ONE- AND TWO- DIMENSIONAL MODELLING OF UPLAND FLOODPLAIN FLOWS IN RESPONSE TO DIFFERENT CHANNEL CONFIGURATION

Vahid Tayefi Nasrabadi

Submitted in accordance with the requirements for the degree of
Doctor of Philosophy

University of Leeds
School of Geography

February 2005

The candidate confirms that the work submitted is his own and that appropriate credit has been given where reference has been made to the work of others.

PAGE NUMBERING AS IN THE ORIGINAL THESIS

Abstract

This research is based on two contexts. First, the research is concerned with a much understudied aspect of flood inundation: upland environments with topographically complex floodplains. Although the presence of high resolution topographic data (e.g. LiDAR) has improved the quality of river flood inundation predictions, the optimum dimensionality of hydraulic models for this purpose has yet to be fully evaluated for situations of both topographic and topological (i.e. the connectivity of floodplain features) complexity. In this research, we present the comparison of three treatments of upland flood inundation using: (a) a one-dimensional model (HEC-RAS) with the domain defined as series of extended cross-sections; (b) the same 1D model, but with the floodplain defined by a series of storage cells, hydraulically connected to the main river channel and other storage cells on the floodplain according to floodplain topological characteristics; and (c) a 2D diffusion wave treatment, again with explicit representation of floodplain structural features. The three models were tested on a 6 km upland reach of the river Wharfe, UK. The results showed that both the extended cross-section and storage cell modes were conceptually problematic. They also resulted in poorer model predictions, requiring incorrect parameterisation of the main river to floodplain flux in order to approach anything like the level of agreement observed when the diffusion wave treatment was assessed. The research concludes that a coupled 1D-2D treatment is likely to provide the best modelling approach, with currently available technology, for complex floodplain configurations.

Second, as a substantive issue, the research is concerned with the effects of channel configuration change (i.e. in-channel morphology) and climate change on flood inundation; the aspect on which mush less attention has been paid. The results show that for the 1 in 0.5 flood event in this study reach, there is a rise of 5.7% and 12.2% to the inundation extent due to 2-year in-channel change (i.e. 10cm rise in bed level) and climate change (i.e. scenario 2050) respectively. The sensitivity of inundated area changes to climate change is strongly conditioned by in-channel sedimentation.

TO MY WIFE, LALEH

Acknowledgment

Table of Contents

Chapter 3: Study area and data sources

Chapter 4: Application of HEC-RAS in normal mode

Chapter 5: HEC-RAS in storage cell mode

Chapter 6: Two-dimensional diffusion wave treatment of floodplain flows

Chapter 7: Floodplain inundation in response to changes in river channel configuration and climate

Chapter 8: Conclusions

List of Figures

Chapter 1

Chapter 3

Chapter 4

Chapter 5

Chapter 6

Chapter 7

List of Tables

Chapter 2

Chapter 3

Chapter 4

Chapter 5

Chapter 6

Chapter 7

List of Pictures

Chapter 1

Introduction and context

1.1 Introduction

Floodplains are a vital part of our environment and their inundation is a natural occurrence. They provide natural storage for floodwater; fertile land for agriculture; valuable habitat for wildlife and plants; and a recreational resource. It is a combination of all these factors which makes this land of such considerable importance to a wide variety of users including conservation groups; farmers; and local communities. Thus, it is vital to have an understanding of floodplain processes in general and floodplain flooding and inundation in particular. Nowadays, flood inundation is taken into account as a major natural hazard in the UK and world-wide and its prediction is a significant task for planners, environmental managers and the insurance industry (see Penning-Rowsell and Tunstall, 1996). As for most rivers, insufficient observations of flood inundation extent are available for determining inundation and, given the infrequent nature of inundation, recourse must be made to some sort of predictive model. Therefore, flood inundation extent prediction using hydraulic models ranging in complexity from a simple planar approximation (i.e. in one dimension) through to fully hydrodynamic models in two dimensions is the key theme in much flood inundation research. Modelling flood extent using three different flow representations on the floodplain is the focus of this thesis.

The reminder of this chapter has three sections. Section 1.2 introduces the research context addressing inundation modelling by a preliminary overview of current literature and thus defines the main issues that dominate the thesis. Section 1.3

summarises the aims and objectives of the research. Section 1.4 outlines the thesis structure.

1.2 Research context

This research has a context based in both a technical issue (representation of flood inundation processes) and a substantive issue (the effects of channel configuration change and climate change on flood inundation). They are addressed in the following sections.

1.2.1 Technical issues

Until relatively recently, the most popular approaches to modelling fluvial hydraulics in general and flood inundation in particular, at the reach scale (1-60 km), have been based on a full treatment or an approximation of the one-dimensional St. Venant equations, solved using numerical solution techniques (see for example Fread, 1984; Samuels, 1990; Fread, 1993; Ervine and MacLeod, 1999). Commonly, this is based on commercial codes such as MIKE11, ISIS, ONDA, FLUCOMP and HEC-RAS. Such schemes describe the river channel and floodplain as a series of cross sections perpendicular to the flow direction and are well suited to parameterization using traditional field surveying methods. Numerical solution of the governing equations for prescribed upstream and down-steam boundary conditions allows the cross-section averaged velocity and water depth at each cross section (i.e. node) to be calculated.

There are issues concerning these models. Samuels (1990) notes that considerable skill is required to determine appropriate cross section location for such models. This is aside from the cost of survey methods, which may limit the number of cross sections that can be considered in a study. Further, due to the simplifying assumptions present in these schemes, representation of flow is limited to bulk flow characteristics (Bates and Anderson, 1993). The models commonly assume planar water levels across the floodplain at each cross section, particularly where levées are located along river banks and water has different elevations between the main channel and the floodplain. This can cause large errors in inundation extent

prediction particularly where floodplains have slight lateral slopes and may also lead to solution instability. The use of cross sections in one-dimensional schemes restricts the representation of the floodplain in relation to topographic characteristics meaning that areas between cross sections are not explicitly represented in the process of flow routing on the floodplain.

More recently, in response to these limitations and given recent advances in numerical methods and computational power, two-dimensional finite difference and finite element models have increasingly been developed and applied to overcome some of the limitations of one-dimensional schemes (see for example Gee *et al.*, 1990; Bates et al., 1992; Feldhaus *et al.*, 1992; Anderson and Bates, 1994; Bates *et al.*, 1995; Nicholas and Walling, 1997; Bates *et al.*, 1998; Bates *et al.*, 1998; Stewart *et al.*, 1999; Nicholas and Mitchell, 2003). These models typically solve the two-dimensional depth-averaged form of the Navier-Stokes equations at a higher spatial resolution than one-dimensional models. Process representation in these models is a logical development of one-dimensional approaches as they include lateral shear, secondary flows and turbulence in the model process representation (Knight and Shiono, 1996). Commonly, these parameters are represented as one lumped parameter (a friction factor) in one-dimensional approaches. Therefore, these approaches are more consistent with known processes (see for example Knight and Shiono, 1996; Hervouet and Van Haren, 1996; Bates and De Roo, 2000) particularly on the floodplain and floodplain/main channel interface where additional processes come into action (i.e. lateral shear layer between floodplain and main channel flows) (Knight and Shiono, 1996) that increase the complexity of flow behaviour.

Two-dimensional models are best employed in conjunction with a DEM of the channel and floodplain surface which, in conjunction with suitable inflow and outflow boundary conditions, allows inundation extent over the study domain and the water depth and depth-averaged velocity in the x and y directions to be computed at each computational node at each time step. Such schemes have shown their capability as a predictive tool in relation to inundation extent and hydraulic field predictions, specifically using TELEMAC (e.g. Galland *et al.*, 1991; Bates *et al.*, 1995; Marks and Bates, 2000; Horritt and Bates, 2002), RMA2 (e.g. Bates *et*

al., 1992, 1995) and *hydro2de* (e.g. Nicholas and Mitchell, 2003). For example, such schemes have been compared successfully to satellite imagery of flood inundation extent (Bates et al., 1997; Horritt and Bates, 2001b) and have provided initial evidence of their ability to correctly reproduce water levels internal to the model domain during dynamic simulations (Bates et al., 1998). Their drawbacks include increased computational cost and less suitability to parameterisation using traditional cross section surveys.

Use of such models has a number of problems. They can be divided broadly into two main groups. First, there are those that relate to the methodological approach (such as representation of wetting and drying processes, turbulence representation and numerical solver used) (Marks and Bates, 2000). Second, there are those that result from (i) parameterisation due to inadequate and inaccurate topographic and friction data provision, particularly the scarcity of detailed topographic data (Bates et al., 1992; Marks and Bates, 2000; Horritt and Bates, 2001a), (ii) simplicity of calibration techniques compared with the complex and distributed structure of two-dimensional models (Bates *et al.*, 1998; Marks and Bates, 2000), and (iii) lack of distributed (for hydraulic fields) and inaccurate (for inundation shorelines) validation data (e.g. Horritt *et al.*, 2001a; Horritt and Bates, 2001a). The constraints arising from availability of topographic and validation data, have been relaxed by the emergence of new data capture techniques using airborne remote sensing, including interferometric synthetic aperture radar (SAR) (e.g. Brackett *et al.*, 1995; Horritt and Bates 2001a), aerial digital photogrametry (Lane, 2000; Westaway *et al.*, 2001, 2003) and laser induced direction and ranging (LIDAR) (e.g. Flood and Gutelius, 1997; Marks and Bates, 2000). The latter can provide a horizontal precision of ±5 cm and a minimum relative precision of ±10-15 cm at horizontal intervals of at least 2 m (Environment Agency, 1997). Using traditional, standard, topographic data (e.g. OS contour line and spot heights) for an 11 km reach of the River Culm floodplain, the vertical precision of each point on the resultant 10 × 10 m DEM was estimated, at best, as ±50 cm (Marks and Bates, 2000). The comparison of inundated areas predicted by a two-dimensional hydraulic model parameterised using novel Lidar data (i.e. high resolution and accuracy) and the Ordnance Survey in conjunction with spot heights data (i.e. low resolution and accuracy), showed an increase of 20% using Lidar data (Marks and Bates, 2000). It

has already been demonstrated that flood hydraulics and inundation extent are affected directly by quite small changes in floodplain topography and indirectly through mesh resolution changes (see Nicholas and Walling, 1997; Hardy *et al.*, 1999; Marks and Bates, 2000; Bates and De Roo, 2000; Horritt and Bates, 2001a, b; Nicholas and Mitchell, 2003)

Despite developments in terms of topographic parameterisation and the existing evidence of its controlling effects on inundation extent, its relative importance to other elements of modelling (i.e. calibration, process representation) is less clearly understood (see Horritt and Bates, 2001b). For instance, complex floodplain topography has been noted as the controlling element of inundation (Nicholas and Walling, 1997) whereas Bates *et al.* (1998) note that friction (in the calibration process) is a more effective parameter in determining inundation extent than floodplain topography. Hardy *et al.* (1999) introduce spatial resolution as a parameter that has a greater effect on model predictive ability than typical calibration parameters, when they applied a two-dimensional finite element to a meandering compound channel. Ignoring calibration effects on the quality of inundation extent predictions, it is crucial to assess the relative importance and value of model parameterisation (in terms of topography), particularly in complex situations, and process representation (in terms of the complexity of flow representation particularly on the floodplain). This can lead to exploration of new modelling strategies and whether or not attention must be paid to improving process representation in inundation models or in gathering more accurate data for their parameterisation (Horritt and Bates, 2001b) and validation. Indeed, simplification of sophisticated flow process representation for floodplain flows to gain the same level of predictive ability (i.e. inundation extent) is a central aim in this research. This has been the central attention of many scientists in the field of inundation modelling. For instance, Horritt and Bates (2002) showed that three hydraulic models, with three different level of process complexity including HEC-RAS (full one-dimensional), LISFLOOD-FP (two-dimensional diffusion wave treatment), and TELEMAC-2D (full two-dimensional), were capable of predicting flood extent and travel times to similar levels of accuracy at optimum calibration when all three models use the same high quality topographic data for parameterisation. Bates and De Roo (2000) found that a diffusion wave treatment out-performed two-dimensional finite element approaches because the simplified treatment of flow

routing on the floodplain allowed a much higher density representation of floodplain topography.

As yet, no consensus exists concerning the level of model process complexity required to achieve satisfactory prediction in terms of flood inundation extent (Horritt and Bates, 2001b). As one-dimensional approximation of in-channel flow is broadly accepted (Cunge *et al.*, 1980; Knight and Shiono, 1996), the question of optimum level of flow process complexity for floodplain flows in relation to inundation extent predictions is still open.

In response to these issues, in this research, three levels of process complexity for floodplain flow representation for inundation modelling are considered. First, in one-dimensional approaches, floodplain zones between cross sections can be treated as units that convey flow parallel to the flow direction in main channel. In this method, water elevations are estimated at each cross section and remain constant across the floodplain. More importantly, the effects of turbulence and dispersion are represented by increasing surface roughness (see Horritt and Bates 2002, Bradbrook *et al.*, 2004).

Second, the floodplain can be represented as storage cells hydraulically connected to the main channel and themselves. The idea of interconnected storage cells on the floodplain was proposed initially by Zanobetti *et al.* (1968, 1970) and Cunge (1975). This state will be aggravated on floodplains with either natural obstacles or man-made structures (dykes, elevated roads field walls, embankments etc.). In such cases, the land surrounding the main channel (i.e. floodplain) may comprise a series of discrete areas acting as storage cells, which hydraulically communicate with their neighbours and/or the main channel. In this sense, the flow direction on the floodplain can be considered to be independent of the direction of main channel flow direction (Fig. 1.1). Water surface elevations in the main channel and on the floodplain in each storage cell will be different.

Fig. 1.1: Schematic form of interconnected storage cells on the floodplain
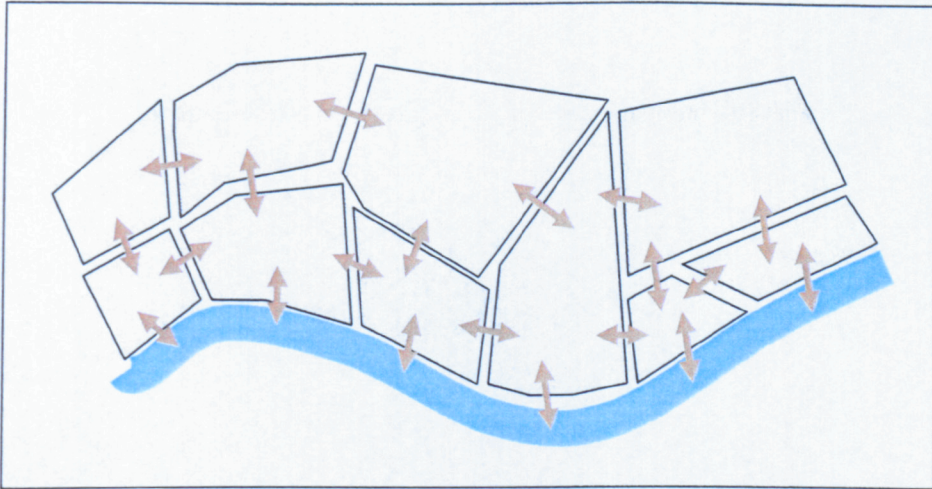
This approach means that once the river overtops, the floodplain is inundated in a manner dictated by local topography at each cell, at least at the beginning of inundation and then hydraulic connectivity between storage cells controls flood inundation extent on the floodplain. Although the two-dimensional unsteady flow equations are not used to explain the flow behaviour on the floodplain in this method (it uses a weir equation and a continuity equation), the physical situation in which channel and storage cells form a two dimensional network for flow movement are perfectly simulated. In such a condition, storage cells can be realistically parameterised with high quality topographic data and flood distribution patterns can be mapped in each cell.

Third, within the last five years, efforts have been made to develop simpler forms of two-dimensional models, kinematic and diffusion wave treatments, in conjunction with high quality topographic data in relation to inundation extent (e.g. Bates and De Roo, 2000; De Roo *et al.*, 2000; Horritt and Bates, 2001a, 2001b, 2002; Bradbrook *et al.*, 2004; Yu and Lane, in press, a and b). Unlike other hydraulic models, the simplified two-dimensional, raster-based models (Fig. 1.2) are specifically designed to predict flood inundation and ignore or minimise the representation of flow processes which are not considered central to this aim. In this approach, the flow between floodplain components is governed using a simple continuity equation. They take the fundamental property adopted in cross-section extension for flood inundation modelling, in which the water surface remains planar

and route water on the floodplain according local topography (e.g. Bradbrook *et al.*, in press).

Figure 1.2: Floodplain cells in a raster-based two-dimensional diffusion wave treatment
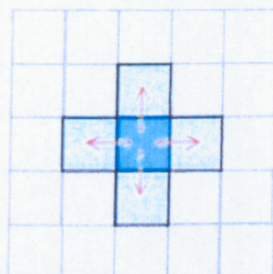
1.2.2 Substantive issues

In the literature, the geomorphological impacts of river flows and flooding; and the influence of different land management activities (i.e. landuse change, clear cutting, urbanisation and etc.) on downstream flooding have been broadly acknowledged (for example see Rothacher, 1973; Harris, 1973; Hollis, 1975; Ziemer, 1981; Lyons and Beschta, 1983; Jones and Grant, 1996; Thomas and Megaham, 1998; Heritage *et al.*, 2001; Phillips, 2002; Hohensinner *et al.*, 2004). However, much less attention has been paid to the impact of river channel configuration (i.e. within-channel morphology) on flood risk and inundation extent. As channel dimensions are not arbitrary and are adjusted through time by the processes of erosion and deposition, they will impact on the conveyance capacity of the river channel. As river conveyance decreases, this may cause river banks to be overtopped more frequently and so result in a greater flood risk. Thus, increased flooding could arise from either a change in hydrological response of the river basin resulting from land management or climate change as well as from the effects of change in channel shape (which may, in turn, be related to a change in sediment delivery due to a hydrological change). The latter has received negligible attention and the over-emphasis on hydrology may mean that the real cause of increased flooding is overlooked. This could have serious implications for watershed managers and planners. In this research, to investigate the effects of channel change on flood inundation, different in-channel cross-sections surveys undertaken in 2002 and

2004 in combination with optimum values of model parameters for the flood considered for this research are used.

The same context applies to the effects of climate change on increased flooding and inundation extent. To date, there is no clear conclusion as to how climate change impacts on flood risk and magnitude given the fact that climate variability is seen to have a strong impact on flood records, masking any observed trend (Robson, 2002). In the UK, to be more specific, long term monthly rainfall series show a tendency to increased winter rainfall and decreased summer rainfall, but with a non-significant trend in the annual rainfall total (IPCC, 2001; Robson, 2002). Under the assumption that flooding is likely to be affected by climate change, evaluation of the effects of climate change on flooding and inundation extent is of great importance so that its effects are not masked by other catchment drivers. In this respect, using the monthly percentage precipitation changes which are available from the UK Climate Impacts Programme 2002 (UKCIP02) for periods 2050s and 2080s, the flood event considered for this study is modified in order to represent the effect of climate change on the inflow hydrograph. Then, using the modified inflow hydrographs for scenarios 2050s and 2080s, the individual effect of climate change and its effect in combination with channel configuration change on inundation extent are studied.

1.3 Aims and objectives

Given the context presented above, the two primary aims of the research are:
(i) to evaluate the performance of hydraulic models with one-dimensional (i.e. in normal and storage mode for floodplain flows) and a simplified two-dimensional process representation in conjunction with high quality topographic data for floodplain inundation extent prediction; and
(ii) to explore the effects of different in-channel configurations due to deposition and erosion, and climate change on inundation extent.

Following from the above aims, the research has 2 main phases. The focus of Phase 1 is technical assessment of flood inundation modelling approaches. The objectives of this phase are:

(i)   to simulate inundation extent using the normal mode of a one-dimensional hydraulic model for floodplain flow representation (i.e. HEC-RAS);

(ii)   to simulate inundation extent using combined storage cells and a one-dimensional hydraulic model (i.e. HEC-RAS); and

(iii)   to simulate inundation extent using a two-dimensional diffusion wave treatment.

This leads to evaluation of these three modelling approaches and identification of an optimal modelling approach. In Phase 2, the effects of in-channel configuration change and climate change on inundation extent are evaluated.

1.4 Thesis structure

The thesis has 7 main chapters. Chapter 2 reviews the definitions and literature concerning all aspects of the application of hydraulic models in relation to shallow open channel flows. These can be categorised into: (i) a review of the fundamentals of open channel flow, with particular reference to two-stage flows including coupling between the main channel and floodplain; (ii) a description of the representation of these fundamentals in existing hydraulic models, with different dimensionality, which are being used to model river channel flows; and (iii) a review of the general concept of model assessment, sensitivity analysis, calibration and validation in relation to hydraulic models.

Chapter 3 describes the study area to which the selected models are applied. In addition, it addresses data needs, including topographic data for parameterisation, friction factors for calibration, and boundary conditions of models used in this research. Data acquisition techniques are also described. In response to a lack of upstream boundary condition data (i.e. inflow hydrographs), hydrological methods are presented in order to estimate the flow rate for the flood considered for this research.

Chapters 4, 5 and 6 are allocated to the application of the hydraulic models considered in this research, including HEC-RAS based on extended cross sections, HEC-RAS based on storage cells and a raster-based two-dimensional diffusion wave treatment. Each chapter describes the theoretical basis on which the model is based. Then, the models are parameterised in terms of topographic data, friction

factors and boundary conditions. For each model application, sensitivity analysis, calibration and validation are performed and the best fit of inundation extent to the observed data using four different accuracy assessment tests is determined. Finally, Chapter 6 presents a final discussion on the performance of the three models including their strengths and weaknesses.

Chapter 7 addresses the effects of in-channel configuration and climate changes on flood inundation. In terms of in-channel configuration change, flood inundation variation resulting from two in-channel cross-section surveys undertaken in 2002 and 2004 are investigated. In this respect, evidence is presented regarding meaningful changes in bankfull discharge and out-of-bank duration, as drivers that control inundation extent, due to in-channel change. In terms of climate change, the inflow hydrograph considered for this research is modified using the monthly percentage precipitation change scenarios for the 2050s and 2080s. The application of the original and modified inflow hydrographs as boundary conditions provide indications of climate change effects on flood inundation. Then, the combined effects of channel change and climate change on flood inundation are investigated.

Chapter 8 concludes thesis. It summarises the results of the thesis; revisits the thesis objectives; discusses and puts into context, the main findings of the study; highlights the limitations of the study; and finally proposes future research directions.

Chapter 2

Modelling floodplain inundation

2.1 Introduction

The last chapter presented the context, aims and objectives of the research. Given the context and aims of the research, a range of hydraulic models with different dimensionality (i.e. 1-d and 2-d) for modelling floodplain flows must be considered. Use of a physically-based model involves a series of stages that can be divided into: (i) analysis of the phenomenon of interest (i.e. reality) in order to generate a conceptual model of that reality and in turn to identify relevant physical rules to describe the conceptualisation; (ii) transformation of physical rules into mathematics and solution of the mathematical model through analytical or numerical solutions, using a set of boundary conditions and expected parameter values; (iii) validation of the model solution against observations (i.e. which are commonly assumed to be reality); and (iv) calibration through which the model prediction is optimised by changing parameter values (see Anderson and Woessner,1992; Bates and Anderson, 2001; Lane 2003). It is necessary to have a clear understanding of the above-mentioned steps, which underpin the structure of this chapter. Hence, description of the fundamental principles of open channel flow, the relevant mathematical equations, the available solver techniques, boundary conditions, simplifications and modifications implemented for the application of the models to floodplain flows, model assessment and sensitivity analysis must all be discussed. These are categorised into: (i) a review of the fundamentals of open

channel flow, with particular reference to two-stage flows including coupling between the main channel and floodplain; (ii) review of the representation of these fundamentals in existing hydraulic models, with different dimensionality, which are being used to model river channel flows; and (iii) review of the general concepts of model assessment, sensitivity analysis, calibration and validation in relation to hydraulic models.

2.2 Principles of open channel flow hydraulics

The term 'hydraulics' is generally related to the application of Fluid Mechanics principles to water, civil and environmental structures and facilities, especially hydraulic structures (e.g. rivers, canals, dams, reservoirs, water treatment plants) (Chanson, 1999). Natural open channels (i.e. streams and rivers) are the focus here. Open channel flow is characterized by the existence of a free surface (the water surface), where surface pressure is atmospheric, and across which shear forces are negligible. The longitudinal profile of the free surface defines the hydraulic gradient and determines the cross sectional area of flow for a given cross-section shape and roughness. Hence, the free surface rises and falls in response to perturbations of the flow (e.g. changes in slope and width). The primary factor in open channel flow analysis is the height of the free surface. The elevation of the free surface (water level) at any point in the channel, with respect to local bank height, defines the head which drives the transfer of flow from river to floodplain. Thus, a prime goal of flow modelling is accurate determination of flow shape in space and time.

2.2.1 Definitions

Free surface flow may be classified in terms of velocity and or depth with reference to both time and space (French, 1994): channel flow may be either or both unsteady in time; and non-uniform in space. *Steady uniform flow* involves constant depth in time and space. This constitutes the fundamental type of flow in an open channel in which the gravity forces are in equilibrium with the resistance forces. It is also the type of flow to which friction formulae, such as the Chezy equation or the Manning equation, are applied without any other treatment of flow hydrodynamics (French, 1994). This type of flow is rare in natural channels. Under the assumption of steady

and uniform flow, the friction slope is equal to the bed slope, and only friction formulae are required to parameterise the momentum equation. *Steady non-uniform flow* involves variation in depth with space, but not through time. Non-uniform flow, also termed varied flow, is further classified as being either: (i) gradually-varied; or (ii) rapidly-varied. Rapidly-varied flow occurs whenever there is a sudden change in channel geometry over a very short distance and this change in geometry dominates over friction effects. Bed slope and channel friction are important because they determine the flow regime under gradually-varied flow conditions. Steady, gradually-varied, flow requires joint application of energy or momentum and frictional resistance equations. *Unsteady flow* involves variation in depth with both time and distance. Conceptually, modelling an unsteady uniform flow is possible. From a practical viewpoint, such a flow is nearly impossible to determine (French, 1994) as it involves simultaneous solution of the energy, momentum and friction equations through time.

2.2.2 The Reynolds number

Two dimensionless indices classify the *state* of the flow according to the above definitions: the Reynolds number; and the Froude number. The ratio of the inertia forces to the viscous forces is known as the Reynolds number. It is used to classify the flow as laminar, transitional, or turbulent:

$$\mathrm{Re} = \frac{UL}{\nu} \qquad \text{(Eq. 2.1)}$$

where Re is the Reynolds number, U is the characteristic velocity of flow (taken as average velocity in open channel flow), L is the characteristic length (taken as the hydraulic radius in open channel flow) and ν is the kinematic viscosity. The kinematic viscosity is calculated as:

$$\nu = \frac{\eta}{\rho_w} \qquad \text{(Eq. 2.2)}$$

where: η is the dynamic viscosity; and ρ_w is the fluid density

A laminar flow $(\text{Re} \leq 500)$ is one in which the viscous forces are of similar magnitude or slightly larger (incorporative terms) than the inertial forces. In such a flow, streamlines are parallel and the fluid particles move along smooth paths. If $\text{Re} \geq 2000$, the inertial forces are large relative to the viscous forces, the inertial forces dominate the situation, and the flow becomes turbulent. In this type of flow, the fluid particles move as eddies in a random fashion. Between these two limits ($2000 \leq \text{Re} \leq 500$), the flow is classified a transitional flow (Singh, 1996).

2.2.3 The Froude number

The second dimensionless parameter which defines the flow regime is the Froude number. Depending upon the magnitude of the ratio of inertial forces to gravity forces, a flow is classified as sub critical, critical, or supercritical. The physical significance of the Froude number may be understood in two different ways; from dimensional analysis (Eq. 2.3); and by consideration of the speed of propagation of a wave of low amplitude and long wavelength (Eq. 2.4).

$$Fr^2 = \frac{inertial}{gravitational} = \frac{\rho L^2 U^2}{\rho g L^3} = \frac{U^2}{gL} \qquad \text{(Eq. 2.3)}$$

$$Fr = \frac{U}{\sqrt{gL}} = \frac{WaterVelocity}{WaveVelocity} \qquad \text{(Eq. 2.4)}$$

where Fr is the Froude number, U is the characteristic velocity of flow (taken as average velocity in open channel flow), L is the characteristic length (taken as flow depth in open channel flow), g is the acceleration due to gravity.

If **Fr** = 1, the inertial and gravitational forces are in equilibrium and the flow is in a critical state. If **Fr** < 1, the flow is in a sub critical state and the velocity of flow is less than the celerity of a gravity wave. Thus, such a wave can propagate upstream against the flow. When the inertial forces are dominant, the Froude number is greater than one and the flow is in a supercritical state. In this state, flow disturbances only travel downstream and the upstream water levels are unaffected by downstream controls (Singh, 1996).

15

In compound channels, where flow has different velocity and depths in the main channel and on the floodplain, more complicated situations may occur. For instance, it is possible that flow in the main channel is very close to critical flow whereas flow on the floodplain, where flow velocity is much lower than the main channel, is still sub critical (Chadwick, 1994). Knight *et al.* (1994) have shown that both sub- and supercritical flow can exist simultaneously in a compound channel.

2.3 Process representation and conceptualisation
2.3.1 Fundamental equations

The equations which describe the flow of the fluid are derived from two fundamental laws of physics; (i) conservation of mass, and (ii) conservation of momentum. These are derived from Newton's laws of motion for a single fluid unit. The law of conservation of mass states that mass cannot be created or destroyed, only converted: mass within a closed system remains constant with time. For an infinitesimal small control volume and an incompressible fluid (i.e. ρ = constant), the continuity equation (conservation of mass) may be obtained in Eulerian form as:

$$\frac{\partial v}{\partial x} + \frac{\partial u}{\partial y} + \frac{\partial w}{\partial z} = 0 \qquad \text{(Eq. 2.5)}$$

where x, y and z denote the space co-ordinates; and u, v and z presents the three components of velocity in the x, y and z directions respectively (Lane, 1998).

The law of conservation of momentum states that a body in motion cannot gain or lose momentum unless some external force is applied: the change of momentum of fluid in a a control volume will equal the sum of all forces applied to the control volume. The forces acting on the control volume are: (i) the surface forces (i.e. pressure and shear forces) acting on the control surface; and (ii) the volume force (i.e. gravity) applied in the centre of mass of the control volume (Chanson, 1999). This law is used to develop the momentum equations for a control volume of an incompressible fluid, known as the Navier-Stokes momentum equations, which are fully described by Lane (1998), ignoring surface wind stresses as:

$$\frac{\partial}{\partial t}(\rho u) + \frac{\partial}{\partial x}(\rho u^2) + \frac{\partial}{\partial y}(\rho u v) + \frac{\partial}{\partial z}(\rho u w) = 2\rho u \zeta \sin \Phi - \frac{\partial p}{\partial x} + \frac{\partial \tau_{xx}}{\partial x} + \frac{\partial \tau_{xy}}{\partial y} + \frac{\partial \tau_{xz}}{\partial z}$$

(Eq. 2.6a)

$$\frac{\partial}{\partial t}(\rho v) + \frac{\partial}{\partial x}(\rho u v) + \frac{\partial}{\partial y}(\rho v^2) + \frac{\partial}{\partial z}(\rho v w) = 2\rho v \zeta \sin \Phi - \frac{\partial p}{\partial y} + \frac{\partial \tau_{xy}}{\partial x} + \frac{\partial \tau_{yy}}{\partial y} + \frac{\partial \tau_{yz}}{\partial z}$$

(Eq. 2.6b)

$$\frac{\partial}{\partial t}(\rho w) + \frac{\partial}{\partial x}(\rho u w) + \frac{\partial}{\partial y}(\rho v w) + \frac{\partial}{\partial z}(\rho w^2) = \rho g - \frac{\partial p}{\partial z} + \frac{\partial \tau_{xz}}{\partial x} + \frac{\partial \tau_{yz}}{\partial y} + \frac{\partial \tau_{zz}}{\partial z}$$

(Eq. 2.6c)

where ρ is the density of water, ζ is the angular rotation of the earth, Φ is latitude, p is pressure, g is the acceleration due to gravity; and τ_{ij} is the shear stress which is given by:

$$\tau_{ij} = \mu \left(\frac{\partial v_i}{\partial x_j} + \frac{\partial v_j}{\partial x_i} \right)$$

(Eq. 2.7)

where μ is the coefficient of the molecular viscosity (dynamic viscosity) in a Newtonian fluid. In Equation set (2.6), the first term on the left-hand side is the momentum acceleration and the next three terms are the momentum advection. The right side of the equations shows the sum of forces acting on the control volume, which include the volume forces (i.e. gravity) acting on the centre of mass of the control volume; and surface forces (i.e. stress forces) including: (i) the pressure forces; and (ii) the resultant of the viscous forces, acting at the control surface (see Chanson, 1999).

Theoretically, these governing equations can be used to solve any open channel fluid flow problem, subject to the assumptions made in their definition. However, there are no industrial tools suitable for solving directly the 3D Navier-stokes

17

equations for free surface flows (Hervouet and Van Haren, 1996). Direct solution of these equations is only possible for very straightforward problems (Lane, 1998). One of the difficulties is movement of the free surface itself, which can cause the extent of the computational domain to vary in time. More importantly, is the problem of turbulence. To solve these equations in the case of a turbulent river flow, a three-dimensional computational grid is required to capture the smallest turbulent motion and time steps must be adopted smaller than the fastest eddies (see Lane, 1998). The provision of such conditions given the current computational power for the reach scale applications is impossible. As a result, a number of assumptions are introduced to simplify solution. The most popular and widely used simplifications are the Shallow Water equations given by Barre de Saint-Venant in 1871. Indeed, in the case of the shallow flow problems that typify most geomorphological and hydrological contexts, three-dimensional equations must be simplified in relation to the hydrostatic pressure assumption, and introduction of special conditions for both the bottom and water surface regarding to atmospheric pressure in large-scale applications, wind stress and Coriolis effects (Lane 1998). The latter are restricted to large-scale applications and are not relevant to this study. In terms of the effect of turbulence on solution, the most common simplification involves a semi-empirical analysis of the effects of turbulent motions on the mean flow properties, called Reynolds averaging (see Lane, 1998). These simplifications and modifications are fully described in the next sections

2.3.2 Three-dimensional shallow flow equations:

As discussed earlier, the full 3-D Navier-Stokes equations describe the three-dimensional hydraulics of fluid flows. In the case of the shallow open channel flow problems, use of these equations needs some modifications and additions.

First, under the assumption of shallow water, the vertical scale may be assumed to be much smaller than the horizontal scale and the boundary layer to be dominant throughout the water depth. This allows Equation (2.6c) to be simplified to the hydrostatic pressure distribution (Rodi et al., 1981).

$$\frac{\partial p}{\partial z} = -\rho g$$

<div align="right">(Eq. 2.8)</div>

Assuming density is constant in all directions, and integrating over depth, Equation (2.8) becomes:

$$p = \rho g (h + z_b)$$

<div align="right">(Eq. 2.9)</div>

where h is the water depth and z_b is the bottom elevation. As mentioned before, at the small-scale application of these questions to river channel systems, it is generally acceptable to ignore the terms associated with the Coriolis effect. Thus, Equations (2.6a) and (2.6b) become (Lane, 1998):

$$\frac{\partial}{\partial t}(u) + \frac{\partial}{\partial x}\left(u^2\right) + \frac{\partial}{\partial y}(uv) + \frac{\partial}{\partial z}(uw) + g\frac{\partial h}{\partial x} + g\frac{\partial z_b}{\partial x} + \frac{1}{\rho}\frac{\partial \tau_{xx}}{\partial x} - \frac{1}{\rho}\frac{\partial \tau_{xy}}{\partial y} - \frac{1}{\rho}\frac{\partial \tau_{xz}}{\partial z} = 0$$

<div align="right">(Eq. 2.10a)</div>

$$\frac{\partial}{\partial t}(v) + \frac{\partial}{\partial x}(uv) + \frac{\partial}{\partial y}\left(v^2\right) + \frac{\partial}{\partial z}(vw) + g\frac{\partial h}{\partial y} + g\frac{\partial z_b}{\partial y} - \frac{1}{\rho}\frac{\partial \tau_{xy}}{\partial x} - \frac{1}{\rho}\frac{\partial \tau_{yy}}{\partial y} - \frac{1}{\rho}\frac{\partial \tau_{yz}}{\partial z} = 0$$

<div align="right">(Eq. 2.10b)</div>

Second, special conditions exist at both the water surface and bottom, causing the normal velocity components the surface and bottom to disappear (Lane, 1998).

Considering the continuity equation (2.5), the shallow flow momentum equations (2.9 and 2.10) and their modifications where necessary and provision of the appropriate boundary conditions (such as the channel topography), modelling a turbulent river flow is theoretically feasible. However, direct application of these equations results in computational problems (Shimizu *et al.*, 1990). The normal state of flow in a fluvial environment is highly turbulent (Reynolds number $> 10^5$) The 3-D computational grid used should be small enough to capture the smallest motion of eddies and time steps chosen should also be smaller than the fastest

eddies (Lane, 1998). For example the smallest scale turbulent motion for a typical fluvial flow can be characterized by the Kolmogorov length scale; with **u** equal to 1 ms^{-1}; the largest length scales of the order of 1m; and kinematic viscosity of 1.0 $\times 10^{-6}$ m^{2}s^{-1}; the required mesh resolution is approximately 0.03mm (Hervouet and Van Haren, 1996). Construction of such a grid for practical purposes is impossible given existing computer power. Younis (1992) showed that the number of grid cells required was a Reynolds number dependence. For a practical application with *Re* in excess of 10^6 direct applications of these equations will be impossible (Bates and Anderson, 2001).

2.3.3 Reynolds Averaging

On the one hand, the flow both in the channel and at the locations of mass and momentum transfer between the main channel and floodplain is fully turbulent which means we are facing a problem of spatial and temporal scale in using the 3-D shallow flow equations. On the other hand, from a practical view point for most hydraulic problems, the details of the instantaneous velocity field are not of vital importance as compared with the mean flow properties. Thus, as mentioned before, the most commonly used approach involves a semi-empirical analysis of the turbulence structure to determine its impacts on the mean flow properties (Lane, 1998). This method, typically termed Reynolds averaging, assumes that each variable (e.g. *v*) can be spilt into a mean value ($\overline{v}_i$) and a random variation (v_i') about it.

$$v_i = \overline{v}_i + v_i'$$

(Eq. 2.11)

It is assumed that the random variations about the mean are normally distributed and hence over a sufficient time period these cancel to zero.

$$\overline{v}_i = \frac{1}{\Delta t}\int_0^{\Delta t} v_i dt$$

(Eq. 2.12)

$$\overline{v}_i' = \frac{1}{\Delta t}\int_0^{\Delta t} v_i' dt = 0$$

(Eq. 2.13)

Reynolds averaging (time averaging) has no effect on the continuity equation, but introduces new terms into the momentum equations, called the turbulent (Reynolds)

shear stresses ($\overline{v_i v_j}$). These represent the transport of momentum that can be attributed to turbulence (Lane, 1998). The stress terms in the momentum equations are then redefined as

$$\frac{\tau_{ij}}{\rho} = \mu \left(\frac{\delta v_j}{\delta x_i} + \frac{\delta v_i}{\delta x_j} \right) - \overline{v_i v_j} \cong -\overline{v_i v_j} \qquad \text{(Eq. 2.14)}$$

Although time-averaging the instantaneous equations removes the need to resolve the small-scale and high-frequency motions, it adds a total of six terms (Reynolds shear stresses) to the momentum equations. The unknown correlations ($\overline{v_i v_j}$) have no physical basis and there are no more equations available to solve them. Therefore, the Reynolds-averaged equations do not close (Olson and Wright, 1990). As there is no direct way of obtaining the Reynolds shear stresses, the only alternative is to model the effects of the Reynolds shear stresses on flow parameters (Younis, 1992). In practice, most turbulence models are based on Boussinesq's assumption (1877) that introduces an eddy viscosity (v_{ij}), which is a coefficient of linear proportionality to calculate the Reynolds shear stress (Younis, 1992).

$$-\overline{v_i v_j} = v_{ij} \left(\frac{\delta v_j}{\delta x_i} + \frac{\delta v_i}{\delta x_j} \right) \qquad \text{(Eq. 2.15)}$$

Lane (1998) provides a detailed discussion of the use of Boussinesq's assumption either to specify a constant eddy viscosity or to determine eddy viscosity using a mixing length hypothesis.

While the discussion so far has been entirely focused on 3-D approaches, many hydraulic problems do not require this level of complexity in order to provide an adequate representation of the flow field. In many circumstances, a modeller may assume that significant flow field variations only occur in a reduced number of dimensions.

2.3.4 Two-dimensional models

In some environmental problems, particularly in geomorphology and hydrology, the major flow field variations of interest only occur in the horizontal dimension. Hence, two-dimensional approaches, which involve depth-integration of velocity to produce depth-averaged values, have been extensively described in the relevant literature (Rodi *et al.*, 1981; Knight and Shiono, 1996). They are increasingly being used in sediment modelling (Nicholas and Walling, 1997, 1998; Walling *et al.*, 1992), geomorphology (e.g. Nelson and Smith, 1989a, b; Bridge and Gable, 1992; Lane *et al.*, 1994a; Miller, 1994; Lane *et al.*, 1999, Yafei and Wang, 1999) and floodplain flow simulations, including flood inundation, (e.g. Gee *et al.*, 1990; Bates and Anderson, 1992; Bates *et al.*, 1992, Bates and Anderson, 1993; Bates *et al.*, 1998; Marks and Bates, 2000; Horritt and Bates, 2001a, b; Bates *et al.*, 1998a; Nicholas and Mitchell, 2003). Depth-averaging using Eq. 2.16, the continuity equation (2.5) and momentum equations (2.10), results in depth-averaged mass (Eq. 2.17) and momentum equations (Eq. 2.18), where capital letters indicate depth-averaged quantities and overbars indicate Reynolds-averaged quantities (Lane, 1998).

$$V_i = \frac{1}{h - z_b} \int_{z_b}^{h} v_i \, \partial z$$

(Eq. 2.16)

$$\frac{\partial h}{\partial t} + \frac{\partial}{\partial x}\left[(h - z_b)\bar{U}\right] + \frac{\partial}{\partial y}\left[(h - z_b)\bar{V}\right] = 0$$

(Eq. 2.17)

$$\frac{\partial}{\partial t}\left(\bar{U}\right) + \frac{\partial}{\partial x}\left(\bar{U}^2\right) + \frac{\partial}{\partial y}\left(\bar{U}\bar{V}\right) = -g\frac{\partial h}{\partial x} - g\frac{\partial z_b}{\partial x} + \frac{1}{\rho}\frac{\partial}{\partial x}\left(\bar{\tau}_{xx}\right) + \frac{1}{\rho(h - z_b)}\frac{\partial}{\partial y}\left(\bar{\tau}_{xy}\right) - \frac{\tau_{bx}}{\rho(h - z_b)} +$$
$$\frac{1}{\rho}\frac{\partial}{\partial x}\int_{z_b}^{h} \rho\left(\bar{u} - \bar{U}\right)^2 \partial z + \frac{1}{\rho(h - z_b)}\frac{\partial}{\partial y}\int_{z_b}^{h} \rho\left(\bar{u} - \bar{U}\right)\left(\bar{v} - \bar{V}\right)\partial z$$

(Eq. 2.18a)

$$\frac{\partial}{\partial t}\left(\bar{V}\right)+\frac{\partial}{\partial x}\left(\bar{U}\bar{V}\right)+\frac{\partial}{\partial y}\left(V^{2}\right)=-g\frac{\partial h}{\partial y}-g\frac{\partial z_{b}}{\partial y}+\frac{1}{\rho}\frac{\partial}{\partial x}\left(\bar{\tau}_{xy}\right)+\frac{1}{\rho(h-z_{b})}\frac{\partial}{\partial y}\left(\bar{\tau}_{yy}\right)-\frac{\tau_{by}}{\rho(h-z_{b})}+$$

$$\frac{1}{\rho(h-z_{b})}\frac{\partial}{\partial x}\int_{z_{b}}^{h}\rho\left(\bar{u}-\bar{U}\right)\left(\bar{v}-\bar{V}\right)\partial z+\frac{1}{\rho(h-z_{b})}\frac{\partial}{\partial y}\int_{z_{b}}^{h}\rho\left(\bar{v}-\bar{V}\right)^{2}\partial z$$

(Eq. 2.18b)

The depth-averaging process introduces two new set of terms into the governing equations: bottom stresses (τ_{bx} and τ_{by}); and dispersion terms (the last two terms in equations 2.18a, b). The bottom stresses in turbulent flow are assumed to be a quadratic function of the depth-averaged velocity:

$$\bar{\tau}_{bi}=C_{f}\rho\bar{V_{i}}\left(\bar{V_{1}}^{2}+\bar{V_{2}}^{2}\right)^{\frac{1}{2}}$$

(Eq. 2.19)

where C_{f} is a friction factor (Darcy-Weisbach). This is justified by Langbein (1966) who applied a random walk model for particles of water to show that channel resistance changes are consistent with the square of velocity. Lane (1998) reports that this method has been used extensively in depth-averaged models (e.g. Dietrich and Whiting, 1998; Nelson and Smith, 1998a,b; Shimizu and Itakura, 1989; Struiksma and Crosato, 1989; Shimizu *et al.*, 1990).

Dispersion terms appear as a result of vertical non-uniformity in the velocity field, representing deviations from the depth-averaged velocities within a vertical profile (Lane 1998). These have a similar physical meaning to the turbulent stresses as they both represent gradients in momentum transport (Rodi, 1980; Rodi *et al.*, 1981). No additional equations arise during the depth averaging, as with the Reynolds shear stresses, and determination of these terms requires closure. Lane (1998) addresses in detail the two key methods in this respect: either a semi-empirical or an empirical treatment of the dispersion terms in order to model their effects on the mean transport of momentum and hence depth-averaged flow velocities. Although, there is still some doubt over the methods used to represent the dispersion terms (see,

Lane, 1998). Rodi *et al.* (1981) note that even in the presence of such three-dimensional effects, in many rivers, the depth-averaging method may be sufficiently accurate for practical purposes, if the width to depth ratio is high and changes in bed elevation are not rapid. Recent advances in numerical methods and computational power have led to hydraulic models becoming more widely available, which are based upon the depth-averaged form of the law of conversation and momentum equations. For instance, TELEMAC-2D and RMA-2 are increasingly being used in relation to sediment modelling (see e.g. Walling and Nicholas, 1997), geomorphology (see e.g. Wang, 1999) and floodplain flow simulations (see e.g. Marks and Bates, 2000; Horritt and Bates, 2002). To use the models, the space domain is divided into a continuum of triangular or rectangular elements, and the governing equations are solved using the numerical methods.

Although the application of these kinds of models was constrained by a lack of precise topographic data for parameterization (see, Bates *et al.*, 1992), the growing availability of high quality remotely-sensed topographic data (see e.g. Horritt and Bates, 2002) is making the two-dimensional hydraulic schemes an increasingly practical flood risk management tool (Bradbrook *et al.*, 2004). Given recent findings in relation to the significance of quality of topographic data on inundation extent (e.g. Marks and Bates, 2000), the possibility that simpler two-dimensional models in combination with these data may provide similar levels of predictive ability is of major interest. In this respect, simpler forms of two-dimensional hydraulic models, based upon a diffusion wave treatment coupled to high resolution topographic data has been seen in the floodplain flow routing literature. (see e.g. Bates and De Roo, 2000; De Roo *et al.*, 2000; Horritt and Bates, 2001a, 2001b, 2002; Bradbrook *et al.*, 2004). These models are usually linked to a one-dimensional model for main channel flows and are fully addressed in the next section.

2.3.5 Two-dimensional diffusion wave treatment

In the last decade, two-dimensional hydraulic models have been developed, which are capable of being applied to rivers over scales of 1-60 km (e.g. Gee *et al.*, 1990; Baird *et al.*, 1992; Feldhaus *et al.*, 1992; Bates *et al.*, 1992, 1995, 1996, 1998a, b; Bates and Anderson, 1993; Marks and Bates, 2000; Nicholas and Mitchell, 2003).

These models have generally shown reasonable correspondence to available field data sets (see e.g. Bates *et al.* 1998). Despite promising results, a number of problems still remain, which can be divided into two groups; (i) those concerning the methodological approach inherent in the modelling procedure (such as representation of wetting and drying processes, turbulence representation and numerical solvers used); and (ii) those that stem from inadequate data provision, particularly of topographic data (Marks and Bates, 2000). Although improvements are required in both aspects, the recent development of novel topographic data capture techniques using airborne LIDAR (laser induced direction and ranging) has already overcome the problem of the lack of high resolution topographic data for parameterisation. The use of such topographic data coupled with two-dimensional hydraulic models facilitates the investigation of the effects of topographic representation upon flood hydraulics on the floodplain in general and flood inundation extent in particular. Current findings have shown that flood hydraulics and inundation extent are substantially controlled by the topographic characteristics of floodplains (Marks and Bates, 2000; Nicholas and Mitchell, 2003). Nicholas and Mitchell (2003) define a two-phase model of flooding, which seems likely to be representative of natural floodplains in general. Within this definition, phase one of flooding occurs immediately after bankfull discharge and marks the beginning of inundation. It is directly controlled by local topography. In phase two the variability of depth and water velocity declines; and the influence of local topography on flow direction is reduced as water moves increasingly in the direction of the dominant floodplain slope. Traditionally, one of the key sources of uncertainty in relation to floodplain inundation predictions has been topographic data (e.g. Marks and Bates, 2000). Considering the recent development of novel topographic data capture techniques using airborne remote sensing, the major issue now appears to be model process complexity (e.g. Bates and De Roo, 2000). It is now well-illustrated that in-channel flow can be routed using one-dimensional approaches (Knight and Shiono, 1996). No consensus yet exists concerning the level of model complexity required to achieve a good prediction of floodplain flow behaviour. For instance, the effect of floodplain sections between cross sections on floodplain flow behaviour is not well represented in one-dimensional methods. These areas are either treated as **conveying,** with an appropriate increase of floodplain roughness to represent the effects of turbulent diffusion, dispersion and surface roughness, or as **storaging,**

hydraulically connected to the main channel and to themselves (Bradbrook *et al.*, 2004). Neither of these methods will describe the connection between river and floodplain correctly. On the other hand, with available high quality topographic data we still do not know how much process complexity is essential for two-dimensional hydraulic models in order to achieve reliable prediction of floodplain inundation. Given the significant influence of topographic characteristics on the hydraulics of floodplain flow (e.g. Bates and De Roo, 2000), the possibility that simpler two-dimensional models coupled with high resolution topographic data may provide similar levels of predictive ability has been of major interest particularly where the prediction of flood inundation in a central aim. This is why the last five years has seen use of a simpler form of two-dimensional hydraulic models, based upon a diffusion wave treatment. In combination with high-resolution topographic data, it sacrifices essential process representation, but also addresses some of the known limitations of one-dimensional modelling of flood inundation (see e.g. Bates and De Roo, 2000; De Roo *et al.*, 2000; Horritt and Bates, 2001a, 2001b, 2002; Bradbrook *et al.*, 2004). Bates and De Roo (2000) showed that the best results in relation to inundation extent have been obtained with a two-dimensional diffusion wave treatment as compared with a planar approximation of the free surface and a relatively coarse resolution two-dimensional finite element method. The results of the work of Horritt and Bates (2001b) indicated that a full two-dimensional model and a two-dimensional diffusion wave treatment coupled to a high resolution DEM can equally simulate the flood shorelines on the floodplain. Horritt and Bates (2002) also showed that under specific circumstances full one-dimensional methods (in their research HEC-RAS) are capable of predicting flood extents to similar levels of accuracy to full two-dimensional and raster-based models (based upon a 2-D diffusion wave treatment). In using one-dimensional methods, model set up commonly requires a priori knowledge of probable flow paths during a flood (Bradbrook *et al.*, 2004), otherwise such predictions may be incomparable with the more sophisticated model results. These findings imply that the question of the optimum level of process representation for floodplain inundation predictions is still open. The two-dimensional diffusion wave treatment, which is applied in this research, is fully described in Chapter 6.

2.3.6 One-dimensional models

The mass and continuity equations (Navier-Stokes equations) may be integrated over an area to produce one-dimensional equations that are basically known as the St Venant equations (2.20 and 2.21) (Cunge *et al.*, 1980). The standard approach to modelling fluvial processes at the reach scale has been one-dimensional models of the full St. Venant equations (Samuels, 1990). To date, the use of such schemes in both engineering and hydrology is dominant (e.g. Cunge *et al.*, 1983; Samuels, 1990; Fread, 1984, 1990, 1993; Niekerk *et al.*, 1992 Rechard, 1997; Ervine and MacCleod, 1999; Bates and Roo, 2000; Horritt and Bates, 2001b). It is generally accepted that, for flow routing, channel flow may be treated as if it is predominantly one-dimensional in the stream wise direction, despite known three dimensional processes being present in all flows particularly once overbank flow starts (Knight and Shiono, 1996):

$$\frac{\partial A}{\partial t} + \frac{\partial Q}{\partial x} = \frac{\partial z}{\partial t} + z\frac{\partial u}{\partial x} + u\frac{\partial z}{\partial x} = 0 \qquad \text{(Eq. 2.20)}$$

$$\frac{\partial u}{\partial t} + u\frac{\partial u}{\partial x} + g\frac{\partial z}{\partial x} + \frac{1}{\rho}\frac{\partial p}{\partial x} - \frac{1}{\rho}\frac{\partial \tau_{xx}}{\partial x} = 0$$

$$\text{(Eq. 2.21)}$$

where u is the horizontal velocity axis in the direction of flow. The momentum equation can be rearranged to yield equation (2.22) (Henderson, 1966), which may be linked to resistance laws to give a stage –discharge relationship.

$$S_f = S_o - \frac{\partial z}{\partial x} - \frac{u}{g}\frac{\partial u}{\partial x} - \frac{1}{g}\frac{\partial u}{\partial t} \qquad \text{(Eq. 2.22)}$$

where S_f is friction slope, S_o is channel slope, $\partial z/\partial x$ is the rate of change of channel depth, $u\partial u/g\partial x$ is the longitudinal velocity gradient, and $\partial u/g\partial t$ is the rate of change of velocity in time.

Various categories of flow may be attributed to the terms in Equation (2.22). Table 2.1 summarizes the four possible forms of simple one-dimensional flow behaviour in open channels.

Table 2.1: Forms of the one-dimensional momentum equation

Type of Flow	Momentum Equation
Kinematic wave (steady uniform)	$S_f = S_0$
Diffusion wave (non-inertia)	$S_f = S_0 - \partial z / \partial x$
Steady non-uniform	$S_f = S_0 - \partial z / \partial x - (u / g)\partial u / \partial x$
Unsteady non-uniform	$S_f = S_0 - \partial z / \partial x - (u / g)\partial u / \partial x - (1 / g)\partial u / \partial t$

For overland flow and many channel flow situations, some of the terms in Equation (2.22) may be neglected (Eagleson, 1970). For example, in a typical shallow stream, if the bed slope is 0.01, the rate of change of water depth ($\partial z/\partial x$) will not exceed 0.001 (Bedient and Huber, 1988). The longitudinal velocity gradient term $(u/g)(\partial u/\partial x)$ and the time rate of change of velocity term $(1/g)(\partial u/\partial t)$ will be typically less than 0.001 (Bedient and Huber, 1988). Thus, the last three terms on the right hand side of Equation (2.22) will be two orders of magnitude less than those for bed slope and may be neglected.

Such schemes describe the river and floodplain as a series of cross sections perpendicular to the flow direction and are well suited to parameterisation using traditional field surveying methods. However, there are problems in using one-dimensional models. First, the resistance laws that are being used in one-dimensional models are based on uniform and steady flow, which does not occur in natural and compound channels. Second, the presence of heterogeneous environments in relation to friction factors particularly between the main channel and the floodplain and also the variation of friction factors with depth for the whole channel (Knight *et al.*, 1989) will lead to difficulties in deriving the correct stage-discharge relationship. Third, there is no continuous representation of topographic features so that the effects of features in areas between cross sections on model output are not explicitly represented, particularly in relation to flood inundation on the floodplain. The values of water depth between cross sections either have to be

overlain on a DEM or linearly interpolated. Fourth, the values of water surface elevation at each cross section are assumed to be constant in the main channel and on the floodplain. This is not usually the case, particularly where there are levées. The last two issues mean that there is no explicit representation of how water moves across the floodplain to create spatial pattern of flood inundation. HEC-RAS, ISIS, MIKE11, FLUCOMP and ONDA are the most common one-dimensional hydraulic models used in practice.

2.4 Flow or friction formulae

As discussed before, the flow of water in channels is governed by the Navier-Stokes equations. One-dimensional versions of these equations are known as the St Venant equations (see, for example, Cunge *et al.*, 1980). Central to these, and requiring special attention, are the resistance laws, which are basically based on uniform flow, but adopted to parameterise friction slope in the St Venant equations. Although uniform flow, and the assumptions required to develop the governing equations, are only rarely satisfied in practice, the concept of uniform flow is fundamental to the understanding and solution of most problems in open channel hydraulics. By definition, uniform flow occurs when: (i) the depth, flow area and velocity at every cross section are constant; and (ii) the energy grade line, water surface and channel beds are all parallel. The stage-discharge relationship for simple prismatic channel may then be readily obtained by applying appropriate uniform resistance formulae.

2.4.1 Basic resistance formulae

The Chezy equation (1769) can be derived with reference to the definition of uniform flow that requires the forces resisting flow to be equal to the forces causing motion (Singh, 1996).

$$\overline{U} = C\sqrt{RS}$$ (Eq. 2.23)

where $\overline{U}$ is the average velocity, C is the Chezy resistance coefficient, R is the hydraulic radius and S is the channel slope.

The Manning equation (1889) was empirically developed, using the characteristics of steady uniform flow (Singh, 1996).

$$\overline{U} = \frac{1}{n} R^{2/3} S^{1/2}$$
(Eq.2.24)

and the equivalent formula for discharge is:

$$Q = \frac{1}{n} A R^{2/3} S^{1/2}$$
(Eq.2.25)

where $\overline{U}$ is the average velocity, n is the Manning resistance coefficient, R is the hydraulic radius, S is the channel slope, Q is discharge and A is the flow area.

For a particular cross-section, Equation (2.25) links the depth (h) via hydraulic radius (R) to the discharge (Q). It should be remembered that the above resistance laws only apply to flow in circular pipes and they may be used to determine steady uniform flow for certain prismatic channels, where energy slope (S_f) is equal to the channel slope (S_o). Using the Manning equation to determine the depth, given the discharge, is normally referred to as a *"normal depth"* criterion. Flood flows are mostly unsteady flows, meaning that the relationship between stage and discharge depends upon whether the discharge is increasing or decreasing. The Manning equation for non-uniform flows, which is dominant in natural channels, is given as:

$$Q = \frac{A R^{2/3}}{n} S_f^{1/2}$$
(Eq. 2.26)

where the friction slope (S_f) for unsteady flows has at least four components based on the simple one-dimensional momentum equation. These components are discussed in section 2.1.7.

As uniform flow can only occur in a channel of constant cross section, natural and complex channels should be excluded. However, in solving the equations for non-uniform flow in natural channels, it is still necessary to solve the Manning equation, as the St. Venant equations still require estimation of a friction slope. Therefore, it is necessary to consider the application of the Manning equation for both non-uniform and irregular channels.

2.4.2 The concept of channel conveyance

To address channel irregularity and its impacts upon the non-uniformity of flow, the concept of channel conveyance (K) has been defined as a measure of the discharge carrying capacity of a channel (Equation 2.27a).

$$Q = KS_f^{1/2}$$
(Eq. 2.27a)

where Q is discharge, K is the conveyance capacity and S_f is the friction slope.

For any given water depth, its value may be found by equating Equation (2.27a) to the Manning equation to give:

$$K = \frac{A^{5/3}}{nP^{2/3}}$$
(Eq. 2.27b)

where A is the flow area, n is the Manning resistance coefficient and P is the wetted perimeter.

Its principal use is in determining the discharge and the energy and momentum coefficients in compound channels, using subdivision of the flow channel into units for which the velocity is uniformly distributed. The conveyance capacities are then calculated, using appropriate sub-area values for A, P, n and R. The individual conveyances are then summed to give the total discharge in the whole channel. As Manning's n varies with flow depth, in particular above bankful level due to the abrupt change in hydraulic radius, adjustments in n values are necessary in order to obtain the correct sub-area conveyance capacities in the main channel and on the floodplain (Knight and Shiono, 1996). Alternatively, a composite roughness may be adopted, based upon aggregation of the sub-area values for the whole channel. Knight (1989) showed that there are differences between the actual and effective roughness values with the composite roughness approach and individual values with the sub-area approach. This means that both the division method and composite roughness methods are essentially flawed. This arises from the fact that simple addition of the individual flows in each sub-area will not necessarily yield the total flow associated with the main channel/floodplain interaction (Knight and Shiono, 1996). Knight and Shiono (1996) report four methods suggested in the literature, including the effects of interactions on the channel division calculations.

The first is based on altering the sub-area wetted perimeter, typically excluding the water height at the main channel and floodplain interface (between the main channel and floodplain sub-division) in the calculation of the wetted perimeter for the floodplain, but including it in the value of the wetted perimeter for the main channel (Wormleaton *et al.*, 1982, Knight *et al.*, 1983, 1984). The second is based on the "coherence" concept of Ackers (1993a). The third, which has been popular, quantifies the apparent shear stresses on the sub-area division. The fourth is based upon dividing the channel by drawing lines along lines of zero shear stress (see Knight and Shiono, 1996).

2.4.3 Roughness coefficients

The value of the roughness coefficient determines the flow resistance of a given channel. Cowan (1956) discussed five primary factors for determination of flow resistance in natural streams and channel ways. Trieste and Jarrett (1987) pointed out 14 factors affecting roughness during large floods. These factors can be classified into seven groups: (1) surficial irregularities, (2) vegetation, (3) obstructions, (4) flow characteristics, (5) geometric variation, (6) meandering, and (7) sediment concentration and debris. It should be noted that the significance of the factors depends upon the spatial resolution used and topographic data entered into a model. These factors are not entirely independent of one another, so that some of them can interact strongly (Singh, 1996). The interaction among the factors may further compound the difficulty of accurately determining flow resistance. Here, the focus is upon Manning's n, as this is the most commonly adopted resistance parameter. It can basically be evaluated directly from discharge and stage measurements for a known cross section and slope, with reasonable accuracy for artificial lined channels and with less accuracy for natural channels due to the variety of channel materials and channel conditions, as mentioned above. Values of the roughness coefficient may also be estimated using "visual comparison" with rivers where it has been measured at a broad range of representative reaches (Hicks and Mason, 1991). The standard references for estimating roughness by visual comparison are Chow (1959), Barnes (1967) and Hicks and Mason (1991). Cowan (1956) developed an approach involving assigning a base-value roughness coefficient appropriate for a straight, uniform, smooth channel with the same bed

32

material by visual comparison, empirical equations or both, then adjusting this base-value by applying correction factors for the effect of bed surface irregularities, shape and size of cross section, obstructions, vegetation and meandering. Similar to the work of Cowan (1956), Arcement and Schnider (1989) presented a base-value approach for the main channel and flood plain with an emphasis on highly vegetated areas. The estimation of the roughness coefficient is associated with other errors that stem from the fact that the value of n may change with stage (particularly with flood flows over bank levels) and with time (due to change in bed material as a result of sediment transport) or season (due to presence of vegetation). An example of such data is given in Table 2.2, where Chow's tables are presented for different channel and floodplain types.

In addition, numerous studies have been undertaken to estimate flow resistance through empirical equations. For instance, using field data collected at sites at various streams in California, Limerinos (1970) defined a relationship between Manning's n and an effective bed particle size as

$$\frac{n}{R^{1/6}} = \frac{c}{a + b\log(R/D)}$$ (Eq. 2.28)

in which a and b are constants that depend on particle size (see Limerinos, 1970), D is the characteristic or effective particle diameter, and c = 0.0926 in English units or 0.113 in metric units. The quantity $n/R^{1/6}$ is interpreted as the roughness parameter.

Bray (1979) analysed data from 67 natural gravel-bed river reaches in Alberta, Canada, and derived an expression for Manning's n of the form

$$n = \frac{0.113y^{1/6}}{1.09 + 2.203\log(y/D_{84})}$$ (Eq. 2.29)

where y is the average depth in a channel.

These approaches aside, errors may be associated with roughness value determination, due to the variable nature of the factors that affect roughness values, which cannot be practically evaluated or precisely measured. For instance, methods in which the estimation of roughness value is based upon grain size at the reach-

scale may be problematic where spatial variation in grain size and sedimentological structure, particularly in coarse-grained channels, leads to difficulties in determining correct roughness values (Lane, 1998). In addition, processes such as secondary circulation and the level of turbulence will impact upon roughness values. In this regard, the variation of the resistance coefficient with the Reynolds number is now well-known through the Colebrook-White equation (Knight and Shiono, 1996). Moreover, the variation of Manning's n with water depth for the main channel and floodplain, particularly above the bankfull level is demonstrated by Knight *et al.*, (1989). Hence, in one-dimensional hydraulic approaches, the roughness parameter not only represents the effects of resistance at the bed upon flow hydraulics but also must include the effects of turbulence and secondary flow (Lane, 2003) that occur in straight open-channel flow. In one-dimensional models, n dominantly controls the magnitude of friction slope and hence, is a major momentum sink. Thus, its values are dependent on the mesh (i.e. cross section spacing) that is being used to discretise the model equations (Yu and Lane, in press, a). Streamwise curvature is another order of complexity in determining roughness values (Knight and Shiono, 1996). These issues mostly cause roughness estimated from grain size at the reach-scale topography to be very different to the effective values required in model application. Indeed, roughness is commonly used as the key calibration parameter and the ultimate values of the friction factor that are used may be very different to those that measured in the field (Lane, 2003).

Table 2.2: Manning's coefficient for a number of qualitatively defined channels and floodplains (after Chow 1959), (a) channels and (b) floodplains.

(a)

Type of channel and description	Minimum	Normal	Maximum
1. Clean, straight, full stage, no riffles or deep pools	0.025	0.030	0.033
2. Same as above, but more stones and weeds	0.030	0.035	0.040
3. Clean, winding some pools and shoals	0.033	0.040	0.045
4. Same as above, but some weeds and stones	0.035	0.045	0.050
5. Same as above, but lower stages, more ineffective slopes and sections	0.040	0.048	0.055
6. Same as 4, but more stones	0.045	0.050	0.060
7. Sluggish reaches, weedy, deep pools	0.050	0.070	0.080
8. Very weeds reaches, deep pools or flood ways with heavy stand of timber and underbrush	0.075	0.100	0.150

(b)

Floodplains (Pasture, No brush)	Minimum	Normal	Maximum
1. Short grass	0.025	0.030	0.035
2. High grass	0.030	0.035	0.050
1. No crop	0.020	0.030	0.040
2. Mature row crop	0.025	0.035	0.045
3. Mature field crop	0.030	0.040	0.050
Floodplains (Brush)	**Minimum**	**Normal**	**Maximum**
1. Scattered brush, heavy weeds	0.035	0.050	0.070
2. Light brush and trees in winter	0.035	0.050	0.060
3. Light brush and trees in summer	0.040	0.060	0.080
4. Medium to dense brush, in winter	0.045	0.070	0.110
5. Medium to dense brush, in summer	0.070	0.100	0.160
Floodplains (Trees)	**Minimum**	**Normal**	**Maximum**
1. Dense willows, summer, straight	0.110	0.150	0.200
2. Cleared land with tree stumps, no sprouts	0.030	0.040	0.050
3. Same as above with heavy growths of sprouts	0.050	0.060	0.080
4. Heavy stand of timber, a few down trees, little undergrowth, flood stage below branches	0.080	0.100	0.120
5. Same as above, but with flood stage reaching branches	0.100	0.120	0.160

2.5 Overbank flow and the idea of a two-stage channel

Natural rivers are typically compound in cross section, consisting of a main channel which carries flow at most times, and one or two adjacent floodplains that are inundated only during overbank flow conditions. The floodplains are an integral part of the whole river system and floodplain flows are natural albeit infrequent consequences of the hydrological flow regime (Knight and Shiono, 1996). Such a system may be defined as a two-stage channel. However, in terms of the role of floodplains in relation to flood flows, they may act as either temporary stores for flood water or provide an additional route for flow conveyance (Bates *et al.*, 1993), depending upon the geomorphologic configuration and topographic characteristics of the floodplain. Thus, the floodplain, or second stage, does not necessarily convey all overbank flows and the flows which are conveyed may be controlled more by topographic characteristics of the floodplain than by the general slope of valley. Up to bankfull level, there is a continuum of hydraulic processes within a river: as the discharge increases, both the flow velocity and water depth increase, and the flow may be reasonably well-described through a one-dimensional treatment, despite the presence of known three-dimensional mechanisms in all flows (Knight and Shiono, 1996). In the case of overbank flows, the in-channel relationship between the discharge and water depth and velocity will no longer be valid (Bhomik and Demissie, 1982), and they must be treated differently. Certain three-dimensional processes begin to be important, particularly at the main channel/floodplain interface (Knight and Shiono, 1996). Once overbank flow starts, under some circumstances, there may be an actual reduction in Q, despite there being a larger flow area. This is because of a reduction in the average flow velocity in the main channel (Zhelezyakov, 1971) as enhanced interaction with the floodplain impacts on in-channel velocities. Once the depth of flow increases on the floodplain, Q will increase significantly due to the increased flow area and simultaneous reduction in relative roughness. There are therefore continua in the depth discharge relationships for both inbank and overbank flows, although a discontinuity will inevitably occur in the stage-discharge curve at bankfull level. Once a channel flows in an out-of-bank condition, the generally slower moving water on the floodplain may retard the faster flowing water in the river channel, thereby creating a shear layer laterally

between the main channel and the floodplain (Rodi, 1980; Knight *et al.*, 1990; Knight and Shiono 1996). In this highly sheared zone, vortices with vertical axes develop at the top of the main channel bank, at the edge of the floodplain, along with larger vortices or eddies that convect high momentum fluid from the main channel onto the floodplain (Knight and Shiono, 1996). In addition to vorticity generated along the vertical axes, helical secondary flows may form in the longitudinal streamwise direction (Knight and Shiono, 1996), as are present in all turbulent flows in non-circular channel sections (Einstein and Li, 1958; Liggett *et al.*, 1965; Tracy, 1965; Melling and Whitelaw, 1976; Perkins, 1979; Imamoto *et al.*, 1993). They may cause perturbations in the distribution of the boundary shear stress if they are strong.

The intensity of interaction between main channel and floodplain flows is dependent upon the relative depth (Knight and Shiono, 1996) and width (Dellurs *et al.*, 1967) of the floodplain. The relative depth is used to describe the ratio between the floodplain depth and the main river depth. The maximum interaction between main channel and floodplain usually occurs at relative depth of around 0.1-0.3, typically at 0.2. Dellurs *et al.* (1967) concluded that the interaction decreases as floodplain width relative to channel width increases.

To understand the nature of these interactions, flow models of varying dimensionality have been developed. The aim of these models is to predict the dependence of flow parameters such as the mean flow velocity, the boundary shear stresses and turbulent field on geometric parameters such as channel slope, sinuosity, cross-sectional shape and surface roughness (Younis, 1996). There is, in principal, no difficulty in attaining the equations that describe the instantaneous fluid motions (Younis, 1996). The problem is in solving them (Hervouet and Van Haren, 1996) due to the practical difficulties of conducting simulations with mesh- and time-step sizes that are sufficiently small to capture the details of both the smallest turbulent motions and the fastest eddies (Younis, 1992, 1996; Lane, 1998). The next section will address the basic principles governing fluid flow, with emphasis on the shallow flow problems that typify most geomorphological and hydrological contexts (Lane, 1998).

2.6 Solution techniques

As described in the above sections, depending on the dimensionality of the model being applied, a series of equations result. This creates one-, two- or three-dimensional systems of differential or partial differential equations that can be solved analytically to yield an exact solution, or numerically for an approximation of the true solution. In the case of the non-linear and non-steady problems associated with irregular topography, difficulties are encountered when considering flow in open channels, and analytical solution is impossible (Huyakorn and Pinder, 1983). Thus, a numerical solution technique must be applied. To use these techniques, the domain of interest is discretised into units constructed from nodal points. The governing partial equations can then be approximated at each node by application of a numerical solver technique. The most popular approximation techniques are: (i) finite difference; (ii) finite element; (iii) finite volume; and (iv) the method of characteristics.

The **Finite Difference Method** discretises the domain internally into a series of continuous regular rectangular sub-areas (cells). The approximations to a continuous solution are defined at isolated points (nodes), which are considered to be representative of the sub-areas of which they are part. The method allows the calculation of an accurate solution of complex differential and partial differential equations in a computationally efficient manner (Hardy, 1997). As the solution cannot be varied (these methods commonly retain the same cell size throughout the domain) the system may be under-represented, such as where there are transfers from channel to floodplain (Zeilke and Urban, 1981), or over-represented in some areas such as low lying floodplains. Computational efficiency becomes less than optimal in the latter situations. In response to the cell size restriction of finite difference methods, the **Finite Element Method** divides the continuum into a series of elements, either triangular, quadrilateral or a combination of both. The solution of the partial and differential partial equations is then defined over the entire domain (see Pinder and Gray (1977) for more detail). The **Finite Volume Method** is relatively new in fluvial hydraulics. The technique divides the fluid domain into a two- or three-dimensional grid of six sided volumes (cuboids). The governing equations are then integrated about each control volume to yield finite volume equations, which then may be solved numerically to obtain a solution (Hardy,

1997). The **Method of Characteristics** transforms the partial differential equations into ordinary differential equations. An example of the method was developed where a rectangular grid was constructed with the size of elements varying throughout the domain depending upon the topographic representation required in particular areas (Schmitz *et al.*, 1983). The method requires considerable computational time, but can honour topographic complexity explicitly.

The properties of a numerical solution that are of vital significance are: (*a*) **consistency**, the approximation should converge to the original partial differential equation as the discrete intervals tend to zero; (*b*) **convergence**, as the grid of discrete points is redefined there should be convergence to the true solution; and (*c*) **stability**, during each spatial or temporal step an error will be introduced, if this error continues within the algorithm, oscillation will occur in the solution and it may become unstable. Given the advantages and disadvantages associated with these techniques, their choice depends upon the nature of the equations to be solved, the characteristics of the environment (e.g. topography), the dimensions considered, as well as the associated computational demands (Hardy, 1997). There is consensus that the finite element solver technique is the most suitable for solution of the equations for free surface flow (Samules, 1985; Gee *et al.*, 1990; Bates and Anderson, 1993, 1996; Anderson and Bates, 1994; Hardy, 1997).

2.7 Model assessment

Building a physically-based numerical model involves a series of stages that can be divided into: (i) analysis of the phenomenon of interest (i.e. reality) in order to generate a conceptual model of that reality and in turn to identify relevant physical rules to describe the conceptualisation; (ii) transformation of physical rules into mathematics and solution of the mathematical model through analytical or numerical solutions, using a set of boundary conditions and expected parameter values; (iii) validation of the model solution against observations (i.e. it is assumed to be reality); and (iv) calibration through which the model prediction is optimised by changing the parameter values (see Anderson and Woessner,1992; Bates and Anderson, 2001; Lane 2003). Of utmost importance to the mathematical modeller is the concept of accuracy, which represents the degree to which their model reproduces reality. To understand discrepancies between model output and reality,

it is essential to explore and to explain all possible uncertainties and errors, which might enter into the model from the first stage of model building to the final stage of model calibration. Sources of errors and uncertainties can be divided into four main groups. First, there are those arising due to exclusion of processes that might matter when describing the system under study during conceptualisation and which introduces parameters into the model. Second, there are those arising from the computational tools and solution techniques chosen. Third, errors and uncertainties may result from parameterisation of model parameters, boundary and initial conditions and the topography of the study domain. Recently, developments have been seen in relation to the detail and accuracy of topographic data provision (see for example Marks and Bates, 2001). Parameterisation in its general sense is used to give value to parameters defined inside the model structure and is essential for initialising the model simulations. These parameters are created as a result of the exclusion and simplification of certain processes during the conceptualisation process (see Lane 2003). Fourth, errors associated with field validation data can occur. This stems from the quality and quantity of validation data taken in the field and the inconsistency between the scale of discretisation of current hydraulic models and field measurement scales (Bates and Anderson, 2001).

As mentioned earlier, any model results are directly affected by the process representation selected inside the model, solution techniques chosen and parameterisation. Thus, there is a fundamental need for any model to be judged. Methods for doing this will depend on the quality and quantity of validation data and validation methods chosen (given the plurality of function attributed with models). Investigation of the model performance may be called **model assessment** (Bates and Anderson, 2001; Lane 2003), which involves two important stages: **verification** and **validation** (Lane, 2003). Verification is the process by which the model is assessed to make sure that it is solving the governing equations correctly. This may involve checking stability of the numerical solution of the model and undertaking sensitivity analysis (Lane 2003). The latter may be used to make sure that the model behaves sensibly in response to changes in boundary conditions or parameter values over a range of parameter uncertainties (Lane, 2003). Validation is the process by which a model is compared with reality to confirm or reject its acceptance. It is of significant importance that a method that is selected for

validation of a model should be consistent with model functionality. A range of functionalities can be assumed for any hydraulic model, including prediction, exploration of processes, and simulation of past and future events. It is common that model output is compared with observations (i.e. conventional validation) to evaluate model predictions. In this sense, no assessment is conducted in relation to the quality of representation of processes in the model. Hence, a question may arise over which aspect of model functionality should be prioritised in model assessment. Most scientists would now accept a quasi-realist position between explanation and advancement of knowledge as a primary aim (i.e. process representation), and prediction as ultimate expression (Richards 1990, Bates and Anderson, 2001). If this strategy in model assessment is chosen, it is obvious that validation in its conventional definition cannot fulfil our objectives and it should only be considered as a general test of model ability. More importantly, using conventional validation methods, as the accuracy that a model represents processes can remain relatively unknown; the cause of divergence between predictions and observations cannot be explained. Hence, errors and uncertainties involved in model application cannot necessarily be traced. In response to the existing weakness in validation methodology, Lane and Richards (2001) explain the necessity of a move from conventional data-driven validation to a model assessment process in which a wider range of criteria are adopted to disaggregate the contribution from conceptual uncertainties, computational uncertainties, data limitations and numerical uncertainties. Similarly, Bates and Anderson (2001) concluded that predictive validation is only one particular aspect of the model assessment process and accordingly a hierarchy of validation aims should be considered. The next section will address issues that constrain conventional validation methods and then introduce alternatives.

2.7.1 Validation of hydraulic models

In conventional validation methods, model output is compared with observations. In the case of hydraulic models, available data sources include external and internal bulk flow measures, vector data (e.g. images of inundation extent); and point scale data (e.g. velocity) (Bates and Anderson 2001).

External and internal bulk flow measures are usually recorded as time series of water levels and discharges, with the latter typical being obtained via a rating curve rather than direct measurement. Given the typically spacing of river gauging stations, internal data are rarely available and external validation is more common. The use of rating curves as a source of external bulk flow measurements for higher flows can be problematic, particularly where they have been constructed using low flow data. Measurement of high flows, out-of-bank flows, is not an easy task. Most rating curves for high and out-of-bank flows, are extrapolated, which leads to significant uncertainties with high flow estimates. This necessitates the evaluation of the model behaviour using other flow measures. Internal flow measures (e.g. inundated area) may be a good alternative as they allow the model behaviour within the modelled domain (flow routing behaviour in the case of hydraulic models) to be critically assessed. Indeed, internal validation of hydraulic models may not be optional but essential. For instance, Bates *et al.* (1998) tested the capability of a two-dimensional finite element (TELEMAC) to simulate both flood routing and stage hydrographs at points internal to the modelled domain. They showed that validation of the model predictions against the downstream reach outflow only confirmed the model's ability as a flood routing tool: further evidence was required if any confidence was to be placed in the distributed flow field predictions. The level of confidence placed in internal predictions will depend upon available data. Horritt and Bates (2002) showed that predictions of flood extent (i.e. an internal prediction) from the LISFLOOD-FP (two-dimensional diffusion wave treatment) model are significantly poorer when the model was calibrated against floodwave travel time as compared with when the model was calibrated against inundation extent. The combined internal and external validation may decrease the effect of equifinality. The equifinality stems from the fact that different sets of input parameters may lead to similar optimum results. Hence, the calibration of hydraulic models against internal and external model outputs may limit the parameter space.

Vector data sources specifically include airborne oblique photography and satellite data sources such as Synthetic Aperture Radar (SAR). These allow accurate determination of flood inundation extent at a specific point in time. For instance, Bates and De Roo (2000) used shoreline derived from oblique air-photo data and ERS-1 SAR for validation of inundation extents reproduced by three different inundation models with varying complexity.

Point scale (e.g. velocity) data for model validation are more associated with the local and field scales. Such data are never routinely available but seem to be the only field data capable of conclusively discriminating between one-dimensional and higher order schemes and between higher order schemes themselves (Bates and Anderson, 2001).

Although validation of hydraulic models against data sources can provide a general assessment of model performance, conventional validation methods themselves may not be effective. First, if a model has been developed incorrectly with respect to its mathematical representation, numerical solution, boundary condition specification and parameterisation, then this may be reflected in divergence between model prediction and independent observations (Lane and Richards, 2001). However, even if a model predicts independent data reasonably well, it will not necessarily be a valid model. In this respect, Beven (1989) emphasizes that hydrological models may produce the 'right results' for the 'wrong reasons'. This stems from the fact that there are a number of degrees of freedom present in the calibration process so that, for instance, the fit between model predictions and field observations in relation to inundation extent may be readily accomplished for a number of model realisations (Marks and Bates, 2000). Second, there is an inconsistency between field measurement scales and the scale of discretisation of current hydraulic models, particularly for models with higher dimensionality. As a result, observations need novel field measurement methods to find spatio-temporal scales closer to prediction scales and rigorous control during field sampling to enhance the quality of observations (Bates and De Roo, 2000, Lane and Richards, 2001, Bates and Anderson, 2001). At least part of the deviation between observed and predicted values may stem from the fact that we do not know how much of reality is represented by observations. For instance, Bates and De Roo (2000) noted that the lack of sufficiently accurate validation data could be a major constraint to validation in hydraulic modelling. They showed that despite access to aerial photography and satellite data sets, a significant degree of uncertainty surrounded inundation extent observations, so that methods of analysis of remotely-sensed data would always under perform. Hence, as the accuracy of validation data increases, evaluating the appropriateness of process representation become easier.

2.7.2 Comprehensive approach to model assessment

The fundamental weaknesses associated with conventional validation methods necessitate testing a wider range of criteria in relation to the capability of a model to predict, to explain and to simulate particular processes in a realistic way. With the same insight, Anderson and Woessner (1992) define validation more comprehensively as a process to demonstrate that a model is 'good', 'correct' or 'sufficient' representation of reality. Lane and Richards (2001) address several aspects of these alternative validation strategies, which are categorized into five groups.

The first is conceptual model assessment, which involves identifying the levels of simplification introduced as a result of assumptions made during model development. This is essential to define the applicable limits of a particular model and the field data needed to initialise and check a model (Lane and Richards 2001).

The second is assessment of computational tests and analytical solutions. The conversion of the mathematics of processes representation into a computer code requires consideration of the levels of accuracy required in a numerical solution, the forms of discretisation (finite element, finite difference), and solution methods to be employed (Lane and Richards, 2001). One way to assess the validity of the conversion is by comparing a numerical solution with an analytical solution (e.g. Horritt 2000, Lane 2003). For many of the partial differential equations, no general solution exists. However, for boundary conditions or a simple geometry a solution of a reduced form of the equations may be directly obtained (Bates and Anderson, 2001). For example, Horritt (2000) used an analytical solution of the two-dimensional St. Venant equations in plan polar coordinates to develop optimal mesh generation strategies for meandering channel flow problems. Testing computer code is another aspect of this stage of model assessment. To make sure that a code is responding in physically-realistic way, sub-models should be tested against relatively simple cases that have already been simulated or observed (Lane and Richards, 2001). An additional aspect of model assessment at this point is consideration of the stability of numerical solution, which is dependent on the time step and scale of spatial discretisation. A well-known criterion for selecting combinations of these elements that maintain stability is the Courant number:

$$\frac{|v|\Delta t}{\Delta x} \leq 1$$

where v is the rate at which a property moves through a spatial domain which has been discretised with a grid cell dimension of Δx and a time step of Δt (e.g. Singh, 1996).

The third approach to model assessment uses sensitivity analysis. Sensitivity analysis can determine whether, in response to boundary condition and input data changes, theoretically realistic model behaviour is experienced (Howes and Anderson, 1988; Lane *et al.*, 1994a; Lane and Richards, 2001) and whether the model is sufficiently sensitive to represent perceived behaviour in real cases (Lane and Richards, 2001). On this basis, undertaking sensitivity analysis may be interpreted as a crucial step in a comprehensive approach to model assessment. However, other roles are attributed to sensitivity analysis that will be addressed in section (2.6.3).

The fourth approach to assessment is based on visualization. One significant aspect of current hydraulic modelling is the simulation of processes evolving dynamically in space and time (Lane and Richards, 2001). For example, in the case of flood inundation extent models, although the ultimate goal of such models is the prediction of the extent of flood inundation, how inundation evolves through time and space is of major importance to make sure that the model can simulate floodplain flows in a realistic way. It is clear that conventional empirical testing, for instance of an inundation extent model, normally involves comparison of flood boundary predictions and a set of static validation data. This may not assess the dynamics of the inundation process. Hasse *et al.* (2000) emphasize visualization of results of simulations and predictions as an important aspect of model assessment. This requires model predictions to be illustrated not as static images but as animations (Lane and Richards, 2001). Although validating the data contained in animations is generally difficult (given available techniques for collecting data) animations provide a better understanding of and confidence in the extent to which the model reproduces the temporally evolving, spatially distributed processes that can be observed through experimentation or in the field (Lane and Richards, 2001).

Finally, there is evaluation against professional standards. Where the use of hydraulic model is well-established, standards for model validation exist. For instance, reference to the model factors such as mass balance, mesh resolution and numerical accuracy have been introduced (Lane and Richards, 2001).

2.7.2 Sensitivity analysis

Sensitivity analysis involves the process of varying model input parameters over a reasonable range (range of uncertainty in values of model parameters) and observing the relative change in model response. Typically, the observed changes in water stage, flow rate, inundation extent or contaminant transport are noted. Functions attributed to sensitivity analysis include: (i) determination of model behaviour to make sure that it simulates processes in a theoretically realistic way in response to representative variation of model input parameter and boundary conditions (e.g. Lane *et al.*, 1994a); (ii) verification of model response to make sure that the model is sufficiently sensitive to represent perceived behaviour in reality (Howes and Anderson, 1998, Lane and Richards 2001); (iii) identification of those parameters to which the model is most sensitive (e.g. Beven 1979a, Lane and Richards 2001); (iv) improvement of model representation through limiting the sensitivity of a particular component (McCuen 1973, Lane and Richards 2001); and (v) assessment of the likely magnitude of error in a model prediction that arises from a particular parameter specification (e.g. Lane *et al.*, 1994, Lane and Richards 2001).

Functions (i) and (ii) may be used as steps in a comprehensive validation method (after Lane and Richards, 2001). For example, in terms of analytical solution assessment, during the numerical solution of hydraulic models, certain types of numerical errors grow to the extent to which the solution begins to oscillate, or the errors become so large that the computation cannot continue. Herein, numerical sensitivity is defined: the process of adjusting parameters that affect the numerical solution in order to obtain the best solution to the equations, whilst still maintaining model stability.

Function (iii) intends to demonstrate the sensitivity of model simulations within the range of uncertainties of the model parameters and determine the most effective input components, which are finally used in the calibration process. Given the

potential impact of error associated with model input data upon model results, this kind of sensitivity analysis is becoming more common. In the hydraulic modelling literature, friction factors, topographic data and boundary and initial conditions receive most emphasis. Errors associated with input data stem from problems with current measurement methods, situations where parameters have a poor physical meaning (measurements become difficult) and spatial and temporal variation of input data. For example, friction factors may vary both spatially and temporarily through a simulation, meaning that the factors have a poor relationship with measurements. This is especially the case as friction factors do not represent only the roughness of the domain surface but also the effects of turbulence, secondary flows, stream curvature and model discretisation into account. In terms of topographic data, the availability of more automated survey techniques such as stereo photogrametry, laser altimetry (Li, 1997) and interferometer radar systems, for both airborne and spaceborne platforms, has decreased uncertainty in topographic data parameterisation, particularly for models with higher dimensionality. As a result of this improvement, the associated elevation models have varying accuracy and resolution, and these effects can be incorporated into sensitivity analysis. For instance, the impact of different DEM resolutions on bulk flow characteristics (Bates *et al.*, 1996) and inundation extent (Hardy *et al.*, 1999; Horritt and Bates, 2001; Yu and Lane, in press a) has been investigated. Bates *et al.*, (1996) showed that spatial resolution directly affects bulk flow characteristics and that there was an optimum level of mesh resolution beyond which results may not significantly alter, a finding confirmed by Hardy *et al.* (1999). Function (iii) of sensitivity analysis is also beneficial in determining the direction of future data collection activities. Data to which the model is relatively sensitive would require greater emphasis in terms of collection as opposed to data to which the model is relatively insensitive. In terms of boundary and initial conditions, errors are often as a result of measurement methods in the field or uncertainties associated with rating curves construction. Anderson and Bates (1994) examined the sensitivity of a two-dimensional hydraulic model in relation to four model parameters: the floodplain friction factor; the domain coefficient depth range; the eddy viscosity; and the flow depth-discharge relationship. They showed that the most sensitive factors are the floodplain friction factor and rating curve. Bates *et al.*, (1998b) add that boundary

and initial conditions are subject to uncertainty even when measured values are used.

Bates and Anderson (2001) conclude that we are in a transition period from a 'data-poor' to a 'data-rich' modelling environment in relation to topography data but the same conclusion cannot be so readily reached for boundary and initial conditions where modellers face the sparse density of the river/tidal gauging networks, the dearth of necessary accuracy in measurement procedures and the lack of rigorous control of field sampling. This is especially the case during extreme events.

Both functions (iv) and (v) of sensitivity analysis involve considering the relative sensitivity of one parameter of a model to the other parameters in that model. Bates et al. (1996), for instance, found that inundation extent is governed by turbulent viscosity and that friction was a secondary factor, particularly when the turbulent viscosity is low. This result contrasts with the work of Bates *et al.* (1992) who found that the bed friction factor was the single dominant factor controlling model output. A possible cause of this discrepancy may be the relative scales of the two studies. Similarly, a comparative sensitivity analysis of model parameters was conducted by Hardy (1997), who demonstrated that the floodplain friction has a far greater effect than channel friction on bulk flow characteristics. In more detail, Hardy *et al.* (1999) explored the relative sensitivity of the friction coefficient in relation to spatial resolution in order to determine whether the friction factor for an event is stationary between different mesh resolutions or whether some kind of feedback occurs.

Undertaking these kinds of sensitivity analyses as part of a validation strategy is, to some extent, questionable. For instance, current methods of sensitivity analysis typically involve perturbing one parameter across a range of possible values while other parameters are held constant. It cannot mirror the real response of a model. In this state, the model is responding · to the imposed condition. However, the behaviour of the model in response to one parameter will depend upon the values taken by other parameters, which means the parameters are inter-correlated and so this provides a relatively restricted understanding of the actual sensitivity (Lane, Richards, 2001). Thus, this method cannot produce the real response of a model. On the other hand, undertaking simulations for all possible combinations of parameter values may be time demanding particularly when the number of parameters is high. In this regard, stochastic methods, such as Generalized Likelihood Uncertainty

Estimation (GLUE) have been presented (see Beven and Binley, 1992). Another issue associated with sensitivity analysis techniques is their lack of essential sophistication when compared to the time/space resolution of the current physically-based distributed models (Bates and Anderson, 1996). Despite rapid development in high time/space resolution modelling, sensitivity analysis methods characteristic of the old generation of lumped hydrology and hydraulic models are still being used. As the first attempts towards consistency between the physically-based distributed model structures and associated sensitivity analyses, a new distributed sensitivity analysis has been introduced by Bates and Anderson (1996).

2.8 Summary of the chapter

The definitions and fundamentals of open channel flows, with particular reference to two-stage flows including coupling between the main channel and floodplain were described in this chapter. Following that, the mathematical representations of these fundamentals, which constitute the existing hydraulic modelling systems, were presented. Strengths and disadvantages of the hydraulic models given their dimensionality in relation to data requirements, process representation, and quality and quantity of their outputs for problems of interest to most geomorphologists and hydrologists were discussed. In the case of floodplain flow simulations including flood inundation prediction, it was noted that two-dimensional depth-average hydraulic models are becoming an increasingly practical tool for determining floodplain inundation extent given the growing availability of high quality remotely-sensed topographic data (Bradbrook et al., 2004; Horritt and Bates, 2002). Given the significant role of topographic data in relation to inundation extent predictions (e.g. Bates and De Roo, 2000), the possibility that simpler forms of two-dimensional models in conjunction with high quality topographic data may provide similar levels of predictive ability was discussed. Simpler forms of two-dimensional approaches in this search were listed as two-dimensional diffusion wave treatments, application of storage cells, where possible, on the floodplain in one-dimensional approaches and normal use of one-dimensional models. For instance, it was noted that two-dimensional diffusion wave treatments represent a simpler form of the full two-dimensional hydraulic models and have obtained credit in floodplain flow simulation literature within the last five years (see e.g. Bates and De Roo, 2000; De

Roo *et al.*, 2000; Horritt and Bates, 2001a, 2001b, 2002; Bradbrook *et al.*, 2004). An in-depth description of the above-mentioned models is discussed in Chapters 4, 5 and 6 respectively. In this chapter, model performance in relation to numerical solution, process representation and comparison of predictions and observations (i.e. flood inundation extent) were discussed under the term model assessment. It was discussed that conventional validation methods may provide only a general assessment of the predictive ability of a hydraulic model and may not give comprehensive evidence in order to demonstrate that a model is able to predict, to explain and to simulate particular processes in a realistic way. In this regard, alternative validation strategies were presented. It was stressed that, in the context of validation strategies, sensitivity analysis is not limited only to (i) determining the relative change in model response due to varying model input parameters, and (ii) identifying those parameters to which the model is most sensitive. Rather, it helps understanding of model responses due to input changes (Howes and Anderson, 1998; Lane and Richards, 2001) and the assessment of likely magnitude of error sources (Lane *et al.*, 1994; Lane and Richards, 2001).

In the next chapter, the study site is presented and its hydrological, geomorphological, climatological and other characteristics are reviewed. A general discussion in relation to data requirements of hydraulic models is given, and then the availability of required data for models considered in this research are detailed. As there is no long-term, measured flow data at the upstream end of the study reach, different hydrological methods are applied to estimate inflow, as the upstream boundary condition.

Chapter Three
Study area and data sources

3.1 Introduction

The previous chapter reviewed (i) the fundamentals of flow in natural channels, particularly the characteristics of flow in two-stage channels; (ii) recent research in relation to the strengths and weaknesses of hydraulic models with different dimensionality for the purposes of flood routing and prediction of flood inundation extent; and (iii) issues concerning validation, calibration and sensitivity analysis of hydraulic models. Given the latest findings in relation to the optimum level of model complexity particularly for determining inundation extent, and also after considering the available data for parameterisation and validation in the reach under study, three models are proposed to fulfil the objectives of the research. The first is a one-dimensional treatment for both main channel and floodplain flows, based upon HEC-RAS. The second involves a one-dimensional treatment of the main channel and application of storage cells for floodplain flow routing, based on compartments arising from natural and man-made obstacles such as walls, roads, embankments, etc. This is applied in a HEC-RAS formulation. The last model considered here is a one-dimensional model of the main channel and a two-dimensional diffusion wave model for routing floodplain flows, integrated with

newly available, high resolution, raster-based Digital Elevation Models. The latter, essentially, reduces the size of compartments on the floodplain to the raster cell size. The main difference between the second and third models is that there is no mathematical treatment of flux on the floodplain in the second model: water in each storage cell is only conveyed to the next storage cell through a weir equation; in the third model, the flows are routed on the floodplain using a diffusion wave treatment. These models are called hereafter HEC-RAS in normal mode, HEC-RAS in storage cell mode and raster-based mode respectively. This chapter describes the study area to which the models are applied, including data needs and data sources. Chapter 4 describes the theoretical basis for one-dimensional water surface profile calculations for steady and unsteady flow routing within HEC-RAS. The application of HEC-RAS in normal mode is presented using a specific flood event for the study site. Issues regarding sensitivity analysis, validation and calibration of the model are also discussed in Chapter 4. Chapters 5 and 6 address the application of HEC-RAS in storage cell and the raster-based modes respectively in the same way. Inundation extent changes in response to river configuration and climate changes are presented in Chapter 7.

3.2 Study site

The study site is located within the upper catchment of the River Wharfe, which is in the southern part of the Yorkshire Dale National Park (Figure 3.1). The Upper Wharfe River extends from the catchment divides to the Skirfare confluence, which lies downstream of Kettlewell and flows in a south-easterly direction. It has an area of 105km^2 with a high point at the top end of the catchment (668m AOD) and a level at the confluence of 186m AOD (Upper Wharfedale 'Best Practice' Project, 1998). The highest point in the catchment is on the left bank towards the bottom of the catchment of 704m AOD (Upper Wharfedale 'Best Practice' Project, 1998). The study reach lies between Hubberholme Bridge and Starbotton, and is nearly 5.5km in length (Figure 3.2). Upstream of Hubberholme, the Wharfe is constrained within a bed rock channel. Downstream, the river is a glaciated valley, which becomes less steep below Hubberholme. In the latter zone, the river is a typical upland bed river and generally single thread, but some well-developed mid-channel bars (Church, 1983) and pool-riffle sequences (Lane et al., 2002a). The river course is generally

sinuous with areas of high meander frequency interlinked with relatively straight reaches. These are placed within a valley with a wide and gentle slope particularly within the study reach. The surrounding moorland has been extensively drained, but some woodland remains (Upper Wharfedale 'Best Practice' Project, 1998). The riparian zone is partly tree-lined with a diverse range of habitats and species (Upper Wharfedale 'Best Practice' Project, 1998). Channel width is within a range of 10 to 15m in the study reach. The river channel is coupled with hillslopes in places, although this is spatially variable (Merrett and Macklin, 1999). The study reach is fed through six tributaries running down the very steep valley sides, which include Gill Beck, Cray Beck, Birk Beck, Buckden Beck, Water Gill and Step Gill.

The average annual rainfall within the period 1981 to 1996 is 1752 mm at Beckemonds, upstream of the study reach (Upper Wharfedale 'Best Practice' Project, 1998). This value may reach up to 2000mm at higher elevations. Rainfall has also been recorded daily at Kettlewell since 1961, where the thirty-year average annual rainfall is estimated 1440 mm (Heritage and Newson, 1997). The average annual evaporation rate at Kettlewell is 433mm (Heritage and Newson, 1997). This area is very sensitive to both localised connective summer thunderstorms and winter cyclones, which tend to produce high-intensity rainfall events (Merrett and Macklin, 1999). Run-off events are highest in late winter, when heavy rainfall onto often-extensive snow cover, can generate high runoff due to enhanced snow melt and low surface infiltration due to the frozen ground. This process leads flood risk to be a major concern. The land use comprises both improved and rough pasture, although some afforestation began from the 1950s onwards (Merrett and Macklin, 1999). On the floodplain, the majority of field boundaries are dry stone walls. Observations suggest that these are largely impervious to flow. These walls impose an important structure on to flood routing with floods constrained by field boundaries except where gates and/or fences are present. River flows are not measured within the catchment but there are five water level recorders between Deepdale and Kettlewell, with only the Deepdale and Kettlewell level recorders now working.

Figure 3.1: The location of Upper Wharfe Catchment in the UK and the study reach in
Upper Wharfe

Figure 3.2: The study reach in Upper Wharfe
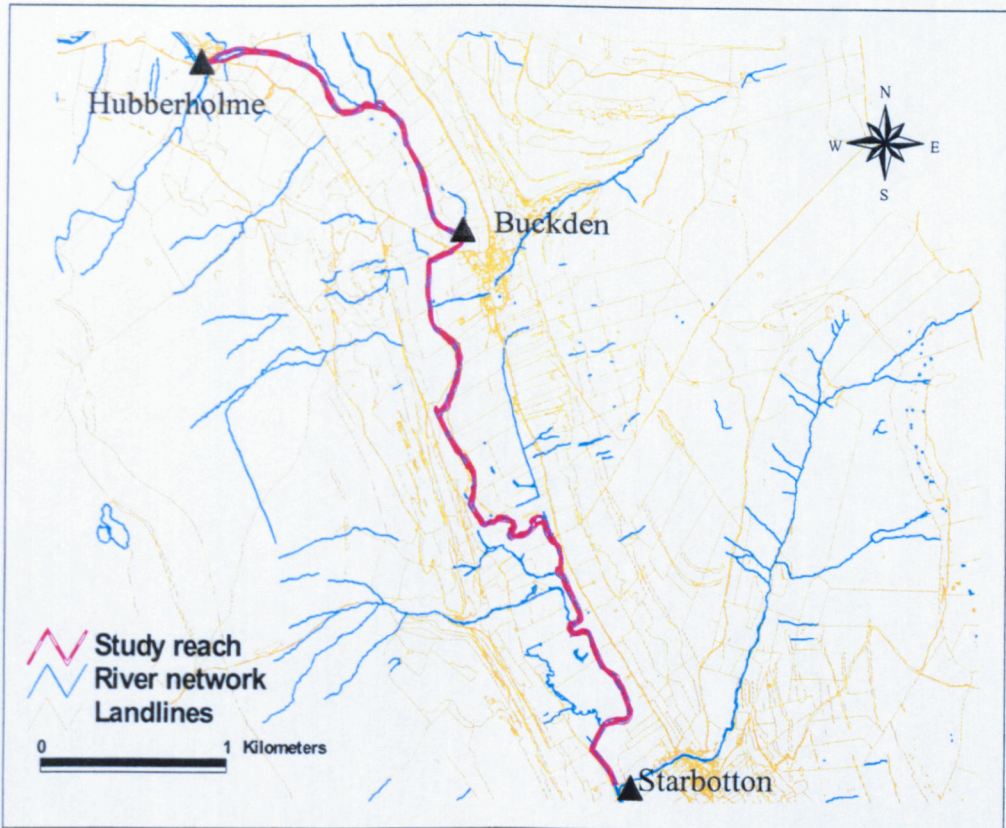
3.3 Data acquisition for hydraulic models parameterisation

The primary data used for flow routing in the main channel and on the floodplain are geometric and flow data. In addition, given the features of any model, there are a series of coefficients that should be determined before any simulation. For instance, contraction and expansion coefficients for one-dimensional models and an eddy viscosity coefficient in the two-dimensional hydraulic models should be identified before any simulation. The coefficients needed to be identified for the three models applied in the research will be discussed in Chapters 4, 5 and 6.

Based upon the process complexity in the hydraulic model in use (e.g. its dimensionality) and, to some extent, the accuracy expected from the simulation results, the nature of the required geometric data would vary. For example, in one-dimensional hydraulic models, the study domain is defined by a series of discrete cross sections, which are perpendicular to the flow direction, both in the main channel and on the floodplain. For a two-dimensional hydraulic model, the study domain is discretised using either finite difference or finite element methods and so

requires distributed topographic data. Given the data needs for topographic parameterisation of the models applied in this research, a series of data sources and techniques are applied that are discussed in the next section in detail.

In terms of geometric data, Table 3.1 presents data needs for each model used in this research.

Table 3.1: Geometric data required for parameterising the models used in this research

Mode	Geometric data needed	Techniques and sources
Normal mode	In-channel cross section, Extension of cross sections on floodplain, joining points between in-channel and floodplain data, Levee elevations,	Surveying (levelling and GPS), Lidar data
Storage mode	In-channel cross section, Levee elevations, storage cell locations and dimensions, Storage cell DEM, Lateral weir locations and dimensions, Location and dimension of hydraulic connection between storage cells	Surveying (levelling and GPS), Lidar and OS landline data
Raster-based mode	In-channel cross section, Levee elevations, Lateral weir locations and dimensions, Floodplain structural characteristics, Floodplain DEM	Surveying (levelling and GPS), Lidar and OS landline data

Flow data are needed as boundary and initial conditions for unsteady flow simulations. Boundary conditions must be established at the open ends (upstream and downstream) of the river system. Boundary conditions are necessary to establish the starting water surface in order to begin calculations. Initial conditions consist of stage and flow data at the exiting nodes, cross sections and storage areas at the beginning of an unsteady flow simulation. The simulated stage and flow data in the first time step of the simulation time are compared with initial values (i.e. initial conditions) established at each node of the system.

River flows are not measured within the catchment but there are five water level recorders between Deepdale and Kettlewell. Only the Deepdale and Kettlewell level recorders are now working. Therefore, hydrological analyses must be conducted to provide flow; which will be discussed in this Chapter. Table 3.2 presents flow data needed for each model given their features.

Table 3.2: Flow data required to parameterise the three models used in this research

Mode	Flow data needed	Technique
Normal mode	(i) Upstream boundary condition (flow hydrograph), Downstream boundary condition (Normal depth), (ii) Initial boundary condition	(i) Hydrological analysis, (ii) steady state simulation
Storage mode	(i) Upstream boundary condition (flow hydrograph), Downstream boundary condition (Normal depth), (ii) Initial boundary condition, storage cell initial flow elevation	(i) Hydrological analysis, (ii) steady state simulation
Raster-base mode	Lateral boundary condition (Lateral inflow hydrographs from main channel)	Estimated from storage mode

3.4 Geometric data sources

Table 3.1 summarised the geometric data required for each model used in this research. These data were required for all aspects of the one-dimensional model, including in-channel cross sections and their extension on the floodplain, storage cells, levees and hydraulic connections data. Data were also required for the floodplain surface and on floodplain structural characteristics in both one-and two-dimensional models. Thus, a series of techniques and data sources were utilised including Real Time Kinematic Geographical Positioning System (RTK GPS), the traditional surveying method (Levelling), Lidar (Light induced direction and range) data, and OS land-line data.

3.4.1 Real Time Kinematic Geographical Positioning System (RTK GPS)

GPS is a satellite navigation system designed to provide instantaneous position, velocity and time information almost anywhere on the globe at any time; and in any weather provided satellite line of sight can be maintained. Its application in this study includes surveying in-channel cross section data; surveying wrack lines and determining the direction of the flood flow on the floodplain as model validation

Picture 3.1: Real Time Kinematic Geographical Positioning System (RTK GPS)

Picture 3.2: Use of GPS to survey cross sections in the study site

data; connecting surveyed and remotely-sensed data; and measuring the systematic errors in Lidar data via comparing GPS data and Lidar data at specific locations. In

this research, a Real Time Kinematic (RTK) GPS is used. This involves two receivers, one that is stationary and a second that is roving, allowing high precision measurements to be obtained in real time. This application is ideal for open-to-the-sky sites. The stationary receiver is the key. It ties all the satellite measurements into a U.K references system (the RINEX network). The roving receivers are then measured with reference to the stationary receivers (i.e. differentially), which after correction should lead to high quality data (±0.002 m in x, y and z) (RTK GPS, User's Manual, 2000). Processing is undertaken using SKI-Pro software. To use the processed data in ArcView and hydraulic models they must be converted to a compatible coordinate system (OSGB36) if the GPS reference station was not initially set with this coordinate system. In this research, RTK GPS is used to obtain: (i) cross section data for the main channel in the one-dimensional model when trees did not have leaves (see Figure 3.3); (ii) flood inundation boundary data on the floodplain as validation data; (iii) the dimensions and locations of hydraulic

Figure 3.3: Cross-section locations determined using GPS along the study site.
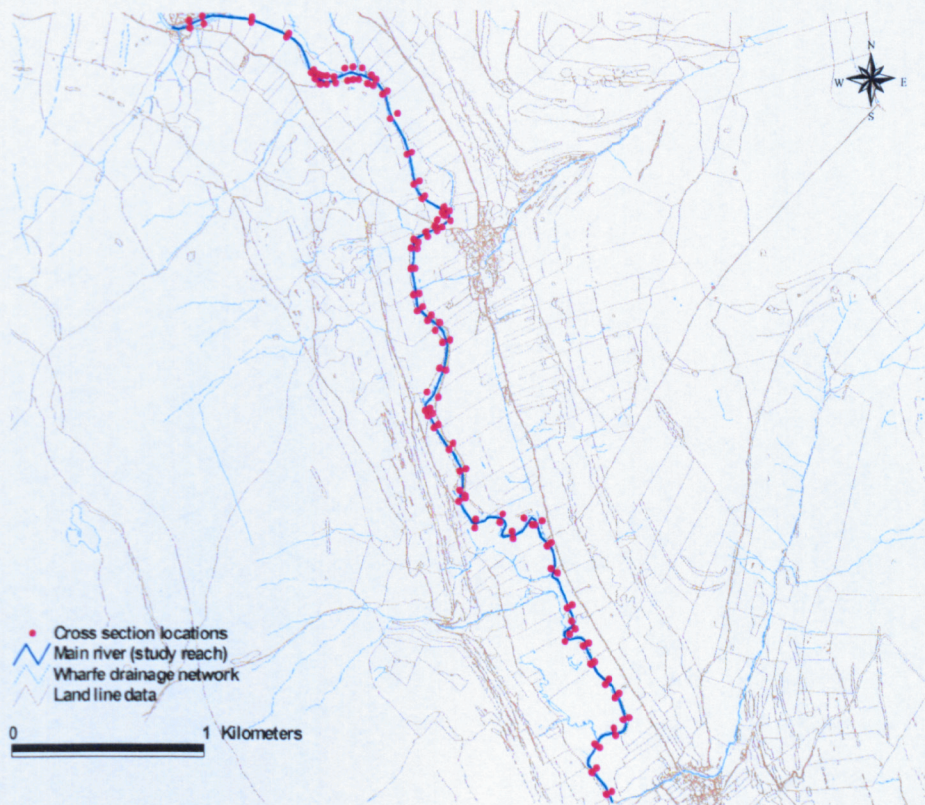
connections between the main channel and floodplain (lateral weirs) and between the storage areas on the floodplain with each other (weirs) (see Figure 3.4); and (iv) the dimensions of the natural and man-made obstacles on the floodplain to prepare a DEM which is the basis of the two-dimensional diffusion wave model.

Figure 3.4: Geographical information collected for part of the study domain using GPS to define and parameterise lateral weirs, storage cell connections and physical obstacle (i.e. walls and fences).
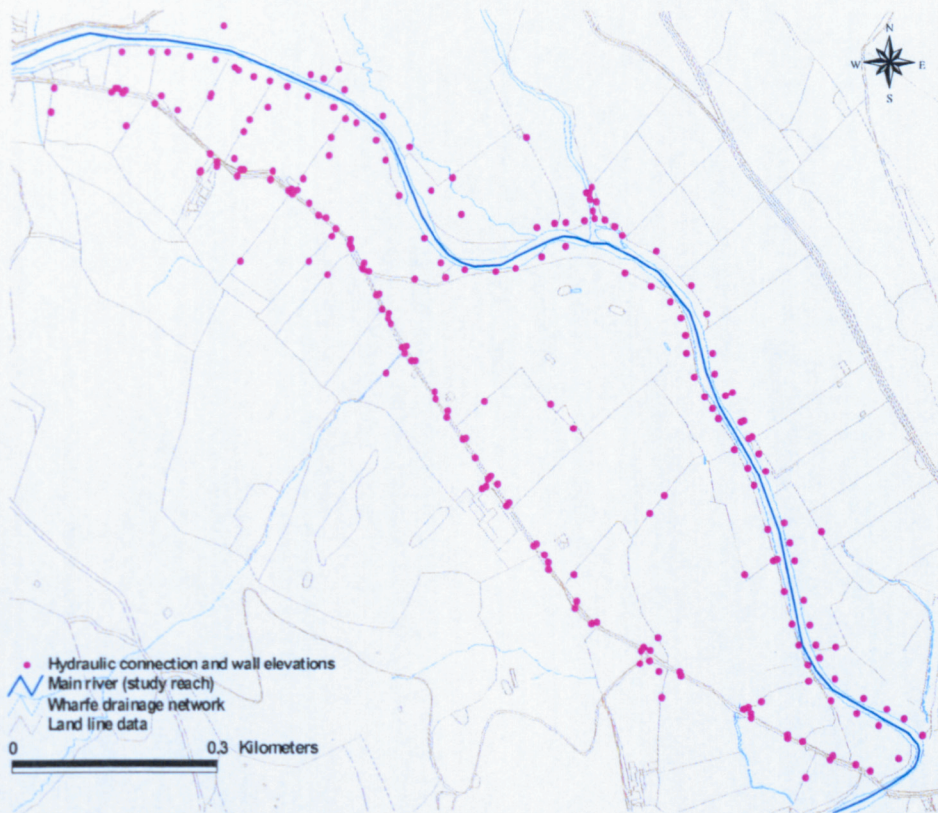
3.4.2 Levelling

As GPS only works when line of sight to satellites can be maintained, additional geometric data had to be collected through levelling in places due to the presence of trees along the river. Levelling is an operation that is used for determining the elevations of points or the differences in elevation between points on the earth's surface. In levelling, a level reference surface, or datum, is established, and an elevation is assigned to it. This datum may be assigned either an assumed elevation or true elevation. In this research, the left and right banks of each cross section were fixed with metal pins and their true elevations were taken with GPS (see Figure

3.3). These elevations are used as the datum for levelling at each cross section, resulting in true elevations for the cross section points.

3.4.3 Lidar data

Lidar (Light Induced Direction and Range) is a remote sensing technique used for establishing ground height and provides a fast and cost-effective tool for obtaining Digital Elevation Model (DEM) data. Vertical precision is of the order of ±0.1 to 0.2 m and can be routinely achieved against "hard" surfaces such as flat paved and asphalt. This degrades to ±0.1 to 0.5 m on "softer" surfaces such as flat grass and scrubs (Huising and Gomes Pereira, 1998). The Environment Agency (U.K) claims a precision of ±0.1 to 0.15 m in general. The precision of the Z values derived from laser measurements is generally better than ±0.25 m according to Gomes Pereira and Wicherson (1999). Spatial precision in the X and Y dimensions is of the order of ±0.5m although Gomes-Pereira and Wicherson (1999) found that it could degrade to 0.8m. Cobby *et al.* (2001) claimed that surface heights under a dense cloud condition with a potential vertical precision of ±0.15-0.20m and sub-meter planimetric accuracy might be produced. From this brief explanation it can be concluded that there are variations in the accuracies achieved by different studies. These can be attributed, in part, to the differences between laser systems employed, flight characteristics, and the terrain being surveyed.

In this research, Lidar is used to create a raster-based Digital Elevation Model as the discretised domain for a two-dimensional diffusion wave model. In addition, it provides detailed topographic information for extending cross sections and parameterising storage areas on the floodplain in the normal and storage cell models respectively. The Lidar data has a resolution of 2 meters. The original Lidar data has been post-processed to standard data quality requirements set by the U.K. Environment Agency for the study site by a separate project (James, 2004). However, some additional image processing was undertaken on the Lidar data to remove errors associated with tree canopies.

61

Figure 3.4-1: The relief-shaded map of part of the Lidar data used in this study
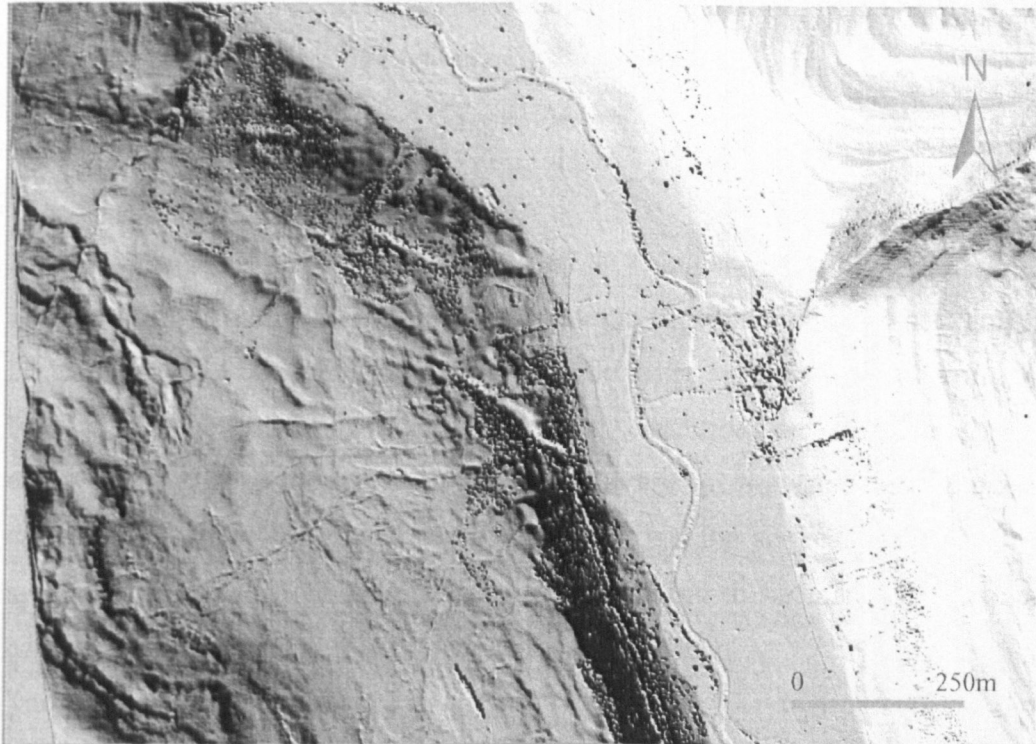
3.4.4 Ordnance Survey (OS) Land-line data

Land-Line is the family name for a range of Ordnance Survey digital map data products that provide detailed information about the topography of Great Britain, including features such as buildings, kerb-lines, hedges and fences, walls, roads, areas of woodland, and etc. Land-Line data are provided at one of three basic scales: 1:1 250, 1:2 500 and 1:10 000. Here, the data are used to define natural and man-made obstacles against flow on the floodplain. Hence, they are useful for establishing storage areas on the floodplain in the storage cell mode of the one-dimensional model. As the dimensions of some of these features are such that they can act as strong obstacles of water flow on the floodplain (i.e. walls) and as they are of a scale that means they are not represented by the Lidar data, additional data are required. For instance, fields on the floodplain are generally divided by stone walls that have up to 0.5 m width. Hence, the walls may not be represented in the Lidar data that originally have 2 m resolution. Another example is the location of gates that hydraulically are of great importance in conveying flow between storage areas on the floodplain. The location of such data had to be collected from OS

Land-line data. Then, their dimensions (e.g. height) were parameterised using GPS data (see Figure 3.4). Field survey was also used to check that field boundaries were impervious (i.e. walls and not fences).

3.5 Flow data

As mentioned above, flow data are needed as boundary and initial conditions for unsteady flow simulations. Boundary conditions (upstream and downstream) must be established at all of the open ends of the river system as the starting water surface. In a sub-critical flow regime, boundary conditions are only necessary at the downstream ends of the river system. If a supercritical flow regime is going to be calculated, boundary conditions are only necessary at the upstream ends of the river system. If a mixed flow regime calculation is going to be made, then boundary conditions must be entered at all ends of the river system.

The upstream end of the river system requires a flow hydrograph or a stage hydrograph and a stage-flow relationship as a boundary condition. There are alternatives for the downstream boundary conditions, including a rating curve and a normal depth assumption (Manning's equation). In the latter case, an energy slope will be required in calculating normal depth (Manning's equation). The influence of a normal depth assumption on model solution can be minimised by making sure that the downstream cross section is located well beyond the area of interest. Initial conditions consist of stage and flow data at all of the exiting nodes, cross sections and storage areas. These values are used at each node, cross section or storage area at the first time step as the assumed values used to be compared against the computed values of the model. The accepted values from the first time step (t time step) will be set as initial conditions for the second time step ($t + 1$ time step).

River flows are not measured within the study site but there are five water level recorders between Deepdale and Kettlewell. Only the Deepdale and Kettlewell level recorders are now working. However, there are some stage data for Hubberholme, which covers records until 2002. The Hubberholme level recorder was observed, as it was not suitable for flow gauging. Therefore, hydrological analyses must be conducted to estimate flow data for the event considered for this research at the upstream of the study reach (Hubberholme). A flood event occurred in 04/02/04

was considered for this study. It should be noted that due to a dry period it was the first meaningful flood event (associated with flood inundation) that occurred since the cross sections were surveyed in 2002. Given available data within the catchment, a range of methods is used to estimate the peak discharge at this point. The methods applied are the Flood Estimation Handbook (FEH) method, a transfer function based upon the ratio between the Deepdale estimated flow data and Hubberholme, a normal depth assumption at Hubberholme and a simulated rating curve at the Hubberholme site.

3.5.1 Flood Estimation Handbook (FEH) method

Flood Estimation Handbook (1999) is the revised version of the Flood Studies Report (FSR) (1975) rainfall-runoff method, one of the principal methods used in the UK for estimating the magnitude of flood of a given frequency of occurrence. Generally, in the FEH rainfall-runoff method, a rainfall input is converted to a flow output using a deterministic model of catchment response. The model used is the unit hydrograph and loss model, which includes three main parameters. The parameters relate to the catchment response to the rainfall (unit hydrograph time to peak), the proportion of rainfall which directly contributes to flow in the river (percentage runoff), and the quantity of flow in the river prior to the event (base flow). The model parameters are derived from observed rainfall and runoff records where possible. If this is not possible, they may be estimated from physical and climatic descriptors of the catchment using a series of established equations. Once the values of the model parameters have been derived for a catchment, the model may be used to estimate the total flow from any rainfall event. The rainfall may be a statistically-derived design event to produce a flood of a specific return period (the T-year flood), or a maximum precipitation (PMP) to produce a probable maximum flood (PMF). Alternatively, the rainfall may be an observed event, the aim being to simulate a notable flood. The latter is the method that is used to estimate the peak flow at the Hubberholme gauging station in this research. The rainfall event data associated with the flood event considered in this research were provided from the Beckmonds rainfall recorder as it was located immediate upstream of Deepdale station and could be reprehensive of the Upper Wharfedale (see Figure 3.1). The rainfall data considered here are presented in Fig. 3.5.

Fig. 3.5: Observed rainfall event for Upper Wharfe River at 4 Feb 2004 (8:15 am to 19:30 pm) at Beckmonds gauge
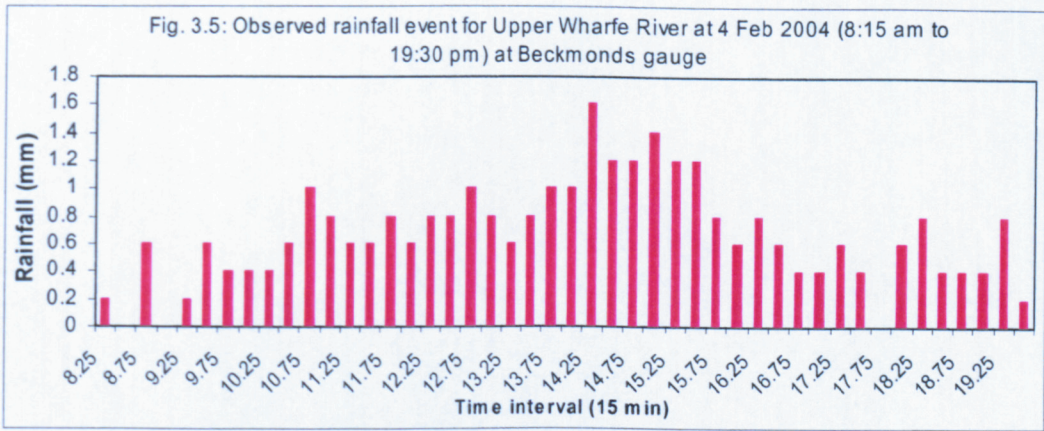
The proportion of the total rainfall input which becomes rapid runoff in the river is referred to as percentage runoff. Estimation of percentage runoff is probably the most important but definitely the most uncertain part of flood estimation using the FEH rainfall-runoff method. The FEH unit hydrograph and loss model assumes that percentage runoff is constant through an event, and is applied to each block of the total rainfall hyetograph. However, in reality, percentage runoff will not be constant, but will increase as soil moisture deficits are reduced and soils become saturated. Percentage runoff, PR, is made up two terms: a standard term *SPR* representing the normal capacity of a catchment to generate runoff; and a dynamic component *DPR* representing the variation in the response depending on the state of the catchment prior to the storm and the storm magnitude itself. The standard percentage runoff, *SPR*, has the dominant role in determining the percentage runoff, *PR*. Given the availability of data within the catchment under study there is no way of estimating directly or observing *SPR* except by access to either the observed or estimated *SPR* data from donor catchments close to the study site. In this case, given there is some data required for estimating SPR in close catchments to the study site, the second method was selected (donor catchment). At three outlets along Wharfe River representing three catchments with different size (Wharfe at Flint Mill Weir, Wharfe at Ilkley and Wharfe at Addingham), SPR is estimated using Equation 3.1, which is base upon catchment descriptors (FEH, 1999)

$$SPR = 72.0 - 66.5\ BFI \qquad \text{(Eq. 3.1)}$$

where *BFI* measures the proportion of the river's long-term runoff that derives from stored sources of the considered catchment. *BFI* typically ranges from 0.1 for relatively impermeable clay catchment to 0.99 for highly permeable chalk catchments (FEH, 1999). The estimated values of *SPR* for three points along Wharfe River are presented in Table 3.3. In addition, the average value of the observed SPR for Wharfe River at Ilkley is available (FEH, 1999) (see Table 3.3). The ratio between the observed and estimated *SPR* at the site that both are available may be applied to correct the estimated values in sites where no observations exist.

Table 3.3: The estimated SPR along Wharfe River downstream the study site

Outlet	SAAR (mm)	Estimated SPR (%)	Observed SPR (%)	Obs./Est.	Corected SPR (%)
Wharfe at Flint Mill Weir	1165	42.8	*********	*******	48.364
Wharfe at Ilkley	1371	46.6	52.7	1.13	52.658
Wharfe at Addingham	1386	46.8	*********	*******	52.884

As there is a notable difference in catchment characteristic (e.g. area, general slope, land use, urbanisation index and annual average rainfall) at the donor catchments (the above three outlets) and the study site, a range of regression equations were established between the corrected values of *SPR* at the donor sites and the study site in order to estimate the value of *SPR* at the study site. For instance, the regression equation that represented the relationship between the Standard Annual Average Rainfall (*SAAR*) and the *SPR* values at the donor catchments is presented in Figure 3.6. Using this regression equation and given the SAAR value at the study site (1727mm), SPR is produced 59.91% at Hubberholme. The estimated value must be used with caution because the number of observed values involved in establishing the regression equation is not reasonable. Moreover, the runoff production is a complicated process and a simple regression equation between SAAR and SPR cannot be a precise approach. As the Wharfe catchment up to Hubberholme is a small part of the donor catchments and located at their upstream, a higher SPR is expected as this part has higher catchment wetness index, smaller size with steeper slope causing a higher value of SPR.

Figure 3.6: Regression made between SAAR and SPR of donor catchmnets

$y = 0.0206x + 24.343$
$R^2 = 0.9997$
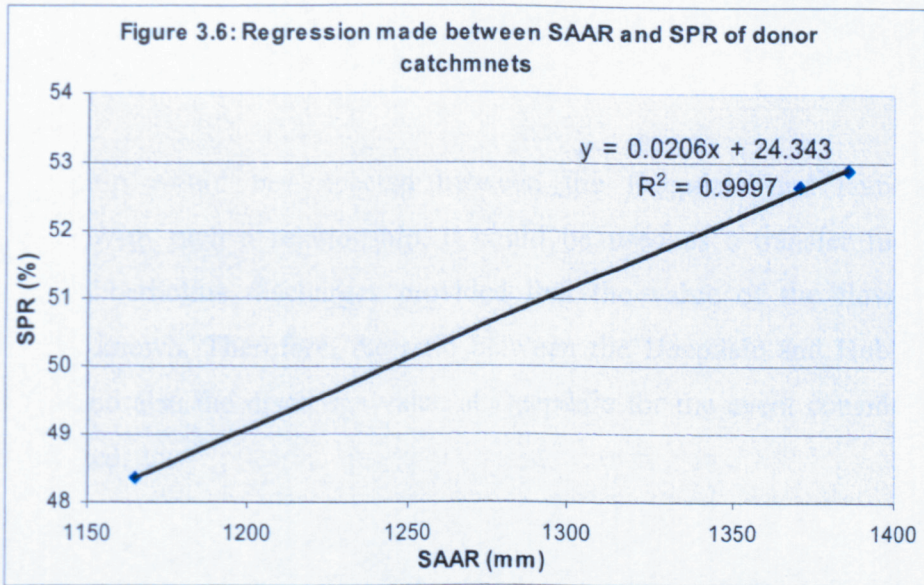
As a further improvement of SPR estimation is not possible hence, a reasonable range of SPR given the estimated value and the study area characteristics relative to the donor catchments is considered. In this respect, three scenarios were considered, using 60%, 70% and 80% SPR values to estimate the peak flow at Hubberholme. The peak flows are estimated as 36.58, 42.35 and 47.73 m^3s^{-1} for the three scenarios respectively. The flow hydrographs are shown in Fig.3.7.

Fig.3.7: Flow hydrogrphs produced at Hubberholme for flood 04/02/04
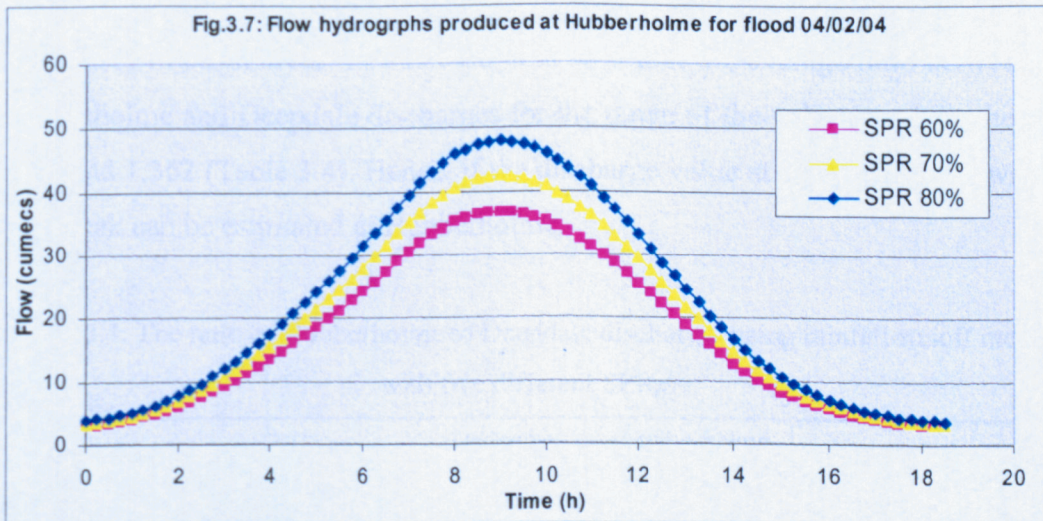
3.5.2 Transfer function based upon discharge values at Deepdale and Hubberholme

A relationship would be expected between the Deepdale and Hubberholme discharges. With such a relationship, it could be used as a transfer function to estimate Hubberholme discharges provided that the value of the flow peak at Deepdale is known. Therefore, the ratio between the Deepdale and Hubberholme discharges and also the discharge value at Deepdale for the event considered here were estimated.

- *The discharge ratio between Deepdale and Hubberholme*

As there are no measured discharge values Hubberholme to estimate the discharge ratio between Deepdale and Hubberholme, discharge ratios were estimated using the FEH method. The results of applying the FEH method to estimation of the flood peak at Deepdale and Hubberholme gauging stations using different *SPR* values for the flood event considered here are presented in Table 3.4. It should be noted that given that Deepdale is located upstream of Hubberholme by less than 2km, the same SPR values were applied for each site in each test. The estimated ratio between the two stations ranges from 1.33 to 1.39. This similarity is not surprising as major differences between discharge values will predominantly arise from differenses in basin areas. In this case, it is seen that the average ratio between the Hubberholme and Deepdale discharges for the range of the values used for the SPR is around 1.362 (Table 3.4). Hence, if the discharge value at Deepdale is known, the flow peak can be estimated at Hubberholme.

Table 3.4: The ratio of Hubberholme to Deepdale discharge, using rainfall-runoff method with five different SPRs%

Method	Deepdale discharge peak, m3s-1	Hubberholme discharge peak, m3s-1	Hubberholme/Deepdale ratio
Rainfall-Runoff method, SPR 50%	22.67	31.50	1.39
Rainfall-Runoff method, SPR 60%	27.41	36.58	1.33
Rainfall-Runoff method, SPR 70%	31.09	42.00	1.35
Rainfall-Runoff method, SPR 80%	34.96	47.73	1.36
Rainfall-Runoff method, SPR 90%	38.84	53.13	1.38
			Average = 1.362

- *Estimation of discharge at Deepdale*

Given the available data at the station, two methods are chosen for estimating the peak discharge value, including the establishment of a rating curve and use of normal depth (Manning's Equation).

- *Rating curve*

A rating curve was established using low flow data at Deepdale (Fig. 3.8). Given the maximum stage observed at Deepdale for the flood event considered here (1.65m) the discharge is estimated 23.22 m^3s^{-1}. Unfortunately, this approach assumes that the low flow stage-discharge relationship can be extended to all flows which is unlikely to be the case.

Fig. 3.8: The rating curve established for Deepdale gauging station

$y = 3E-05x^{2.6556}$
$R^2 = 0.962$
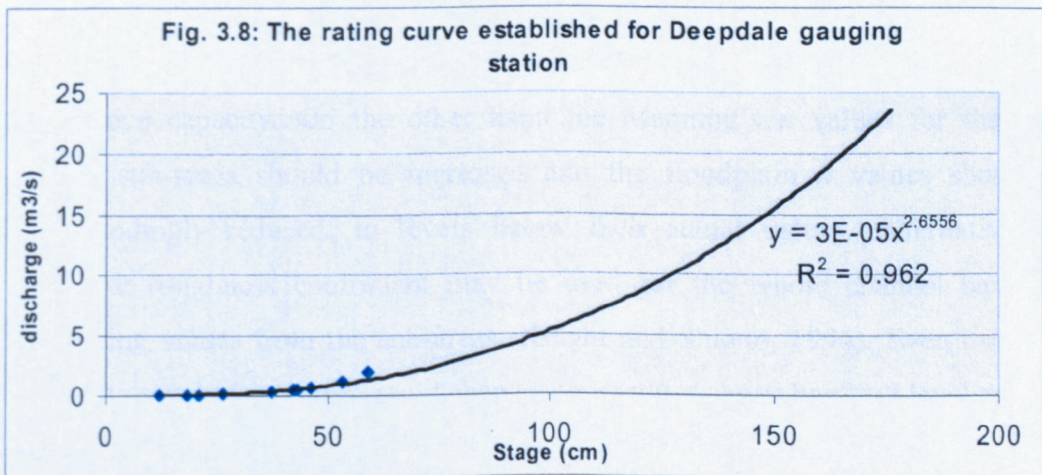
- *Normal Depth*

Using the Manning equation (Eq.3.2), the estimation of discharge, Q, can be linked to the flow area, A, the hydraulic radius, R, the friction slope, S_f, and the Manning's n as the resistance coefficient as seen below.

$$Q = (AR^{2/3}S_f^{1/2})/n$$ (Eq. 3.2)

69

It should be noted that this resistance law only applies to flow in circular pipes, and although it may be used for certain prismatic channels the equation is not suitable for flow in very complex cross sections. This is because (i) there is commonly a heterogeneous roughness distribution around the wetted perimeter in natural cross sections; (ii) the roughness value varies with depth of flow; and (iii) there is commonly a difference between the actual and estimated roughness values for flow above the bankfull level (see Knight and Shiono, 1996). The latter is because interaction processes between the main channel and floodplain are ignored. To overcome part of the difficulty, the division of the whole channel to sub-areas including the main channel and floodplain is advocated. However, even this may not be enough. One example of the difficulty in applying this approach is reported for the River Seven at Montford, using measured friction slope and overbank velocity data (Knight *et al.*, 1989). Knight *et al.* (1989) showed that, for flows above the bankfull level, there is an abrupt decrease in the hydraulic radius, and Manning's *n* for the whole channel must be decreased in order to obtain the correct conveyance capacity. On the other hand the Manning's *n* values for the main channel sub-areas should be increased and the floodplain *n* values should be correspondingly reduced, to levels below their actual values. Alternatively, a composite roughness coefficient may be used for the whole channel based on aggregating values from the sub-areas (Knight and Shiono, 1994). Even using the composite roughness values, rapid changes in *n* values above bankfull level are seen (Knight and Shiono, 1994). It should be clear from this brief description that the early simple division and composite roughness methods are essentially flawed, since the simple addition of the individual flows in each sub-area does not necessarily equal the total flow due to the main channel/floodplain interaction process. Knight and Shiono (1994) describe four variations on the channel division method in order to simulate the interaction process as accurately as possible. The option used here to deal with this difficulty is based on altering the sub-area wetted perimeter, typically excluding the length *ab* in the calculation of the floodplain wetted perimeter (sections A and C), but adding the *ab* length to the main channel wetted perimeter (see Figure 3.9).

Fig. 3.9: Exculding ab length from floodplain wetted periemete calculation at Deepdal cross section
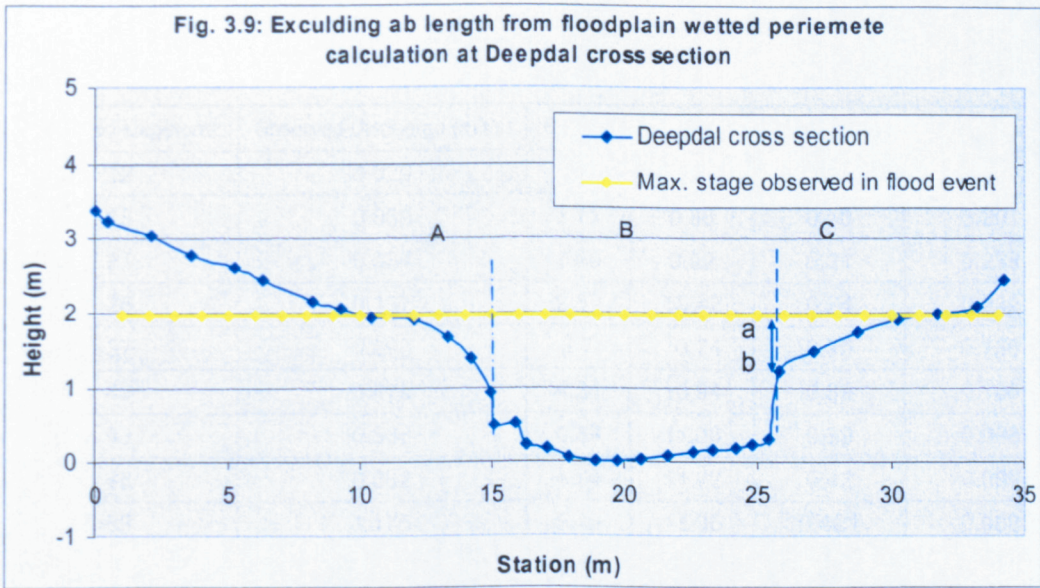
To estimate the discharge value using the mentioned method, n values for higher water depths in the main channel, friction slope (in this case bed slope), flow area and wetted perimeter at the main channel and floodplain sub-areas are needed.

In the case of Deepdale, the cross section characteristics and bed slope were surveyed. In the case of bed slope, a total length of 200m, 100m of upstream and downstream of the Deepdale gauging station, within the main channel were surveyed. Based on the surveyed data, the best estimation of the friction slope at this point is 0.0005. The flow area and the wetted perimeter values for the flood event considered in the research at each three sub-areas are summarised in Table 3.5.

Table 3.5: Flow hydraulics at Deepdale cross section for the peak stage observed at flood event 04/02/04

Sub-area	Flow area, A (m2)	Wetted perimeter, P (m)	Hydraulic radius, R
A	1.47	3.07	0.48
B	17.65	14	1.26
C	1.61	4.46	0.36

Given that there are some measured stages and discharges at Deepdale, the variation of n values with water depth can be determined, using the Manning equation (Table 3.6). It was assumed that the n values have the same values for main channel and floodplain. The variation of Manning's n with stage can be generally plotted and extended to estimate n values for a given stage. Figure 3.10 shows the best regression made between stage data and the n values.

71

Table 3.6: Estimation of *n* values using the observed stage and discharge data at Deepdale

Observed stage(cm)	Observed Discharge (m3/s)	Flow A.	Wetted P.	Hydraulic R.	Estimated *n*
12	0.029	1.14	9.74	0.12	0.209
18	0.059	1.71	9.86	0.18	0.201
21	0.084	1.99	9.92	0.21	0.238
26	0.137	2.57	10.42	0.24	0.232
37	0.298	3.7	10.74	0.35	0.136
42	0.479	4.24	10.94	0.39	0.105
43	0.538	4.39	11.06	0.39	0.098
46	0.662	4.74	11.22	0.42	0.089
53	1.175	5.46	11.36	0.481	0.063
59	1.918	6.08	11.48	0.54	0.046

Fig. 3.10: the regression equation made between n values and water level at Deepdale gauging station

$$y = 0.0413x^{-0.9214}$$
$$R^2 = 0.8091$$
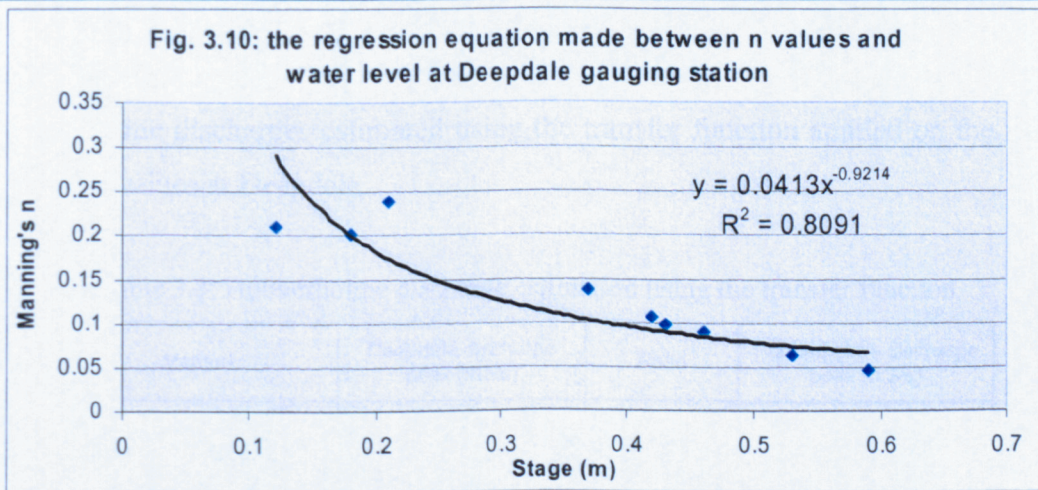
Given the peak stage observed at the flood event 04/02/04 at Deepdale (1.65m), the associated value of the Manning's *n* is estimated 0.026 for whole cross section areas.

The data necessary to estimate discharge values using the Manning equation are now available at Deepdale gauging station. Table 3.7 presents the estimated discharge values using the rating curve, the sub-area method (conventional method) and the revised sub-area method in which the *ab* length of the floodplain wetted perimeter is excluded and then added to the main channel wetted perimeter. As expected, these recalculations show that the rating curve method appears to over-estimate the peak flow.

Table 3.7: The discharge values estimated using the revised sub-division, conventional sub-division and rating curve method at Deepdale gauging station

Method	Sub-area	Flow A. (m2)	Wetted P. (m)	Hydraulic R.	n value	Bed Slope	Q (m3/s)
The revised sub-area (Exclusion of ab length from floodplain wetted perimeter)	A	1.47	3.07	0.48	0.026	0.0005	0.78
	B	17.65	14	1.26	0.026	0.0005	17.71
	C	1.61	4.46	0.36	0.026	0.0005	0.7
							Total 19.19
The conventional sub-area	A	1.47	3.79	0.39	0.026	0.0005	0.67
	B	17.65	12.84	1.37	0.026	0.0005	18.72
	C	1.61	4.9	0.33	0.026	0.0005	0.66
							Total 20.05
Rating curve							23.22

Having obtained the discharge values at Deepdale, the next step is to transfer the discharge values to the Hubberholme discharge values, using the ratio between the Deepdale and Hubberholme discharges (see Table 3.4). Table 3.8 shows the Hubberholme discharges estimated using the transfer function applied on the three discharge values at Deepdale.

Table 3.8: Hubberholme discharge estimation using the transfer function

Method	Deepdale discharge peak (m3/s)	Ratio	Hubberholme discharge peak (m3/s)
Revised sub-area	19.19	1.36	26.14
Conventional sub-area	20.05	1.36	27.31
Rating curve	23.22	1.36	31.63

3.5.3 Hubberholme rating curve used in previous studies

Under a three-year project in relation to improving the management of the land and waters of the Upper Wharfe, JBA was commissioned to develop a hydraulic model as part of this project by the Environment Agency. The results of this part of the project have provided simulated rating curves for different cross sections of the River Wharfe. JBA used HEC-RAS as the hydraulic model for simulating a flood event that occurred in early December 1999 with a return period of a little over three years. Figure 3.11 shows the rating curve simulated for Hubberholme gauging station by JBA in 2000.

Fig. 3.11: The simulated rating curve at Hubberholme by JBA

$$y = 231.69x^{0.0032}$$
$$R^2 = 0.9984$$
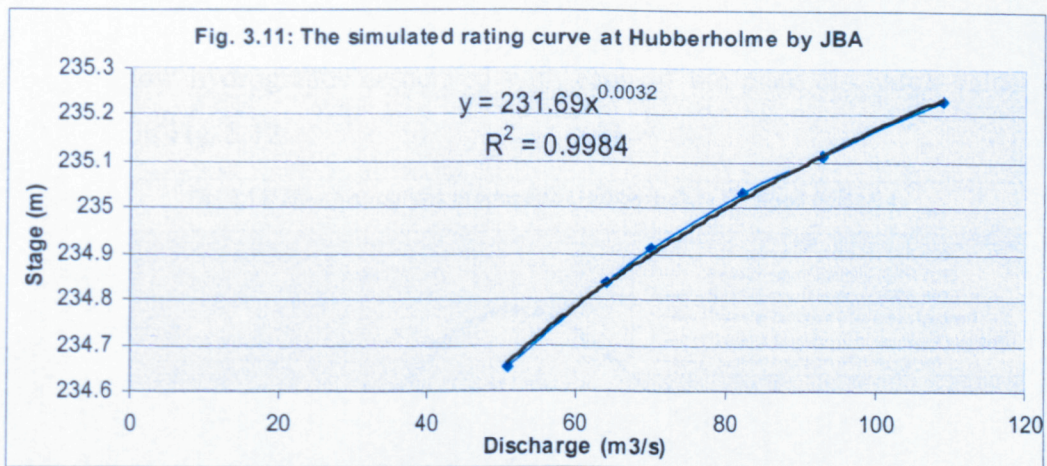
Considering the observed peak stage at the Hubberholme gauging station for flood event 04/02/04 (233.6-233.8m AOD) the peak flood using this rating curve is estimated as between 17 and 22.2 m^3s^{-1}.

3.5.4 Selection of the flow peak at Hubberholme for the flood event of 04/02/04

The peak flow rate at the Hubberholme gauging station has been estimated using: (i) the FSR rainfall-runoff method with three SPR%; (ii) the transfer function based upon the ratio of Hubberholme to Deepdale discharge values, in which different methods are used for estimating the peak discharge at the Deepdale gauging station; and (iii) the rating curve produced from previous studies at the Hubberholme gauging station. The results are presented in Table 3.9.

Table 3.9: Range of the peak discharge values estimated at Hubberholme gauging station using different methods

Methods used to estimate the peak flow at Hubberholme	Discharge (m3/s)
FSR rainfall-runoff method-SPR 60%	36.58
FSR rainfall-runoff method-SPR 70%	42.35
FSR rainfall-runoff method-SPR 80%	47.73
Transfer function (Revised sub-area at Deepdale)	27.62
Transfer function (Conventional sub-area at Deepdale)	31.62
Transfer function (Rating curve at Deepdale)	26.49
Rating curve obtained from previous studies, JBA (2000)	17-22.2

Table 3.9 has a wide range values for the flow peak at the Hubberholme gauging station. Flow hydrographs associated with each of the peak discharge values are presented in Fig. 3.12.

Fig. 3.12: Flow hydrogrphs produced at Hubberholme for flood 04/02/04
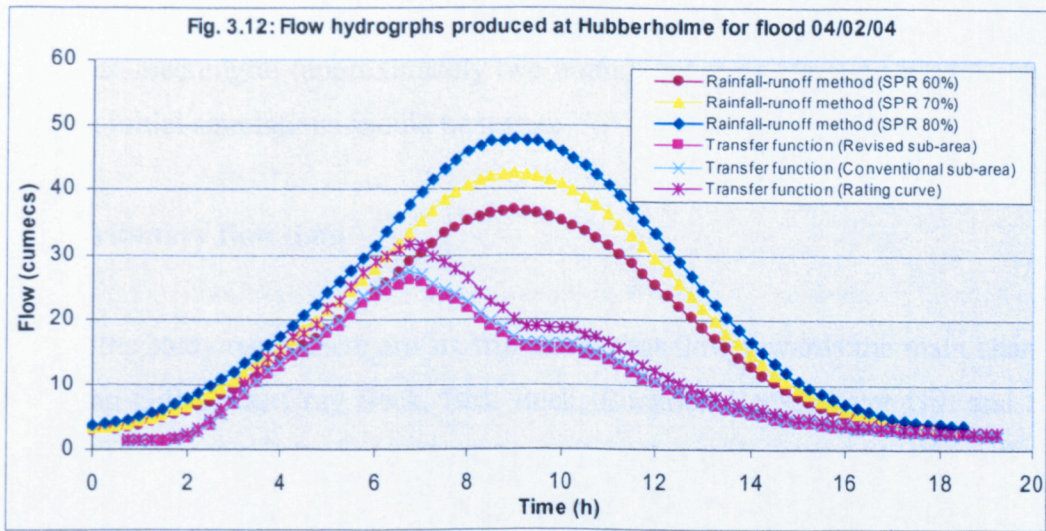
Given the uncertainty associated with the methods used here, it is difficult to justify any of the estimations as being the best estimation. Major uncertainty sources associated with the methods used here commonly stem from (i) determination of the SPR% values in the FEH method; (ii) the determination of Manning's n in the normal depth method; and (iii) the lack of flow data for out-of-bank flows in the rating curve method. Moreover, Figure 3.12 shows differences in the shape of the estimated hydrographs at Hubberholme, which may affect the flood simulation along the study reach. Thus, after the model (normal mode) was set up, initial simulations were conducted, using the estimated peak values and hydrograph shapes, to assess the effects of upstream boundary conditions on model predictions. As the stage data at Hubberholme have not been involved in the estimation of flow data at this site, any simulation that could satisfy the observed stage data (validation data) at the Hubberholme gauging station was chosen as the final discharge value at this point (see Chapter 4).

If the timing of the flow peaks in Figure 3.12 is studied, it is seen that two main timings exist: (i) one that is associated with the transfer function method; and (ii) the Rainfall-Runoff method timing, regardless of the SPR% values used. It should be noted that the timing associated with the transfer function is initially based upon the timing of stage data measured at Deepdale. Then, the flow hydrographs have

been shifted given the travel time calculated between the two stations. The comparison of stage data in 2000 between Deepdale and Hubberholme revealed that the travel time between the two gauging stations ranges from 30 to 45 minutes. Hence, Figure 3.12 indicates that the differences between the timing of the flow peaks are meaningful (approximately two hours) and their effect on model outputs through initial simulations should be tested.

3.5.5 Tributary flow data

Within the study reach there are six tributaries that flow towards the main channel, including Gill Beck, Cray Beck, Birk Beck, Buckden Beck, Water Gill and Step Gill. Given that some stage and flow data at low flow condition had been collected by a separate project, rating curves for 5 of the tributaries were created. As the stage data within the period of the flood event considered in the research were available for the mentioned tributaries, the relevant flow hydrographs were produced. Figure 3.13 shows the estimated flow hydrographs for the flood event 04/02/04 for each tributary within the study site.

Fig 3.13: Flow hydrographs estimated at the tributaries within the study site for flood event 04/02/04
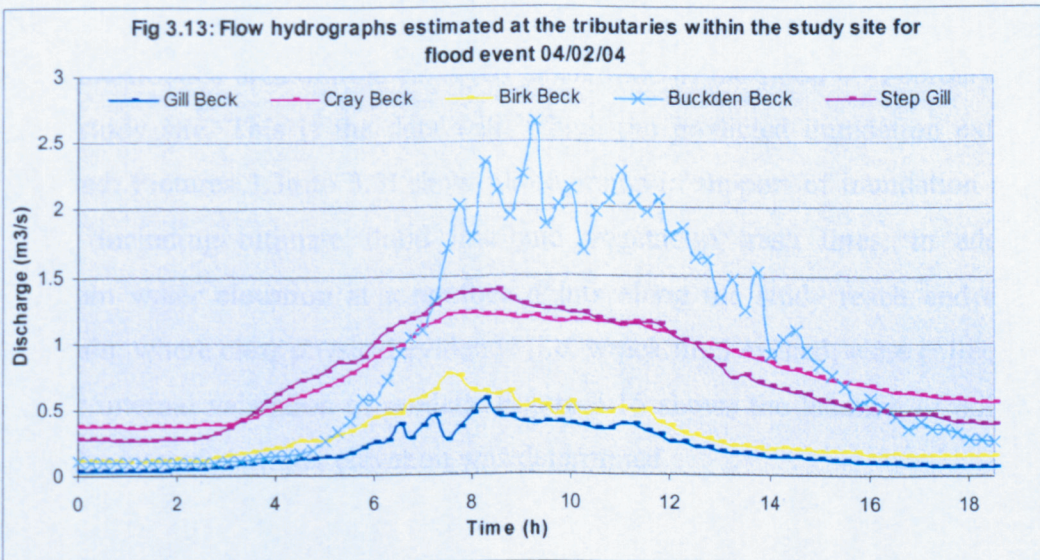
Figure 3.13 shows that the Buckden Beck and Gill beck tributaries have the highest and lowest contributions to the main channel flows with 2.65 and 0.56 m^3s^{-1} respectively. As seen, the timing of the flow peaks is approximately coincident, with a longer time-to-peak for Buckden Beck. This is not surprising given that Buckden Beck has a longer basin. If the timing of the peak flows in the main

channel at Hubberholme (Figure 3.12) and in the tributaries (Figure 3.13) are compared, it is clear that there is a consistency between the timing of the flow peaks of the tributary hydrographs and those resulting from rainfall-runoff methods. In contrast, the flow peak timing resulting from the transfer function show early peaks in the tributaries as compared to main channel flow peaks. This is not surprising as the time-to-peak in the rainfall-runoff model has a very poor representation of catchment structure.

The significance of tributaries should be studied in two aspects: (i) they are hydraulically connected to the main channel and subsequently affect the main channel conveyance; and (ii) they directly contribute to inundation processes on the floodplain. The latter may lead to errors in observed inundation data where the predicted inundation area is sourced only from overtopped in-channel flows.

3.6 Validation data

Inundation extent associated with the flood event considered here was surveyed using GPS, ground photographs and observational evidence including vegetation trash lines, distribution of overbank fines and flattened vegetation. Figure 3.14 shows the flooded area outline surveyed at the time of the flood 4th February 2004 in the study site. This is the data with which the predicted inundation extent is compared. Pictures 3.3a to 3.3l show photographs in support of inundation extent survey, including ultimate flood line and vegetation trash lines. In addition, maximum water elevation at a number points along the study reach and on the floodplain, where clear physical evidence (i.e. wrack line) existed, were collected as data for internal validation of models. Figure 3.15 shows the location of points in which the maximum water elevation was determined.

Figure: 3.14: Inundation extent observed at the time flooding (04/02/04) using GPS, ground photographs and observational evidence

0 _____ 1 Kilometers
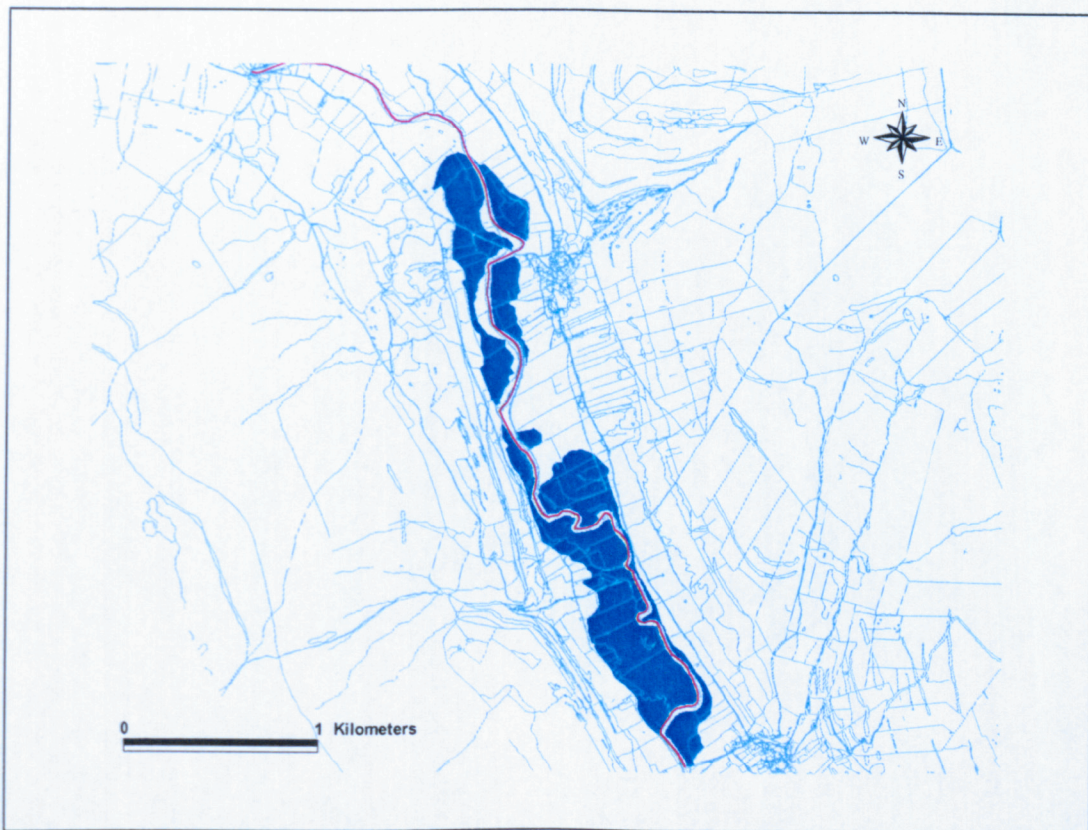
Picture 3.3: Photographs showing flood shorelines and wrack lines for the flood 4th February 2004

(a)

(b)

(c)

(d)

(e)

(f)

(g)

(h)

(i)

(k)

(l)

Figure 3.15: Points at which maximum water elevation was measured after flooding
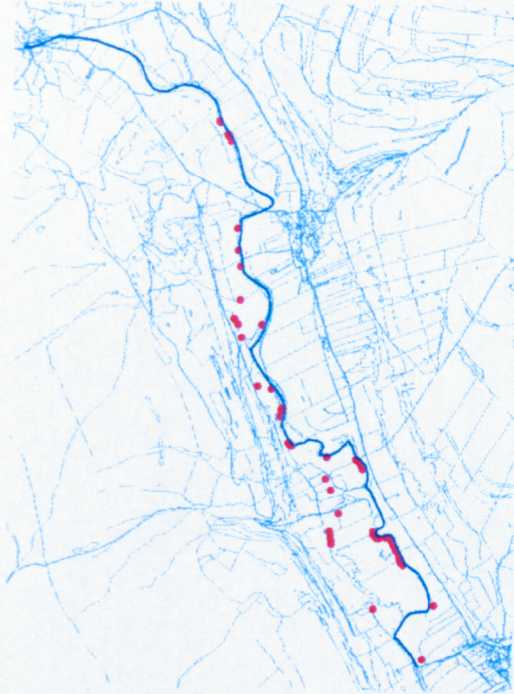
3.7 Accuracy assessment techniques

Before the calibration of hydraulic models can be performed, analysis techniques must be defined to undertake an accuracy assessment between the predicted and observed flood extent, as it is this measure that will be optimised by the calibration process. The accuracy assessment is based upon a simple comparison of the number of pixels or hectares of a category predicted (e.g. inundation areas predicted) and observed data (reference or validation data). In the simplest sense, a non-site specific accuracy assessment is undertaken so that only total areas for predictions are compared with observation regardless of the location of these areas. This approach only describes the level of disagreement and not where that disagreement is to be found.

In response to this limitation, site specific assessment, which is based upon comparing prediction and observation data on a locational basis, is used. The foundation of this assessment is an error matrix. An error matrix is a square array of numbers set out in rows and columns that express the number of units (pixels, polygons or clusters) assigned to a particular category of predictions relative to a

particular category of observations (Figure, 3.16). In most cases, the rows represent predictions and the columns represent the reference data considered to be correct.

Figure 3.16: Mathematical example of error matrix

		j = Columns (reference)			**row total**
		1	**2**	**3**	n_{i+}
1		n_{11}	n_{12}	n_{1k}	n_{1+}
i = Rows (predictions) **2**		n_{21}	n_{22}	n_{2k}	n_{2+}
3		n_{k1}	n_{k2}	n_{kk}	n_{k+}
column total	n_{+j}	n_{+1}	n_{+2}	n_{+k}	n

The number of rows and columns is dependent upon the number of classifications considered for accuracy assessment. For example, in this research, inundated and non-inundated areas are considered for classifications, flowing guidance in Yu and Lane (in press a).

Initially, a single value representing the accuracy of the entire classification (i.e. overall accuracy) is presented. The overall accuracy is computed by comparing a sample of locations of prediction data with the same locations as observation data and keeping track of agreement. Overall accuracy is simply the sum of the correctly predicted units (i.e. the major diagonal) divided by the total number of units in the entire error matrix (Equation 3.3).

$$Overall..accuracy = \frac{\sum_{i=1}^{k} n_{ii}}{n}$$

(Eq. 3.3)

In this research, the total area for inundated and not-inundated classifications that are correctly predicted (i.e. where they agree with inundated and not-inundated

observations) is divided by the entire area of floodplain to give overall accuracy. There are two main reasons why the overall accuracy may not be a reliable statistic in relation to model performance. First, the overall accuracy is strongly dependent upon the area that is defined floodplain (Yu and Lane, in press a). Second, the statistic may suggest a good performance in a poor model if the area that is never inundated data is large.

In response to this limitation, Kappa analysis, which is a discrete multivariate technique in accuracy assessment, has been developed (Congalton and Green, 1999). Kappa is computed for an error matrix and shows how well predictions agree with observation data. Moreover, it can be used to determine if one error matrix is significantly different than another (Bishop *et al.*, 1975). The result of performing a Kappa analysis is a KHAT statistic (actually $\hat{K}$, an estimate of Kappa) which is another measure of accuracy (Cohen, 1960). This measure seems to be more reliable than overall accuracy because although it is based on the difference between the actual agreement in the error matrix (i.e. $n_{11} + n_{22} + ... + n_{kk}$) as with overall accuracy, it recognises the chance agreement which is indicated by the row and column totals. For each error matrix, a Kappa value can be calculated using Equation 3.4.

$$\hat{K} = \frac{n \sum_{i=1}^{k} n_{ii} - \sum_{i=1}^{k} n_{i+} n_{+i}}{n^2 - \sum_{i=1}^{k} n_{i+} n_{+i}}$$ (Eq. 3.4)

where $n_{i+} = \sum_{j=1}^{k} n_{ij}$ and $n_{+i} = \sum_{i=1}^{k} n_{ij}$.

The KHAT values range from +1 to −1 but since there should be a positive correlation between predictions and observations, positive KHAT values are expected. A prefect agreement is achieved at KHAT = 1 (Congalton and Green, 1999).

As the KHAT value is attributed to an entire error matrix, it means that the Kappa analysis still remains partly dependent on the dry area of floodplain. Therefore, in the context of floodplain inundation modelling, both the overall accuracy and Kappa analysis introduce bias into results if the non-inundated area is large. Hence, it is useful to look at the agreement for an individual category within an error

matrix. For instance, in the case of flood inundation prediction, the model accuracy may only be assessed in relation to inundated area. In the simplest of terms, model performance can be assessed using a measure of fit ($F\%$) in order to compare the predicted inundated area with the observed inundation area (see Bates and De Roo, 2000, Horritt, and Bates, 2001a, Horritt and Bates, 2002).

$$F\% = \frac{IA_{obs} \cap IA_{mod}}{IA_{obs} \cup IA_{mod}} \times 100 \qquad \text{(Eq. 3.5)}$$

where IA_{obs} and IA_{mod} are inundated areas observed and modelled respectively. Equation 3.5 can be rewritten for an error matrix for a specific category (ith) of predictions (i.e. inundated area):

$$F_i = \frac{n_{ii}}{n_{i+} + n_{+i} - n_{ii}} \qquad \text{(Eq. 3.6)}$$

F varies between 0 for a model with no overlap between predicted and observed inundated areas and 1 for a model where these coincide perfectly. The problem with this statistic is that it does not correct the results for the bias that can arise from chance agreement. Hence, the conditional Kappa coefficient has been developed as a variant of the Kappa statistic. The maximum likelihood estimate of the Kappa coefficient for conditional agreement for the ith category is given by

$$\hat{K}_i = \frac{nn_{ii} - n_{i+}n_{+i}}{nn_{i+} - n_{i+}n_{+i}} \qquad \text{(Eq. 3.7)}$$

If the ith category is assigned to the inundated area, use of Equation 3.7 corrects for the chance agreement ($n_{i+}n_{+i}$) that would be expected from random patterns.

The four accuracy measures (overall accuracy, Kappa, F and Conditional Kappa) described above may disagree with each other. This is because each measure reflects different information contained within the error matrix. Hence, in the calibration process in this research all mentioned measures are estimated in order for a better understanding of model performance.

3.8 Summary of Chapter

This chapter has presented the characteristics of the study site location and separately reviewed data needs for the hydraulic models considered for the research. The data needs were described in detail for each model. Following that, techniques used to provide them were presented. Geometric data were provided using Lidar data and OS Land-line data as data sources, along with techniques and tools such as surveying (levelling) and GPS. The flow data attributed to the flood event considered for the research (as an upstream boundary condition) was estimated using different hydrological methods. The methods yielded a wide range of the flow peaks that must be calibrated through initial simulations (Chapter 4) in order to choose the best estimate of the flow data at Hubberholme. The shorelines associated with the flood event considered here were surveyed using GPS in support of ground photographs and observational evidence. Finally, analysis techniques were defined to undertake accuracy assessments between the predicted and observed flood extent, as the measure that should be optimised by the calibration process. Chapter Four reviews the fundamentals of the one-dimensional hydraulic model, HEC-RAS, and discusses initial application of the model to the study site. After detailed analyse has been performed, sensitivity analysis of the model is completed thereby allowing a greater understanding of model behaviour for an upland river reach to be gained. Then, the performance of the model in relation to inundation extent prediction, using different accuracy assessment techniques, is evaluated.

Chapter 4
Application of HEC-RAS in normal mode

4.1 Introduction

The last chapter provided a review of data needs and the techniques that are essential to parameterise hydraulic models. This chapter addresses the application of a one-dimensional hydraulic model, for which HEC-RAS is selected in this research. First, the governing equations for steady and unsteady flow calculations and the boundary conditions required within HEC-RAS are described. After an in-depth description of the model, initial simulations are then undertaken to choose the optimum flow hydrograph estimation in relation to the upstream boundary condition for the flood event considered (04/02/04). A set of scenarios with variable friction factor, spatial (i.e. cross section spacing) and temporal (i.e. time step) resolution and flood magnitude are simulated in order to assess the sensitivity and stability of the model application in such an environment. This allows a greater understanding of the model behaviour to be obtained and helps to calibrate the model predictions against the most sensitive variables. Finally, for the event considered here, a comprehensive accuracy assessment in relation to inundation extent prediction for all scenarios is undertaken. Once the optimum inundation extent associated with the flood event considered here is gained, the model capabilities and limitations in relation to prediction of inundation extent are discussed.

4.2 Introduction to HEC-RAS

HEC-RAS is a hydraulic model developed by the Hydrologic Engineering Centre (HEC) of the US Army Corps of Engineers. In 1964, HEC released the HEC-2 computer model to aid hydraulic engineers in stream channel analysis and floodplain determination. HEC-2 quickly became the standard stream hydraulic analysis program, and its capabilities were expanded in the ensuing years to provide for, among other things, bridge, weir and culvert analysis. Due to increased use of Windows-based personal computing software, HEC released in the early 1990's a Windows-compatible counterpart to HEC-2 called the River Analysis System (RAS). HEC-RAS has a graphical user interface programmed in Visual Basic, to which are attached flow computation algorithms programmed in FORTRAN, many of which are derived from the original HEC-2 model. HEC-RAS can calculate flow hydraulics for steady and unsteady states using flow rate (steady state), hydrographs (unsteady state), channel cross section data, roughness of the river channel (Manning's n) and suitable boundary conditions. The model can deal with a full network of channels, a dendritic system, or a single river reach. It also deals with flow structures within and out of river, such as bridges, weirs, lateral weirs and gates.

HEC-RAS basically describes the river channel and floodplain as a series of discrete cross sections perpendicular to the flow direction. The finite difference procedure for solving the flow equations then defines the topography of the system domain according to the cross sections. Water surface elevation and other hydraulic characteristics of flow are calculated at each cross section and all hydraulic structures defined in the domain (e.g. lateral weirs). Finally, to simulate flood inundation extent, values of water depth at each cross section are either overlain onto a DEM or linearly interpolated between them.

4.3 Steady flow calculation procedure within HEC-RAS

Under steady state, time-dependent terms are not included in the flow calculations. In steady state, flow is assumed to be gradually-varied because we assume that a hydrostatic pressure exists at each cross section. At locations where the flow is

rapidly varied, the model switches to the momentum equation or other empirical equations. Hence, the energy and momentum equations for flow calculations in steady state within HEC-RAS are described below.

4.3.1 Energy equation

Water surface elevations are calculated from one cross section to the next cross section by solving the Energy equation with an iterative procedure called the standard step method (Fig. 4.1). The Energy equation is presented as follows:

$$Y_2 + Z_2 + \frac{\alpha_2 V_2^2}{2g} = Y_1 + Z_1 + \frac{\alpha_1 V_1^2}{2g} + h_e \qquad \text{(Eq. 4.1a)}$$

where Y_1 and Y_2 are the depth of water at cross sections 1 and 2, Z_1 and Z_2 are the elevation of the main channel at sections 1 and 2, V_1 and V_2 are the average velocities (total discharge/total flow area) at sections 1 and 2, α_1 and α_2 are the velocity weighting coefficients at sections 1 and 2, g is the gravitational acceleration and h_e is the energy head loss.

Fig. 4.1: Terms used in the energy equation (HEC-RAS, Hydraulic Reference, 2000)

91
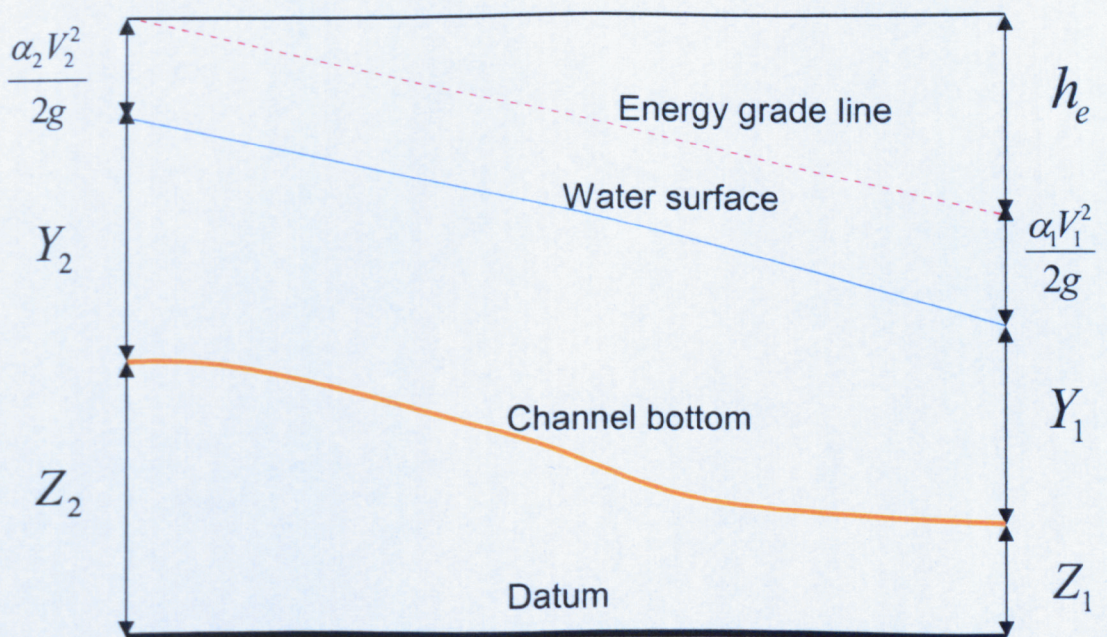
Given the river channel geometry and flow hydraulics, different water surface elevations are expected between the main channel and on the floodplain. As HEC-RAS is a one-dimensional model, only a single water surface and therefore a single mean energy should be computed at each cross section. For a given water surface elevation, the mean energy is obtained by computing a flow weighted energy from all subsections of a cross section. To do this, the mean velocity head is obtained by computing a flow weighted velocity head over the cross section. The velocity-weighting coefficient (α) accounts for the error in using the average velocity instead of a velocity distribution. Alpha (α) is calculated as follows:

$$\alpha = \frac{\left[Q_1 V_1^2 + Q_2 V_2^2 + ... + Q_n V_n^2\right]}{Q\bar{V}^2}$$

(Eq.4.1b)

where Q_1, Q_2, and Q_n are the discharge, V_1, V_2 and V_n are the velocity of sub-sections 1, 2 and n^{th} of a cross section, Q is the total discharge of the cross section and $\bar{V}$ the average velocity of the cross section.

The energy head loss (h_e) between two cross sections is comprised of friction losses and contraction and expansion losses. The energy head loss is calculated via Equation 3.2 as follows:

$$h_e = L\bar{S}_f + C\left|\frac{\alpha_2 V_2^2}{2g} - \frac{\alpha_1 V_1^2}{2g}\right|$$

(Eq. 4.2)

where L is the discharge weighted reach length, $\bar{S}_f$ is the representative friction slope between two sections and C is the expansion and contraction loss coefficients

Depending on the length specified for flow in the main channel and on the floodplain, the distance weighted reach length, L, is calculated as:

$$L = \frac{L_{lob}\bar{Q}_{lob} + L_{ch}\bar{Q}_{ch} + L_{rob}\bar{Q}_{rob}}{\bar{Q}_{lob} + \bar{Q}_{ch} + \bar{Q}_{rob}}$$

(Eq. 4.3)

where L_{lob}, L_{ch}, L_{rob} are the cross section reach lengths specified for flow in the left overbank, main channel, and right overbank respectively, $\overline{Q}_{lob}$, $\overline{Q}_{ch}$, $\overline{Q}_{rob}$ are the arithmetic average of the flows between sections for the left overbank, main channel, and right overbank respectively.

4.3.2 Friction losses

To evaluate the friction loss ($L\overline{S}_f$) in HEC-RAS, the representative friction slope ($\overline{S}_f$) for a reach and L (as defined by Equation 4.3) should be calculated. The friction slope (slope of energy gradeline) at each cross section is computed from Manning's equation as follows:

$$S_f = \left(\frac{Q}{K}\right)^2 \qquad \text{(Eq. 4.4)}$$

where Q and K are the total discharge and conveyance for a cross section respectively.

On this basis, HEC-RAS uses the following expression for the representative reach friction slope:

$$\overline{S}_f = \left(\frac{Q_1 + Q_2}{K_1 + K_2}\right)^2 \qquad \text{(Eq. 4.5a)}$$

where subscripts 1 and 2 relate to variable values at the upstream and downstream end of the reach under study.

Given the channel irregularity and its impacts upon the non-uniformity of flow, the concept of channel conveyance (K) has been defined as a measure of the discharge carrying capacity of a channel (Eq. 4.5b)

$$Q = KS_f^{1/2} \qquad \text{(Eq. 4.5b)}$$

where Q is the discharge, K is the conveyance capacity and S_f is the friction slope.

4.3.3 Contraction and expansion losses

Contraction and expansion of flow due to changes in the cross section are common causes of energy loss within a reach (between two cross sections). HEC-RAS assumes that a contraction or expansion is occurring whenever the velocity head downstream relative to the velocity head upstream is greater or smaller respectively. Contraction and expansion losses in HEC-RAS are evaluated by the following equation:

$$h_{ce} = C \left| \frac{\alpha_1 V_1^2}{2g} - \frac{\alpha_2 V_2^2}{2g} \right| \qquad \text{(Eq. 4.6)}$$

where C is the contraction or expansion coefficient. Typically C values are evaluated empirically for different situations (see Section 4.7.3).

4.3.4 Solution method

The unknown water surface elevations are calculated from one cross section to the next cross section by solving equation 4.1 (i.e. the Energy equation) and 4.2 with an iterative procedure called the standard step method. This is the primary procedure for computing water surface profiles between cross sections in steady and gradually varied flows. Given the flow and water surface elevation at one cross section, the goal of the standard step method is to compute the water surface elevation at the adjacent cross section. For sub-critical flow (most rivers exhibit sub-critical flow), the computations begin at the downstream boundary and proceed upstream. For supercritical flow, the computations begin at the upstream boundary and proceed downstream. Assuming sub-critical flow, the procedure takes the following steps:

(a) The downstream cross-section water surface elevation is assumed to be known (either from boundary condition data or the previous time stem model calculation.

(b) Assumption of a water surface elevation, or initial condition, at the upstream cross section (Fig. 4.1).

(c) Computation of the associated conveyance and velocity head values at the upstream cross section based on the assumed water surface elevation.

(d) Calculation of friction slope and the energy head loss (friction loss, and contraction/expansion loss) between the upstream section (from b and c) and the downstream section (a).

(e) Solution of the energy equation (Eq. 4.1) using the values from (c) and (d) to compute the water surface elevation at the upstream section.

(f) Comparison of the computed water surface elevation (from e) with the value assumed in the first step (from b) and adjustment of the water surface elevation used in (b).

(g) Repetition of (b) to (f) until the assumed and computed water surface elevations are within a predetermined tolerance.

The calculation then moves to the reach immediately upstream using the result from (g) as the input to (a).

The standard step method in HEC-RAS is constrained by 40 iterations as the maximum number iterations for balancing the water surface. If the maximum number of iterations is reached before a balanced water surface is achieved, the procedure will then calculate critical depth as the final water surface elevation. Once a balanced water surface elevation has been obtained for a cross section, checks are made to ascertain that the elevation is on the right side of the critical water surface elevation (e.g. above the critical elevation for sub-critical profile).

4.3.5 Momentum equation

The energy equation is only applicable in HEC-RAS when the flow is gradually-varied. For situations in which the water surface passes through critical depth (transient from sub-critical to supercritical or vice versa), the momentum equation should be applied. There are several instances where a transition can occur. These include significant changes in channel slope, bridge constrictions, drop structures and weirs, and stream junctions. In some of these situations, empirical equations can be applied (such as at drop structures and weirs) but in terms of a hydraulic jump, flow hydraulics at bridges and stream junctions, the momentum equation must be applied (HEC-RAS, Hydraulic Reference, 2001).

The momentum equation is derived from Newton's second law of motion:

$$\sum F_x = ma \qquad \text{(Eq. 4.7)}$$

Applying Newton's second law of motion to a body of water constrained by two cross sections (Fig. 4.2), the following expression for the change in momentum over a unit time can be written:

$$P_2 - P_1 + W_x - F_f = Q\rho\Delta V_x \qquad \text{(Eq. 4.8)}$$

where P is the hydrostatic pressure force at locations 1 and 2, W_x is the force due to the weight of water in the x direction, F_f is the force due to external friction losses from 2 to 1, Q is discharge, ρ is the density of water, and ΔV_x is change in velocity from 2 to 1, in the x direction.

Fig. 4.2: Application of momentum principle (HEC-RAS, Hydraulic Reference, 2000)
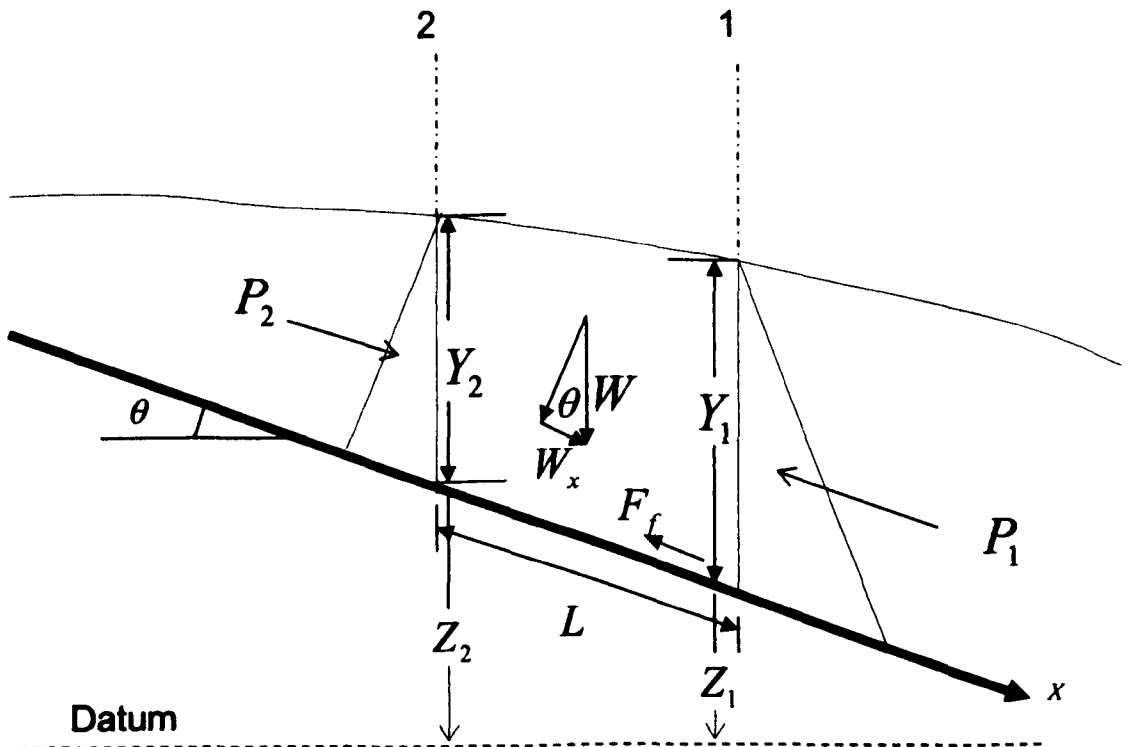
4.3.6 Hydrostatic pressure forces

The force in the x direction due to hydrostatic pressure is:

$$P = \gamma A \bar{Y} \cos\theta \qquad \text{(Eq. 4.9)}$$

where $\bar{Y}$ is the distance from the water surface to the centroid of the cross-section area. The assumption of hydrostatic pressure is valid for slopes less than 1:10 (approximately 6 degrees). Given that the slope of most river channels is far less than 1:10, $\cos\theta$ can be set to 1 (Chow, 1959). Therefore, the equations for the hydrostatic pressure force at cross sections 1 and 2 can be presented as:

$$P_1 = \gamma A_1 \bar{Y}_1 \qquad \text{(Eq. 4.10)}$$

$$P_2 = \gamma A_2 \bar{Y}_2 \qquad \text{(Eq. 4.11)}$$

where γ is the unit weight

of water, A is the wetted area of the cross section at locations 1 and 2, and $\bar{Y}$ is the depth measured from the water surface to the centroid of the cross sectional area at locations 1 and 2.

4.3.7 Weight of water

The weight of water is calculated via:

$$W = \gamma \left(\frac{A_1 + A_2}{2} \right) L \qquad \text{(Eq. 4.12)}$$

$$W_x = W \times \sin\theta \qquad \text{(Eq. 4.13)}$$

$$Sin\theta = \frac{z_2 - z_1}{L} = S_0 \qquad \text{(Eq. 4.14)}$$

$$W_x = \gamma \left(\frac{A_1 + A_2}{2} \right) L S_0 \qquad \text{(Eq. 4.15)}$$

where L is the distance between sections 1 and 2 along the x axis, S_0 is the slope of channel, based on mean bed elevations, and Z is the mean bed elevation at locations 1 and 2.

4.3.8 External friction

The friction force is opposite to the flow direction and calculated via:

$$F_f = \tau \overline{P} L \qquad \text{(Eq. 4.16)}$$

where τ is the shear stress and $\overline{P}$ is the average wetted perimeter between sections 1 and 2. The shear stress is determined through:

$$\tau = \gamma \overline{R} \overline{S}_f \qquad \text{(Eq. 4.17)}$$

where $\overline{R}$ is the average hydraulic radius and $\overline{S}_f$ is the slope of energy grade line (friction slope).

Substituting Equation 4.17 back into Equation 4.16:

$$F_f = \gamma \left(\frac{A_1 + A_2}{2} \right) \overline{S}_f L \qquad \text{(Eq. 4.18)}$$

4.3.9 Functional form of the momentum equation

Considering the momentum equation derived from Newton's second law of motion (Eq. 4.19):

$$ma = Q \rho \Delta V_x \qquad \text{(Eq. 4.19)}$$

where $\rho = \dfrac{\gamma}{g}$, $\Delta V_x = (\beta_1 V_1 - \beta_2 V_2)$ and β is the momentum coefficient that accounts for a varying velocity distribution in irregular channels, this equation can be rewritten as:

$$ma = \frac{Q\gamma}{g} (\beta_1 V_1 - \beta_2 V_2) \qquad \text{(Eq. 4.20)}$$

Finally, by substituting Equations 4.10, 4.11, 4.15, 4.18 and 4.20 back into Equation 4.8, the functional form of the momentum equation (4.21) used in HEC-RAS for steady state is achieved.

$$\frac{Q_2^2 \beta_2}{g A_2} + A_2 \overline{Y}_2 + \left(\frac{A_1 + A_2}{2} \right) L S_0 - \left(\frac{A_1 + A_2}{2} \right) \overline{S}_f L = \frac{Q_1^2 \beta_1}{g A_1} + A_1 \overline{Y}_1$$

$$\text{(Eq. 4.21)}$$

4.4 Unsteady flow calculation procedure within HEC-RAS

For unsteady flow calculations, the time-dependent terms are included in the calculations and water flow under any situation is governed by the principals of conservation of mass (continuity) and conservation of momentum. These principals are presented mathematically in the form of partial differential equations. These equations are explained below.

4.4.1. Continuity equation:

Conservation of mass for a control volume states that the net rate of flow into the volume be equal to the rate of change of storage inside the volume. In other words, the general equation of continuity states that inflow minus outflow equals rate of change of storage.

$$\frac{\partial A}{\partial t} + \frac{\partial Q}{\partial x} = q$$

Assuming that Δx is small and the fluid is incompressible, the change in mass in the control volume is equal to:

$$\frac{\partial A}{\partial t}\Delta x = \left[\left(Q - \frac{\partial Q}{\partial x}\frac{\Delta x}{2} \right) - \left(Q + \frac{\partial Q}{\partial x}\frac{\Delta x}{2} \right) + q\Delta x \right] \qquad \text{(Eq. 4.22)}$$

where q is the rate of lateral flow per unit length of channel and A is the total flow area. Simplifying and dividing Equation 4.22 by Δx yields the final form of the continuity equation for unsteady flow calculations

$$\frac{\partial A}{\partial t} + \frac{\partial Q}{\partial x} - q = 0 \qquad \text{(Eq. 4.23)}$$

Fig. 4.3: Elementary control volume for derivation of continuity and momentum equations
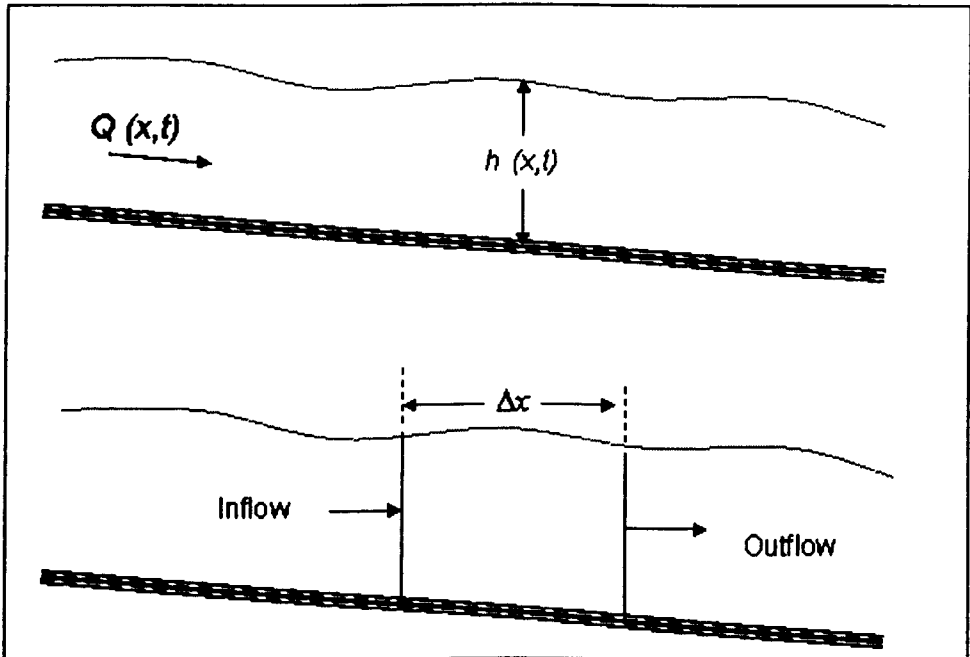
4.4.2 Momentum equation

The momentum equation in the x direction is produced from a force balance on the river element according to Newton's second law of motion. The following forces are acting on the area of control volume:

Hydrostatic force $\qquad F_1 = F_H = \gamma \dfrac{\partial \left(\bar{h} A \right)}{\partial x} \Delta x,$ $\qquad$ (Eq. 4.24)

Gravity force $\qquad F_G = \gamma A \dfrac{\partial z_0}{\partial x} \Delta x = \gamma A S_0 \Delta x,$ $\qquad$ (Eq. 4.25)

Friction force $\qquad F_f = -\gamma A S_f \Delta x,$ $\qquad$ (Eq. 4.26)

where γ is the specific weight of water (ρg), $\bar{h}$ is distance from the water surface to the centroid of pressure prism, S_f is the friction slope, S_0 is the bed slope, and z_0 is the invert elevation.

The three forces acting on the volume of fluid are defined above. The only component that is needed to be defined is the momentum flux. The flux entering or leaving the control volume may be written respectively as:

$$\rho\left(QV - \frac{\partial QV}{\partial x}\frac{\Delta x}{2}\right) \qquad \text{(Eq. 4.27)}$$

$$\rho\left(QV + \frac{\partial QV}{\partial x}\frac{\Delta x}{2}\right) \qquad \text{(Eq. 4.28)}$$

Therefore, the net rate of momentum (momentum flux) entering the control volume is:

$$-\rho\frac{\partial QV}{\partial x}\Delta x \qquad \text{(Eq. 4.29)}$$

Since the momentum of fluid in the control volume is $\rho Q\Delta x$, the rate of accumulation of momentum may be written as:

$$\frac{\partial}{\partial t}\rho Q\Delta x = \rho\Delta x\frac{\partial Q}{\partial t} \qquad \text{(Eq. 4.30)}$$

Recalling the principles of conservation of momentum, the net rate of momentum (momentum flux) entering the control volume (Eq. 4.29) plus the sum of all external forces acting on the volume change [(Eq. 4.24) + (Eq. 4.25) +(Eq. 4.26)] is equal to the rate of accumulation of momentum (Singh, 1996) (Eq. 4.30). Then, we will have:

$$\rho\Delta x\frac{\partial Q}{\partial t} = -\rho\frac{\partial QV}{\partial x}\Delta x - \rho g A\frac{\partial h}{\partial x}\Delta x - \rho g A\frac{\partial z_0}{\partial x}\Delta x - \rho g A S_f\Delta x \qquad \text{(Eq. 4.31)}$$

The elevation of water surface, z, is equal to $z_0 + h$, therefore:

$$\frac{\partial z}{\partial x} = \frac{\partial h}{\partial x} + \frac{\partial z_0}{\partial x} \qquad \text{(Eq. 4.32)}$$

where $\partial z/\partial x$ is the water surface slope.

Substituting Equation 4.32 into Equation 4.31 and dividing Equation 4.31 by $\rho\Delta x$ and moving all terms to the left side yields the final form of the one-dimensional

momentum equation. This equation is valid for negligible lateral inflow to the control volume (see Singh, 1996).

$$\frac{\partial Q}{\partial t} + -\frac{\partial QV}{\partial x} + gA\left(\frac{\partial z}{\partial x} + S_f\right) = 0 \qquad \text{(Eq. 4.33)}$$

4.4.3 Application of unsteady flow equations within HEC-RAS

Figure 4.4 illustrates the two-dimensional characteristics of the interaction between the main channel and floodplain flows. When the river is rising, water moves laterally away from the main channel, inundating the floodplain and filling possible storage areas. As the depth increases, the floodplain begins to convey water downstream, generally along a shorter path than that of the main channel. When the river stage is falling, water moves toward the channel from overbank flow. Hence, two-dimensional flow occurs at higher river stage where the interaction between the channel and floodplain flows exists.

This two-dimensional flow can often be accurately approximated by a one-dimensional representation. A common approach is to ignore over bank conveyance entirely, assuming that the overbank flow is used only for storage (HEC-RAS, Hydraulic Reference, 2001). This assumption may be suitable for large rivers where the channel is confined by levées and the remaining floodplain is either heavily vegetated or an off-channel ponding area. Off-channel ponding areas can be modelled as storage areas that exchange water with the river through hydraulic connections.

Fig. 4.4: Channel and floodplain flows (HEC-RAS, Hydraulic Reference, 2001)
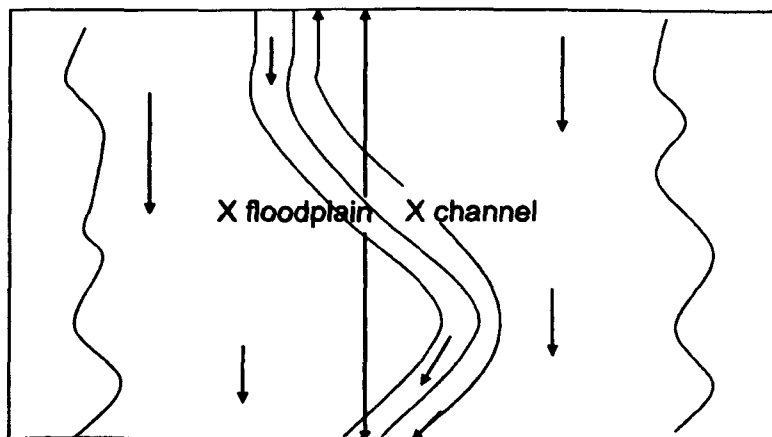
Fread (1976) and Smith (1978) approached this problem by dividing the channel into two separate channels. In this sense, the continuity and momentum equation should be rewritten for each channel. To simplify the problem, they assumed a horizontal water surface at each cross section normal to the direction of flow, such that the exchange of momentum between the channel and floodplain was negligible and that discharge was distributed according to conveyance.

$$Q_c = \phi \cdot Q \qquad \text{(Eq. 4.34)}$$

where Q_c is flow in channel, Q is the total flow, ϕ is equal to $K_c /(K_c + K_f)$, K_c is conveyance in the channel, and K_f is conveyance on the floodplain.

Expanding on earlier work, Barkau (1982) manipulated the finite difference equations for the channel and floodplain and defined a new set of equations that were computationally more convenient. Using a velocity distribution factor, he combined the convective terms. Further, by defining an equivalent flow path, Barkau replaced the friction slope terms with an equivalent force. Equations 4.35 and 4.36, derived from the work of Barkau, are the basis for the unsteady flow solution within HEC-RAS software.

$$\frac{\partial A}{\partial t} + \frac{\partial(\phi Q)}{\partial x_c} + \frac{\partial[(1-\phi)Q]}{\partial x_f} = 0 \qquad \text{(Eq. 4.35)}$$

$$\frac{\partial Q}{\partial t} + \frac{\partial(\phi^2 Q^2 / A_c)}{\partial x_c} + \frac{\partial((1-\phi)^2 Q^2 / A_f)}{\partial x_f} + gA_c\left[\frac{\partial Z}{\partial x_c} + S_{fc}\right] + gA_f\left[\frac{\partial Z}{\partial x_f} + S_{ff}\right] = 0$$
$$\text{(Eq. 4.36)}$$

where the subscripts c and f refer to the channel and floodplain respectively.

4.4.4 Numerical solution methods

The final forms of the continuity and momentum equations used within HEC-RAS are outlined above. The most successful and accepted procedure for solving the one-dimensional unsteady flow equations is the four-point implicit scheme, also known as the box scheme. Hence, the mentioned equations are approximated using

implicit finite differences and solved numerically using the Newton-Raphson iteration technique.

4.5 Application of HEC-RAS in normal mode

HEC-RAS describes the river channel and floodplain as a series of discrete cross sections perpendicular to the flow direction. The finite difference procedure for solving the governing equations then defines the topography of the system domain according to the available cross-section data. In this sense, the real topographic characteristics between cross sections in the main channel and, more importantly, on the floodplain are not considered. The change of topographic features between two adjacent cross sections is assumed to be linear and obtained thorough interpolation. After entering suitable boundary conditions, water surface elevations are calculated at all cross sections for either a set of flow data (steady flow simulation) or by routing hydrographs through the system (unsteady flow simulation). To simulate flood inundation extent, water depth values at each cross section at any time step are either overlain onto a digital elevation model, (a DEM), or linearly interpolated between them. Therefore, there are two separate steps to simulating flood inundation extent. The data needed to perform unsteady flow simulations are divided into two main categories: geometric data (Section 4.6) and unsteady flow data (Section 4.7).

4.6 Geometric data

The basic geometric data requirements to run HEC-RAS in normal mode comprise the connectivity of the river system (called the river system schematic), cross-section data, reach lengths, energy loss coefficients (friction losses, contraction and expansion losses, structure-related losses), and stream junction information. Hydraulic structures data (bridges, culverts, weirs....etc.) are also assigned as part of geometric data that should be parameterised.

4.6.1 The river system schematic

The river system schematic is needed to define how the river system is configured. The conventional approach to entering the river system schematic into HEC-RAS is

by drawing and connecting the various reaches of the system in the geometric data editor. HEC-RAS is able to model river systems that range from a single reach to complicated networks. This leads to a drawback. To allow a range of networks to be simulated, HEC-RAS uses its own coordinate system so that the coordinate of any given point is based on its river station along a one-dimensional stream centreline, location along the cross section line and elevation. This coordinate system is specially designed for HEC-RAS and does not match any real-world coordinate systems. For example, where HEC-RAS displays a stream as a straight-line in model coordinates, it may be represented as a curved line in a real-world coordinate system. Fortunately, HEC-RAS has been modified so that it is able to accept any coordinate system. Hence, an extension of ArcView GIS called HEC-GeoRAS has been developed to process geospatial data for use in HEC-RAS. It means that HEC-GeoRAS creates an import file for HEC-RAS that contains most of the necessary geometric data, and displays the river system in HEC-RAS in a real-world coordinate system. As seen in Fig. 4.5, the stream line and cross sections that are created in HEC-RAS are schematically illustrated whereas they are derived from a real-world coordinate system (in Fig. 4.6) using HEC-GeoRAS. Furthermore, HEC-GeoRAS is able to convert the hydraulic modelling output to GIS format in order to map flood inundation extent under real-world coordinates.

Fig. 4.5: The schematic illustration of the river system in HEC-RAS
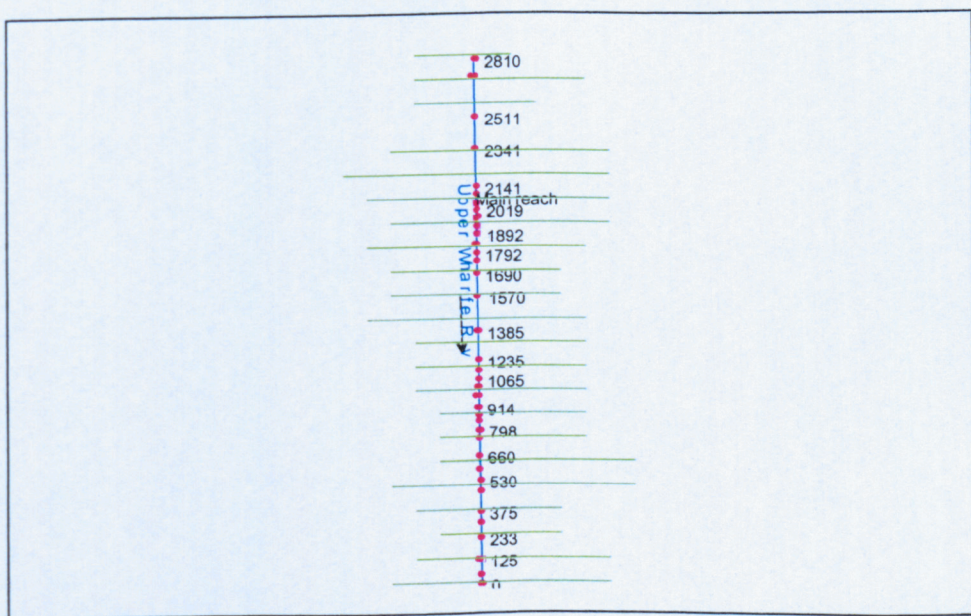
Fig. 4.6: The exhibition of the river system in real-world coordinate system, using HEC-GeoRAS (for the upstream section of the study reach)
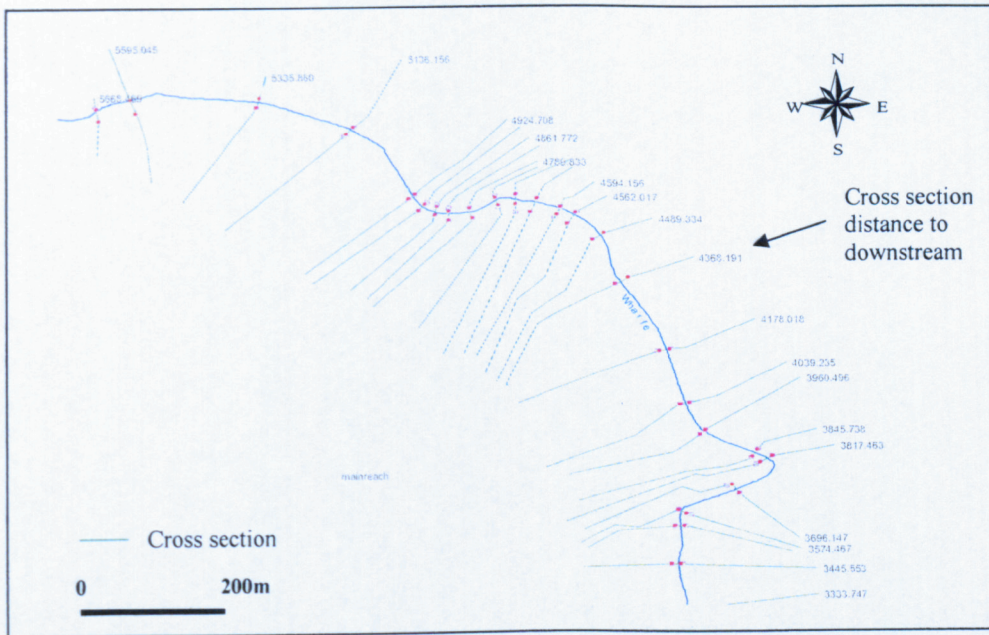
When performing a hydraulic study it is normally necessary to extend the reach both upstream and downstream of the study reach. Gathering additional upstream data is necessary where any upstream impacts due to construction alternatives within the study reach are to be evaluated. More importantly, extension of data collection downstream is necessary in order to prevent any effects of user-defined boundary conditions affecting the results within the study reach. Therefore, to prevent any computed error within study reach, estimated boundary conditions should be placed far enough downstream such that the computed profile in the area of interest converges on an answer that does not depend on the type or the location of the downstream boundary condition.

As shown in Chapter 3, there were five tributaries flowing towards the study domain, terminated either in the main channel or on the floodplain. In HEC-RAS, for those which are connected to the main channel, tributary inflow hydrograph can be added to the main channel hydrograph of a cross section that is located immediate upstream of where the tributary joins the main river. As there is no way of simulating tributary flows terminating at floodplain areas in HEC-RAS, a similar method as described above was used to simulate the flow of these kinds of tributaries. This may be problematic in relation to inundation extent data because

flows that are directly involved in flood inundation on the floodplain are conveyed to the main channel. This means that the observed inundation data includes the contribution of flow the floodplain but they are not essentially included in the simulated inundation extent. Thus, part of discrepancies between predictions and observations may be attributed to tributary parameterisation.

4.6.2 Cross section geometry

Cross section geometry specification includes determination of the ground surface profile at each cross section and the measurement of the distance between cross sections (reach length) within the main channel and on the right and left floodplain. Energy loss coefficients (friction coefficient and contraction and expansion coefficients) and stream junction data are also assigned as part of geometric data specification and must be determined. The cross-section should be perpendicular to the flow direction and extend across the entire floodplain. Cross sections are required at representative locations within the reach, where there are considerable changes in bed slope, discharge, roughness and channel and floodplain shapes or at locations where water-related structures exist. Where abrupt changes occur, several cross-sections should be used to describe adequately the reach regardless of the cross-sectional spacing. Cross-section spacing is also a function of stream size, slope and the uniformity of cross section shape. In general, large uniform rivers, with flat slopes normally require fewer cross-sections than rivers with complex configurations and steeper slopes. To provide the in-channel cross-sectional data, surveying techniques such as levelling and GPS are used in this research. Cross-sectional data across the entire floodplain are extracted from remotely sensed Lidar data along each cross section.

When the cross-sections are spaced far apart, and the changes in hydraulic properties are great, the solution of the governing equation may become unstable. In such situations the flow area, depth and/or velocity varies rapidly, it is necessary to add additional cross sections to keep the solution stable. This usually occurs in the complicated reaches (e.g. meandering reaches, steep reaches and reaches with high levees). Hence, cross section spacing should always be tested to ensure that the water surface profiles are estimated as accurate as possible.

4.6.3 Energy loss coefficients

Several types of energy loss coefficients may be utilized by HEC-RAS to evaluate energy losses: (a) Manning's n or equivalent roughness, K, values for friction loss; (b) contraction and expansion coefficients to evaluate the transition losses, and (c) bridge, culvert and weir loss coefficients to evaluate looses related to their shape, size and entrance and exit conditions.

- *Manning's n*

Selection of an appropriate value of Manning's n is crucial to the accuracy of a computed water profile. The value of Manning's n is highly variable and generally depends upon a number of factors including: surface roughness, vegetation, channel irregularities, channel alignment, scour and sedimentation, obstructions, shape and size of the channel, seasonal change, temperature, suspended material and bed load. In general, given the significance of n values for computed water profiles its values should be calibrated whenever water surface profile information (gauged data as well as high water marks) is available. When gauged data are not available, values of n computed for similar stream conditions or obtained from experimental data should be used as guides in selecting n values. Therefore, given that estimation of a precise value of n for any specific reach seems impossible, a realistic range of its values must be considered. There are several methods for determining Manning's n values for typical channels (e.g. Chow, 1959). Visual comparison is one of these methods. This includes pictures of selected rivers and calibrated n values for a range of flows may be utilized as a guide to n value determination (Fasken, 1963; Barnes, 1967; Hicks and Mason. 1991).

Although there are many factors that affect the determination of n values, the most important ones are: (i) the type and size of materials that compose the bed and banks of the channel; and (ii) the shape of channel. On this basis, Cowan (1956) developed a procedure for estimating the effects of these factors to determine the value of n for a channel. The value of n may be computed by

$$n = (n_b + n_1 + n_2 + n_3 + n_4)m \qquad \text{Eq. (4.37)}$$

where n_b is a base value of n for a straight, uniform , smooth channel in natural materials, n_1 is a correction factor for the effect of surface irregularities, n_2 is a value for variations in shape and size of the channel cross section, n_3 is a value for obstruction, n_4 is a value for vegetation and flow conditions, and m is a correction factor for meandering of the channel. The data required to parameterise the equation 4.37 are provided in Arcement and Schneider (1989).

Several tabulated values for the base value of n and adjusting factors are presented (e.g. Cowan, 1956; Aldridge and Garrett, 1973; Arcement and Schneider, 1989). However, Limerinos (1970) presented an equation to estimate the base value of n, in which the base value of n is related to hydraulic radius and particle size based on samples from 11 stream channels having bed materials ranging from small gravel to medium-sized boulders.

$$n = \frac{(0.0926)R^{1/6}}{1.16 + 2.0\log\left(\dfrac{R}{d_{84}}\right)}$$

Eq. (4.38)

where R is hydraulic radius in feet (data range was 1.0 to 6.0 feet) and d_{84} is the particle diameter in feet, that equals or exceeds the diameter of 84 percent of the particles (data range was 1.5 to 250 mm). An example of tabulated values of Manning's n was presented in Chapter 2.

- *Contraction and expansion coefficients*

Contraction and expansion of flow occurs due to changes in cross section shape between two adjacent cross sections. The contraction and expansion losses (transition losses) are estimated through multiplying the contraction and expansion coefficients, experimentally evaluated, by the absolute difference between velocity heads between two cross sections (see Eq. 4.6). The contraction and expansion coefficients for sub-critical flows are selected based on the recommended standard values in Table 4.1 (HEC-RAS, Hydraulic Reference, 2001). The maximum value for these coefficients is one.

Table 4.1: Sub-critical flow contraction and expansion coefficients (HEC-RAS, Hydraulic reference, 2001)

Situation	Contraction	Expansion
No transition loss computed	0.0	0.0
Gradually transitions	0.1	0.3
Typical bridge sections	0.3	0.5
Abrupt transitions	0.6	0.8

For supercritical cases, these coefficients should be considered to be lower as the velocity heads in supercritical flow are greater, and small changes in depth may result in large changes in velocity head. Hence, using contraction and expansion coefficients that would be typical for sub critical flows may lead in over-estimation of the energy losses in supercritical cases (HEC-RAS, Hydraulic Reference, 2001).

4.7 Unsteady flow data

Unsteady flow data are needed in order to perform an unsteady flow analysis in HEC-RAS. Unsteady flow data consist of boundary conditions (external and internal) and initial conditions.

4.7.1 Boundary conditions

Boundary conditions must be established at all of the open ends (upstream and downstream) of the river system as the starting water surface. A starting water surface is necessary in order for the model to begin calculations. Upstream ends of the river system can be modelled using a flow hydrograph, a stage hydrograph or combined stage and flow data as a boundary condition. There are additional alternatives for downstream boundary conditions, including a rating curve and a normal depth assumption (Manning's equation).

4.7.2 Initial conditions

Initial conditions consist of stage and flow data at all of the existing nodes (cross sections) and water elevation of each storage area of the river system. These values

are used at each node and at the first time step as the assumed values used to be compared against the computed values of the model. The accepted values from the first time step (t time step) will be set as initial conditions for the second time step (t +1 time step). Specifying an initial stage value at any node in the domain before unsteady flow simulation, the model performs a steady flow backwater run to compute the corresponding stages at each node as the initial conditions for the first time step. The influence of initial conditions is lost after a certain period of time. This is because at each time step, the flow field simulated in the previous time step is assigned as the initial value.

4.8 HEC-RAS model (in normal mode) set up

Within the study site (Hubberholme to Starbotton), 58 cross sections were surveyed by levelling and GPS. Following that, the reach length (cross section distances) for the left overbank, right overbank and main channel were specified. The cross section profiles were extended on the floodplain using Lidar data. The Manning's n value was estimated using Equation (4.37) and also consideration of n values in previous studies. The range 0.035-0.065 was chosen for calibration. Given the uncertainties associated with the estimation of n values, this range enables the full range of possible friction values to be explored. In addition, friction values are used, to some extent, for compensating flow representation, and hence the actual value may be shifted and so a wider range should be selected. The contraction and expansion coefficients for sub-critical flows were selected based on the recommended standard values (See Table 4.1). Given the study reach characteristics, in which a gradual transition was recognised, 0.1 and 0.3 were selected as the Contraction and Expansion coefficients respectively. A number of estimations of flow hydrographs were produced as upstream boundary conditions in Chapter 3. All flow hydrographs were simulated initially as upstream boundary conditions with a reasonable Manning's n value. Any of the flow hydrographs that can satisfy the validation data (herein the observed stage data at the upstream boundary condition), were selected as boundary conditions at the upstream end. Given that there are no measured data at the down stream of the study reach, the Normal Depth (Manning Equation) was set as the downstream boundary condition. This option uses the Manning equation to estimate a stage for each computed flow.

Thus, the effect of using this type of boundary condition is limited to stage calculations. When applying this, the boundaries should be placed far enough down stream, such that its effects will not affect the results in the reach of interest particularly at the downstream end. To use the normal depth as downstream boundary condition in HEC-RAS, a friction slope should only be entered for the reach in the vicinity of the boundary condition. Initially the friction slope was set within the range 0.001-0.005. However, the effects of friction slope on predicted stage and its optimum value at the downstream end of the reach were tested through sensitivity analysis and initial simulations respectively.

As mentioned before, there are five major tributaries contributing to the main channel within the study reach. There are two methods to model stream tributaries: (i) using stream junctions as locations where two or more streams come together or split apart; and (ii) directly adding tributaries inflow hydrographs where a tributary comes to the main channel. In this research, the second method is chosen, meaning that all tributaries' flow hydrographs are connected to the main channel.

The river system of the study domain along with the surveyed cross sections is shown in Figure 4.7.

Fig. 4.7: The one-dimensional model (HEC-RAS) in normal mode parameterised for the study site

113
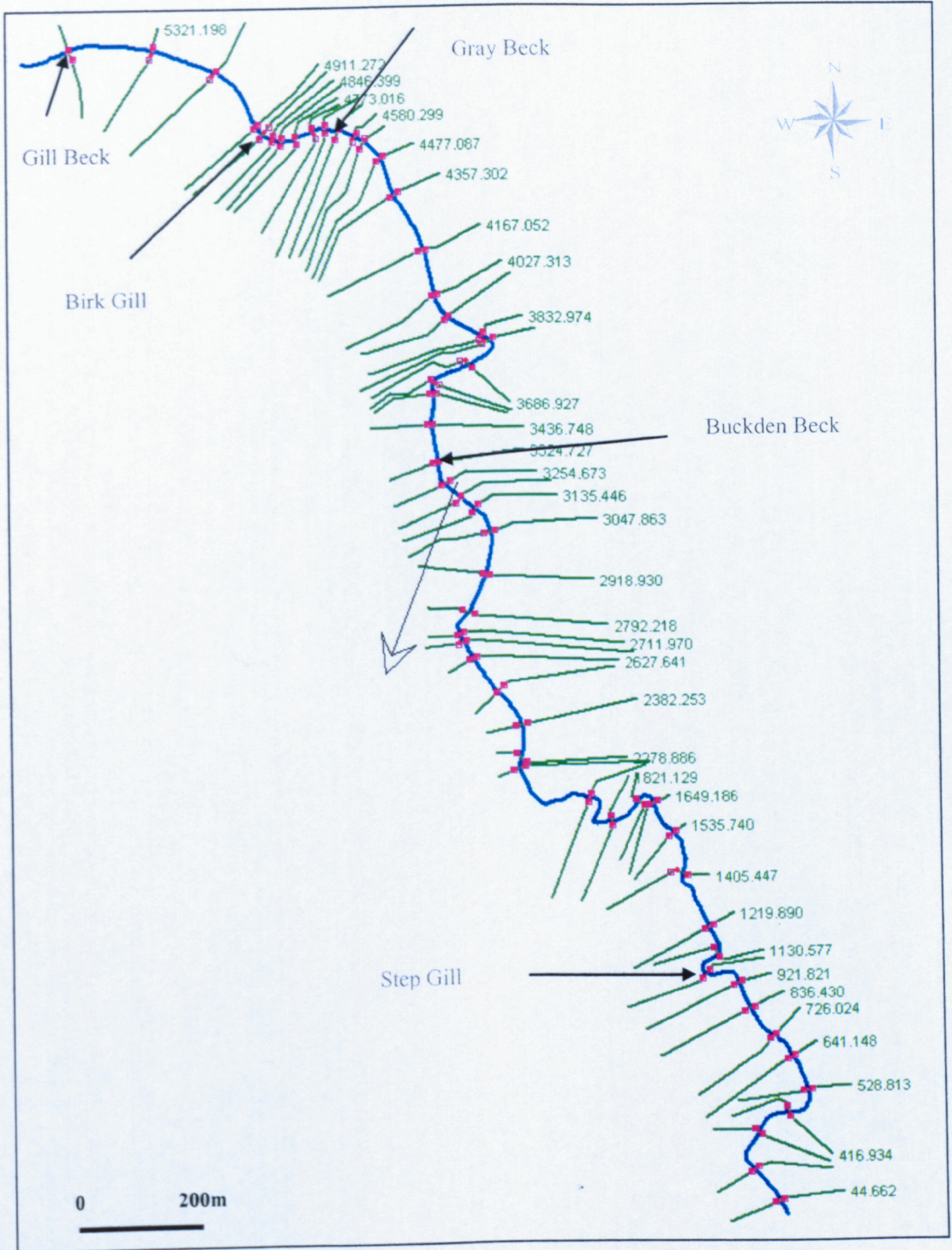
4.9 Initial simulations

A number of estimations of flow peaks were produced to predict upstream boundary conditions (Chapter 3). The HEC-RAS model in normal mode was initially run in steady mode using the peak flow data (see Table. 3.9) along with a reasonable range of geometric coefficients to test which peak flow satisfies the observed data (stage data) at the upstream end. As the produced flow data at Hubberholme are independent of the stage data observed at this gauging station, the stage data can be used as independent validation data. Therefore, if any of the flow peaks used in the steady state simulations produced the maximum stage observed during the flood event (04/02/04) at Hubberholme, it can be considered as a feasible selection flow peak for the upstream boundary condition

A set of steady simulations using the estimated peak flows were simulated. The results of the simulations showed (Table 4.2) that the peak value obtained using the Rainfall-runoff Method (FEH, 2000) with a SPR of 80% (47.73 m^3/s) adequately reproduced the observed stage data at upstream end of the reach. Hence, it was selected as the peak flow for the upstream boundary condition in this research.

Table 4.2: Comparison between the maximum stage simulated and observed at Hubberholme, using the estimated flow peaks as upstream boundary condition under steady simulations.

Methods used to estimate the peak flow at Hubberholme	Flow peak (m3/s)	Simulated peak stage (m)	Observed peak stage (m)
FSR rainfall-runoff method-SPR 60%	36.58	233.21	233.6-233.8
FSR rainfall-runoff method-SPR 70%	42.35	233.32	233.6-233.8
FSR rainfall-runoff method-SPR 80%	47.73	233.51	233.6-233.8
Transfer function (Revised sub-area at Deepdale)	27.62	233.03	233.6-233.8
Transfer function (Conventional sub-area at Deepdale)	31.62	233.12	233.6-233.8
Transfer function (Rating curve at Deepdale)	26.49	233.00	233.6-233.8
Rating curve obtained from previous studies, JBA (2000)	17.00-22.20	232.72-232.90	233.6-233.8

It is obvious that the original hydrograph associated with the selected flow value has an artificial, symmetric shape (Fig. 4.8). Utilising the stage data trend at Hubberholme, a shape-scaled hydrograph was produced, with the same flow peak (Fig. 4.8). Thus, it was necessary to perform unsteady simulations to define the effect of the hydrograph shapes on the model output (i.e. inundation extent).

Fig. 4.8: Flow hydrographs for flood 04/02/04 at Hubberholme based on stage-based shape and rainfall-runoff model-based shape (symmetrical)
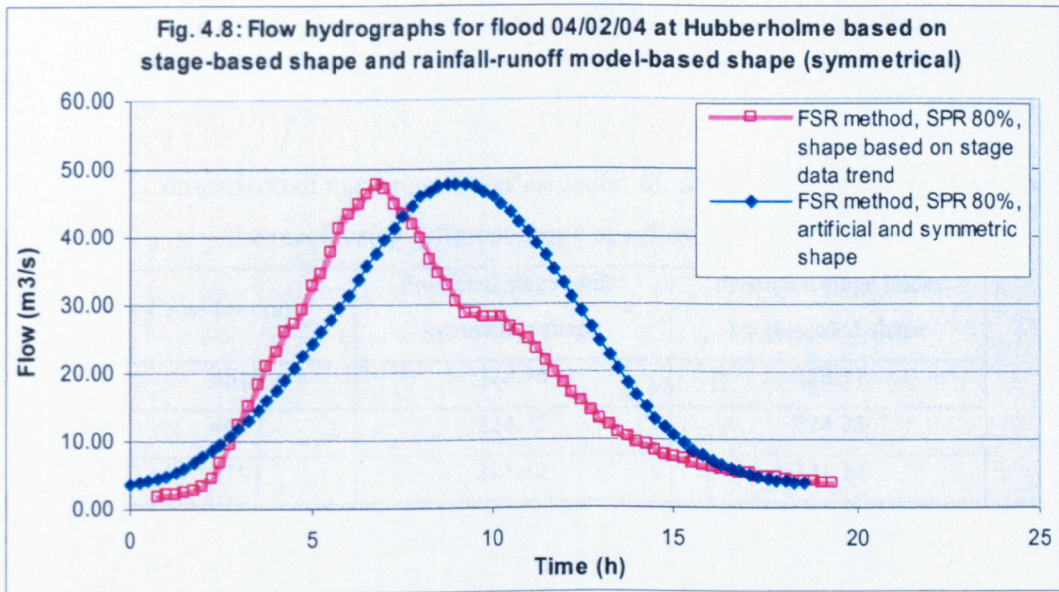
Again, selecting reasonable values of parameters involved in model parameterisation (i.e. Manning's n; Expansion and Contraction coefficients; and friction slope), two scenarios with different hydrograph shapes but the same value of peak flow were established. Comparison of the results observed shows that hydrograph shape does not have a major effect on predicted stage (as prime control of floodplain inundation) along the reach but it strongly affects the timing of the flood wave. Figure 4.8a shows downstream stage data predicted using the above hydrographs. As seen, the stage data under the symmetric shape simulation predicts water elevation only 0.04 m higher than the stage-scaled shape. In contrast, it indicates that the difference in timing of the peak stage data at the downstream end of the reach is around 4h. Comparison of predicted stage data along the reach for the two scenarios reveals the same conclusion, meaning that there is not a major difference in predicted stage data as a result of the different shape of inflow hydrographs (see Table 4.3). Outflow hydrographs predicted using the above scenarios are associated with more changes in the estimated peak values so that the symmetric hydrograph resulted in a higher flow peak in order of $2m^3/s$ than the hydrograph with stage-based shape. The effect of hydrograph shape on timing of outflow hydrographs was similar to stage predictions. Hence, it is expected that timing of flood wave has a direct effect on the timing of floodplain inundation. As the ultimate objective of the research is focused on prediction of inundation extent

without considering the timing of inundation, the maximum inundation extent predicted using the two scenarios was compared.

Table 4.3: Comparison of maximum water elevation for a number of cross sections along the reach using different shape of inflow hydrograph.

Cross section	Predicted stage under symmetric shape	Predicted stage under stage-scaled shape
4819	228.76	228.77
4027	224.75	224.75
3191	221.12	221.14
2248	218.30	218.33
1219	216.42	216.43
528	215.69	215.67
44	215.4	215.36

Fig. 4.8a: Downstream stage data predicted using diffrent shape hydrographs as upstream boundary conditions
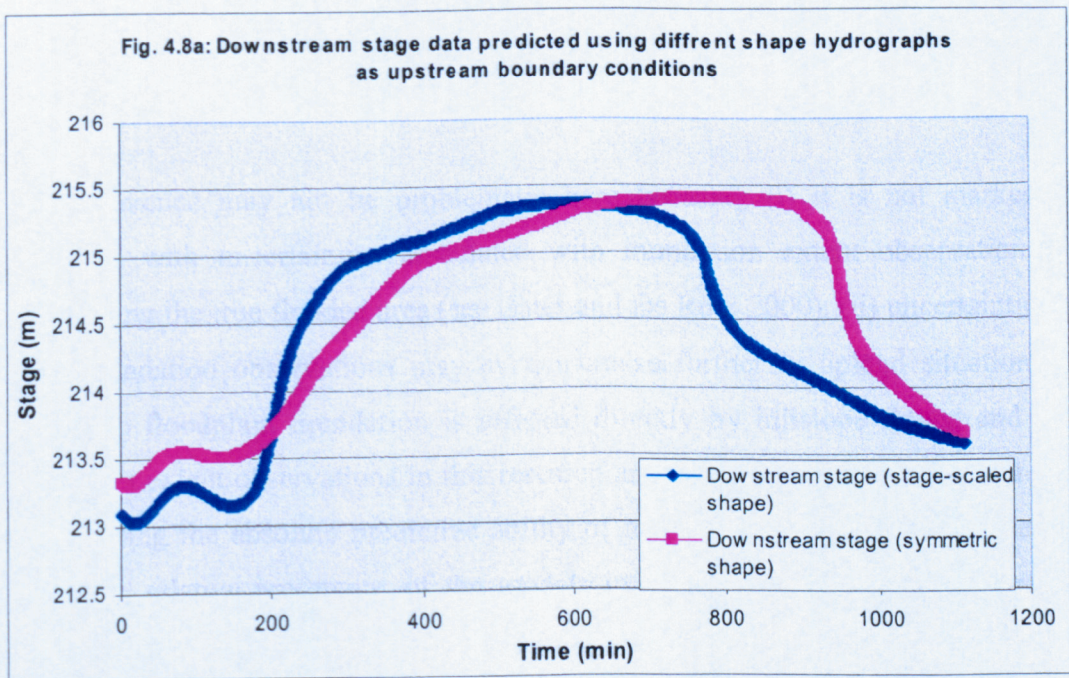
The maximum inundation extent predicted using inflow hydrographs with the symmetric and stage-scaled shapes are presented in Figure 4.8b. Comparison of the predicted inundation extents shows that the symmetric shape of inflow hydrograph is associated with a 2.5% increase in flooded area.

Figure 4.8b: comparison of inundation area due to change in inflow hydrograph shape, (a) stage-scaled shape and (b) symmetric shape.
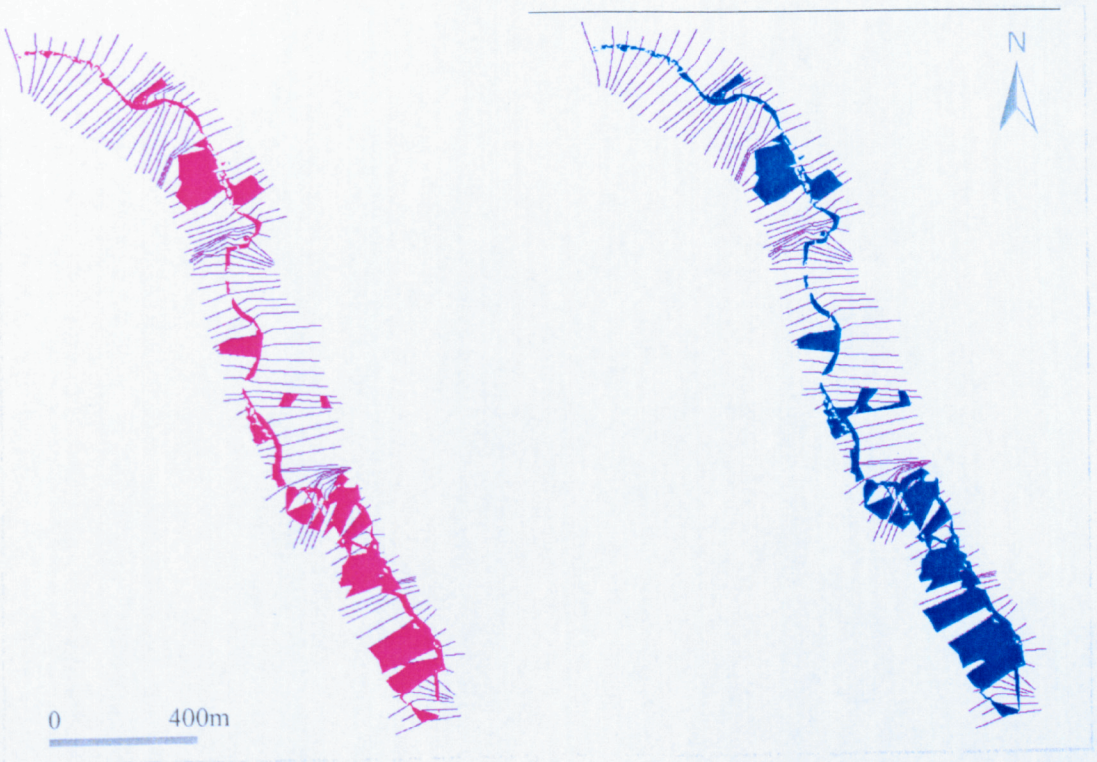
This difference may not be problematic here because; (i) it is not marked as compared with uncertainties associated with inundation extent observations in representing the true flooded area (see Bates and De Roo, 2000), (ii) uncertainties in flood inundation observations may even increase further in upland situations in which the floodplain inundation is affected directly by hillslope flows; and (iii) inundation extent observations in this research are not assigned as a single date set for assessing the absolute predictive ability of models used but it will be used to assess the relative preference of the models in relation to inundation prediction. Hence, the shape of the flow hydrograph as the upstream boundary condition in all hydraulic models in this research is based upon the stage record for the Hubberholme gauging station scaled to a peak discharge of $47.73m^3/s$ (Fig. 4.8).

4.10 Sensitivity analysis of HEC-RAS in normal mode for this study site

It is of paramount importance that model response (HEC-RAS in normal mode) is explored in such a way that an acceptable level of domain representation is

achieved. This requires sensitivity analysis so that; (i) it can be established that the model is physically representative of the domain of the study site and responds in a realistic way in response to representative variation of model input data and boundary conditions (e.g. Lane *et al.*, 1994); (ii) when the model is calibrated against the observed data, parameters to which the model is most sensitive have been identified (e.g. Beven 1979, Lane and Richards 2001); and (iii) the assessment of the likely magnitude of error in a model prediction that arises from a particular parameter specification is established (e.g. *Lane et al.*, 1994, Lane and Richards 2001). In order to assess these, sensitivity analysis is the process of varying: (i) model physical parameters over a reasonable range; and (ii) numerical solver elements; in order to observe the relative change in model response. Typically, the observed changes in water stage, flow rate, inundation extent and model stability are noted (Bates *et al.*, 1998).

4.10.1 Sensitivity analysis variables

In this case study, scenarios based upon physical parameters, boundary conditions and elements associated with numerical solution (parameters that might affect numerical solution) were selected for sensitivity analysis. In this case, we isolated: (i) a reasonable range of Manning's *n* values; (ii) the effect of boundary condition variation by using a range of statistical flood events at the upstream and downstream ends; and (iii) elements associated with numerical solution include various time and distance intervals (time step and cross section spacing respectively). There are other physical parameters that can be involved in sensitivity analysis. These are friction slope at the downstream boundary (i.e. a downstream boundary condition) and expansion and contractions coefficients. The effects of these two parameters on flow characteristics and model behaviour was significantly less than others. The effects of friction slope were removed by placing the downstream boundary far enough from the study domain so that any effects were not noted in the study domain. In terms of contraction and expansion coefficients, as there is no sharp change in river configuration, it was found that they had a negligible impact on flow characteristics for this study site.

The Manning's *n* values were estimated using Equation (4.37) and consideration of previous studies'*n* values (JBA, 2000). Given them, the range 0.035-0.055 was

chosen for sensitivity analysis purpose. In the same way, a range of 0.04-0.08 was selected for Manning's *n* values for floodplain area.

The flood event of the 4th of February 2004, which was identified as the main flood event for the research, was of the scale of a 1 in 0.5 year event, based on previous hydrological analysis in this catchment (JBA, 2000). However, flood events with higher return periods were included for sensitivity analysis in order to check the scope of the model's ability as a predictive tool for this study site. Using growth factors for Upper Wharfe, flood events with 2-, 5-, and 10-year return periods were developed for Hubberholme, with magnitudes of 70.4, 92.8 and 108.5m^3/s respectively.

Assessment of the effects of spatial and temporal resolution on model outputs is rarely explored in hydraulic models. Hence, there is no template for testing spatio-temporal resolution but it should be tested in order to gain optimal solution. In terms of computational intervals, consideration must be taken to avoid instabilities in the solution. The computational interval should be small enough to describe accurately the rise and fall of the hydrographs being routed. Consideration must also be given to hydraulic structures, such as bridges, culverts, weirs and gated spillway. The structures result in abrupt changes in stage and flow at specific times. For example, when flow just begins to go over a lateral weir, the change in stage and flow can be dramatic. These types of rapid changes can cause instability. The only solution to this problem is to shorten the computational interval.

In terms of computational time, the largest time step for which the model remains stable and solves the equations accurately should be selected. On the other hand, smaller time steps should be chosen if results change significantly between time steps even if the model remains stable. HEC-RAS provides a basis for selecting a suitable time step. As long as the Courant Condition is satisfied, the corresponding time step provides model stability and accuracy. However, it can be restrictive and the user may have to use very short time steps to satisfy it even when longer time steps will still maintain stability and accuracy (Eq. 4.39).

$$C = V_W \frac{\Delta t}{\Delta x} \leq 1.0 \qquad \text{Therefore} \qquad \Delta t \leq \frac{\Delta x}{V_W} \qquad \text{(Eq. 4.39)}$$

where C is the Courant Number, V_w is the flood wave speed, which is normally greater than the average velocity, Δt is the computational time step, and Δx is distance between cross sections.

Another way to set a practical computational time step for medium and large rivers is as follows (HEC-RAS, Users Manual, 2000):

$$\Delta t \le \frac{T_r}{20} \qquad \text{(Eq. 4.40)}$$

where T_r is the time of rise of the hydrograph to be routed.

In other words, if the flood wave goes from its base to its peak in 20 hours, then the computational interval should be equal to or less than 1 hour. Given the flood considered for the research, the computational time is approximated 15 minutes. Based upon this estimation a range of computational time steps including 1sec, 30sec, 1min, 15min and 30min were selected as variables for the sensitivity analysis.

In terms of distance intervals (in this case cross section spacing), three scenarios are established using linear interpolation between the surveyed cross sections. These include cross section spacings up to 50m, up to 120m and up to 200m (original surveyed cross sections).

4.10.2 Sensitivity analysis results: downstream friction slope and expansion and contraction coefficients

As noted before, as there are no measured data at the downstream end of the study site. Normal Depth (Manning Equation) was chosen as the downstream boundary condition in normal mode of HEC-RAS in this research. This method estimates a stage for each computed flow and hence, its effect is limited to stage calculations at downstream. To use the method, an estimate of friction slope at the downstream boundary is required. It is usually assumed to be equal to bed slope. A range of 0.01-0.0005 was chosen for sensitivity analysis purposes. The effect of friction slope on stage calculations for the event considered here is shown in Figure 4.9. As seen, the scope of effectiveness of the factor is only limited to the first 700 m

upstream from downstream boundary and afterwards there is no difference in estimated stage profiles using different friction slopes. In addition, the comparison of a number of observed stage data against the estimated stage values is shown in Figure 4.9. Accordingly, the value of 0.0005 can be considered as the best estimate for friction slope downstream of the study site.

Fig. 4.9: The effect of friction slope on downstream stage data where normal depth is used as downstream boundary condition
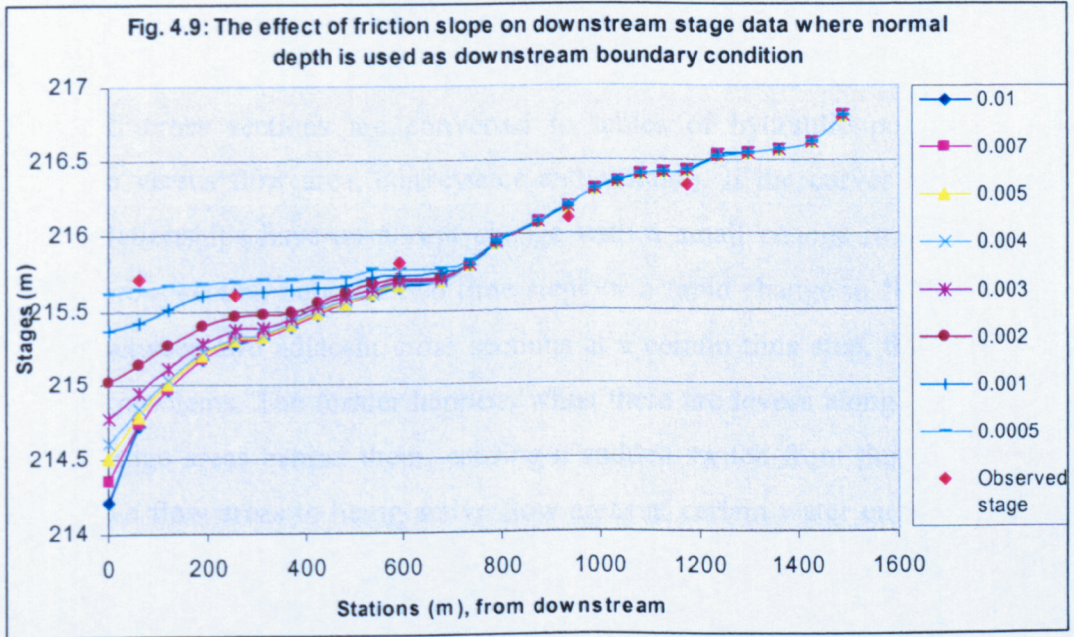
Considering Table 4.1 there are four options to choose values for Expansion and Contraction coefficients. Scenarios were designed using the whole range of the coefficients to check their effects on the model output. No marked change was seen in the model output due to change of Contraction and Expansion coefficients. Hence, the recommended values for gradual transitions (HEC-RAS, Hydraulic Reference, 2001) will be used for actual simulations

4.10.3 Sensitivity analysis results: stability

Table 4.4 presents the simulations performed for sensitivity analysis of HEC-RAS in the normal mode for this specific study site, using a physical parameter, n, boundary condition, upstream inflow hydrograph, and elements associated with numerical sensitivity, distance and time intervals. The floodplain's n value was left constant at 0.06 at this stage in the sensitivity analysis as negligible sensitivity was

found (see 4.11.5). As shown in Table 4.4, 180 scenarios were defined to simulate the behaviour of the model in relation to scope of stability and feasibility of the model, the effects of the main channel friction (in here Manning's n) on bulk flow data (in here downstream flow and stage data), and the effects of distance intervals and time steps on the model's results.

An unstable numerical model is one for which certain types of numerical errors grow to the extent to which the solution begins to oscillate or the errors become so large that the computations cannot continue. In a one-dimensional model like HEC-RAS, all cross sections are converted to tables of hydraulic properties (flow elevation versus flow area, conveyance and storage). If the curves that represent these relationships have an abrupt change with a small change in elevation at a certain cross section between two time steps or a rapid change in flow hydraulics occurs between two adjacent cross sections at a certain time step, they may cause stability problems. The former happens when there are levees along the river with large storage areas behind them, causing a sudden switch from these areas being ineffective flow areas to being active flow areas at certain water elevations within two continuous time steps. Instability often happens when the model goes to critical depth at a certain cross section, causing over-estimation and under-estimation of the depth at the next cross section upstream and down-stream respectively. It, in turn, causes the changes in flow area, flow depth and flow velocity to become too high and the model becomes unstable.

Table 4.4: Simulations performed for sensitivity analysis of HEC-RAS in normal mode in the study site, using flood magnitude, main channel friction, time steps and cross section spacing variables.

1 in 0.5 flood	Manning's n 0.035					Manning's n 0.045					Manning's n 0.055				
spacing	1 sec	30 sec	1 min	15 min	30 min	1 sec	30 sec	1 min	15 min	30 min	1 sec	30 sec	1 min	15 min	30 min
Up-to 50m	1*	2	3	4	5	6	7	8	9	10	11	12	13	14	15
Up-to 125m	16	17	18	19	20	21	22	23	24	25	26	27	28	29	30
Up-to 200m	31	32	33	34	35	36	37	38	39	40	41	42	43	44	45

1 in 2 flood	Manning's n 0.035					Manning's n 0.045					Manning's n 0.055				
Spacing	1 sec	30 sec	1 min	15 min	30 min	1 sec	30 sec	1 min	15 min	30 min	1 sec	30 sec	1 min	15 min	30 min
Up-to 50m	46	47	48	49	50	51	52	53	54	55	56	57	58	59	60
Up-to 125m	61	62	63	64	65	66	67	68	69	70	71	72	73	74	75
Up-to 200m	76	77	78	79	80	81	82	83	84	85	86	87	88	89	90

1 in 5 flood	Manning's n 0.035					Manning's n 0.045					Manning's n 0.055				
Spacing	1 sec	30 sec	1 min	15 min	30 min	1 sec	30 sec	1 min	15 min	30 min	1 sec	30 sec	1 min	15 min	30 min
Up-to 50m	91	92	93	94	95	96	97	98	99	100	101	102	103	104	105
Up-to 125m	106	107	108	109	110	111	112	113	114	115	116	117	118	119	120
Up-to 200m	121	122	123	124	125	126	127	128	129	130	131	132	133	134	135

1 in 10 flood	Manning's n 0.035					Manning's n 0.045					Manning's n 0.055				
Spacing	1 sec	30 sec	1 min	15 min	30 min	1 sec	30 sec	1 min	15 min	30 min	1 sec	30 sec	1 min	15 min	30 min
Up-to 50m	136	137	138	139	140	141	142	143	144	145	146	147	148	149	150
Up-to 125m	151	152	153	154	155	156	157	158	159	160	161	162	163	164	165
Up-to 200m	166	167	168	169	170	171	172	173	174	175	176	177	178	179	180

Stable simulation   Unstable simulation

* Numbers are attributed to file referencing in the hydraulic model.

The results presented in Table 4.4 indicate that, as the magnitude of floods increase, the stability of the model generally decreases. It means that the model is more feasible for smaller floods than floods with return periods bigger than 5 years in this particular reach. However, the stability of the model for smaller floods is not unconditional and it depends upon certain combinations of distance intervals, time steps and main channel friction. The model is unconditionally unstable for higher cross section spacings (up-to-200m), but the results show that there is no major

123

difference between spacings of up-to-125 m and up-to-50 m for smaller flood magnitudes (1 in 0.5 and 1 in 2 floods) in relation to model stability. Hence, the cross section spacing of up-to-125m may be accepted as the optimal representation of geometry of the study site: the largest spacing that produces stable solutions. Stability can be achieved by selecting a time step that satisfies the Courant condition within reasonable cross section spacing and main channel friction values, which affects the Courant condition as well.

As low and high values of Manning's n applied within the reasonable range of flood magnitudes (flood smaller than 5-year return periods) produce stable simulations under different combinations with other factors, there is no clear preference over main channel friction values in relation to model stability. It means that this range of Manning's n values can be used for calibration.

4.10.4 Sensitivity analysis results: the effects of cross-section spacing on bulk flow characteristics

The effects of cross-section spacing on the downstream bulk flow characteristics are investigated. The two cross-section spacings of up-to-50 m and up-to 125 m along with three different main channel n values (0.045, 0.055 and 0.065) and the flood magnitudes of 0.5 and 2 year return periods are considered. As simulations that are associated with the cross-spacing of up-to-200 m and the 1 in 5 years flood were numerically unstable (see Table 4.4), they are not considered here. Table 4.4-1 presents the simulations considered here and provides a framework for comparing the effects of cross-section spacing on the downstream bulk flow characteristics with respect to the flood magnitude and friction value. The floodplain friction factor remained unchanged for these scenarios.

Table 4.4-1: A framework considered for investigating the effects of cross section spacing on flow characteristics.

Cross section spacing	50m			125m		
n	0.045	0.055	0.065	0.045	0.055	0.065
1 in .5 years flood	S1*	S2	S3	S4	S5	S6
1 in 2 years flood	S10	S11	S12	S13	S14	S15

Stable simulation
Unstable simulation
* Numbers are attributed to file referencing in the hydraulic model

Figures 4.9-1 to 4.9-4 show the changes of downstream stage and flow hydrographs in response to different cross-section spacing, main channel *n* value and flood magnitude. The results show that changes of bulk flow characterises due to the change in cross-section spacing are negligible and these characteristics dominantly controlled by flood magnitude and main channel friction factor in this particular case study.

Figure 4.9-1: The effects of cross section spacing on the buld downstream flow characteristics using the n channel 0.055 and the 1 in 0.5 years flood

Figure 4.9-2: The effects of cross section spacing on the bulk downstream flow characteristics using the n channel 0.065 and the 1 in 0.5 years flood

Figure 4.9-3: The effects of cross section spacing on the bulk downstream flow characteristics using the n channel 0.045 and the 1 in 2 years flood

Figure 4.9-4: The effects of cross section spacing on the bulk downstream flow characteristics using the n channel 0.055 and the 1 in 2 years flood

4.10.5 Sensitivity analysis results: the effect of main channel friction on bulk flow characteristics

A feasible range of Manning's *n* for the main channel was selected to analyse the sensitivity of the model performance in relation to bulk flow characteristics. The channel friction was changed from a starting value of 0.035 and increased in increments of 0.005 up to a maximum value of 0.06. If the corresponding values are taken from Table 2.2 allowing actual qualitative description to be applied to the values, the channel are changed from '*clean, straight, full stage with no riffles or*

126

pools' through to *'stony, weedy with pools'*. The floodplain's *n* value remains constant at an *n* value of 0.06.

If the output flow and stage hydrographs are analysed (see Figure 4.10 and 4.11) it is clear that the main channel friction factor controls the bulk output characteristics. By increasing the channel from a natural smooth channel (low Manning's n values) to a hydraulic rough channel (high Manning's n values) there are major changes in peak flow and stage values, trends in the rising and declining limbs of flow and stage hydrographs, and timings of peak flows and stages.

Fig. 4.10: The effect of channel friction on the outflow hydrographs (cross section 416)

Fig. 4.11: The effect of channel friction on the output stage hydrographs (cross section 416)
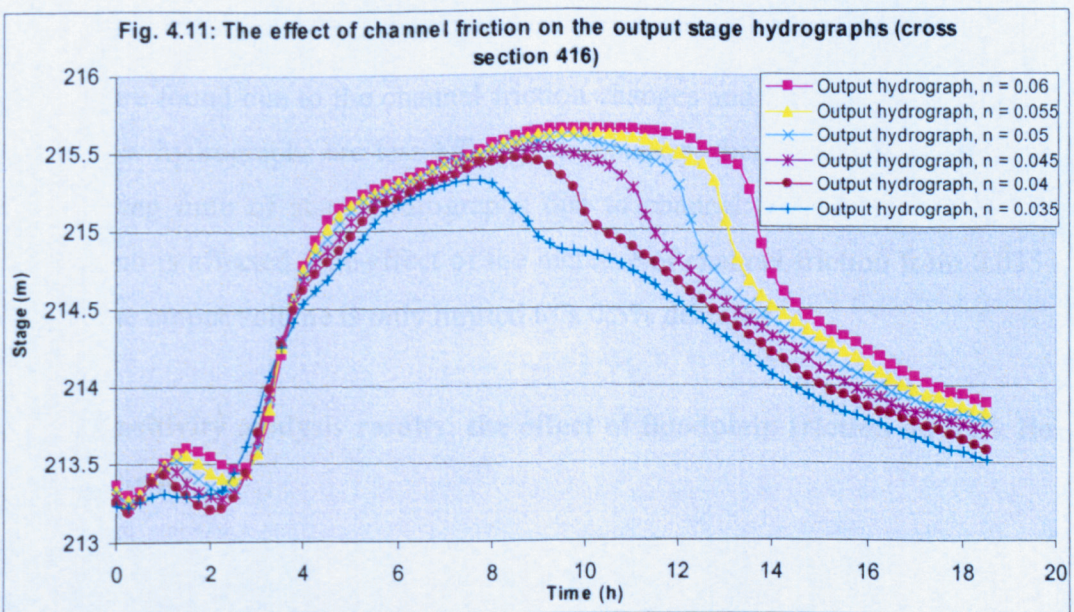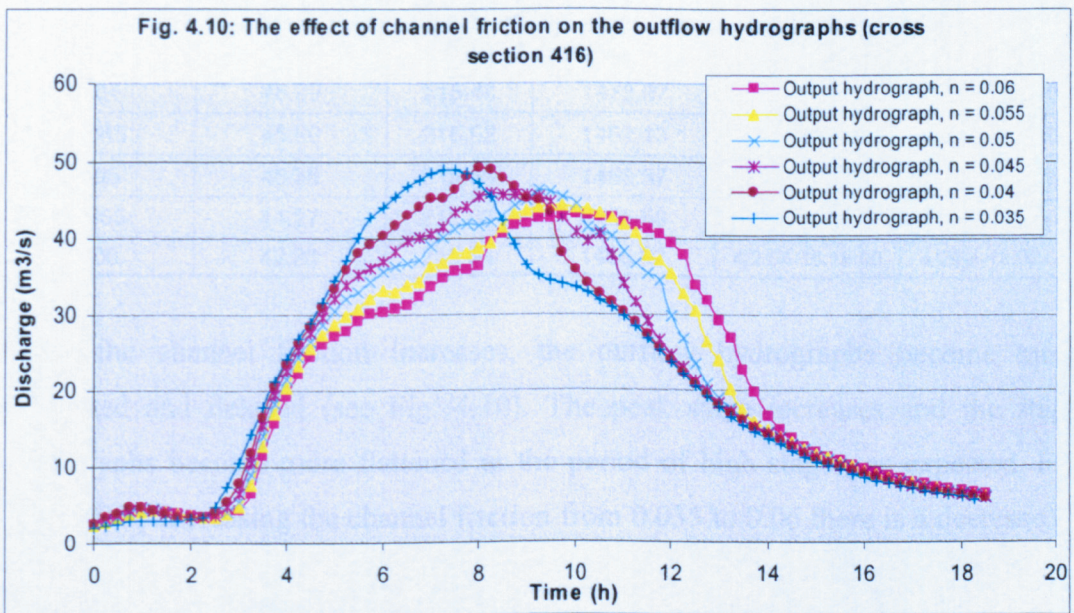
It should be noted that the downstream hydrographs used to investigate the effects of main channel friction variation on flow characteristics were upstream of the influence of the downstream boundary condition.

The changes can be observed if Table 4.5 is studied summarising the other bulk flow characteristics.

Table 4.5: The effect of channel friction on bulk flow characteristics in normal mode of HEC-RAS

Channel friction (Manning's n)	Peak Discharge (m3/s)	Peak stage (m)	Output volume (1000 m3)	Real time of peak flow	Real time of peak stage
0.035	48.89	215.31	1474.34	4/2/04-15:45:00	4/2/04-15:45:00
0.04	48.99	215.46	1473.07	4/2/04-16:15:00	4/2/04-16:45:00
0.045	45.69	215.52	1462.13	4/2/04-16:30:00	4/2/04-17.15:00
0.05	46.25	215.59	1468.37	4/2/04-17:30:00	4/2/04-17:45:00
0.055	44.27	215.62	1465.56	4/2/04-18:00:00	4/2/04-18:00:00
0.06	42.99	215.64	1466.92	4/2/04-18:15:00	4/2/04-18:00:00

When the channel friction increases, the outflow hydrographs become more attenuated and delayed (see Fig. 4.10). The peak stage increases and the stage hydrographs become more flattened at the period of high stages, as expected. For instance, by increasing the channel friction from 0.035 to 0.06 there is a decrease of 12.1% in the peak discharge (from 48.89 to 42.99 m^3/s), an increase of 33cm in the peak stage (from 215.31 to 215.64m) and a delay of 2-2.5h in relation to time to peak flow and stage. The central 50% of outflow hydrographs are where most changes are found due to the channel friction changes and the first and last 25% of the outflow hydrographs are less affected. In contrast, there is no major difference in the rising limb of stage hydrographs due to channel friction changes but the falling limb is affected. The effect of the increase of channel friction from 0.035 to 0.06 on the output volume is only limited to a 0.5% decrease.

4.10.6 Sensitivity analysis results: the effect of floodplain friction on bulk flow characteristics

The floodplain Manning's n was increased in increments of 0.01, from 0.03 up to 0.08. This range, given Table 2.2, represents floodplains associated with 'short grasses' to 'Medium to dense brush in summer'. To analyse the effect of floodplain

friction on the bulk flow characteristics the main channel friction was kept constant at the value of 0.05 (Manning's $n = 0.05$). If the output flow and stage hydrographs are studied (see Figures 4.12 and 4.13), using a 1 in 0.5 flood event (peak flow 47.73 m^3/s), it is seen that there is no considerable change in outflow hydrographs due to floodplain friction changes. The consequence of changing the floodplain friction on output stage hydrographs is even more limited.

Fig. 4.12: The effect of floodplain friction on the outflow hydrograph, using a 1 in 0.5 flood event (cross section 416)

Fig. 4.13: The effect of floodplain n on output stag hydrograph, using a 1 in 0.5 flood event (cross section 416)
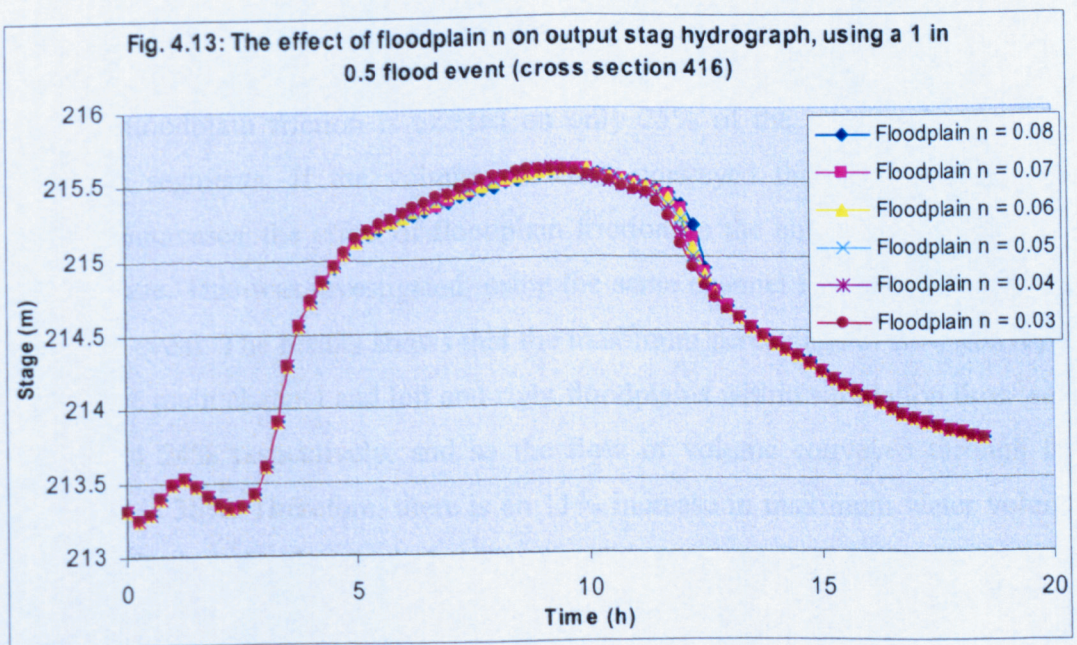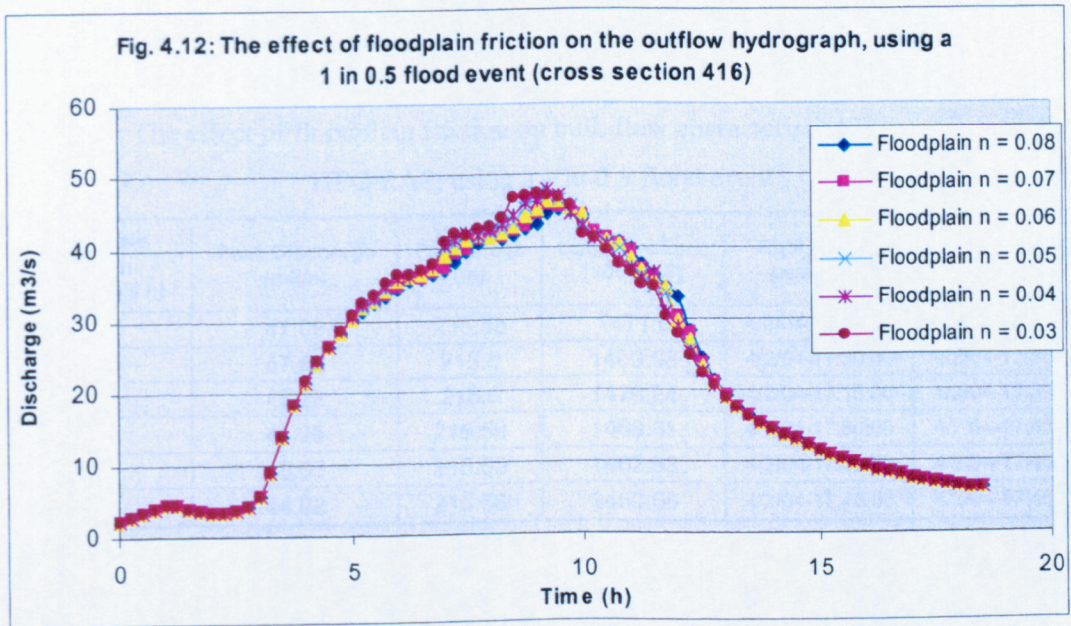
More details of output bulk flow characteristics are predicted in Table 4.6. By increasing the floodplain friction factor from 0.03 to 0.08 there is a reduction in the peak values of the outflow hydrographs by 2.01m^3/s (4.5%) whereas there is no change in peak stages. Comparison of output water volume changes due to the floodplain friction increase from 0.03 to 0.08 shows a decrease of 0.8%. In addition, the effect of floodplain friction change on the timing of peak flows and stages at the downstream boundary is constrained to only a range of 15 to 30 minutes and there is no major shift in the time to the flow and stage peaks.

Table 4.6: The effect of floodplain friction on bulk flow characteristics in normal model of HEC-RAS, using a 1 in 0.5 flood event

Floodplain friction (Manning's n)	Peak Discharge (m3/s)	Peak stage (m)	Output volume (1000 m3)	Real time of peak flow	Real time of peak stage
0.03	47.09	215.58	1471.6	4/2/04-17:15:00	4/2/04-17:30:00
0.04	47.67	215.6	1469.98	4/2/04-17:30:00	4/2/04-17:30:00
0.05	47.28	215.6	1470.24	4/2/04-17:15:00	4/2/04-17:30:00
0.06	46.25	215.59	1468.31	4/2/04-17:30:00	4/2/04-17:45:00
0.07	45.53	215.59	1462.83	4/2/04-17:30:00	4/2/04-17:45:00
0.08	44.98	215.58	1460.58	4/2/04-17:45:00	4/2/04-17:45:00

These results are achieved when the main channel Manning's n remains constant with a value of 0.05. Using this value of n and a 1 in 0.5 flood event at the study site, the maximum percentage of flow conveyed through main channel and left and right floodplains are estimated as 75, 9 and 16% at a certain time step. It means the effect of floodplain friction is exerted on only 25% of the water volume of the floodplain segments. If the volume of water conveyed through the floodplain segments increases, the effect of floodplain friction on the bulk flow characteristic may increase. This was investigated, using the same channel friction factor and a 1 in 2 flood event. The results shows that the maximum percentage of flow conveyed through the main channel and left and right floodplains within simulation time were 64, 12 and 24% respectively, and so the flow of volume conveyed through the floodplain is 36%. Therefore, there is an 11% increase in maximum water volume conveyed through the floodplain in a flood with two-year return period. Figure 4.14 and 4.15 show the consequence of floodplain friction changes on the downstream flow and stage hydrographs respectively. Comparison of Figure 4.14 and 4.15 with 4.12 and 4.13 indicates that there is a similar behaviour of bulk flow characteristics

due to floodplain friction changes despite an 11% increase in floodplain flow volume at maximum state.

Fig. 4.14: The effect of floodplain friction on outflow hydrographs, using a 1 in 2 flood event (cross section 416)

Legend:
- Floodplain n = 0.05
- Floodplain n = 0.06
- Floodplain n = 0.07
- Floodplain n = 0.08

Y-axis: Discharge (m3/s)
X-axis: Time (h)
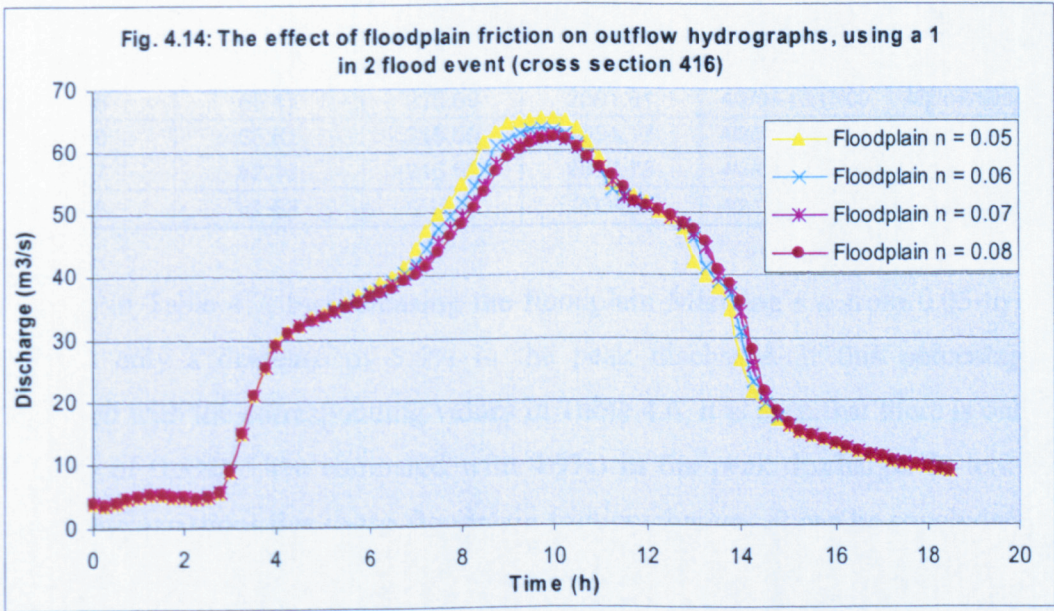
More details of bulk flow characteristic changes due to floodplain friction changes are shown in Table 4.7. Table 4.7 presents the results of simulations that are numerically stable.

Fig.4.15: The effect of floodplain friction on output stage hydrographs, using a 1 in 2 flood event (cross section 416)

Legend:
- Floodplain n = 0.05
- Floodplain n = 0.06
- Floodplain n = 0.07
- Floodplain n = 0.08

Y-axis: Stage (m)
X-axis: Time (h)

131
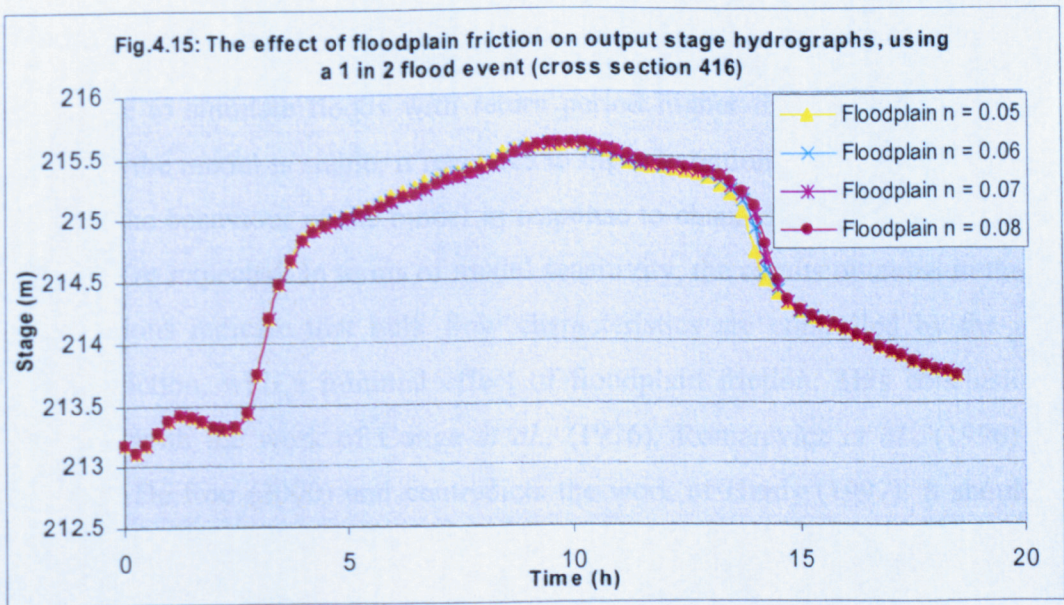
Table 4.7: The effect of floodplain friction on bulk flow characteristics in normal model of HEC-RAS, using a 1 in 2 flood event

Floodplain friction (Manning's *n*)	Peak Discharge (m3/s)	Peak stage (m)	Output volume (1000 m3)	Real time of peak flow	Real time of peak stage
0.05	65.17	215.59	2081.61	4/2/04-18:15:00	4/2/04-18:15:00
0.06	63.61	215.59	2054.17	4/2/04-18:00:00	4/2/04-18:00:00
0.07	62.16	215.59	2037.73	4/2/04-18:15:00	4/2/04-18:15:00
0.08	61.63	215.6	2034.8	4/2/04-18:15:00	4/2/04-18:15:00

As seen in Table 4.7, by increasing the floodplain Manning's *n* from 0.05 to 0.08 there is only a decrease of 5.4% in the peak discharge. If this percentage is compared with the corresponding values in Table 4.6, it is seen that there is only an increase of 0.5% (5.4% compared with 4.9%) in the peak discharge. In terms of peak stage variations due to the floodplain friction changes, it can be concluded that flood plain friction has no effect on the downstream peak stages for flood magnitude considered here. Similar to Table 4.6, no major shift in the timing of peak flow and stage hydrographs is seen.

4.10.7 Sensitivity analysis: discussion

Model behaviour reveals that the model does not simulate processes in a realistic way in response to reasonable variation in model input data. For instance, the model is not able to simulate floods with return period higher than 5 years. Within the range that the model is stable, it responds to input variations in a realistic way. For instance, the behaviour of the model in response to channel and floodplain friction changes is as expected. In terms of model sensitivity, the results obtained in the last three sections indicate that bulk flow characteristics are controlled by the main channel friction, with a minimal effect of floodplain friction. This conclusion is consistent with the work of Cunge *et al.*, (1976), Romanwicz *et al.*, (1996) and Bates and De Roo (2000) and contradicts the work of Hardy (1997). It should be noted that models used by these researchers are based upon different physical process. For instance, Bates and De Roo (2000) used a two-dimensional diffusion wave treatment for floodplain flows whereas Hardy (1997) applied TELEMAC-2D that solves second order partial differential equations for depth averaged free surface flow derived from the full three-dimensional Navier Stokes equations. It is

obvious that different process inclusion in each model would mean that the friction value has a different physical meaning. In a 1D model, the friction term accounts for the energy loss due to planform variations including the effects of lateral shear, secondary flows and bed friction. For a 2D finite element model these losses are represented directly in the domain geometry at the element scale and only subsumed within the friction term at the sub-grid cell (see Knight and Shiono, 1996, Horritt and Bates, 2000). Thus, although the effect of friction coefficients on bulk flow characteristics cannot absolutely be compared between different physically-based models, it can be concluded that in one-dimensional models the effects of main channel friction on bulk flow characteristics are dominant.

4.11 Calibration and Validation of HEC-RAS in normal mode

Given the results of the sensitivity analysis presented in this chapter, friction coefficients for the channel and floodplain remain unconstrained and therefore are treated as calibration coefficients for the model. Although this is likely to be a major source of model error, the lack of alternative techniques for parameterising friction means that calibration is currently the only way forward. The extent and dimensionality of the parameter spaces were determined given the sensitivity analysis undertaken. Manning's n values for the channel range from 0.04 to 0.06 with increments of 0.005. Values for the floodplain range from 0.04 to 0.07 with increments of 0.01. This enables the full range of possible friction values to be explored in relation to optimum calibration. Given the aim of the research, which is the comparison of the predictive ability of models used in relation to inundation extent, the model calibration is performed versus the observed inundation data.

The flood event that happened on the 4th February 2004 with a peak flow of 47.73 m^3/s and a 18.5h duration (see Chapter3) was used as the upstream boundary condition in the study reach. The boundary of inundation extent was collected using RTK GPS at the time of flooding. Before the calibration can be performed, analysis techniques must be defined to perform an accuracy assessment between the predicted and observed flood extent, as it is this measure that will be optimised by the calibration process. The next section describes the basic analysis techniques needed to perform an accuracy assessment.

4.11.1 Application of accuracy assessment of the model results

As previously mentioned, HEC-RAS in normal mode was used to predict the maximum inundation extent at the study site, using a flood wave with a peak discharge 47.73m^3/s and 18.5h duration on the 4th February 2004. The model was calibrated using Manning's n values for the channel ranging from 0.04 to 0.07, with increments of 0.005, and for the floodplain ranging from 0.04 to 0.07, with increments of 0.01. Theses ranges were selected given the results of the sensitivity analysis undertaken in the previous section. The predicted water levels at each cross section are converted to inundation extent via a secondary processing step using HEC-GeoRAS. The resultant inundation extents are validated against the observed inundation extent resulting from the flood event 4th February 2004 (see Chapter 3).

Model performance was assessed using the four accuracy measures described in Chapter 3. To do that, inundated areas predicted using HEC-GeoRAS for all simulations performed here and also inundated areas observed using RTK GPS were converted to grids with the same pixel size in order to calculate the content of error matrices associated with each simulation. Figure 4.16 presents the maximum inundation extent predicted using the normal mode of HEC-RAS for the range of the Manning n values used in the main channel (from 0.04 to 0.07) and the n value of 0.06 for the floodplain area.
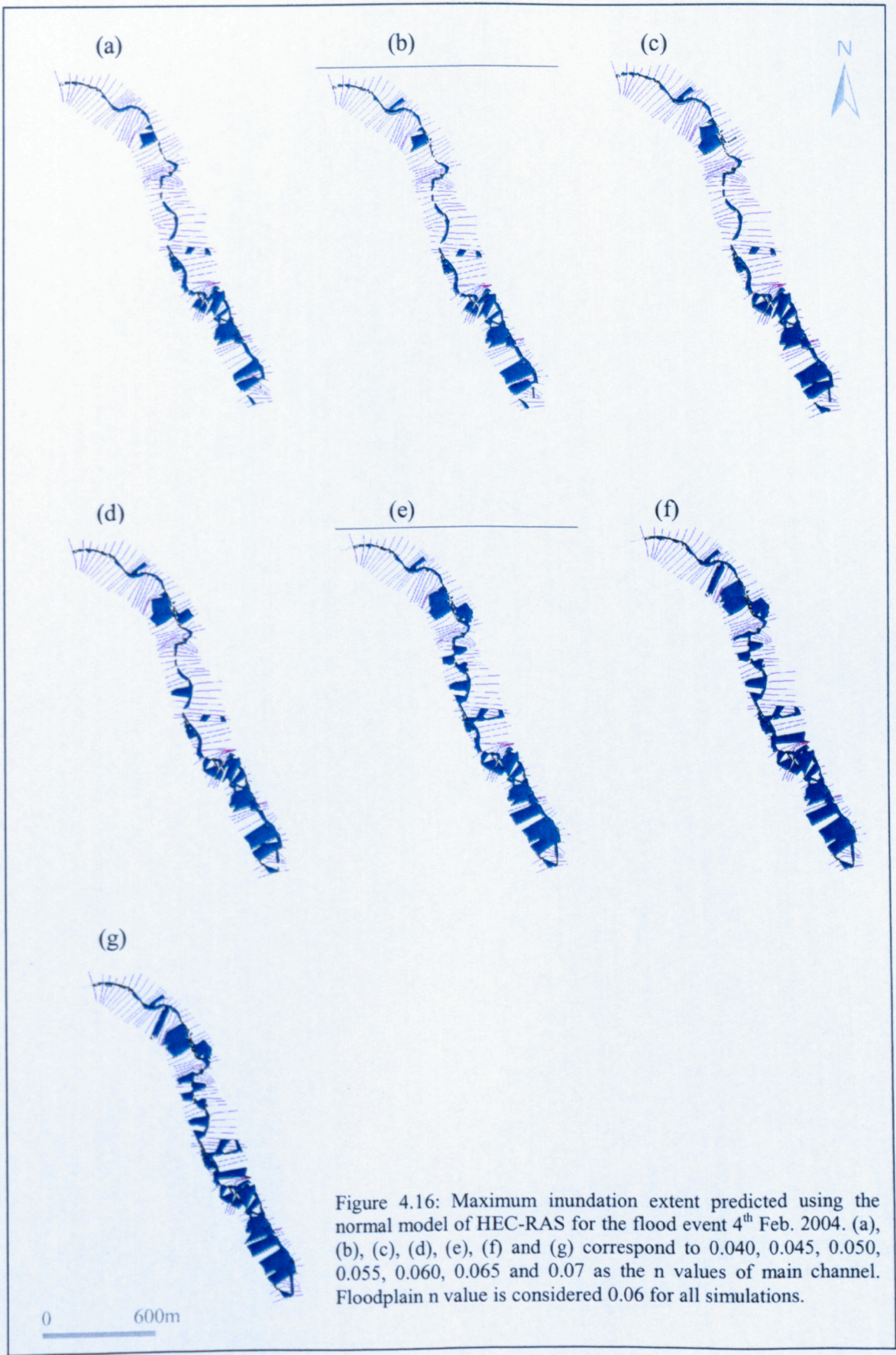
Figure 4.16: Maximum inundation extent predicted using the normal model of HEC-RAS for the flood event 4th Feb. 2004. (a), (b), (c), (d), (e), (f) and (g) correspond to 0.040, 0.045, 0.050, 0.055, 0.060, 0.065 and 0.07 as the n values of main channel. Floodplain n value is considered 0.06 for all simulations.

0   600m

Table 4.8 presents the performance of the model in relation to inundation extent using the four different accuracy coefficients. As expected, the model is more sensitive to channel friction than floodplain friction in relation to inundation extent. For instance, by changing floodplain friction from 0.04 to 0.07 in simulations where the channel friction is 0.055, no improvements in the predictions of wet area are seen. However, for higher channel friction values, level of agreement is more sensitive. Indeed, by increasing main channel friction, more water is expected on the floodplain. At this state, floodplain friction plays a more effective role in the routing process of flow on the floodplain. It can explain the difference between the effect of floodplain friction at the top and bottom of Table 4.8. More importantly, by changing floodplain n values, no marked changes were noted in bulk flow characteristics (see Section 4.11.5) but accuracy statistics in relation to inundation extent is sufficiently affected by floodplain friction (see Table 4.8). This suggests that inundation extent does depend on floodplain n values. As mentioned before, as channel friction increases, the model improves in terms of agreement between the predicted and observed inundation data. This is regardless of the kind of accuracy assessment method used. The agreement between the predicted and observed inundation data may be improved by using even higher n values in the main channel (i.e. higher water elevation and in turn, more water on the floodplain and more inundation). Thus, having a high agreement value in Table 4.8 does not necessarily mean optimal results in terms of inundation extent prediction. Hence, the model performance, given in Table 4.8, is uncertain and must be verified using numerical performance and other validation data as well.

Table 4.8: Accuracy assessments undertaken for HEC-RAS in normal mode in relation inundation extent

n (channel)	Accuracy method	n (floodplain)			
		0.04	0.05	0.06	0.07
0.04	Overall accuracy	0.51	0.54	0.54	0.54
	Kappa analysis	0.14	0.17	0.17	0.17
	Conditional Kappa	0.07	0.10	0.10	0.10
	Fit	0.18	0.22	0.22	0.22
0.045	Overall accuracy	0.52	0.54	0.54	0.54
	Kappa analysis	0.15	0.18	0.19	0.19
	Conditional Kappa	0.08	0.11	0.11	0.11
	Fit	0.21	0.25	0.25	0.25
0.05	Overall accuracy	0.57	0.57	0.57	0.57
	Kappa analysis	0.22	0.22	0.22	0.22
	Conditional Kappa	0.13	0.13	0.13	0.13
	Fit	0.29	0.30	0.30	0.30
0.055	Overall accuracy	0.59	0.59	0.59	0.59
	Kappa analysis	0.25	0.25	0.25	0.25
	Conditional Kappa	0.15	0.15	0.15	0.15
	Fit	0.34	0.34	0.34	0.34
0.06	Overall accuracy	0.68	0.67	0.64	0.64
	Kappa analysis	0.39	0.38	0.33	0.32
	Conditional Kappa	0.27	0.26	0.22	0.21
	Fit	0.50	0.49	0.44	0.43
0.065	Overall accuracy	0.77	0.75	0.73	0.72
	Kappa analysis	0.47	0.46	0.43	0.42
	Conditional Kappa	0.36	0.34	0.33	0.31
	Fit	0.58	0.57	0.53	0.53
0.07	Overall accuracy	0.85	0.85	0.84	0.81
	Kappa analysis	0.53	0.53	0.51	0.49
	Conditional Kappa	0.42	0.40	0.37	0.36
	Fit	0.62	0.63	0.61	0.61

To make a definite judgement in relation to the predictive ability of the model, the numerical performance of the model can also be considered in terms of overall mass balance errors and computational efficiency. Mass balance errors for each combination of channel and floodplain friction values are calculated and presented in Table 4.9.

Table 4.9: computational performance and mass balance errors for HEC-RAS in normal model

mass balance test	n (floodplain)			
n (channel)	0.04	0.05	0.06	0.07
0.040	0.01	0.02	0.03	0.04
0.045	-0.01	0.01	0.01	0.01
0.050	0	0.01	0.01	0
0.055	0.01	0.01	0.01	0.02
0.060	0.02	0.05	0.03	0.01
0.065	0.02	0.05	0.02	0.02
0.070	0.03	0.04	0.03	0.02

As seen in Table 4.9, mass balance errors range from 0 to 0.05 m^3/s of the inflow hydrograph at the upstream boundary condition. There are no objective criteria to accept or reject a simulation given mass balance errors (Bates and De Roo, 2000) but the range observed here is less than errors that may be associated with the estimation of upstream boundary conditions, process representation in the model (i.e. neglect of infiltration, rainfall and runoff from hillslopes etc.). Therefore, the mass balance errors found here probably have a negligible effect on the predicted inundation extent.

To make a definite judgement in relation to the value of n that results in the best prediction of inundation area, comparisons between the maximum water levels predicted and observed during the flood for a number of points on the floodplain (i.e. internal validation) were conducted. Figure 4.16-1 shows the location of these points that were measured immediately after flooding as supplementary validation data. Table 4.10 presents the predicted maximum water levels using different n values against the observed data for the corresponding cross sections. The difference between the observed and predicted maximum water levels is presented as quantified values. It should be mentioned that the positive and negative values in the quantified values in Table 4.10 are considered as under-prediction and over-prediction of maximum water levels respectively on the floodplain.

Figure 4.16-1: Points at which maximum water elevation was measured after flooding
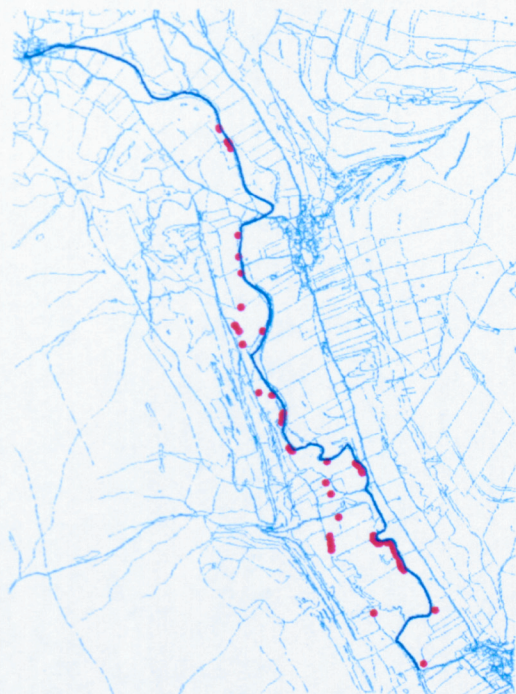
Table 4.10: Comparison of predicted and observed water elevation at a number of cross sections along the study reach

Cross section	Observed water level	Simulated water level n = 0.055	Absolute error n =0.055	Simulated water level n = 0.060	Absolute error n =0.060	Simulated water level n = 0.065	Absolute error n = 0.065	Simulated water level n = 0.070	Absolute error n = 0.070
4357	226.10	225.93	0.17	226.02	0.08	226.19	-0.09	226.22	-0.12
4263	225.80	225.69	0.11	225.76	0.04	225.85	-0.05	225.87	-0.07
4167	225.30	225.25	0.05	225.29	0.01	225.32	-0.02	225.36	-0.06
4120	225.00	225.11	-0.11	225.12	-0.12	225.13	-0.13	225.12	-0.12
3528	222.76	222.70	0.06	222.83	-0.07	222.84	-0.08	222.91	-0.15
3380	222.25	221.93	0.32	222.07	0.18	222.07	0.18	222.06	0.19
3324	221.89	221.70	0.19	221.81	0.08	221.83	0.06	221.88	0.01
2918	220.09	220.10	-0.01	220.23	-0.14	220.19	-0.10	220.22	-0.13
2179	218.25	218.11	0.14	218.16	0.09	218.18	0.07	218.17	0.08
1821	217.55	217.30	0.25	217.36	0.19	217.36	0.19	217.34	0.21
1470	216.60	216.61	-0.01	216.62	-0.02	216.64	-0.04	216.64	-0.04
1086	216.15	216.37	-0.22	216.40	-0.25	216.45	-0.30	216.43	-0.28
585	215.80	215.71	0.09	215.77	0.03	215.82	-0.02	215.81	-0.01
44	215.55	215.36	0.19	215.44	0.11	215.57	-0.02	215.56	-0.01
Mean			0.09		0.01		-0.03		-0.04
STDEV			0.14333		0.12527		0.125748		0.132

The statistics in Table 4.10 show that the minimum mean difference between the observed and predicted water levels is obtained using the n value of 0.06. Using the n value of 0.06, maximum water levels at the specified points are over-predicted by

0.01m in average. The comparison between the standard deviation obtained using different n values indicates that scenarios attributed to the n values of 0.06 and 0.065 have the lower standard deviation. Generally, the scenario that is attributed to the lower mean difference can be accepted as the best prediction. Therefore, as the prediction of water elevations along the study reach is of a higher accuracy using n values of 0.06, the inundation extent that is associated with that is assigned as the maximum ability of this model in relation to inundation extent prediction. Figure 4.17 shows the best agreement between the flooded areas predicted in normal mode of HEC-RAS, using the n values of 0.06 and 0.04 for main channel and floodplain respectively, and the flooded areas observed during flooding.

Fig. 4.17: Best-fit prediction of inundation extent using HEC-RAC in normal mode with the *n* values 0.06 and 0.04 for main channel and floodplain respectively for a flood with peak discharge of 47.73m³/s.
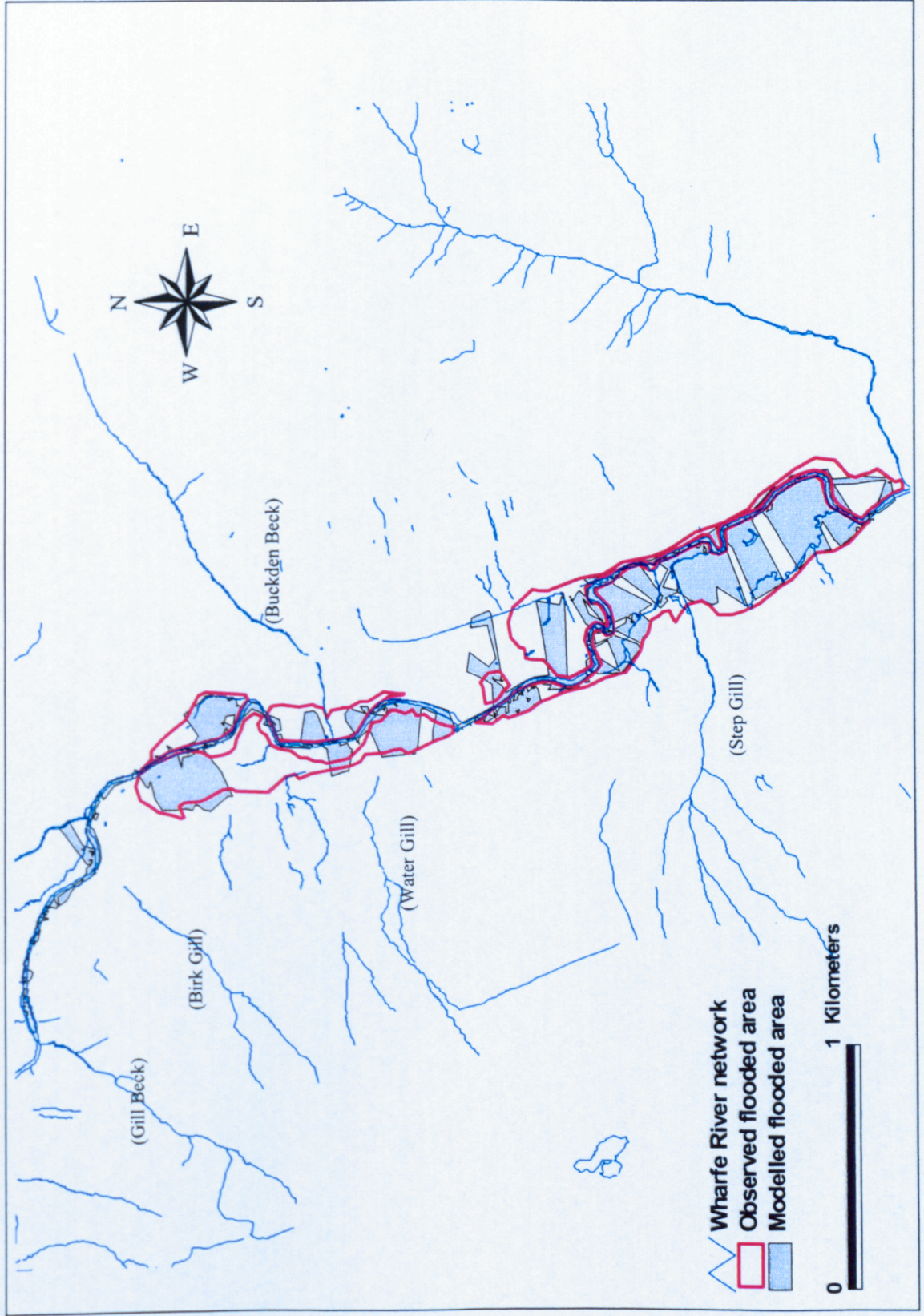
4.12 Discussion

HEC-RAS in normal mode was applied to a 5.5km upland section of the River Wharfe between the gauging stations of Hubberholme and Starbotton for the flood event that occurred in February 2004 with a peak flow of 47.73m3/s. Based on the sensitivity analysis results, the range of 0.04-0.07 with increments of 0.005 and 0.01 was selected as n values for the main channel and floodplain respectively. Considering a two-stage calibration, the model output was calibrated against the shorelines obtained using RTK GPS (see Figure 4.16-1), a number of photographs taken at the time flooding and a number of internal maximum water elevations measured during flooding within the study domain (see Figure 4.16-3). There were no measured flow and stage data at the downstream gauging station for validating the dynamic simulations of the reach. Model ability in relation to inundation extent prediction was assessed using accuracy agreement tests between predictions and observations, considering computational performance, and internal validation. Using HEC-GeoRAS, maximum water surface elevations calculated at each cross section of the model were overlaid onto a high resolution DEM (i.e. 2-meter resolution) to create inundation extents. Although the measure of the Conditional Kappa indicates the actual ability of a model for prediction of a specific category of predictions, for instance wet area, (see Section 3.7), the measure of Fit is chosen as it enables us to compare model performance for different modelled reaches and flood events (e.g. Bates and De Roo, 2000; Aronica et al., 2002). This measure is equal to 100% when the predicted and observed shorelines coincide. The best performance of the model correctly simulated 50%, ($F\%$), of inundated and non-inundated areas of the potential floodplain area (see Table 4.8). This is shown in Figure 4.17, which provides a comparison of model predicted inundation extent with the shorelines derived from GPS data. The model performance obtained here seems not to be promising when compared with performance of 69.5% of a planar approximation model applied to a 35 km reach of the River Meuse in The Netherlands, in which predictions were compared with air photography and SAR imagery (see Bates and De Roo, 2000). Horritt and Bates (2002) showed that model performance in terms of inundation extent is directly a function of the quality of validation data. The performance of HEC-RAS in terms of F reduced from 64.83%

to 41.79% in terms of optimum calibrations for two different events due to the different sources of validation data (Horritt and Bates, 2002). The poorer performance of HEC-RAS in this research site as compared with similar studies (see Bates and De Roo, 2000; Horritt and Bates, 2002) may be attributed to two causes. First, the under-prediction of inundation may stem from under-estimation of the inflow hydrograph (i.e. upstream boundary condition). This cannot be the major cause for under prediction of inundation because maximum water elevations measured at a number of points within the study reach (along the reach and on the floodplain) indicate a good correspondence with predicted stages. Second, it may be attributed to the quality of validation data used. If portions of the floodplain in which inundation seems to be under-predicted are studied, these portions are mostly located on the floodplain where tributaries are connected to the main channel and floodplain. The tributaries connected to the main channel contribute to in inundation as well as main channel (i.e. Buckden Beck and Step Gill in Figure 4.17). More importantly, another group of the tributaries are those which are not connected directly to the main channel and only convey flows from hillslopes to the floodplain (i.e. Birk Gill and Water Gill in Figure 4.17). Thus, it seems that lower performance of the model in some extent can be explained by uncertainties involved in validation data (i.e. over-estimation). However, it is expected that use of models with higher complexity of flow representation may result in improvements in predicting inundation extent.

4.13 Summary of the chapter

The principles of one-dimensional models, with an emphasis on HEC-RAS and its steady and unsteady flow calculation procedures, were described. The model was applied and parameterised using an estimated inflow hydrograph, surveyed cross sections and determination of the relevant coefficients. Then, the model was applied to an upland reach of the River Wharfe in order to predict inundation extent. The model performance in terms of F at its optimum calibration was capable of predicting 50% of the inundated and non-inundated areas. It seemed that the reason why the model performance was lower than expected (compared with similar studies) relates to uncertainties involved in shoreline position. The main source of

these uncertainties is flows coming from hillslopes coupled to floodplain. Such performance should be compared with other models considered in the research (i.e. HEC-RAS in storage cell mode and two-dimensional diffusion wave treatment) to determine the optimum level of process complexity in relation to inundation extent prediction. In response to such needs, Chapters 5 and 6 are assigned to the description and application of the storage cell mode of HEC-RAS and a two-dimensional diffusion wave treatment of floodplain flows in the study site.

Chapter 5

HEC-RAS in storage cell mode

5.1 Introduction

In Chapter 4, the ability of the normal mode of HEC-RAS (a one-dimensional hydraulic model) in relation to prediction of flood inundation extent in an upland floodplain was investigated. The results showed that the best predictions of the model range from 40 to 50% (i.e. $F\%$) of the observed data for the event considered here. This approach assumed that the river-floodplain system was acting as a two-stage conveying channel. However, the complexity of the floodplain is such that, in reality, the floodplain is a series of storage cells that only convey when adjacent storage cells connect. Thus, the aim of this chapter is to develop a storage cell approach in which high-resolution topographic data (i.e. Lidar data) and associated field survey are used to model the floodplain as a series of storage cells. This modelling approach is applied and tested for the reach under study and flood event considered for the research. This is the first time that such a modelling system in conjunction with high-resolution topographic data has been applied for floodplain inundation extent prediction. Based on considering the sensitivity of the modelling system against calibration parameters, the model is verified in relation to whether or not calibration parameters have an effect on model response that is consistent with expectations and whether the results are more reliable and accurate than the normal mode of HEC-RAS for flood inundation prediction.

5.2 Storage cell concept

There are drawbacks related to the results of one-dimensional models that originate from violation of one or more basic assumptions including the one-dimensionality of the flow, uniformity of velocity and horizontality of water level across the cross section. This level of dimensionality may sufficiently satisfy flow behaviour in the main channel (Knight and Shiono, 1996) but cannot perfectly explain flow behaviour on the floodplain where complex topographic characteristics play a dominant role in relation to both flow distribution on the floodplain and flood inundation extent (e.g. Hardy *et al.*, 1999, Bates and Anderson, 2001, Nicholas and Mitchell, 2003). This means that once the river overtops, the floodplain is inundated in a manner dictated by local topography at least at the beginning of inundation. Indeed, such flow may never return to the main channel during the falling limb of the flood hydrograph. This state will be aggravated on floodplains with either natural obstacles or man-made structures (dykes, elevated roads, field walls, embankments etc.). In such cases, the land surrounding the main channel (floodplain) may comprise a series of discrete areas acting as storage cells, which connect with their neighbours and/or the main channel. In this sense, the flow direction on the floodplain may be independent of the direction of main channel flow (Fig. 5.1).

Fig. 5.1: Schematic form of interconnected storage cells on the floodplain

146
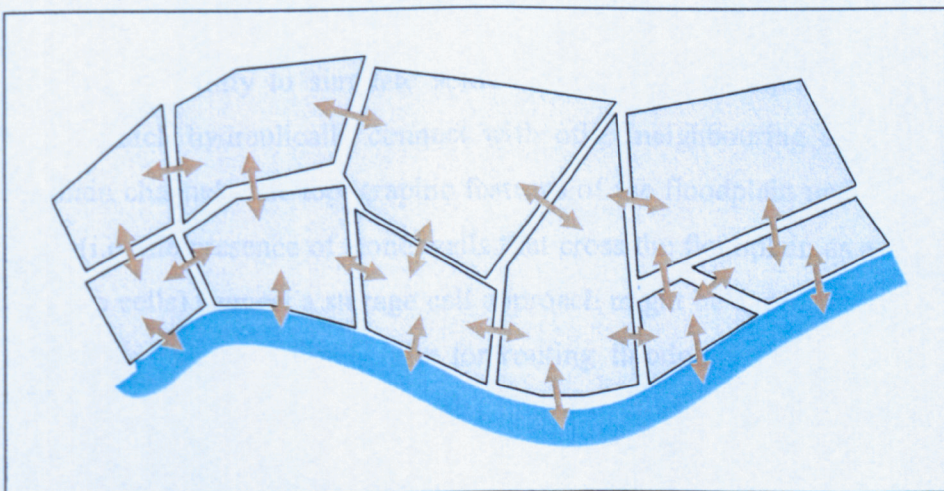
To deal with such situations, Zanobetti *et al.* (1968, 1970) and Cunge (1975c) proposed considering the floodplain as interconnected storage cells. They assumed that the water surface is horizontal in each cell and water level is solved using the continuity equation in each cell. Flow exchanges across cell boundaries are calculated based on water levels in the adjacent cells and some form of boundary condition (e.g. a weir equation). Although the two-dimensional unsteady flow equations are not used to explain the flow behaviour on the floodplain, the physical situation in which channel and storage cells form a two-dimensional network for flow movement are perfectly simulated. Thus, this approach may have considerable advantages over one-dimensional models in simulating flow situations that are clearly physically multidimensional. Use of such models may become more appropriate in relation to flood inundation extent prediction as high-resolution topographic data are becoming increasingly available for providing the detailed topography of each cell. In such a condition, storage cells can be realistically identified and flood distribution patterns mapped in each cell at a resolution defined by the size of the storage cell.

Use of one-dimensional approaches also assumes that water levels across cross sections are horizontal. Thus, it can be problematic as a sudden shift from the floodplain being an ineffective flow area to being an effective flow area can result, especially where there are large areas behind levees overtopped. This can cause stability problems for one-dimensional modelling approaches. This also necessitates consideration of alternatives for floodplain flow simulation.

HEC-RAS has the ability to simulate some or all of the floodplain flow using storage areas which hydraulically connect with other neighbouring storage areas and/or the main channel. The topographic features of the floodplain under study in this research (i.e. the presence of stone walls that cross the floodplain as a series of discrete storage cells) suggest a storage cell approach might be appropriate. Thus, a network of interconnected storage cells for routing floodplain flows (quasi two-dimensional model), which are hydraulically linked to a one-dimensional treatment of the flow in the main channel (default for HEC-RAS), are established in this thesis (see Figure 5.2).

Figure 5.2: A simple schematic floodplain representation by storage cells concept in HEC-RAS
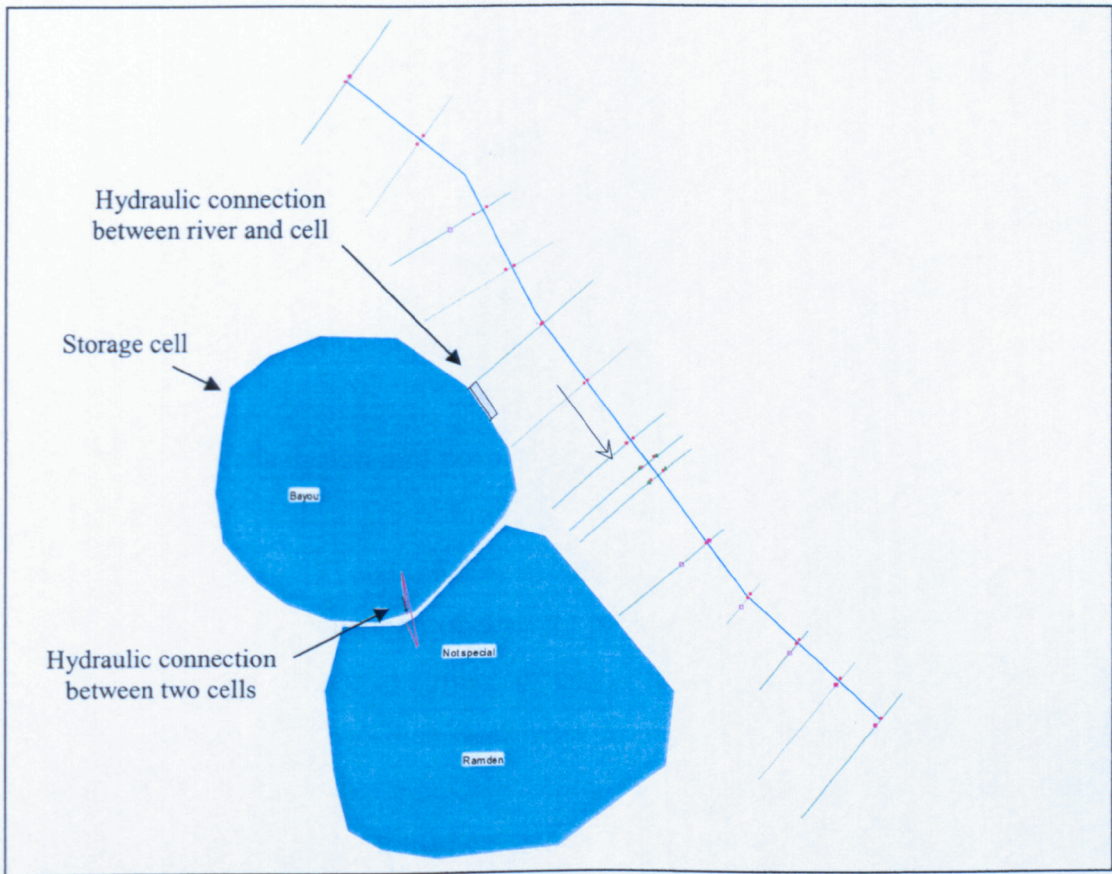
5.3 Storage cell mode of HEC-RAS and data requirements

Flow in the main channel in the storage mode of HEC-RAS is routed in a similar way as in the normal mode of HEC-RAS, using a one-dimensional wave treatment. Hence, the main channel is discretised and parameterised in the same way as the normal mode except that cross sections are not extended across the floodplain where storage cells are located. In this case, no cross sections had to be extended on the floodplain as the river banks are engineered and there are levees along the reach with large potential flow areas behind them. This was the reason for the instability problems in the normal mode of HEC-RAS (Chapter 4). To avoid section extension problems, storage cells were extended to the nearest river bank in all cases. Given the results of HEC-RAS in normal mode, the main channel is parameterised using the cross section spacing up to 125 m. The boundary and initial conditions are defined in the same manner as in the normal mode. Only the

floodplain environment is treated differently as compared with the normal mode. For storage cell definition, a series of areas crisscrossed by natural obstacles and man-made structures (dykes, elevated roads, field walls, embankments etc.), which were hydraulically connected to neighbouring areas, was specified. In addition, the characteristics of connection points between the connected areas were investigated in the field (i.e. location, number of connections, and dimensions). In the next section, the issues of storage cell specification on floodplains, and their parameterisation in this particular reach, are discussed. Following that, hydraulic connections and the governing equations applied in here are described.

5.3.1 Storage cells design and parameterisation

Ordnance survey (OS) Landline data specify roads, field walls, and fences, and can be used to obtain a collection of discrete bounding areas. This is basically a GIS task. The cells were updated through extensive fieldwork in order to validate and to modify (where necessary) them and more importantly, to identify their hydraulic connections to the neighbouring cells and/or the main channel. The first step in the analysis yields a series of bounding areas with a wide range of cell sizes. In some cases, cells should be joined together to make a single cell. In others, there is a limitation in relation to the number of hydraulic connections that a cell may have (default for HEC-RAS is 8 connections for each cell). Thus, some of storage cells have to be divided into the smaller cells to meet the condition. In this state, hydraulic connection is set across the cell boundaries. A total of 61 storage cells were finally designed for the floodplain in this reach (see Figure 5.3).

Fig: 5.3: Final storage cell design on the floodplain, using a combination of Landline data and site visit and modifications in order to meet HEC-RAS constraints
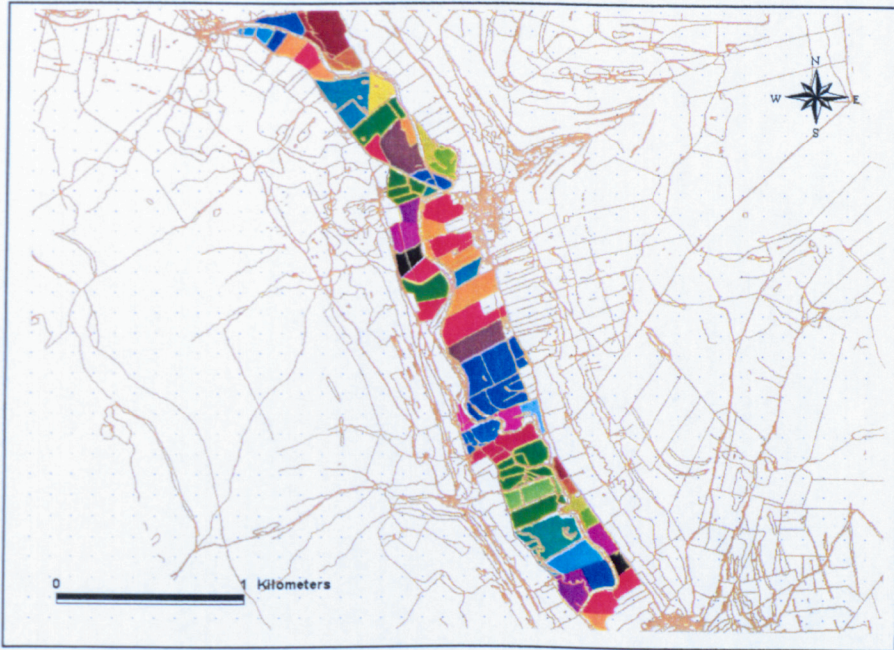
There are two options for describing the storage cells in terms of their functionality (capacity and change through time). First, we can imagine the wetted area to be constant, and as the elevation of water changes through time a simple multiplication of area by elevation results in the volume of water in each storage cell. Second, as wetted area is rarely constant through time in each storage cell but is usually a function of water elevation change, volume-water elevation relationships can be used to describe the storage cell capacity. The data requirement for the first method is only a predefined minimum elevation of each storage cell. In the second approach, the detailed topography data to define the cell capacities for each elevation contour line are needed. As Lidar data are available for the research area, a volume-elevation curve for each storage cell can be defined (e.g. Figure 5.4). Based on the second method, once water fluxes are conveyed into a cell, a contour line for water elevation can be specified according to the volume of water conveyed into the cell. The water level continues to rise in a cell until either the flux into the cell reverses or the water level reaches the elevation of a hydraulic connection segment and makes a new connection with other cell. In this case study, in total for 61 storage cells the corresponding Lidar data were obtained and their volume-elevation relationships were drawn.

Figure 5.4: (a) storage cell specified using Landline data, (b) Lidar data used to describe volume-elevation relationship for the cell, and (c) the curve showing the volume-elevation relationship for this specific cell
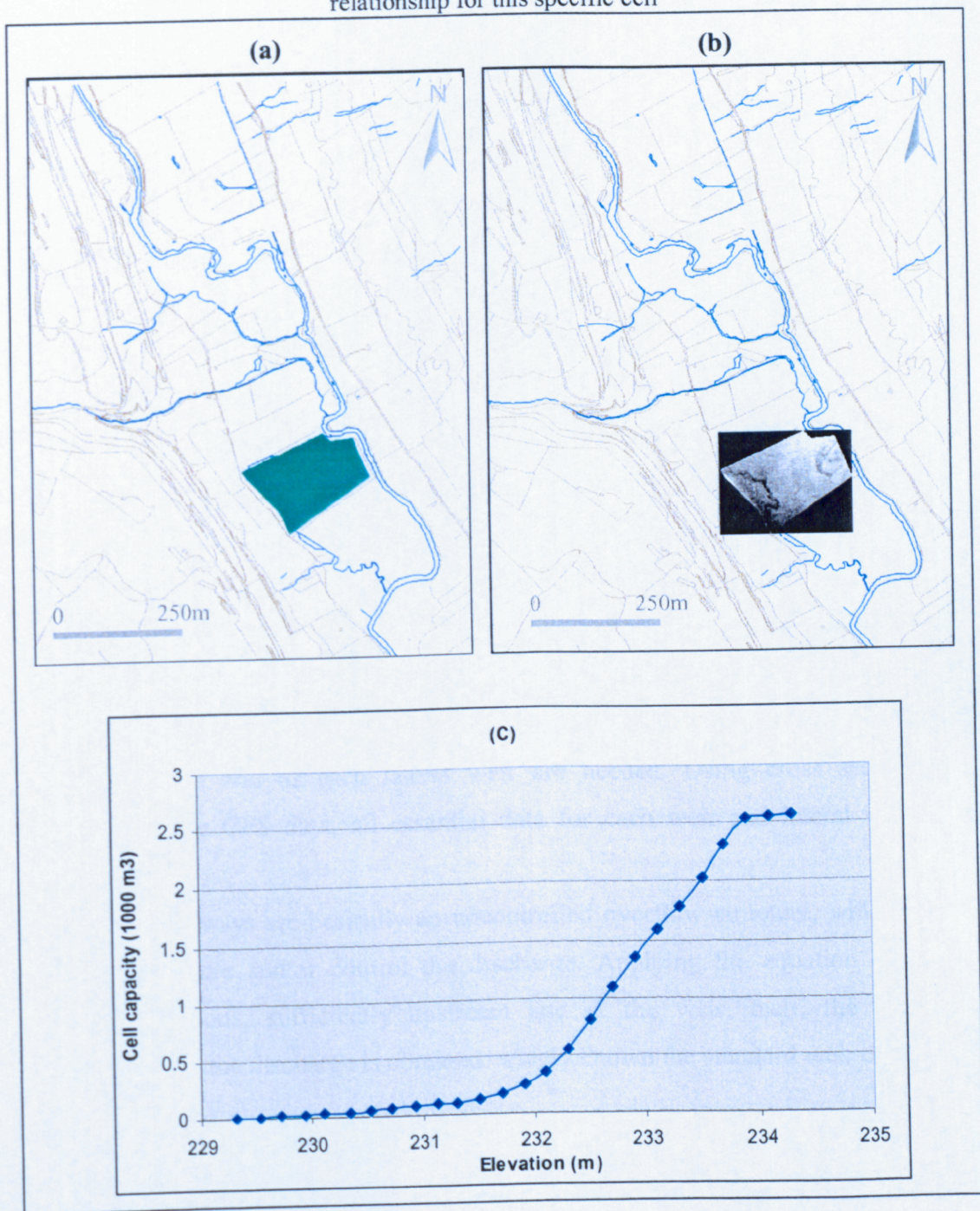
5.3.2 Hydraulic connections

There are two kinds of hydraulic connections that are used, both for connections between storage cells and connections between storage cells and the main channel. The total number of hydraulic connections for each storage cell should not exceed

eight in the HEC-RAS system. In addition, long hydraulic connections between storage cells and the main river may lead to instability in the model solution. In this regard, initial simulations were undertaken. The results showed that the maximum length of hydraulic connection for this particular study reach, so that the model remains stable, should not exceed 100m. It should be noted that the model may become unstable due to other reasons (e.g. temporal resolution). Hence, some storage cells have to be divided to smaller ones to overcome this limitation. Hydraulic connections between the storage cells are made by weirs and between the storage areas and the main channel by lateral weirs. The only difference between the normal weirs and lateral weirs is that, as lateral weirs are located alongside the river channel, the weir itself and the water surface across the weir as well, has a slope (Fig. 5.6). Where normal weirs are used between storage cells, both the weir segment and water level over the weir are assumed to be horizontal. A total of 171 hydraulic connections in the form of lateral weirs between the main channel and storage cells on the floodplain, and a total of 51 weirs between storage cells, were finally established. To use weirs as hydraulic connections between storage cells, their dimensions should be determined, including width, and height and absolute bed elevation. To establish a lateral weir, their lengths and bed elevation at the beginning and end of each lateral weir are needed. Using cross section data acquired using GPS data, all essential data for each weir and lateral weir were determined.

Weirs or spillways are basically an uncontrolled overflow structure, which can be used to measure and/or control the discharge. Applying the equation of energy between sections, sufficiently upstream and at the weir itself, the following expression for the discharge is obtained, widely known the standard weir equation.

$$Q = CLH^{2/3} \hspace{2cm} \text{(Eq. 5.1)}$$

where Q is discharge in cfs, C is a dimensionless discharge coefficient, L is the length of spillway crest and H is the upstream energy head above the spillway crest. As the pressure distribution on the crest may not be hydrostatic and also due to different weir geometry, roughness, and inflow conditions, the discharge characteristics over the weir may be affected hence, the discharge coefficient has

been identified. The discharge coefficient for all different types of weirs should, if possible, established by calibration (Graf, 1998). However, numerous correlations have been proposed for C in the literature (e.g. Chanson, 1999). Typical values will range from 0.5 to 4 depending upon the shape of the spillway crest (i.e. broad-crested, ogee-shaped and sharp-crested weirs), dimensions of the weir and the upstream total head.

The weir equation is usually used for weirs crossing the river (inline weirs) such that the water surface and weir segment are parallel. Thus, this equation can be utilised for hydraulic connections between storage cells (Fig. 5.5). It should be noted that within a storage cell there is no outflow as long as the water level is below the absolute elevation of the evacuating weir segment(s). Once the water level reaches that critical point, flow is only conveyed to the next storage cell(s) using the weir equation. Hence, under any condition, there is no flux flow within storage cells on the floodplain. The analysis assumes that flow within a storage cell is not required to connect hydraulic connections. This issue is addressed through diffusion wave modelling in Chapter 6.

Fig.5.5: A sample of weir as a hydraulic connection between two storage cells
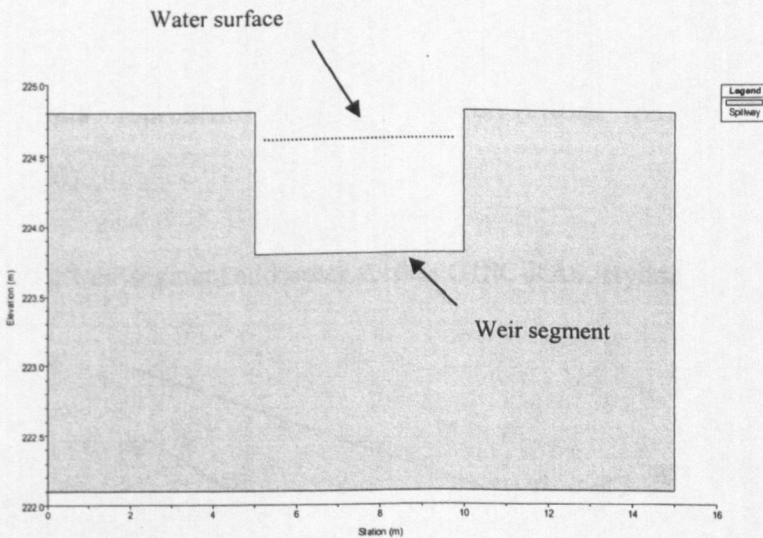
Fig.5.6: A sample of lateral weir as a hydraulic connection between a storage cell and the main channel
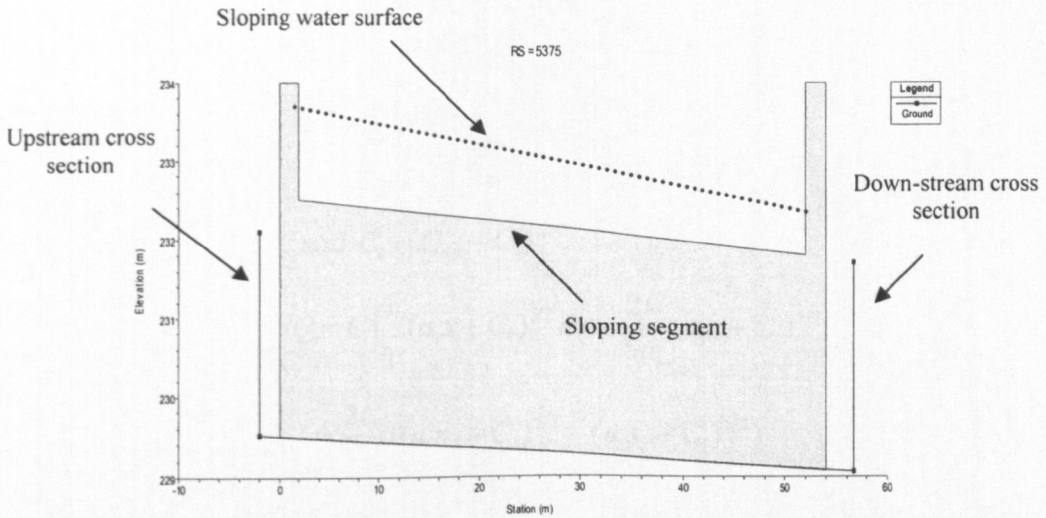
In the case of lateral weirs, the water surface across the weir has a slope. Additionally, the weir itself could be on a slope (Fig. 5.6). Because of this, an equation suitable for weirs with sloping segments and water surface should be derived. The definition for a sloping line representing the water surface and the weir segment are shown in Fig. 5.7. The constants a_{ws} and a_w represent the slope of the water surface and the weir segment, respectively, while the variables C_{ws} and C_w are constants representing the initial elevations (HEC-RAS, Hydraulic Reference, 2000).

Fig 5.7: Sloping weir segment and water surface (HEC-RAS, Hydraulic Reference, 2000)
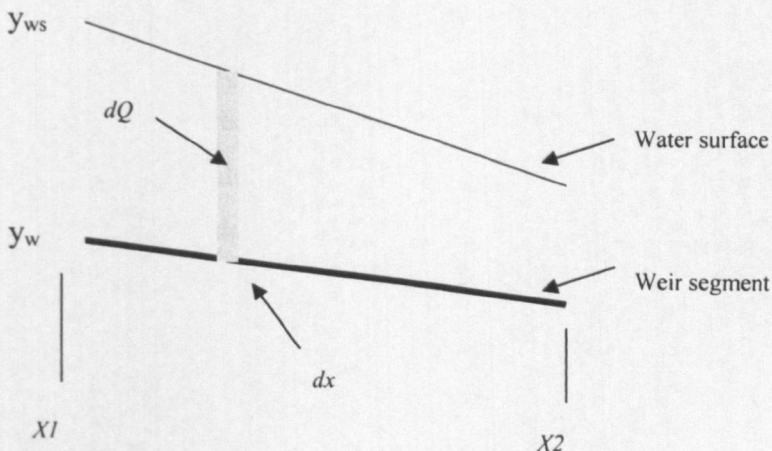
The following general equation is derived for a sloping weir and water surface by integrating the standard weir equation:

$$dQ = C(y_{ws} - y_w)^{3/2} dx$$

$$dQ = C(a_{ws}x + C_{ws} - a_w x - C_w)^{3/2} dx$$

$$dQ = C((a_{ws} - a_w)x + C_{ws} - C_w)^{3/2} dx$$

Assuming $a_1 = a_{ws} - a_w$ and $C_1 = C_{ws} - C_w$

$$\int_{x_1}^{x_2} dQ = C\int_{x_1}^{x_2} (a_1 x + C_1)^{3/2} dx = \frac{2C}{5a_1}(a_1 x + C_1)^{5/3}$$

$$Q_{x_1-x_2} = \frac{2C}{5a_1}((a_1 x_2 + C_1)^{5/2} - (a_1 x_1 + C_1)^{5/2}) \qquad \text{(Eq. 5.2)}$$

The above equation is valid as long as a_1 is not zero. When a_1 is zero, the water surface is parallel to weir segment, and the original weir equation can be applied.

Figure 5.8 shows part of the floodplain in the storage cell mode of HEC-RAS, including a series of connected storage cells on the floodplain along with their hydraulic connections (i.e. weirs and lateral weirs). Figure 5.9 shows the final set up of HEC-RAS using storage cells and hydraulic connections on the floodplain for the whole study area.

5.3.3 Mapping of floodplain inundation extent

To predict inundation extent over the floodplain using storage cells, it is first necessary to map flow distributions over each storage cell at peak water level. To do that, the peak water level at each storage cell is extracted for each simulation. This water level is considered as a *"critical elevation"* for a particular cell. All pixels that have elevations less than the *"critical elevation"* are considered as flooded areas in that particular cell. This calculation is conducted for all storage cells using GIS software. By merging the separate inundation extent predictions for each storage cell, the inundation extent predictions for the entire floodplain result. Thus, in the storage cell mode, the production of the inundated area map is completed as separate step.

155

Figure 5.8: A schematic exhibition of part of floodplain represented by storage cells and their hydraulic connections (i.e. weirs and lateral weirs)
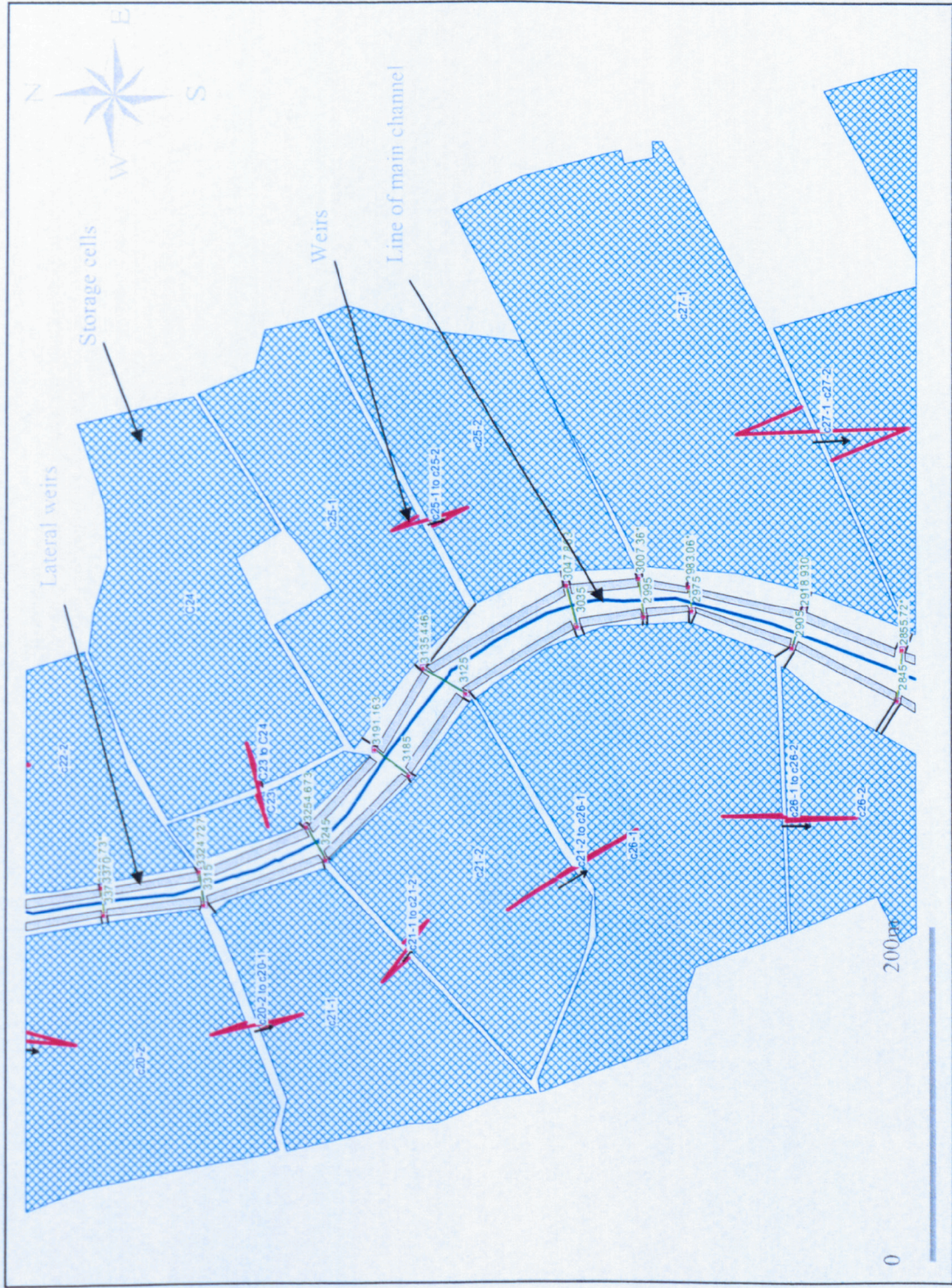
Figure 5.9: The final set up of HEC-RAS using 61 storage cells and 222 hydraulic connections on the floodplain

157
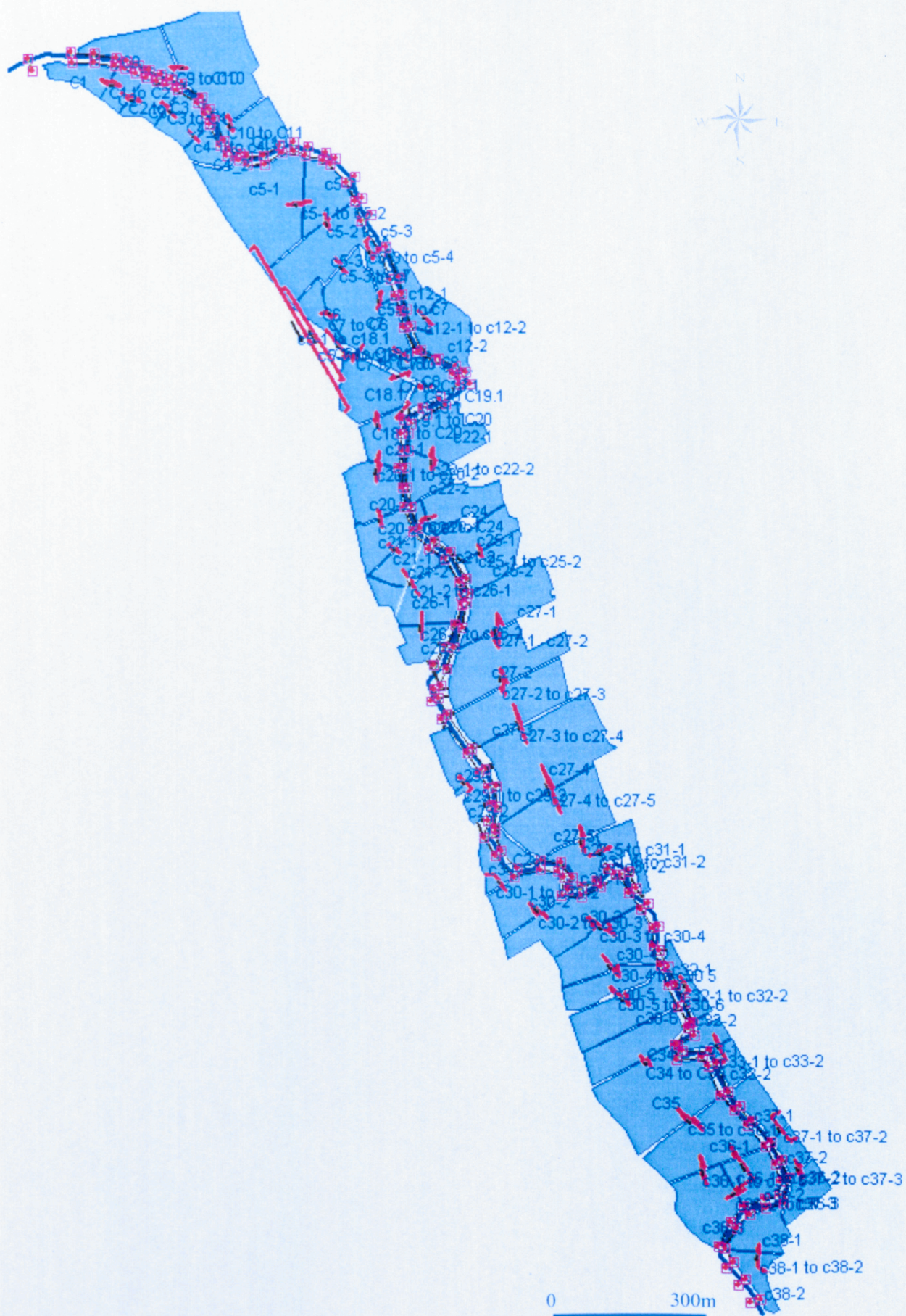
5.4 Sensitivity analysis of HEC-RAS in storage cell mode

In Chapter 4, the necessity and importance of sensitivity analysis in hydraulic modelling were discussed. Once again, sensitivity analysis scenarios were defined: (i) to assess the scope, feasibility and capacity of the hydraulic model used here; and (ii) to specify the degree of model sensitivity to parameters linked to the model structure.

As with the normal mode of HEC-RAS, scenarios based upon physical parameters, boundary conditions, and elements associated with numerical solution (parameters that might affect numerical solution) were selected for sensitivity analysis. Herein, the physical parameter is a reasonable range of Manning's n values for only the main channel as there is no flux on the floodplain (i.e. within storage cells), the effect of boundary condition variation using a range of statistical flood events at the upstream end of the river, and elements associated with numerical solution including various time step issues. It should be noted that the cross section spacing is not changeable due to the maximum number of hydraulic connections that a cell may have and it was fixed at the optimum distance identified in the last chapter (up to 125m). As mentioned before, the Manning's n value was estimated using Equation (4.37) and consideration of the previous study's n values. Thus, a range of 0.035-0.06 with increments of 0.005 was chosen for sensitivity analysis.

The flood event of the 4th of February 2004, which was identified as the main flood event in the reach of interest during the study period, is of the scale of a 1 in 0.5 year flood (using the previous hydrological analysis in this catchment, JBA, 2000). However, flood events with higher return periods were undertaken for sensitivity analysis in order to check the scope of the model's ability as a predictive tool for this study site. Using growth factors determined for the Upper Wharfe, flood events with 2-, 5-, and 10-year return periods developed at Hubberholme gauging station, with peak discharges of 70.4, 92.8 and 108.5m^3/s respectively.

As there is no certain guide for selecting time steps, it should be tested to gain optimal solutions. For the normal mode of HEC-RAS, given the calculations performed, 1sec, 30sec, 1min, 15min and 30min were selected as time steps for the sensitivity analysis. In this application, more attention must be paid to time step variation given the presence of hydraulic connections. In such cases, the time step

must be smaller to satisfy the Courant condition. Hence, time steps of 1sec, 5 sec, 30 sec, 1min and 5 min were selected.

Table 5.1 summarises the simulations performed for sensitivity analysis of HEC-RAS in the storage cell mode for this specific study site, in response to varying n, upstream inflow hydrograph (i.e. flood return period), and time step variation.

Table 5.1: Scenarios undertaken to do sensitivity analysis for HEC-RAS in the storage cell mode

Spacing up to 120	Manning's n 0.035					Manning's n 0.04					Manning's n 0.045				
Flood return period	1 sec	5 sec	30 sec	1 min	5 min	1 sec	5 sec	30 sec	1 min	5 min	1 sec	5 sec	30 sec	1 min	5 min
0.5	181*	182	183	184	185	186	187	188	189	190	191	192	193	194	195
2	196	197	198	199	200	201	202	203	204	205	206	207	208	209	210
5	211	212	213	214	215	216	217	218	219	220	221	222	223	224	225
10	226	227	228	229	230	231	232	233	234	235	236	237	238	239	240

Spacing up to 120	Manning's n 0.05					Manning's n 0.055					Manning's n 0.06				
Flood return period	1 sec	5 sec	30 sec	1 min	5 min	1 sec	5 sec	30 sec	1 min	5 min	1 sec	5 sec	30 sec	1 min	5 min
0.5	241	242	243	244	245	246	247	248	249	250	251	252	253	254	255
2	256	257	258	259	260	261	262	263	264	265	266	267	268	269	270
5	271	272	273	274	275	276	277	278	279	280	281	282	283	284	285
10	286	287	288	289	290	291	292	293	294	295	296	297	298	299	300

☐ Unstable simulation   ☐ Stable simulation

* Numbers are attribute to file referencing of the hydraulic model

5.4.1 The scope of stability of the model (HEC-RAS in storage cell mode)

The results of Table 5.1 show that, for almost all the values of Manning's n selected, the model is stable for all flood magnitudes, provided that the model is only run under the smallest time step used (i.e. 1 second intervals). Compared with HEC-RAS in normal model, the model shows more stability and there is no preferred stability zone as the size of flood is increased. As noted in Chapter 4, a major weakness of HEC-RAS in normal mode, that could cause the model to become unstable, is sudden changes in flow area with only a small change in elevation between two continuous time steps. The possibility of this happening was greater for bigger flood magnitudes. Table 5.1 shows that using the storage cell mode on the floodplain reduces the possibilities for this and the model is stable regardless of the size of flood event being used. In terms of model stability and feasibility, HEC-RAS in storage cell mode is preferred relative to HEC-RAS in

normal mode. The model behaviour also shows that a wider range of Manning's n values is available for calibration (all values chosen except $n = 0.035$ for which the model becomes unstable).

5.4.2 The effect of main channel friction on bulk flow characteristics

The range of Manning's n values used in Table 5.1 provides for a qualitative description of actual roughness of the main channel (see 4.2.9). Hence, in relation to sensitivity analysis, the channel friction was selected from a starting value of 0.04 and increased in increments of 0.005 up to a maximum value of 0.06. If the output flow and stage hydrographs are analysed (Figures 5.11 and 5.12), it is seen that changes in main channel friction has no major effect on outflow hydrographs and its effect is limited to changes in stage hydrographs. In general terms, it can be concluded that the sensitivity of outflow characteristics in one-dimensional models, where floodplains are represented by a series of storage cells, which are hydraulically connected to each other as well as to the main channel, is less than models that represent floodplains through extended cross-sections. As there is a current emphasis on using floodplain storage to attenuate downstream flows, this research emphasises the need to give very careful attention to how floodplain are represented in one-dimensional models.

Fig. 5.11: the effect of main channel friction on outflow hydrographs

160

Fig. 5.12: The effect of main channel friction on down-stream stage hydrographs
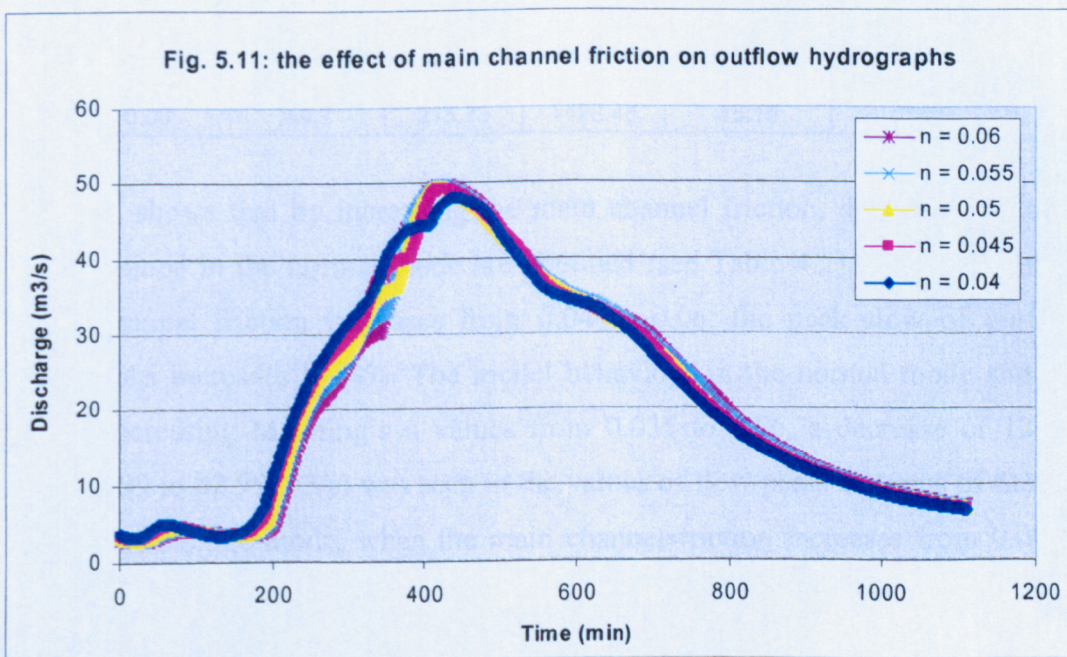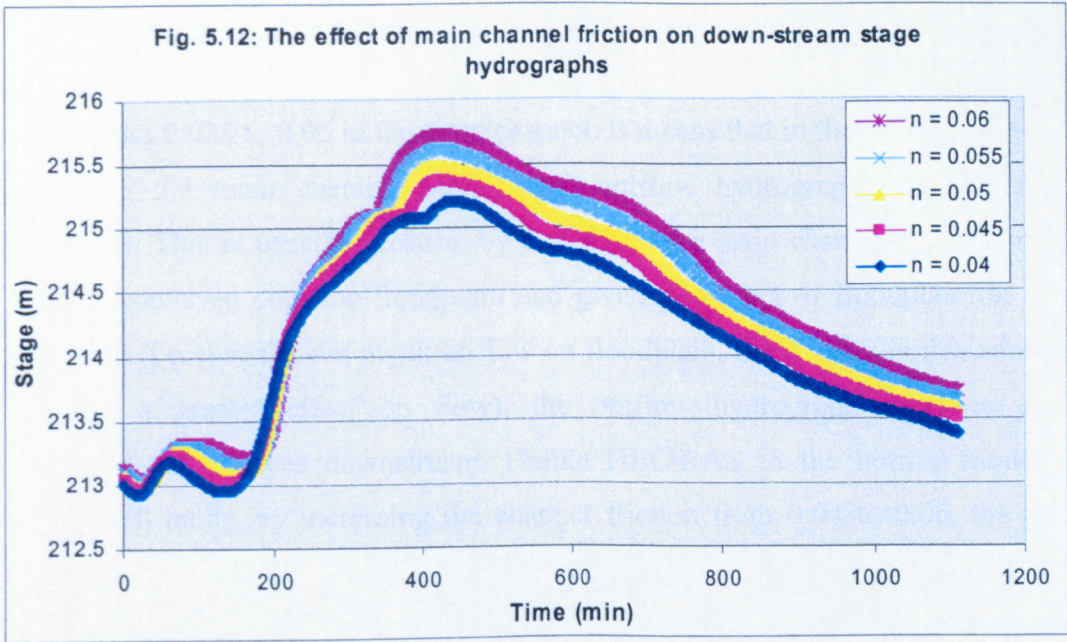
To justify such a conclusion, Table 5.2 shows some of the quantitive bulk flow characteristics obtained using HEC-RAS in storage cell mode.

Table 5.2: The effect of channel friction factor on bulk flow characteristics in the storage cell mode of HEC-RAS.

Channel friction (Manning's n)	Peak Discharge (m3/s)	Peak stage (m)	Output volume (1000 m3)	Real time of peak flow (4th Feb 2004)	Real time of peak stage (4th Feb 2004)
0.04	47.9	215.2	1441.57	15:32	15:32
0.045	49.2	215.37	1438.41	15:17	15:16
0.05	49.47	215.49	1434.11	15:16	15:16
0.055	49.56	215.61	1430.9	15:17	15:16
0.06	49.7	215.73	1428.45	15:19	15:19

Table 5.2 shows that by increasing the main channel friction, different results to those obtained in the normal mode are obtained (see Table 4.2). Table 5.2 shows that if channel friction increases from 0.04 to 0.06, the peak flow of outflow hydrographs increases by 4%. The model behaviour in the normal mode showed that by increasing Manning's n values from 0.035 to 0.06, a decrease of 12.1% (from 48.99 to 42.99 m3/s) was seen in the values of flow peak. In terms of time to peak in the storage mode, when the main channel friction increases from 0.04 to 0.06, the time to peak of outflow hydropaths shows a decrease of around 13min. Such behaviour was not seen when the value of the main channel friction was

161

changed in the normal mode of HEC-RAS in the previous Chapter (section 4.11.3). Rather, the time to flow peak was delayed by 2 to 2.5h due to the change of n values from 0.035 to 0.06 in the main channel. It means that in the normal mode, by increasing the main channel friction, the outflow hydrograph becomes more attenuated. This is usually because, by increasing the main channel friction, more water is conveyed onto the floodplain and given the effect of floodplain on flow behaviour (i.e. given lower depth of flow on floodplain, the friction in this area has therefore a greater effect on flow), the outflow hydrograph becomes more attenuated and delayed downstream. Unlike HEC-RAS in the normal mode, in storage cell mode, by increasing the channel friction from 0.04 to 0.06, the peak discharge downstream increased from 47.9 to 49.7m3/s (4%) and there is a reduced change in timing of the peak flow (13 minutes versus 2 hours in the normal mode application). This is because in the storage cell mode of HEC-RAS, there is much less flux on the floodplain. Once any flow is conveyed into a storage cell on the floodplain, it settles into the deepest areas of that cell with no flux until the water level reaches the critical levels of the next hydraulic connections. From this point onwards, the hydraulic relationship between two cells is managed with a weir equation. In the storage cells used for the floodplain in this research, there was no major elevation difference between the lowest points in storage cells and the level of weir segments. It means that the capacity of cells to keep water in them is not as marked and the floodplain does not delay flow in the same way as it does in normal mode. In storage cell mode, as soon as flow is conveyed on to floodplain, it is transferred to downstream storage cells with only a short delay in relation to the effects of storage of water on the floodplain cells. There is no representation of flux effects, which will slow floodplain flow velocities, and so reduce the ease with which water is conveyed downstream. Thus, by increasing n values in the main channel in storage cell mode, the peak discharge values can actually increase and time to peak become shorter.

In terms of downstream stage hydrographs, as expected, increasing n values increase peak stage downstream. Table 5.2-1 shows that the change of n values from 0.04 to 0.06 caused an increase of 0.53m (from 215.2 to 215.73m) in peak stage and a decrease of 13min in relation to time to stage peak. The corresponding values in normal mode due to the change of n values from 0.04 to 0.06 are 0.33m and a delay of 2 to 2.5h in time to peak stage. Compared with the normal mode, the

effects of the change of n values on the timing of peak flow and stage are not marked. Both the models showed similar behaviour in relation to the effects of the friction factor changes on peak stages at the downstream.

Comparison of output water volume changes due to the main channel friction increase from 0.04 to 0.06 shows a 0.9% decrease in output water volume whereas the corresponding value in normal mode was a 0.5% decrease. This will be because of a better representation of storage effects up to the critical levels at which storage cells connect.

The general comparison between outflow and stage hydrographs (i.e. 4.10 and 4.11 versus 5.11 and 5.12) resulting from the normal and storage cell modes of HEC-RAS reveals that the effect of main channel friction change on outflow and stage hydrographs is marked in relation to shape of hydrographs in normal model; this is much less the case in storage cell mode. Different shape of downstream stage hydrographs is referred to floodplain flow representation in each mode. Momentum effects in normal mode push hydrographs forward and storage effects in storage cell mode push them backward.

The effect of main channel friction on bulk flow characteristics using flood events bigger than the one that occurred on the 4th Feb 2004 (i.e. 1 in 0.5 flood event) was investigated. Table 5.2-1 compares the effect of two values of the main channel friction factor between two values (0.045 and 0.055) on bulk flow characteristics using flood events with 0.5-, 2- and 5-year return periods at the study site. It shows that the effect of main channel friction changes on bulk flow characteristics is found regardless of the flood event magnitude despite there being more flow volume on floodplain in bigger flood events. It means that the response of the floodplains represented using storage cells to floodplain flow is not a function of the flow volume conveyed on to the floodplain but rather the capacity of the floodplain storage which is the similar for all flood magnitudes. This may have implications in relation to floodplain management.

Table 5.2-1: Comparison of main channel friction changes on bulk flow characteristics
using different flood event magnitude

Flood Return Period	Channel friction (Manning's n)	Peak Discharge (m3/s)	Change (%)	Peak stage (m)	Change (%)	Output volume (1000 m3)	Change (%)	Time of peak flow (4th Feb 2004)	Time of peak stage (4th Feb 2004)
1 in 0.5	0.045	49.2		215.37		1438.4		15:17	15:16
1 in 0.5	0.055	49.56	0.7%+	215.61	0.1%+	1430.9	0.4%-	15:17	15:16
1 in 2	0.045	69.66		215.8		2019.8		15:00	15:00
1 in 2	0.055	69.75	0.1%+	216.1	0.1%+	2011.7	0.4%-	15:02	15:02
1 in 5	0.045	93.8		216.25		2694.6		14:59	14:59
1 in 5	0.055	92.66	1.2%-	216.6	0.2%+	2684.6	0.5%-	15:02	15:02

5.4.3 Summary of the sensitivity analysis on bulk flow characteristics

The sensitivity of bulk flow characteristics in the storage cell mode application has been analysed using 180 scenarios. Time step, main channel friction factor and flood magnitude variation were the parameters used to establish the scenarios. The results show that the model in storage cell mode overcomes the existing weaknesses found in normal mode that result in its instability. The storage cells mode can simulate the entire range of flood magnitudes used in the research provided that smallest time step application is used (i.e. 1 second). Unlike in the normal mode, where the bulk flow characteristics were controlled by main channel friction, in the case of storage cell mode, due to the special effect of storage cells on floodplain flows (i.e. no treatment of flux on the floodplain), the effects of main channel friction change on bulk flow characteristics were more complicated. When main channel friction was changed in the storage cell mode, peak discharge increased (rather than decreased, as in normal mode). In contrast, downstream stage hydrographs in response to main channel friction change showed behaviour similar to the normal mode although the shape of stage hydrograph remained unchanged. To explain such behaviour in the storage cell mode in relation to outflow and stage hydrographs in response to main channel changes, two processes that act at the same time must be clarified. First, by increasing the main channel friction in storage cell mode, lower velocities in the main channel and more delay in the flow reaching its peak value downstream is expected (i.e. flow hydrograph intends to become

more attenuated and delayed) so that this process results in a high water level in the main channel and, in turn, more water is transferred onto floodplain. Second, the existence of more water on floodplain, in the presence of no treatment of flux effects in the storage cells, causes rapid downstream transfer of flow. These two processes act against each other. It is worth commencing on the conceptual difference between normal and storage cell modes, as both have been shown to be problematic in practice. From a priori consideration, the normal mode is problematic because it allows conveyance of water downstream for all floodplain flows as it does not block downstream flux even when blockage exist. Thus, it represents momentum effects only and not discontinuities in flows due to physical blockage. The storage cell mode represents this effect explicitly by conceptualising the floodplain as discrete cells, with hydraulic connections. However, aside from points of connections there is no representation of momentum effects to whole floodplain flux rates. Hence, the storage cells allow flux to be too rapid on the floodplain. Thus, conceptually, both models are inadequate: normal mode for assuming that a two-dimensional routed flow can be reduced to flux between extended cross sections; and storage cell mode for assuming that floodplains are a series of storage ponds that are not affected by dynamic flux transfer processes. In response to the limitations, a compromise solution is favoured, recognising both storage and flux routing effects (see Chapter 6).

Given the limitations mentioned in relation to both normal and storage cell modes, it is worth considering further which of these modelling approaches result in a better inundation extent prediction. In turn, this may help to understand that which aspect of a modelling system (i.e. flow process representation, topographic parameterisation, calibration and validation data) are more crucial in inundation extent prediction.

5.4.4 Calibration and validation of HEC-RAS in storage cell mode

Given the sensitivity analysis undertaken in section 5.4.3, the n values in the range 0.04-0.06 with increments of 0.005 were chosen to calibrate model predictions against the observed inundation extent. The flood event that occurred on the 4th February 2004, with a peak flow of 47.73 m^3/s and a 18.5h duration (see Chapter 3), was used as the upstream boundary condition in the study reach. The boundary

of inundation extent as validation data had been collected using RTK GPS at the time of flooding (Chapter 3). In addition, parts of the river banks where water leaves the main channel or return to the main channel during flooding were measured in order to assess lateral weir behaviour (i.e. predicted data) under different input data. The measures used in the calibration process were explained in Chapter 3. Four accuracy measures: Overall accuracy; KHAT; Fit; and Conditional Kappa; were estimated for each simulation in order to assess the model's ability to predict inundation extent. These measures may disagree with each other. This is because each measure reflects different information contained within the relevant error matrix. Hence, the determination of all these measures may result in a better understanding of model performance. As additional data were measured in the field during flooding, accuracy assessments were conducted for lateral weir performances and comparisons between the predicted and observed water elevations in some storage cells are undertaken.

Table 5.3 shows the accuracy assessments performed for the lateral weirs overtopped. As seen, as the main channel friction factor increases, the agreement between predictions and observations increases, as expected, as a result of water depth increases in the main channel. This trend stops with Manning's $n = 0.06$ and the accuracy measures decrease (Table 5.3). If the values of the four measures used here are considered as indices for choosing the best fit between predictions and observations, the n value of 0.05 produces the best fit. With consideration of Conditional Kappa measure as the only index, the model predicts the best fit by using the n value of 0.055. Both the overall accuracy and Kappa analysis introduce bias into the results because they are attributed to an entire matrix: the results depend on the number of non-overtopped lateral weirs included in the accuracy assessment (i.e. the size of the flood). Hence, they are not very precise as the number of non-overtopped lateral weirs is large here. In terms of the Conditional Kappa and measure of Fit, both indicate the agreement for an individual category within an error matrix but the Conditional Kappa is preferred because it corrects the bias that may arise from chance agreement. Hence, based on the Conditional Kappa, the model is optimised using the n value of 0.055 in relation to where flow leaves or returns to the main channel.

Table 5.3: Accuracy assessments conducted in relation to where flow leaves or enters in to the main channel using different n values

n (channel)	Accuracy method	value
0.040	Overall accuracy	0.83
	Kappa	0.64
	Conditional Kappa (Overtopped)	0.49
	Fit	0.63
0.045	Overall accuracy	0.91
	Kappa	0.81
	Conditional Kappa (Overtopped)	0.71
	Fit	0.81
0.050	Overall accuracy	0.94
	Kappa	0.88
	Conditional Kappa (Overtopped)	0.82
	Fit	0.88
0.055	Overall accuracy	0.92
	Kappa	0.85
	Conditional Kappa (Overtopped)	0.86
	Fit	0.85
0.060	Overall accuracy	0.85
	Kappa	0.71
	Conditional Kappa (Overtopped)	0.84
	Fit	0.75

Subsequently, the comparison between predicted and observed inundation extents required to complete the error matrix information for each scenario is accomplished. Figure 5.13 shows the error matrices created for each simulation considered in the calibration process. Based on the error matrices, four accuracy assessments were performed and their results are presented in Table 5.4. Table 5.4 shows that as the value of n increases, the agreement between predictions and observations rises and this trend does not stop. This means that a higher agreement between predictions and observations is dependent on more water on the floodplain, which is obtained using a higher n value in the main channel even where this results in water leaving the channel across weirs where it was not observed to do so. The question that we are concerned with is not which Manning's n value results in the best fit between predictions and observations of inundation extent in storage cell mode given that, in the reasonable range of n values, there is not much difference in model performance for inundation extent prediction. Rather, the question is that when the performance of lateral weirs is estimated at better than 85% (using n =

Figure 5.13: Error matrix produced for each simulation considered for calibration process in relation to inundation extent prediction ability of HEC-RAS in storage cells mode, (a), (b), (c), (d) and (e) error matrices are associated with *n* values of 0.04, 0.045, 0.05, 0.055 and 0.06 in the main channel respectively

(a)

	Observed wet	Observed dry	
Predicted wet	12031	242	12273
Predicted dry	19257	21649	40906
	31288	21891	53179 Floodplain total

(b)

	Observed wet	Observed dry	
Predicted wet	14399	492	14891
Predicted dry	16889	21399	38288
	31288	21891	53179 Floodplain total

(c)

	Observed wet	Observed dry	
Predicted wet	15910	642	16552
Predicted dry	15378	21249	36627
	31288	21891	53179 Floodplain total

(d)

	Observed wet	Observed dry	
Predicted wet	17228	794	18022
Predicted dry	14060	21097	35157
	31288	21891	53179 Floodplain total

(e)

	Observed wet	Observed dry	
Predicted wet	18361	1251	19612
Predicted dry	12927	20640	33567
	31288	21891	53179 Floodplain total

Table 5.4: Results of four accuracy assessments performed in relation to the accuracy of inundation extent prediction through storage cell mode

n (channel)	Accuracy method	value
0.040	Overall accuracy	0.63
	Kappa	0.33
	Conditional Kappa (Inundated)	0.20
	Fit	0.38
0.045	Overall accuracy	0.67
	Kappa	0.39
	Conditional Kappa (Inundated)	0.25
	Fit	0.45
0.050	Overall accuracy	0.70
	Kappa	0.44
	Conditional Kappa (Inundated)	0.29
	Fit	0.50
0.055	Overall accuracy	0.72
	Kappa	0.47
	Conditional Kappa (Inundated)	0.32
	Fit	0.54
0.060	Overall accuracy	0.73
	Kappa	0.49
	Conditional Kappa (Inundated)	0.35
	Fit	0.56
0.065	Overall accuracy	0.74
	Kappa	0.51
	Conditional Kappa (Inundated)	0.37
	Fit	0.58

0.055 in Table5.3), the performance of the model in relation to inundation extent prediction showed to be relatively similar, if the floodplain treatment is adequate and given that floodplain topography is identified at the highest resolution possible. This difference becomes clear by comparing Tables 5.3 and 5.4, illustrating different levels of agreement. There are a number of reasons for this difference. First, as the study area is located in an upland floodplain, the general slope of the floodplain is higher than lowland floodplains and this may result in little storage in each storage cell on the floodplain. Second, in the storage cell mode, there is no flux on the floodplain, meaning that, as soon as the volume of water in each cell exceeds its storage limit, additional water is transferred downstream without any delay. This may be the reason that no attenuation is seen in the outflow hydrographs when the n values increase in the main channel (see Figure 5.11). The only delay

that may occur is attributed to the capacity of hydraulic connections in conveying flow between storage cells. This may lead to blockage and back water effects in cells and hence larger flooded area occurs. Third, water fills storage cells from the lowest points upwards (see initial stages of Figure 5.4c), regardless of location from which the water comes into the cell. This means that, in a certain storage cell, if there is only potential restriction in relation to capacity of the hydraulic connections (no blockage and back water effects), as the volume of flow into a cell increases (as a result of increase of n in the main channel) no change may occur in the inundation extent associated with water stored in that cell. The inundated area in each cell is as a result of water stored in the cell before potential blockage effects (i.e. storage capacity) and additional water stored due to potential blockage and back water effects. Hence, in storage cell mode, flows that leave the main channel do not necessarily change the inundated area, which this is the main weakness of the storage cell mode in relation to inundation extent prediction. From this brief explanation, the lower performance of the model for inundation extent prediction (Table 5.4) as compared with predictions of where flow leaves or returns to the main channel (Table 5.3) is explained. This justification is of great significance where there are gaps between predicted inundated areas (as in the middle of the study reach, Figure 5.15). If the downstream half of the study reach in relation to inundated area is studied (Figure 5.15), there are no gaps in predicted inundated areas between cells. This is due to blockage and back water caused by the channel river configuration downstream so that all flood flows are conveyed through the main channel at the outlet of the study reach. This causes the storage capacity of cells in this part of the study reach to increase and hence, inundated areas appear continuous between the storage cells. In other words, if storage cells are too large, floodplain flux effects become important, and this will lead to poor agreement as storage cells will automatically put water in the lowest elevations in the storage cell rather than routing it across the storage cell. What is defined as the critical size depends on channel configuration in relation to flood size. It is less of an issue for big floods when a storage cell may be fully inundated or for little floods where channel configuration encourages full inundation.

As mentioned before, to make a definite judgement in relation to the predictive ability of the model, the numerical performance of the model can also be compared

in terms of overall mass balance errors and computational efficiency. Mass balance errors for each simulation performed here are summarised in Table 5.5.

Table 5.5: Mass balance errors for HEC-RAS in storage cells mode for simulations considered for calibration process

n (channel)	Mass error (%)
0.04	-0.01
0.045	-0.02
0.05	-0.03
0.055	-0.03
0.06	-0.03

Table 5.5 shows that mass balance errors range from 0.01 to 0.03m^3/s of the inflow hydrograph at upstream boundary condition. As Bates and De Roo (2000) explained there are no objective criteria to accept or reject a simulation with given mass balance error values. This becomes more difficult when we still do not know the values of error associated with the estimation of upstream boundary conditions and the effect of simplifications made in relation to process representation in the model structure on predictions. Like HEC-RAS in the normal mode, the mass balance errors found here probably have a minimal effect on the predicted inundation extent.

The best performance of the storage cell mode of HEC-RAS in relation to inundation extent is still uncertain because, as the n value in the main channel increases, the agreement between prediction and observations of inundated area improves (see Table 5.4). This is regardless of the kind of accuracy assessment method used. Table 5.4 shows the best performance of the model in the range simulated is attributed to Manning's n 0.065. Since model performance is dependent on water depth on the floodplain, by using higher n values, better performance is expected. To make a definite judgement in relation to the value of n that results in the best prediction of inundation area, comparisons between the maximum water levels predicted and observed during the flooding for a set of points on the floodplain (i.e. internal validation) were conducted. Table 5.6 presents the predicted maximum water levels using different n values as compared the observed data on the floodplain. The difference between the observed and predicted maximum water levels is presented as quantified values.

Table 5.6: Comparison between the predicted and observed water levels (absolute and quantified values) on the floodplain, using different friction factor in the main channel

Flood 1 in 0.05	Predicted peak water level (m), using								Observed
Cell	n = .050 absolute	n = .050 quantified	n = .055 absolute	n = .055 quantified	n = .060 absolute	n = .060 quantified	n = .065 absolute	n = .065 quantified	water level (m)
c34	215.98	0.27	216.12	0.13	216.25	0.00	216.38	-0.13	216.25
c35	215.95	0.15	216.08	0.02	216.21	-0.11	216.33	-0.23	216.10
c20-1	221.37	0.03	221.42	-0.02	221.47	-0.07	221.53	-0.13	221.40
c20-2	220.88	0.02	220.94	-0.04	221.01	-0.11	221.10	-0.20	220.90
c21-1	220.46	0.04	220.50	0.00	220.54	-0.04	220.60	-0.10	220.50
c21-2	220.03	0.07	220.09	0.01	220.16	-0.06	220.24	-0.14	220.10
c26-1	219.84	0.06	219.87	0.03	219.90	0.00	219.94	-0.04	219.90
c26-2	219.83	0.07	219.86	0.04	219.88	0.02	219.92	-0.02	219.90
c29-1	218.62	0.08	218.70	0.00	218.78	-0.08	218.86	-0.16	218.70
c30-2	217.42	0.08	217.45	0.05	217.47	0.03	217.52	-0.02	217.50
c30-3	216.85	0.05	216.91	-0.01	216.96	-0.06	217.02	-0.12	216.90
c30-4	216.78	0.04	216.82	0.00	216.86	-0.04	216.91	-0.09	216.82
c30-6	216.60	-0.20	216.64	-0.24	216.69	-0.29	216.74	-0.34	216.40
c36-1	215.84	0.26	215.96	0.14	216.07	0.03	216.20	-0.10	216.10
c36-2	215.82	0.18	215.93	0.07	216.04	-0.04	216.17	-0.17	216.00
c36-3	215.80	0.20	215.91	0.09	216.02	-0.02	216.15	-0.15	216.00
Mean		0.09		0.02		-0.05		-0.13	
STEDV		0.11		0.09		0.08		0.08	

It should be noted that the positive and negative values in the quantified values in Table 5.6 indicates under-prediction and over-prediction of maximum water levels respectively on the floodplain. The difference between the observed and predicted water levels (i.e. quantified values) for the specified points is plotted in Figure 5.14. Table 5.4 shows that that the minimum of the mean difference between the observed and predicted water levels is obtained using an n value of 0.055. Using the n value of 0.055, maximum water levels at the specified points is under-predicted by 0.02m on average. The second best prediction is achieved using the n value of 0.06. The comparison between the standard deviation obtained using the n values 0.055 and 0.06 indicates that there is no meaningful difference between them (0.09 versus 0.08) and hence, the scenario that is attributed to the lower mean difference can be accepted as the best prediction. Therefore, as the prediction of water elevations along side the study reach is of a higher accuracy using the n value

Fig. 5.14: The relative difference between the observed water levels and the predicted ones using different *n* values
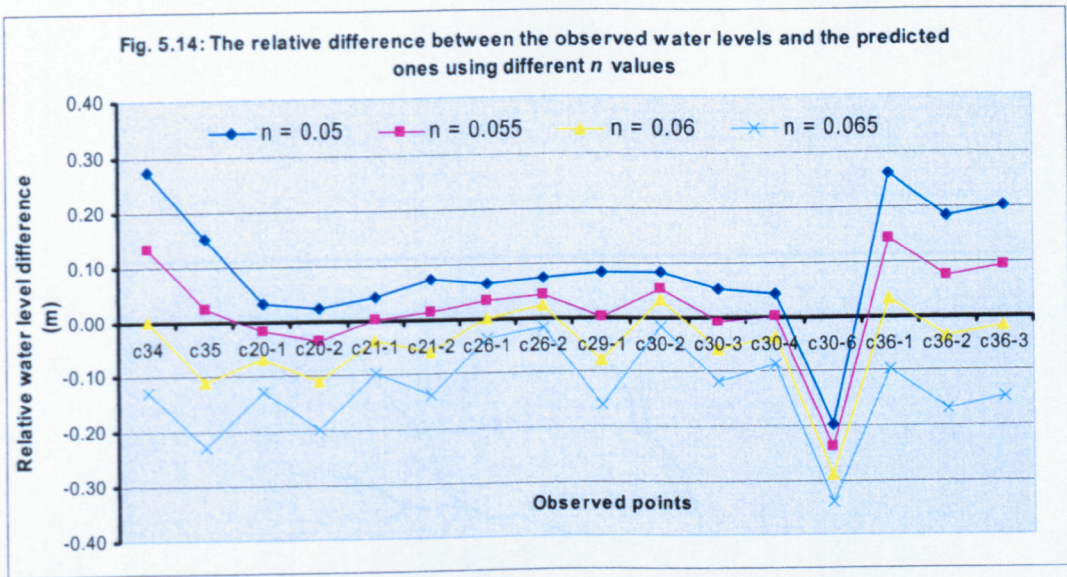
of 0.055, the inundation extent that is associated with that is assigned as the best ability of this model in relation to water level. It should be noted that storage cells used for comparing the predicted and observed water elevations on the floodplain (see Table 5.6) are located mostly in the downstream half of the reach, where the back water and blockage effects in storage cell model result in a good match between predictions and observations. This may explain different main channel *n* values associated with the best inundation predictions in these models (0.060 and 0.055 for normal and storage cell models respectively). Figure 5.15 shows that the best agreement between the flooded areas predicted in storage cell mode and the flooded areas observed during flooding is 54% in terms of F. The selection of the *n* value of 0.055 as the best estimate of the friction factor for the main channel in relation to the prediction of water elevations on the floodplain is consistent with what was obtained in relation to the performance of the lateral weirs of the model.
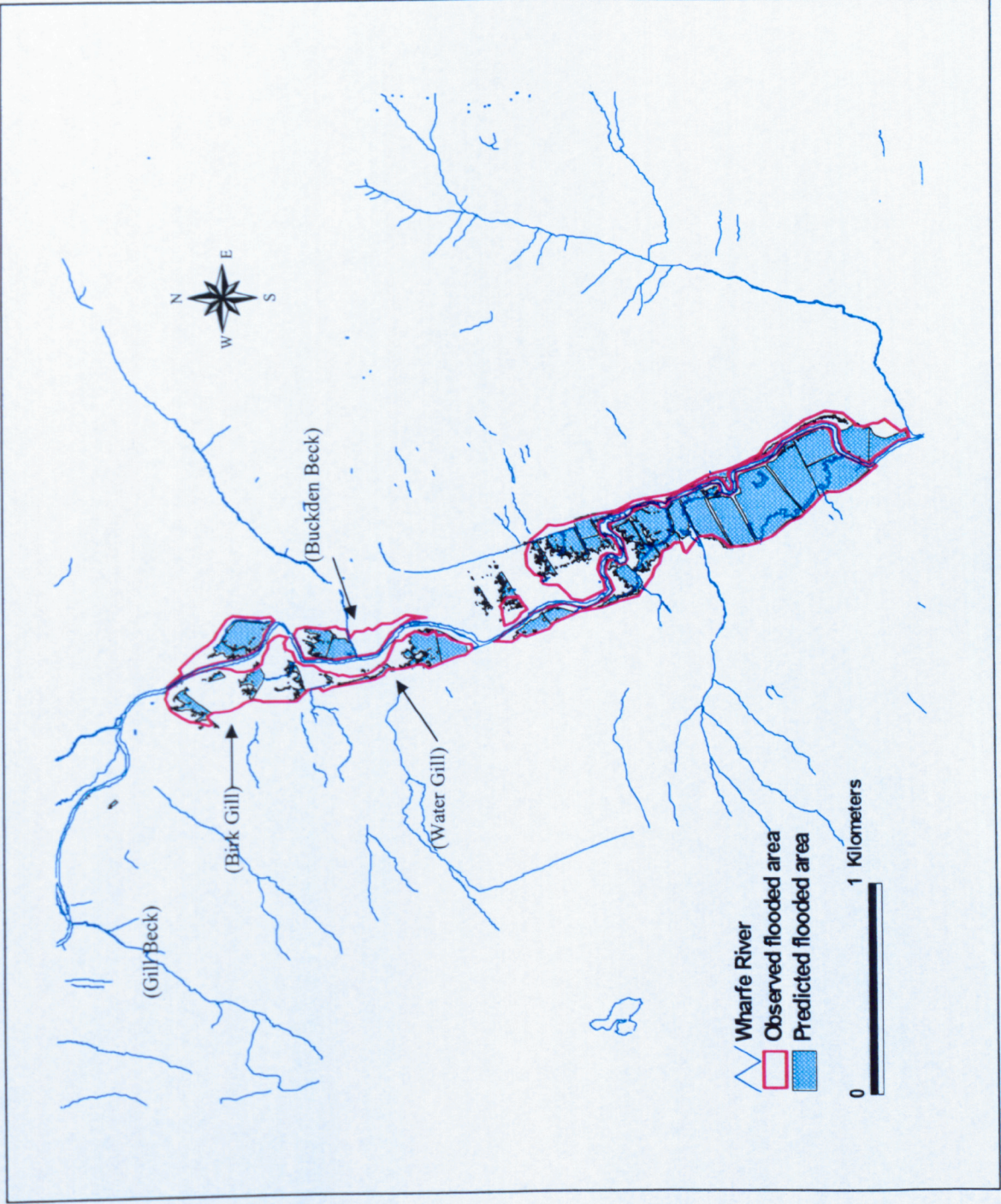
5.5 Discussion

The storage cell mode of HEC-RAS was applied to the study reach for the flood event considered in this research. The best measure of fit (i.e. F%) was estimated as 54% using an n value of 0.055 in the main channel. As mentioned before, inundation of the floodplain in storage cell mode is controlled by the storage capacity of each storage cell and as soon as water level reaches a critical elevation (i.e. the elevation of hydraulic connections between storage cells), water is conveyed without any delay to downstream part of the reach as there is no treatment of flux effects on the floodplain. The only potential delay that may occur is due to the conveyance capacity defined by hydraulic connections and flood magnitude, which may cause blockage and backwater effects between cells. This effect becomes more significant in downstream cells of the domain as any flow that leaves the main channel is conveyed immediately to these cells provided that continuous hydraulic connections exist. On this basis, upstream cells are usually less inundated and downstream cells fully inundated aided by the downstream channel configuration. Less inundation of upstream cells and a better correspondence between predicted and observed inundation extents in downstream cells reflects this (Figure 5.15). Thus, inundation extent in the storage cell mode is not a function of the volume of flow that leaves the main channel, but the primary storage capacity (i.e. storage capacity below critical elevation of a hydraulic connection) of a cell and the potential effects of backwater and blockage. This reflects the failure of the storage cell approach to represent flux effects explicitly. Indeed, the main problem with the storage cell approach in this environment is that the storage cells are not true storage cells where the residence time of water in each cell significantly exceeds the flood duration time. As with the normal mode, the storage cell approach represents only a very poor treatment of actual floodplain processes. On the other hand, this chapter has shown that model performance results do depend on validation data. Validation data in this study are associated with some uncertainty, stemming from the contribution of tributary and hillslope flows to inundation extent. These uncertainties are less attributed to the location of shorelines as they were surveyed using GPS and supported with ground surveys and observational evidence. These are mostly resulted from the effects of hillslope and tributary flows on the floodplain. Although lateral inflow hydrographs resulting from tributaries

within the study domain were considered as boundary conditions in the simulations undertaken, they were connected to the main channel and so affect flood inundation unrealistically. This is true due to an inappropriate model design rather than uncertainties in validation data. However, what is crucial here is that the predicted and observed inundation extents cannot properly be compared with each other as part of the observed inundation extent has a non-main channel source. This may be explained by disagreement between predicted and observed inundation extent over parts of the floodplain that are affected by tributaries of Birk Gill, Buckden Beck and Water Gill (see Figure 5.15).

Despite the poor representation of flow on the floodplain in storage cell mode, the topographic characteristics of each cell are dominant role in determining flood inundation patterns within each storage cell. The high degree of agreement between predicted and observed shorelines at cells which are completely inundated reveals the significant contribution of topography to the inundation process.

In terms of the comparison of performance of storage cell and normal modes of HEC-RAS, both the normal and storage cell modes achieve relatively similar measure of fit at their optimum calibration, 50% for the normal mode and 54% for the storage cell mode. Despite the similarity of agreement between results, Figure 5.16 appears very different predictions of actual inundation extent, in which inundation extents derived from these two models are compared. This is due to different representation of floodplain flows on which the modes are based. In storage mode, little attention is paid to the effects of floodplain flux routing and the model performance is controlled by storage and blockage effects on the floodplain. This generally causes under-prediction of inundation extent particularly for upstream storage cells (see Figure 5.16). In terms of normal mode, the emphasis is on only momentum effects in downstream direction (may be a sufficient assumption in straight floodplain, narrow valley, low storage of the floodplain, simple topography of the floodplain). In addition, the planar approximation of water elevations on the floodplain particularly where the floodplain is protected by levées, which have a higher elevation than other parts of floodplain, results in over prediction of inundation extent. More importantly, in storage cell mode, the effect of floodplain topographic characteristics in predicting the precise location of shorelines is evident, particular where the inundation extent is less affected by

176

hillslope/tributary flows (compare Figure 5.15 and 5.16). As the effect of validation data on model performance is well acknowledged, the performance of the models used here might vary if a better validation date set was used.

5.6 Summary of Chapter

The storage cell concept for routing floodplain flows was tested, using an one - dimensional model in the main channel and 61 storage cells on the floodplain that they are hydraulically connected to the main channel and themselves. The boundaries of storage cells were defined using Landline data and field observations. In total, 171 hydraulic connections were established using field observations and parameterised using GPS and Lidar data. The model showed that it was able to simulate a wide range of flood magnitudes. The results of the model sensitivity to main channel n values showed that inundation extent in this mode is less affected by the volume of water that leaves the main channel but it depends on the primary capacity of storage cells and potential blockage effects. The model performance for the flood considered in this research was estimated as 54% at the optimum calibration, not a marked improvement as compared with normal mode. The comparison of lateral weir performances and the predictive ability of the model in relation to inundation extent revealed that the model was able to predict at better than 85% where water leaves the main channel but an inadequate flow process representation on the floodplain meant that the model could not produce reasonable results for inundation extent. Also, it was discussed that validation data were, to some extent, responsible for poor performance of the model. Finally, comparisons were conducted between the normal mode and storage cell conceptualisations and then their practical implications in the case study were reviewed.

In response to limitations expressed using normal and storage cell modes of HEC-RAS, a higher level of process complexity for floodplain flows based on two-dimensional diffusion wave treatment as a compromise solution, is used in the next chapter for inundation prediction.

Figure 5.16: Comparison of inundation extent derived from normal and storage cell modes at their best calibration

Wharfe river network
Normal mode
Storage cell mode

0   1 Kilometers
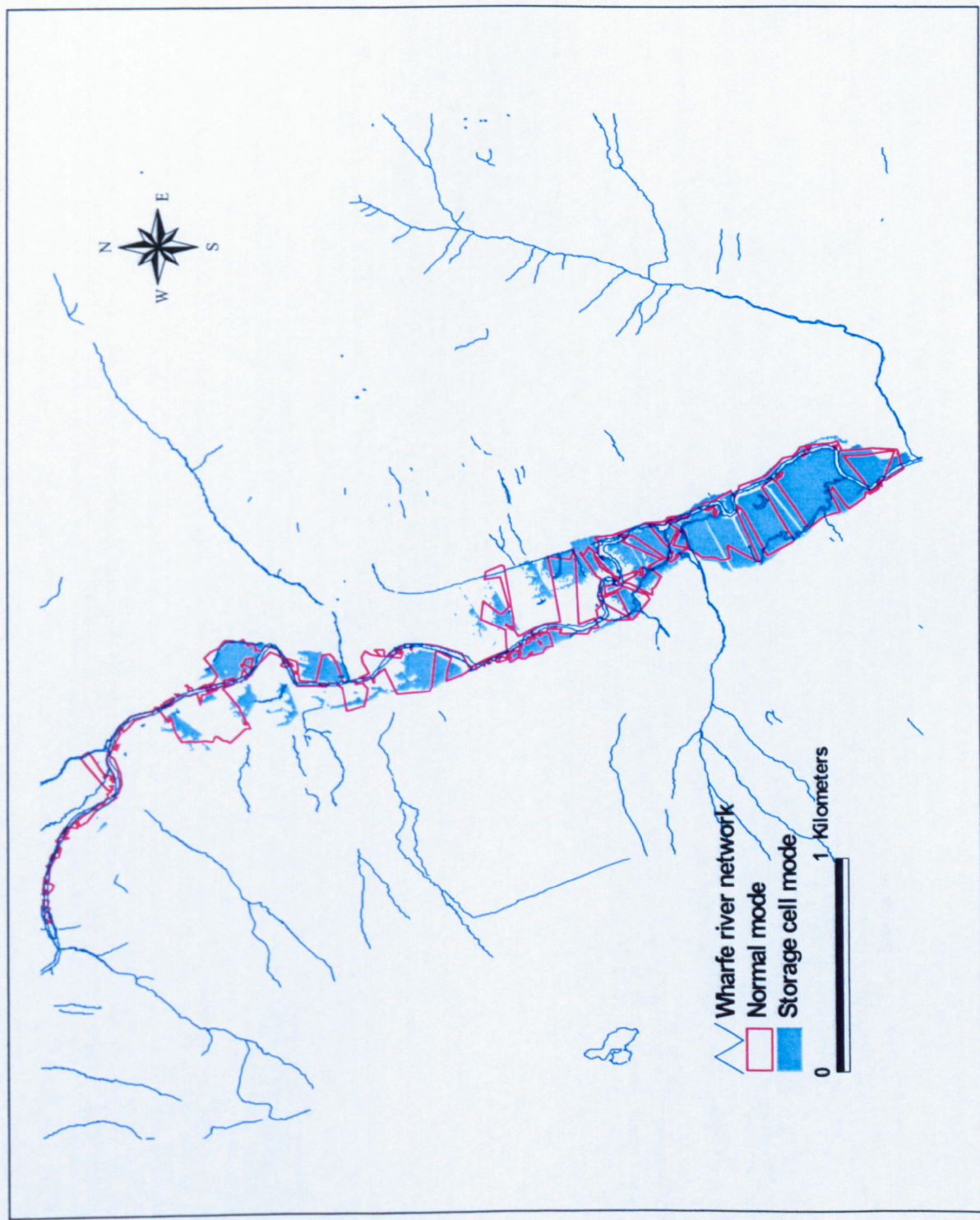
Chapter 6

Two-dimensional diffusion wave treatment of floodplain flows

6.1 Introduction

Physical hydraulic models have indicated that, whilst in-channel flows may be satisfactorily described by a one-dimensional representation, out-of-bank flows that incorporate significant two and three-dimensional effects invalidate such an approach (Sellin *et al.*, 1993; Ervine *et al.*, 1994; Knight and Shiono, 1996). Recognition of these limitations has led to development of two-dimensional finite element techniques for the simulation of the flood events along reach scale (1-60 km) compound channels (Gee *et al.*, 1990; Feldhaus *et al.*, 1992; Bates and Anderson, 1992, Bates and Anderson, 1994; Bates *et al.*, 1995, 1996, 1998; Stewart *et al.*, 1999). These models allow two-dimensional prediction of inundation and also provide the potential to investigate inundation mechanisms. The models have often been constrained by the limited spatial resolution of available topographic data sources and the cost of acquiring such data through ground survey (e.g. Bates and De Roo, 2000). Previously, flood inundation modelling has been constrained by the scarcity of detailed topographic data (e.g. Bates *et al.*, 1992; Marks and Bates, 2000). This is particularly problematic where flood routing is affected by complexity in topographic features (e.g. urban areas, rural areas with structurally complex floodplain due to natural or man-made obstacles; and the isolated ponding areas) (Yu and Lane, in press a, b). With the

179

growing availability of high quality remotely sensed floodplain topographic data (i.e. Lidar and Synthetic Aperture Radar, SAR), there has been a shift from a data-poor to a data-rich environment in relation to floodplain flow modelling (Marks and Bates, 2000; Bates *et al.*, 2003). This is making two-dimensional flood inundation modelling an increasingly practical flood analysis tool (Bradbrook *et al.*, in press).

As yet, no consensus exists concerning the level of model process complexity required to achieve a satisfactory prediction in terms of flood inundation extent (Horritt and Bates 2000). Such a conclusion is supported if the recent modelling studies in relation to inundation extent prediction are reviewed. For instance, Horritt and Bates (2002) showed that three hydraulic models with three different level of process complexity including HEC-RAS (full one-dimensional), LISFLOOD-FP (two-dimensional diffusion wave treatment), and TELEMAC-2D (full two-dimensional) are capable of predicting flood extent and travel times to similar levels of accuracy at optimum calibration where all three models use the same high quality topographic data for parameterisation. Bates and De Roo found that a diffusion wave treatment out-performed a two-dimensional finite element approach because the simplified treatment of flow routing on the floodplain allowed a much higher density representation of floodplain topography.

Attempts have been made to develop a simplified form of two-dimensional floodplain flow routing based upon a two-dimensional diffusion wave treatment (e.g. Bates and De Roo, 2000; De Roo *et al.*, 2000; Horritt and Bates, 2001a, 2001b, 2002, Bradbrook *et al.*, 2004; Yu and Lane, in press a, b). These approaches focus on floodplain flow representation, as one-dimensional representation of in-channel flows is broadly accepted by scientists for the cases of interest to hydrologist (e.g. Sellin and Willets, 1996; Knight and Shiono, 1996). The appeal of a simplified two-dimensional approach is based upon the fact that recent studies have demonstrated that floodplain topographic features have a controlling role in flow distribution on floodplain environments (see Nicholas and Walling, 1997; Hardy *et al.*, 1999; Marks and Bates, 2000; Bates and De Roo, 2000; Horritt and Bates 2001a,b; Nicholas and Mitchell, 2003). Hence, there is the possibility that simpler models in conjunction with high quality topographic data for floodplain areas may provide similar levels of predictive ability (in terms

of inundation extent) to more complicated models. The availability of high quality topographic data for floodplain environments has provided opportunities for simpler models to be tested in this context. In addition, the results presented in Chapters 4 and 5 have shown the drawbacks of normal and storage model approaches. The former only represent the momentum effects of floodplain flows without considering blockage and storage effects that may be caused by physical obstacles on the floodplain. The latter emphasizes storage effects caused by floodplain topographic characteristics. However, the way flow processes on the floodplain are represented in the storage mode, leads to an overly rapid flux rate on the floodplain. Hence, a model representing a compromise solution is favoured. In response to this need, two-dimensional diffusion wave treatments have recently been introduced (e.g. Bates and De Roo, 2000; Yu and Lane, in press a, b). They sacrifice process representation in relation to treatment of the two-dimensional depth-averaged momentum equations and also address known problems of one-dimensional modelling of flood inundation. For instance, the diffusion wave approach directly models floodplain zones located between cross sections whereas in one-dimensional treatments, such zones are not well represented and the only parameter that may compensate such geometrical effects is floodplain roughness, although careful design of model geometry may help the weakness.

In this chapter, a two-dimensional diffusion wave treatment is described and linked to a one-dimensional hydraulic model for in-channel flow routing in order to predict the inundation extent resulting from the flood of 4th February 2004. The model responses (i.e. inundation extent) are analysed by changing the resolution of topographic data and floodplain roughness. Then, the model is calibrated and validated against the observed shorelines. Using four accuracy assessment tests, the model performance in terms of inundation extent at optimum calibration is assessed. Finally, the predictive ability of the model as compared with the normal and storage cell modes of HEC-RAS in relation to inundation extent is determined.

6.2 Raster-based two-dimensional diffusion wave model

As mentioned above, these types of models are relatively recent (Bates and De Roo, 2000; Horritt and Bates, 2001a, 2001b, 2002, Yu and Lane, in press a, b). They are based on the same idea as the storage cell concept (i.e. they are quasi two dimensional) (Cunge *et al.*, 1975, 1980) but the size of cells is reduced down to the elevation data resolution. By using high quality topographic data, these types of models are particularly suitable for topographically complex floodplains. These floodplains are characterised by natural obstacles and man-made structures (dykes, elevated roads field walls, embankments etc.) abandoned channels and drainage ditches, and small urban areas as well. Natural or structural features on the floodplain generally act to block areas of floodplain, particularly under shallow flows, and so control the timing and direction of flow in the larger domain. These may affect both inundation extent and inundation timing considerably. For instance, Nicholas and Mitchell (2003) emphasize the effects of abandoned channels and floodplain drainage ditches on floodplain inundation, particularly in the initial stage of flooding. In one-dimensional models, these effects (topographic features) are usually represented either by changing roughness coefficient values during the calibration process or establishing storage cells on the floodplain (see Chapter 5). In raster-based models, the study domain is discretised into raster grid cells with flood flows routed according to the real local slope on the floodplain (i.e. a directional treatment). Spatially-varying roughness coefficients over the floodplain can then be used as part of a distributed calibration (Horritt and Bates, 2001a).

In raster-based models, water levels are updated using the continuity equation at each cell while the fluxes between cells are estimated using water levels in the adjacent cells and one of the following approximations: uniform flow, gradually varied flow, diffusive wave or a weir equation. For instance, Bates and De Roo (2000); and Horritt and Bates (2001b) have used kinematic (i.e. uniform flow) and diffusive wave treatments as methods that route flow rates between adjacent cells. In the last chapter, weir equations were used to estimate fluxes between storage cells on the floodplain.

These types of models are closely related to the Digital Elevation Models (DEM) used to derive them and this simplifies the input of data and visualisation of

results. Raster based models are able to underlay the highest resolution raster grids in order for inundation calculations at spatial scales in which full two-dimensional hydraulic models at a resolution comparable to raster cell sizes are not computationally feasible.

Raster-based models are specifically designed to predict flood inundation and less attention has been paid to the representation of the processes associated with routing. In other words, inundation prediction ability is maximised at the expense of other aspects of the hydraulics, such as flood routing (Bates and De Roo, 2000). In general, the raster-based models have a number of advantages in terms of formulation simplicity, low computational cost, limited calibration factors and ready integration with newly available high-resolution data sources. Their disadvantages include: (i) simplified representation of flow processes due partially to the poor representation of momentum transfers on the floodplain, and between the main river and floodplain; and (ii) issues associated with numerical solution, including strong sensitivity to discretisation in time and space (Yu and Lane, in press, a)

In this research, a raster-based diffusion wave model that has been developed in a separate research project by Yu and Lane (in press, a) for floodplain inundation extent in urban areas is linked to a one-dimensional hydraulic model that routes flow within main channel (i.e. HEC-RAS). This link is made using the lateral weirs established in the storage cells mode of HEC-RAS (see Chapter 5) along the study reach. The lateral weir results provide the transferred flow data (i.e. entering and leaving the floodplain) between the main channel and the floodplain at any specific location along the study reach and at any specific time step during flooding. Hence, these data can be used continuously as input data at the main channel/floodplain boundary for the floodplain model.

6.3 Two-dimensional diffusion wave model description

The basic component of the raster-based inundation model is a raster Digital Elevation Model of resolution and accuracy sufficient to identify the elements of the floodplain topography (dykes, embankments, depressions, walls, buildings and former channels) considered necessary to distribute flood flows on the floodplain. The optimum resolution cannot be known a priori and may only be

determined after calibration. It should be guessed as a starting point. Having defined the basic data source, the next step is to select the process representation complexity. The optimum level of process complexity must be so that it sacrifices process representation but not so far that this undermines the capability of the model to route water to the covered parts of the floodplain. This may be achieved using a diffusion wave treatment of the depth-averaged momentum equations in which the inertial terms (i.e. acceleration and advection terms) are lost (Bradbrook *et al.*, 2004). In addition, using a raster-based inundation model involves local topographic characteristics in routing flows on floodplains independent of flow elevations in the main channel. This overcomes some of the limitations found in one-dimensional modelling of flood inundation.

For the first time, Bates and De Roo (2000) developed LISFLOOD-FP as a raster-based inundation model that was based on the most basic dynamic wave routing scheme available: a kinematic wave approximation. Horritt and Bates (2002) improved the model so that floodplain flows could be treated under a diffusive wave approximation too. The raster-based model used in this research (Yu and Lane, in press, a) takes a similar structure to the work of Bradbrook *et al.* (2004) and is described in terms of continuity and momentum (diffusive wave approximation) equations. The model follows Horritt and Bates (2002) but improvements in terms of wetting and drying processes have been made.

The simplest way to achieve distributed routing of water over the floodplain is to consider each grid cell as a storage volume for which a continuity equation is solved (see Figure 6.1). The continuity equation states that the change in volume in each cell over time (i.e. a time step) is equal to the fluxes into and out of it.

$$\frac{dV}{dt} = Q_{up} + Q_{down} + Q_{left} + Q_{right} \qquad \text{Eq. (6.1)}$$

where V is the cell volume, t is time and Q_{up}, Q_{down}, Q_{left}, Q_{right} are the flow rates (either positive or negative) from upstream, downstream, left and right adjacent cells, respectively.

184

Having set the calculation area (a DEM for potential floodplain) and specified the inflow boundary (i.e. inflow hydrograph), the next step is to represent the likely flow distribution across the boundary. To do that, the total inflow across the boundary is partitioned according to the depth in the cell at the start of the time step. The general form of the Manning equation for an irregular cross section is:

$$Q = \frac{AR^{2/3}S^{1/2}}{n}$$
Eq. (6.2)

where Q is the flux between cells, A is the cross sectional area at the interface of the two cells, R is the hydraulic radius at the interface of the two cells, S is the water surface slope between the two cells (i.e. energy slope) and n is the Manning friction coefficient. It is a common practice in hydraulic analysis (e.g. ISIS, HEC-RAS) to split compound cross sections into a series of sub-divisions and to calculate flow conveyance in them separately. Bradbrook et al., (2004) note that if the flow across the face of each cell is treated as separate sub-division, assuming the regular grids the flow area is given by $A = w.d$ where w is the width of the cells and d is the flow depth at the interface. In this state, the wetted perimeter, P, will be equal to the flow width since the ground level is assumed to be uniform across the cell. Thus, the hydraulic radius is equal to the depth of flow at that cell, $R = \dfrac{A}{P} = \dfrac{w.d}{w} = d$ and Manning equation takes the form:

$$Q = \frac{wd^{5/3}S^{1/2}}{n}$$
Eq. (6.3)

Equation 6.3 is used to partition the total inflow between the wet cells that lie on the boundary. Thus, for a total inflow of Q_{in}, the inflow to cell i, ($Q_{in,i}$), of n wet cells along the boundary is given by:

$$Q_{in,i} = Q_{in} \frac{d_i^{5/3}}{\sum_n d_i^{5/3}}$$
Eq. (6.4)

Figure 6.1 shows a centrally-located grid cell (i, j) and four cells adjacent to it, which may connect directly with the central cell. To calculate flow rates between the central cell and any of these cells two parameters, the energy slope (S) and the effective depth (h), in the Manning equation should be determined.

Figure 6.1: Flow orientation for a single central cell

	$(i+1, j)$	
$(i, j-1)$	(i, j)	$(i, j+1)$
	$(i-1, j)$	
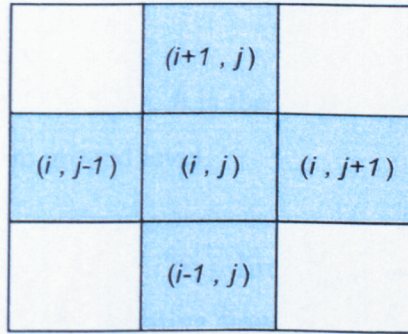
In each orthogonal direction, the energy slope is given by the difference in water levels between the cells divided by the distance between the cell centres. Water is allowed to flow out from the source cell to the adjacent cells only if the energy slope is positive.

$$S_i = \frac{h_{i,j} - h_{i\pm1,j}}{w}$$

Eq. (6.5)

$$S_j = \frac{h_{i,j} - h_{i,j\pm1}}{w}$$

Eq. (6.6)

Outflow from a grid cell is only allowed into two of the orthogonal directions, determined by the vector sum of the energy slopes. The vector sum of the energy slopes along i and j directions is determined as:

$$S = \sqrt{S_i^2 + S_j^2}$$

Eq. (6.7)

Another parameter that should be determined to solve the Manning equation is the flow depth, d. The effective flow depth is determined as the difference between the water level at the source cell and the ground level at either the source or destination cell, which ever has the higher elevation. This is because in complex topography the effect of local low points and local high points at the source and destination cells may results in an inaccurate estimation of the effective flow depth. Hence these effects should be removed. The actual flow depth between a source cell and a destination cell in each i or j direction can be calculated as:

$$d_i = h_{i,j} - \max\lfloor g_{i,j}, g_{i\pm1,j} \rfloor \qquad \text{Eq. (6.8)}$$

$$d_j = h_{i,j} - \max\lfloor g_{i,j}, g_{i,j\pm1} \rfloor \qquad \text{Eq. (6.9)}$$

where d is the effective flow depth, h is the water surface elevation at the source cell and g is the maximum ground level.

As the effective flow depth in the i or j direction may have a distinct value, the effective flow depth as a representative flow depth for the source cell in the line of steepest slope is then calculated by the arithmetic mean of the two effective flow depths as:

$$d = \frac{d_i S_i^2 + d_j S_j^2}{S^2} \qquad \text{Eq. (6.10)}$$

where d is the effective flow depth at the interface of the source and destination cells, d_i and d_j are the effective flow depths at the directions i and j, S_i and S_j are the energy slopes at the directions i and j and S is the vector sum of the energy slope.

Substituting equations (6.7) and (6.10) into equation (6.4) provide all parameters necessary to solve Manning's equation discretised in a regular grid. Having solved the Manning's equation in a regular grid, the diffusive wave equation over the grid can then be solved in order to route flow vectors at both i and j orthogonal directions. The flow can only go to up to two adjacent cells at each time step. The flow equations that are derived from the discretisation of the diffusive wave equation over the domain grid are as follows:

$$Q_i = Q\frac{S_i}{S} = \frac{wd^{5/3}S_i}{nS^{1/2}} = \frac{wd^{5/3}\left(\dfrac{h_{i,j} - h_{i\pm1,j}}{w}\right)}{n\left[\left(\dfrac{h_{i,j} - h_{i\pm1,j}}{w}\right)^2 + \left(\dfrac{h_{i,j} - h_{i,j\pm1}}{w}\right)^2\right]^{1/4}}$$

Eq. (6.11a)

$$Q_j = Q\frac{S_j}{S} = \frac{wd^{5/3}S_j}{nS^{1/2}} = \frac{wd^{5/3}\left(\dfrac{h_{i,j}-h_{i,j\pm1}}{w}\right)}{n\left[\left(\dfrac{h_{i,j}-h_{i\pm1,j}}{w}\right)^2 + \left(\dfrac{h_{i,j}-h_{i,j\pm1}}{w}\right)^2\right]^{1/4}}$$

<div align="right">Eq. (6.11b)</div>

Using equation (6.11a) and (6.11b) the flow rates into and/or out of the grid cells in two dimensions are calculated at every time step. The change of water depth (? d) in each of the grid cells can then be estimated at the beginning of each time step by:

$$\frac{\Delta d}{\Delta t} = \frac{\displaystyle\sum_{d=1}^{4}Q_{in(i,j)}^d - \sum_{d=1}^{4}Q_{out(i,j)}^d + Q_{inf\,low}}{w}$$

<div align="right">Eq. (6.12)</div>

where Δt is the time step, $\sum Q_{in}$ is the net inflow into a cell from the adjacent cells, $\sum Q_{out}$ is the net outflow from a cell into the adjacent cells and $Q_{inf\,low}$ is inflow into a cell from upstream boundary.

Having calculated the flow magnitude in each of the two orthogonal directions, flow velocity can be estimated via

$$v_i = \frac{Q_i}{wd_i}$$

<div align="right">Eq. (6.13a)</div>

$$v_j = \frac{Q_j}{wd_j}$$

<div align="right">Eq. (6.13b)</div>

These equations can be shown to be equivalent to a two-dimensional discretised form of the diffusive wave equation, which is obtained from the full St. Venant equations by neglecting the local and convective acceleration terms in the momentum equation (Horritt and Bates, 2001a; Bradbrook *et al.*, 2004). In the method used here, the flow between cells is solely a function of the component of free surface gradient in either the i or the j directions. In the diffusive approach derived from a two-dimensional depth-averaged momentum equation, the i and j components of the flow are linked (Horritt and Bates, 2001b).

6.3.1 Wetting and drying processes

The flow depth calculated for each grid cell on the floodplain is assigned as the average flow depth over that whole cell. In terms of the wetting process, once a cell receives water at a specific time step, the wetting front edge lies within the cell. In most cases it will take a couple of time steps to become fully wetted. If this process is not represented, it can lead to overly rapid diffusion of flow across the floodplain. To deal with this problem, an assumption is made where water is not allowed to flow out of a cell until the wetting front has crossed the cell. This is based on a wetting factor for each cell (Bradbrook *et al.*, 2004) that represents the percentage of a cell that is wet. The wetting factor is estimated as follows

$$\%wet = \max\left(1, \frac{v\Delta t}{\Delta x}\right) \qquad \text{Eq. (6.14)}$$

The water is not allowed to flow out a cell as long as the wetting factor is less than one (i.e. the cell is not fully wet). The wetting factor is updated each time step as water advances over a grid cell. Although the wetting factor is essential for water to exit from a cell, it is not a sufficient condition. In addition, a minimum water depth must be set for each cell so that before this depth is reached no flux across cell faces is allowed.

When the water volume leaving a cell is bigger than one entering the cell, the cell is drying. In this sense, the water depth may be reduced to zero or even a negative value. This may causes two kinds of problems. First, negative depths are impossible. Second and more importantly, to have continuous inundation areas and to avoid the creation of isolated wet cells it is vital that partially wet cells are accurately maintained during the drying process. To deal with this, a minimum water depth is set after which no more outflow is allowed during the drying process (Bradbrook *et al.*, in press). If the sum of the inflow and outflow balances the minimum depth, then the outflow flux (and therefore inflow fluxes to other cells) is scaled by a drying factor, d_f :

$$d_f = \frac{w^2(d - d_{min})}{\Delta t \left(\sum_{d=1}^{4} Qin_{i,j}^d - \sum_{d=1}^{4} Qout_{i,j}^d - Q_{inf\ low} \right)} \qquad \text{Eq. (6.15)}$$

The drying factor ensures mass balance as the floodplain dries. The value of the minimum depth will depend upon the scale of reach and the model grid size. It may be desirable to have lower values for longer reaches in order to prevent significant attenuation of the flood volume. The minimum value of water depth (d_{min}) for the model used in this research is set as 0.01m (see Bradbrook et al., 2004).

6.3.2 Model solution

Model solution is based upon explicit forward differencing. Hence, the solution strongly depends upon grid resolution and time step. In general, the smaller the time step, the greater the model accuracy. As with most numerical models, the selection of the time step is therefore a compromise between accuracy and computational demand (Bradbrook et al., 2004). With explicit forward differencing, the maximum time step should be small enough so that any surface disturbance does not propagate beyond the boundaries of a grid cell. In general terms, the time step must be less than the time for flow to travel the cell width.

As the solution is explicit, the Courant condition can be applied as a necessary but not sufficient condition to determine the stability and accuracy of model solution at each time step:

$$\Delta t \leq \frac{w}{v + \sqrt{gd}} \qquad \text{Eq. (6.16)}$$

where d is the maximum water effective depth, w is the cell width and v is the flood wave velocity and g is acceleration due to gravity. The $\sqrt{gd}$ term is not strictly necessary with the formulation used here as there is no explicit treatment of inertial terms. Time steps longer than time required for flow to travel the cell width, may violate the Courant condition and lead to model instability. Traditional methods for determining time steps involve finding the smallest t

among those calculated for each grid point. The value of the denominator of the Equation (6.16) is stored for each wet cell and the maximum of this parameter within the domain is used in determining the maximum value of the time step for the next iteration. Over complex topography this value usually needs to be downscaled further (Bradbrook *et al.*, in press).

6.3.3 Model boundary conditions

Boundary conditions consist of an inflow hydrograph along each contact pixel between the main channel and floodplain. The hydrograph is produced using a weir equation along the reach for each specific lateral weir, resulting from using a one-dimensional hydraulic model (see Chapter 5) in the main channel. The hydrographs represent flow transfers to and from the floodplain (i.e. negative and positive flow rates respectively). In this state, it is assumed that the floodplain is protected by a long embankment that essentially acts as a continuous, broad-crested weir. This can be identified from topographic data (e.g. Lidar data). In this case the lateral weirs made in the storage cell mode of HEC-RAS (see Chapter 5) are overlaid on Lidar data in order to specify contact pixels between the main channel and floodplain. Applying a weir equation, the flux to the floodplain is determined based upon the predicted water level in the main channel (see section 5.2.2).

Outflow boundary conditions also need to be determined, relating to when and how water leaves the calculation domain. The method used here is based upon the work of Bradbrook *et al.*, (2004). Once water reaches an outflow boundary, at the end of each time step, the water depth in cells that are on the other side of the outflow boundary are set to be equal to the water depth in the adjacent cell. In this state, the water surface slope is the same as the bed slope across the boundary. If this results in a zero or reverse water surface slope (i.e. back into the calculation domain), then the water depth on the other side of the boundary is recalculated such that the water surface slope finds a nominal downstream slope. During the next time step, the outflow across the boundary is calculated depending on the water surface slope across the boundary (which will be either equal to the bed slope or zero). Mass conservation is checked at each time step to ensure that total

outflow is equal to the total inflow minus the increase in floodplain storage during that time step if there is water flowing out of the outflow boundary.

6.4 Model application (i.e. Raster-based 2D diffusion wave treatment)
6.4.1 Data requirements

The model was applied to the study reach considered for the research, a 5.5 km length of the River Wharfe. The basic data required for the model is a Raster Digital Elevation Model derived from Airborne Laser Altimetry (i.e. Lidar) with accuracy sufficient to identify both the channel (i.e. location) and those elements of the floodplain topography (dykes, embankments, walls, roads, fences etc.) considered necessary for flood inundation prediction. Specification of these elements was improved using OS Landline data. In this case, all obstacles that have implications for free distribution of the floodplain flow, including walls and fences, were identified in the OS base map. Then, an extensive field survey using a Global Positioning System has been performed to collect information necessary to correct the DEM through increasing the elevation of floodplain pixels to correctly represent walls etc (see Figure 6.1).

As there are embankments for flood protection along almost all of the study reach on both sides of the river, the hydraulic connection between main river and floodplain was made via lateral weirs. The positions of the lateral weirs were specified on the base map using their coordinate systems gained from geometric data from the storage cell model (see Chapter 5).

There is an issue here in that the resolution and accuracy needed to specify elements that are on the floodplain cannot be known a priori (see Bates and De Roo, 2000) and may vary between applications. The original Lidar data had a resolution of 2 meters. The original Lidar data has been post-proceeded to (i) standard data quality requirements for environmental studies, guaranteeing a precision of ± 0.25m throughout and improving to ± 0.15m in relatively flat areas with solid reflectance surfaces (Environmental Agency, 1997), as part of a separate project (James, 2004); and (ii) removal of errors resulting from tree canopies within the study areas. The 8m resolution was selected for simulations undertaken in this research (see section 6.4.2.1).
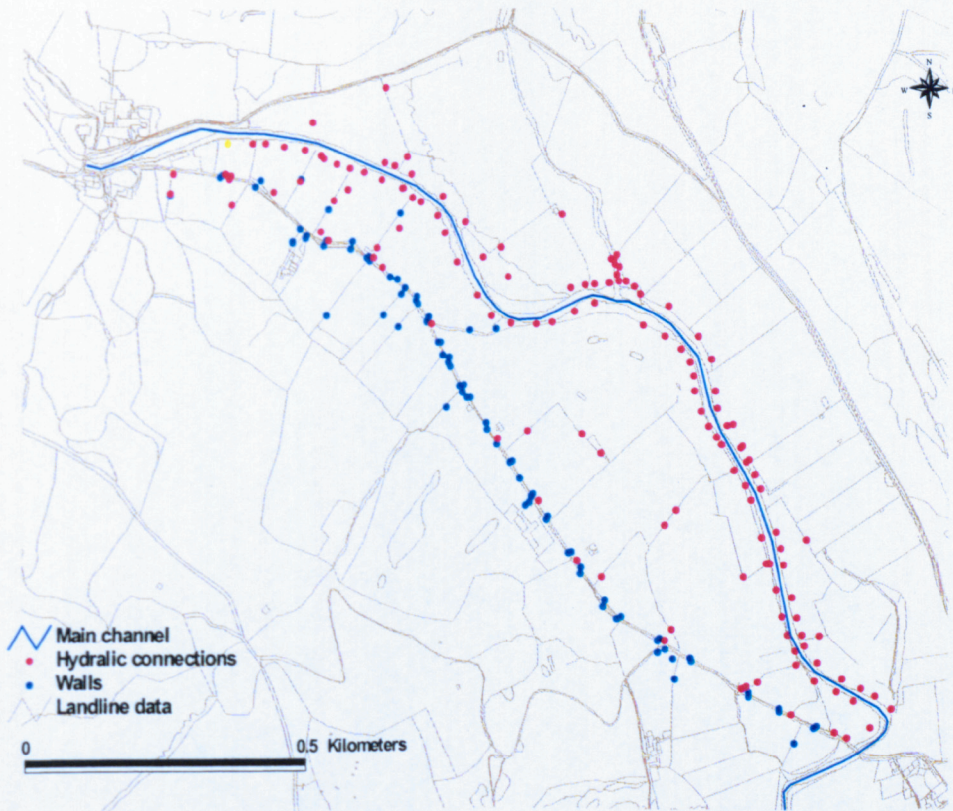
Once, the basic component of the model (i.e. a Digital Elevation Model of the floodplain) is specified, the only parameter needed for each cell on the floodplain to route water is a user-defined friction coefficient, which is given based upon the selected range of Manning's n for this particular floodplain (see section 4.11.3).

In terms of boundary conditions, the only data required to run the model are inflow and outflow boundary conditions produced using a one-dimensional hydraulic model for the main channel flow (i.e. storage cell mode of HEC-RAS). The main channel model provides flux data for each lateral weir established along the river and was entered to the floodplain model manually.

The flood considered for the study occurred on the 4th February 2004 with a peak flow of 47.8 m^3/s and duration of 18.5h (see sections 3.5.4 and 4.10). This was used to estimate flux from the main river to the floodplain. Given the results obtained in the last two chapters, lateral weir outflows produced using Manning's $n = 0.055$ and 0.060 in the main channel in the storage cell mode were considered as input flow hydrographs for the raster-based two-dimensional diffusion model. However, to have a better understanding of the raster-based model behaviour in

relation to inundation extent prediction, a wider range of main channel roughness values, including 0.045 and 0.065, was considered. This will allow us to compare the performance of the three models used in the study in the light of main channel friction changes.

6.4.2 Sensitivity analysis of the raster-based 2-d diffusion wave model

As with the normal and storage mode of HEC-RAS, scenarios based upon physical parameters and boundary conditions were established for sensitivity analysis. The only physical parameters required are a reasonable range of Manning's n values for only floodplain areas. This range should be selected based upon the fact that the friction coefficient in this model (i.e. 2-d diffusion wave model) may have a different physical meaning due to: (i) the kind of flow processes included in routing of floodplain flows; and (ii) the removal of elements of floodplain areas that may have implications for floodplain flow behaviour. In the latter case, the effect of these elements on floodplain flow (e.g. walls, fences, houses) is usually compensated by increasing the friction factor value. Similar to the normal mode of HEC-RAS, the range of 0.03-0.08 with increments of 0.01 was selected as friction factor values on the floodplain for sensitivity analysis. As mentioned before, a lateral inflow boundary condition produced using the n value of 0.06 for the main channel in the storage cell mode (as optimum calibrated value) was considered for the raster-based model. To evaluate the raster-based model behaviour in relation to inundation extent variations in response to increased inflow on to the floodplain resulting from the main channel friction changes (i.e. lateral inflow boundary condition change due to main channel friction change), a wider range of the main channel n values (0.065, 0.060, 0.055 and 0.045) was selected. The effect of boundary conditions (i.e. lateral inflow hydrographs from main channel onto floodplain) variation were analysed using a range of statistical flood events in the main channel that, in turn, produced different lateral inflow hydrographs for the raster-based model on the floodplain. As with the normal and storage cell modes of HEC-RAS, boundary conditions are based upon flood events with 0.5- (i.e. flood event of the 4th February 2004), 2-, 5- and 10-year return periods, estimated for Hubberholme gauging station. In terms of the sensitivity of model predictions to spatial resolution, the research

relied on the results obtained by Horritt and Bates (2001a) and Yu and Lane (in press, a), which are discussed in the next section.

6.4.2.1 The effect of mesh resolution on inundation extent prediction

Previously, flood inundation modelling was constrained by the spatial resolution of available topographic data (see for example Marks and Bates, 2000). Hence, model resolution has been much finer than the resolution of the topographic data used to drive a simulation. Recently, with the increased availability of high resolution topographic data (e.g. Lidar), a new research area has emerged based upon integrating true large data sets with lower-resolution numerical inundation models (e.g. the finite element methods) in a optimum manner that makes maximum use of the information content of the data available (Bates *et al.*, 2003). This is not a central aim of this research as raster-based models enable high-resolution digital elevation models acquired by airborne laser altimetry and stereo-photogrametry to be incorporated into the models with lower data redundancy. However, there have been studies of mesh dependence effects on model results using finite element methods (e.g. Horritt, 2000; Hardy *et al.*, 1999). Some comment is required in relation to similar issues.

The effect of spatial scale on flood inundation predictions has been investigated by Horritt and Bates (2001a), and Yu and Lane (in press, a). These studies, qualitatively and quantitatively, have shown that the raster-based models are quite sensitive to spatial resolution for situations where the inundation extent is not confined by the topography of the floodplain, which depends on the size of the flood (Yu and Lane, in press, a). Horritt and Bates (2001a) showed that the increase of spatial resolution (decreasing grid size) allows the model to represent more accurately water storage near the channel and hence the retardation of the floodwave caused by this process. They found an optimal scale of 100 m so that running the model using a higher resolution than this led to neither an improvement nor degradation in inundation predictions, when the model was applied to a 60 km reach of the river Seven, UK, with a 435 m^3/s peak flow at the upstream end of the reach, a bankfull discharge of 180 m^3/s and channel width of 40 m. In that research, models with 10 to 100 m resolution were chosen as good predictors of inundation extent. Yu and Lane (in press, a) showed that 4 and 8 m
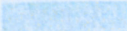
resolutions were associated with the best fit between model inundation extent predictions and observed data, where a flood event with the peak value of $563 m^3/s$ was simulated on a 4 km length reach of the river Ouse, UK. They applied four different spatial resolutions, 4, 8, 16 and 32 m, and the same model that is used in this research. The difference in the obtained optimum spatial resolution in the above studies (4/8 m versus 100 m) in relation to inundation prediction may be attributed to the different length scales of the reaches studied, local floodplain configuration with respect to flood magnitude and model structure (kinematic treatment versus diffusion wave treatment). Thus, we use the 8 m resolution as optimal in this research. This is justified for three reasons. First, the length scale of the reach being studied here (5.5 km) is of the same order as the one that Yu and Lane (in press, a) used. Second, the scale of channel width here is of the order of 10 to15 m and the floodplain is laterally confined by hillslopes in places along the river channel. Given the floodplain confinement, the 8 m resolution was felt to represent the effect of storage of near-channel water most efficiently in this research (Horritt and Bates, 2001a). Third, the same model (a diffusion wave treatment) is being applied here as opposed to the model structure (a kinematic wave treatment) that Horritt and Bates (2001a) used.

6.4.2.2 Model stability

The results of Table 6.1 show that the raster-based model is unconditionally stable and feasible for the whole range of statistical flood events applied, regardless of the floodplain Manning's n value need. In this respect, compared with normal and storage cells mode of HEC-RAS, the raster-based model is preferable.

Table 6.1: Scenarios undertaken to do sensitivity analysis for raster-based model in relation to model stability

| Flood return period | Floodplain n | | | | | |
	0.03	0.04	0.05	0.06	0.07	0.08
0.5	301*	302	303	304	305	306
2	307	308	309	310	311	312
5	313	314	315	316	317	318
10	319	320	321	322	323	324

       Stable simulation   Unstable simulation

* Numbers are attributed to file referencing in the hydraulic model

6.4.2.3 The effect of main channel friction on inundation extent prediction

The flood event considered for this research was simulated using the storage cell mode of HEC-RAS in the main channel to produce inflow hydrographs entering onto the floodplain over the lateral weirs in the raster-based model. The raster-based model behaviour in relation to inundation extent variations in response to inflow boundary variations imposed by main channel friction changes (i.e. lateral inflow boundary condition change due to main channel friction change) was evaluated using the n values of 0.045, 0.055, 0.060 and 0.065 as the main channel friction in the storage cell mode. The changes in inundation extent on the floodplain over time, using different n values in the main channel are presented in Figure 6.2. During the simulations, the n value of 0.06 was chosen as the floodplain friction factor. As seen in Figure 6.2, maximum inundation extent is affected by main channel friction; the larger the main channel n value the greater the inundation extent. If Figure 6.2 is studied, it shows that by increasing the n value from 0.045 to 0.055 and from 0.055 to 0.065, maximum inundation extent increases by 35% and 19% respectively.

Fig. 6.2: The spread of inundation areas on the floodplain over time, using different n values in the main channel
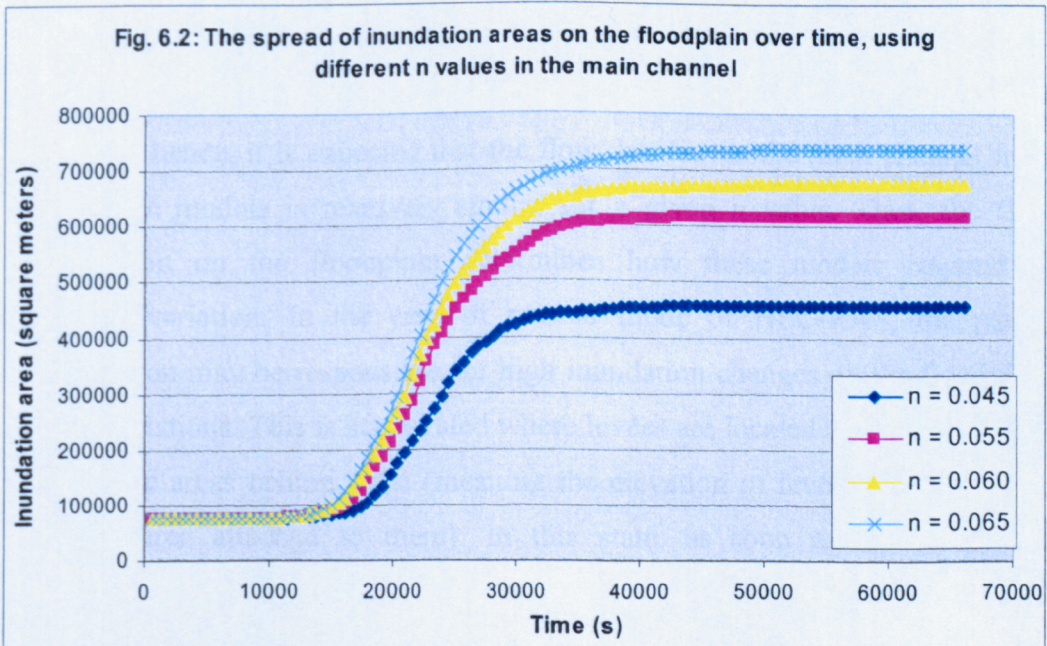
The lower percentage of increase in maximum inundation when the n value changes from 0.055 to 0.065 may be attributed to the floodplain confinement. It should be noted that the main channel friction factor is not involved directly in the raster-based model formulation but it only affects lateral inflows (i.e. volume, rate, location of outflow from main channel) as boundary conditions for the raster-based model.

The model behaviour in relation to maximum inundated area variation in response to main channel n changes is compared with corresponding scenarios in the normal and storage cell modes of HEC-RAS (Table 6.2).

Table 6.2: percentage of inundation area increase due to changes of the main channel n values for the three models used in this research

	From 0.045 to 0.055	From 0.055 to 0.060	From 0.055 to 0.065
Normal mode	44%	35%	57%
Storage cell mode	21%	9%	16%
Raster-based model	35%	9%	19%

As seen in Table 6.2, the highest and lowest percentage of inundation increase due to the main channel n value rise is associated with the normal and storage cell modes of HEC-RAS respectively. The raster-based model response to these changes is in between. It should be noted that the flow in the main channel is simulated using the same one-dimensional model (i.e. HEC-RAS) in the three models and hence, it is expected that the flow that leaves the main channel from any of these models is relatively similar for a given n value. Thus, the flow representation on the floodplain determines how these models respond to inundation variation. In the case of normal mode of HEC-RAS, the planar approximation may be responsible for high inundation changes on the floodplain due to n variations. This is accelerated where levées are located along rivers, with large storage areas behind them (meaning the elevation of levées is higher than floodplain area attached to them). In this state, as soon as the levées are overtopped, since the model is one-dimensional, assuming a planar water surface across the floodplain, the entire floodplain is incorrectly considered as flooded area. The failure to treat momentum transfer on the floodplain results in an overly rapid transfer of floodplain flow particularly in the upper and middle part of the

reach, and may explain the low percentage of inundation area increase in the storage cell model. As seen in Table 6.2, using progressively higher n values in the main channel (more water on the floodplain) eventually results in blockage and backwater effects (see section 5.4.4) that hold water on the floodplain for longer periods. In general, the behaviour of storage cell and diffusion models (i.e. inundation extent variation) is relatively similar in response to higher n value changes (0.055-0.060 and 0.055-0.065). This may be attributed to floodplain confinement in this particular case study, which limits the spread of inundation laterally. However, a big difference in inundation extent response in the storage cell and diffusion models (21% versus 35%) when the n increases from 0.045 to 0.055 is seen. In the storage cell mode, by using lower n values in the main channel, less water is transferred onto floodplain (initial stage of flooding on floodplain) and the water is then transferred to the downstream without any delay (lack of momentum transfer) and hence contributes less to flood inundation than in the diffusion model.

Maximum flood inundation extents predicted using the two-dimensional diffusion wave treatment on the floodplain for different n values used in the main channel are presented in Figure 6.3.

Fig. 6.4: Change of inundation extents predicted using the raster-based model under different n value in the main channel and a fixed n value, 0.06, on the floodplain. (a), (b), (c) and (d) are attributed to the n values of 0.045, 0.055, 0.060 and 0.065 for the main channel.

(a)

(b)

Legend (panel c):
- Observed shorlines
- Modelled inundation
- Land lines
- Main channel
- 0 — 1 Kilometers

(c)

Legend (panel d):
- Observed shorlines
- Modelled inundation
- Land lines
- Main channel
- 0 — 1 Kilometers

(d)
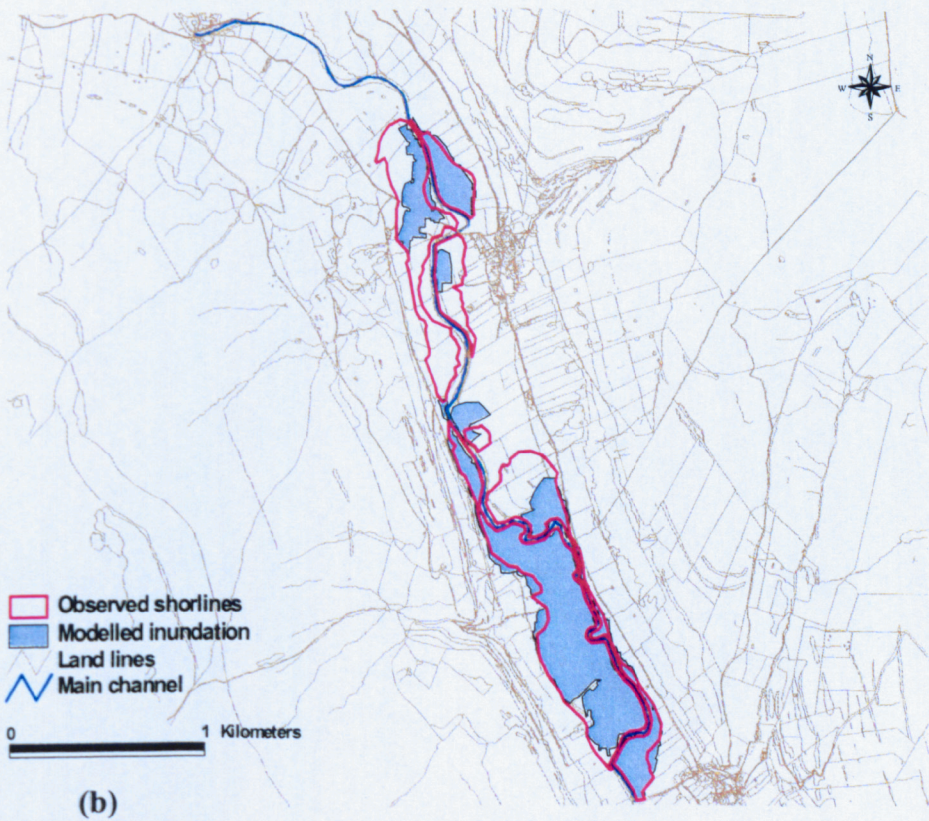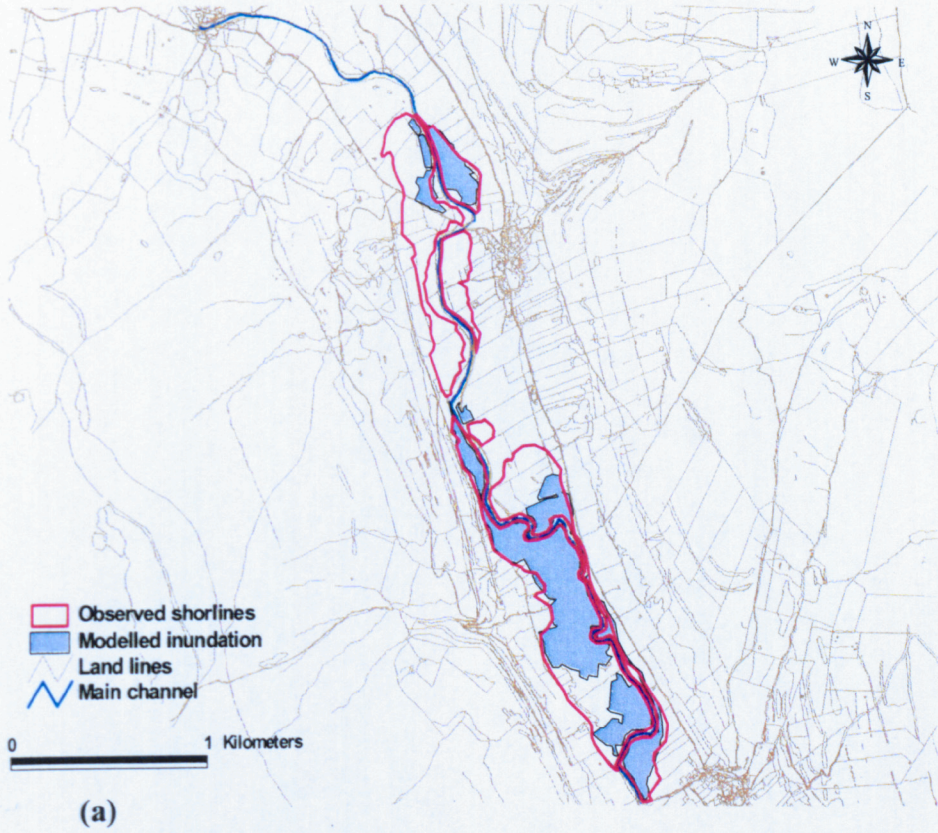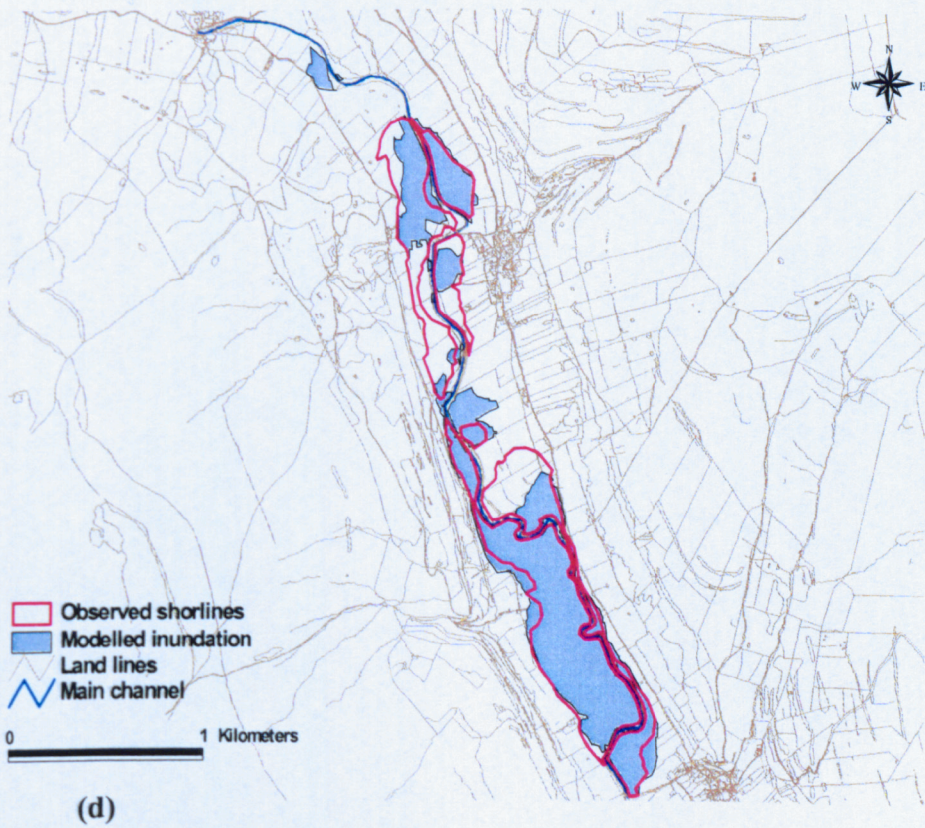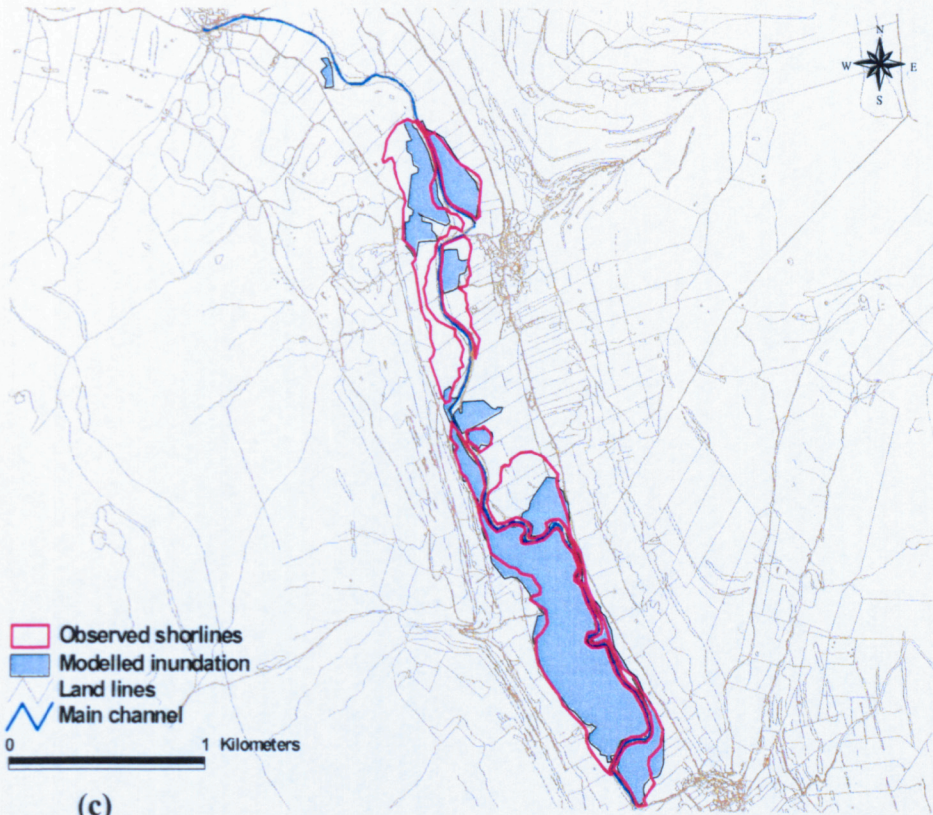
6.4.2.4 The effect of floodplain friction on inundation extent prediction

Having defined inflow hydrographs as boundary conditions for the raster-based model using the *n* value of 0.06, scenarios were defined using seven different Manning's *n*, (0.03, 0.04, 0.05, 0.06, 0.07, 0.08 and 0.5), values to evaluate the effect of floodplain friction on inundation extent prediction. The change in inundated extent on the floodplain over time, using different *n* values is presented in Figure 6.5. Figure 6.5 shows that the maximum predicted inundation extent, regardless of the location of inundated areas, is independent of the friction factor value within reasonable ranges of the parameter space (0.03 to 0.08). Using a reasonable range of *n* values (0.03 to 0.08), floodplain inundation begins at *c*.15000 s into the simulation. Within this range, the rate of increase of inundation is relatively unchanged. Using a Manning's *n* of 0.5, the rate of increase of inundation is reduced but the maximum area inundated remains relatively unchanged. By increasing *n*, the speed of the wetting process can be reduced but the size of increase required to achieve a major change is beyond the reasonable range of *n* values considered for floodplain areas. This matches the findings of Yu and Lane (in press, a) and Horritt and Bates (2001a).

Fig. 6.5: The spread of inundated areas through simulation time using different Manning's n values
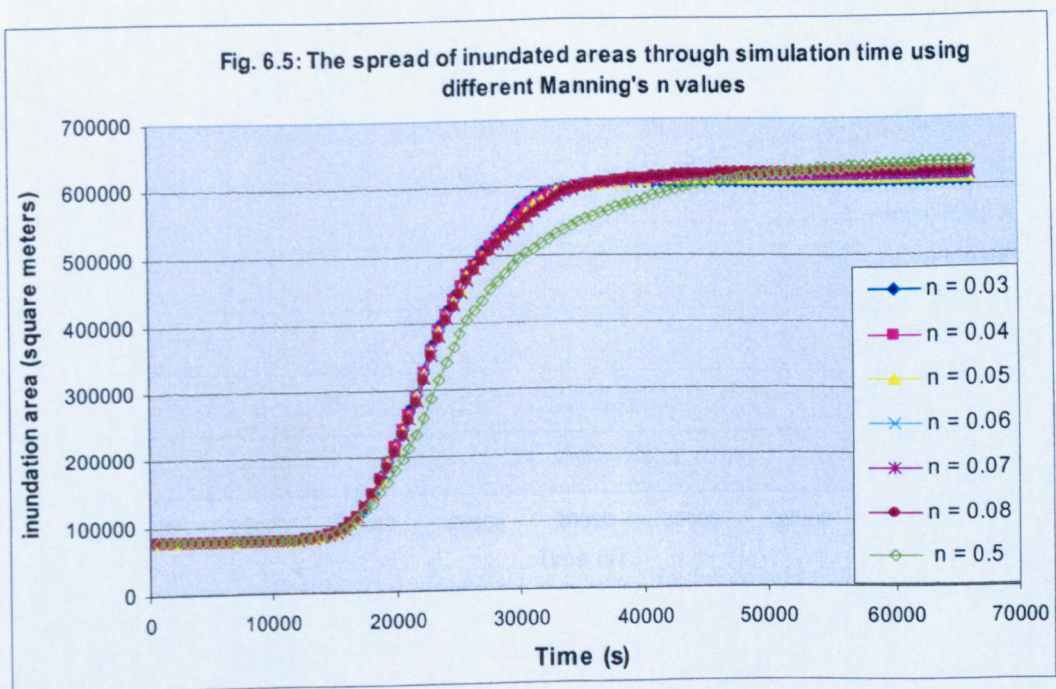
As the two-dimensional diffusion wave treatment of floodplain flows is a recent development, there is little understanding of the effects of n upon floodplain flow routing, where much of the topographic complexity is contained in the model solution at finer mesh resolution. The low sensitivity may be expected because of poor representation of inertial processes in a diffusion wave model. However, it may also be due to floodplain confinement. If the floodplain areas were unconfined, the effect of n values on inundation may be clearer (Yu, Lane, in press, a). This is supported by inspection of Figure 6.5 for the period 22000-35000 s (see Figure 6.6). This is the only period when the 0.03 to 0.08 curves separate from each other (maximum separation occurs at 30000s). As soon as floodplain confinement is reached, they converge to a maximum value, the ultimate limit of inundation extent on the floodplain. This, value remains unchanged through the simulation time (see Figure 6.5). Thus, as floodplain width increases, the effect of Manning's n on the inundation process may increase. Previous work using raster-based models (Horritt and Bates 2001a and Yu and Lane, in press, a) was conducted on floodplains with lateral confinement and the need to apply this kind of model on wider floodplains in order to evaluate the effect of n on inundation extent is important.

Fig. 6.6: The spread of inundated areas through simulation time using different Manning's n values
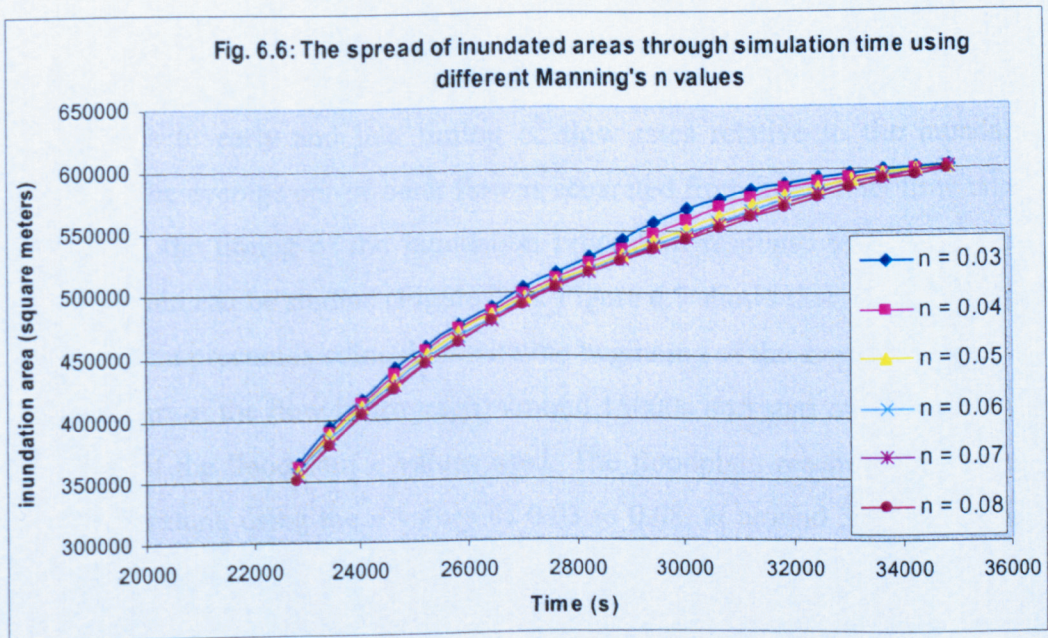
Thus, where the inundated areas remain laterally confined, the timing of inundation is relatively unimportant in relation to the maximum inundation extent. Although the wetting process is relatively independent of n values (within the range 0.03 to 0.08), the effect of n values may affect other flow characteristics (e.g. wave travel time) on the floodplain. As the model being used here is designed as an inundation extent predictor, it cannot address other aspects of flow routing.

If the floodplain inundation process is compared with the average out-of-bank flow through the reach it may indicate the relative timing of flood inundation in relation to out-of-bank flows. To assess this, an average estimate of bankfull flow for the study reach is needed. Table 6.3 lists the bankfull discharges of cross sections that contribute to floodplain flooding, using the flood event used in the research and a Manning's n of 0.06. Once in-channel flows reach the bankfull discharges at these cross sections, flow leaves the main channel and leads to floodplain inundation. Hence, the average bankfull discharge for these cross sections is estimated at 30.4 m³/s (see Table 6.3).

A flow hydrograph was selected from the middle of the study reach in order to show the relative timing of in-channel flow in relation to the floodplain inundation process. The consideration of the flow hydrograph from the middle of the reach reduces errors made if an upstream or downstream flow hydrograph was selected due to early and late timing of flow rates relative to the inundation process. If the average out-of-bank flow is separated from in-channel flow on this hydrograph, the timing of the inundation process in response to flows entering into floodplain can be studied (Figure 6.7). Figure 6.7 shows that the beginning of the inundation process is coincident with the beginning of the average out-of bank flow (red part of the flow hydrograph) around 15000s into start of the simulation, regardless of the floodplain n values used. The floodplain reaches its maximum inundation extent, using the n values of 0.03 to 0.08, at around 35000 s whereas the declining limb of the flow hydrograph shows that flow is still leaving the main channel and actively involved in the floodplain inundation process. The declining limb of the flow hydrograph stops adding any flow to the floodplain at approximately 40000 s into the simulation. The fact that the maximum inundation extent is reached before the out-of-bank flow stops (given the dimensions of the

floodplain) may indicate lateral confinement of the floodplain. Further inflow onto the floodplain after its maximum inundation extent is reflected in the depth of water on the floodplain. On the other hand, using a Manning's n of 0.5 on the floodplain, the maximum inundation extent is coincident with the end of flow leaving the main channel (end of the red part of the flow hydrograph on the declining limb). Although this is theoretically more meaningful in terms of timing between flood inundation and flow leaving the main channel, the n value required for this is beyond the acceptable range of n values for floodplain environments. The choice of which description is more valid for the floodplain and event used here depends upon dynamic validation data for inundation extent.

Table 6.3: Lists of cross sections contributed in floodplain flooding and the corresponding bankfull discharges, using the flood event considered for the research and n value of 0.060.

Cross section	Bankfull discharge, m3/s	Cross section	Bankfull discharge, m3/s
4345	28.5	1335	26.32
4255	26.18	1286	27.99
4160	32.42	1275	23.66
4120	30.64	1205	24.28
4115	32.06	1170	37.47
4070	33.96	1165	30.32
4020	34.03	1125	32.79
3520	38.43	1120	33.47
3480	39.01	1080	32.7
2710	37.14	1030	33.85
2680	35.85	920	36.6
2620	43.36	830	28.75
2615	35.05	825	36.94
2235	25.5	780	28.8
2175	25.86	775	31.88
2105	25.93	715	26.4
2035	25	640	30.34
1965	26.77	635	35.38
1870	26.94	575	31.35
1820	27.49	520	34.98
1765	27.82	470	33.62
1760	21.93	410	29.11
1710	21.58	355	31.48
1705	26.62	350	30.79
1635	21.17	300	30.8
1528	26.94	295	31.29
1350	25.43		

		Sum	Average
		1612.97	30.4334

Fig. 6.7: Relative timing of average out-of-bank flows to inundation process
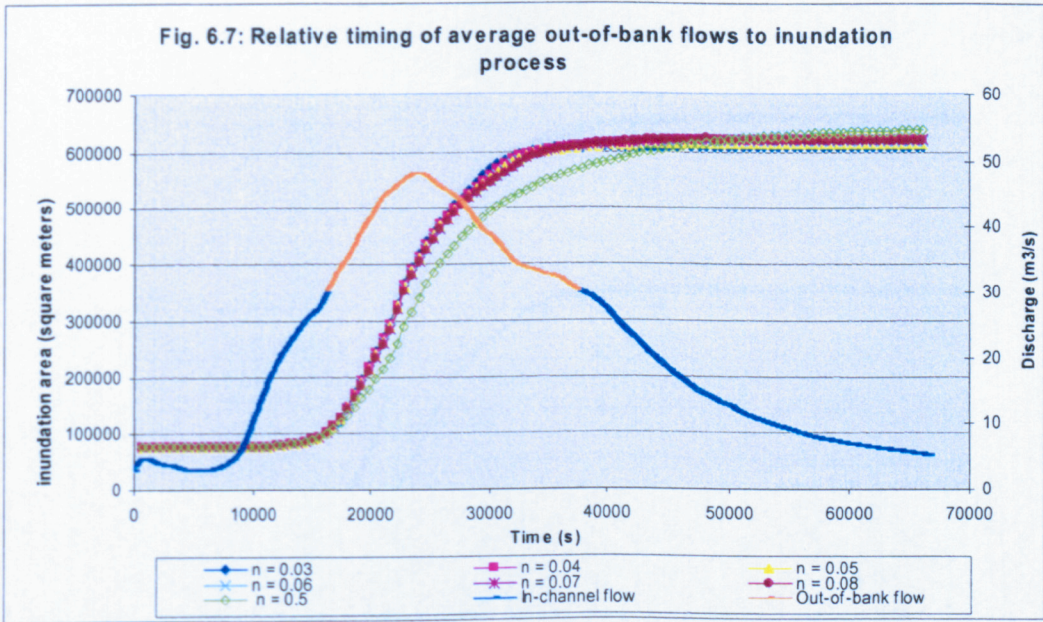
As long as there is no such validation data, the role of the friction factor in the diffusion wave model is obscured. As the validation data for the considered event is collected for the maximum extent of inundation, a definite conclusion in this regard is difficult. Regardless of the role of Manning's n in the flood inundation process in this particular floodplain, the fact is evident that the maximum inundation extent remains constant for different n values and it can be compared with the maximum observed inundation extent to evaluate the model performance in this respect.

6.4.3 Inundation extent in response of different flood magnitude

To investigate flood inundation on the floodplain in response to different flood magnitudes, the trend of inundation on this particular floodplain using two flood magnitudes (1 in 0.5 years (i.e. the flood that occurred on 4th Feb. 2004 with a peak discharge of 47.7 m^3s^{-1}) and 1 in 2 years with a peak discharge of 67.1m^3s^{-1}) were investigated. Figure 6.8 presents the timing of flood inundation on the floodplain using the two flood flows. The trend of inundation timing on this particular floodplain and with these two hydrographs is similar and independent of flood magnitude. In terms of the change of inundation area due to flood magnitude, Figure 6.8 shows that the 2- year return period flood resulted in an increase in 64% in inundation extent.

Fig. 6.8: The progress of inundation extent on the floodplain, using two different flood magnitudes
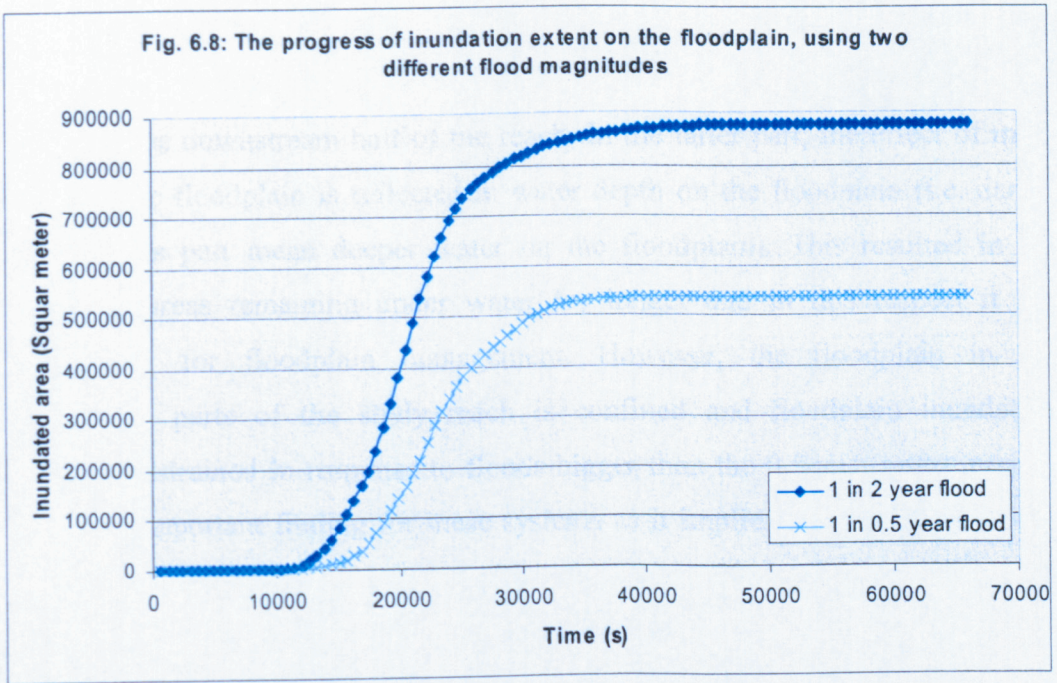
Figure 6.9 shows the location of areas predicted as flooded, using two different flood magnitudes (i.e. 0.5 and 2 year return period).

Figure 6.9: Visual comparison of inundated areas, using two different flood magnitudes, (a) 0.5-year return period flood and (b) 2-year return period flood.
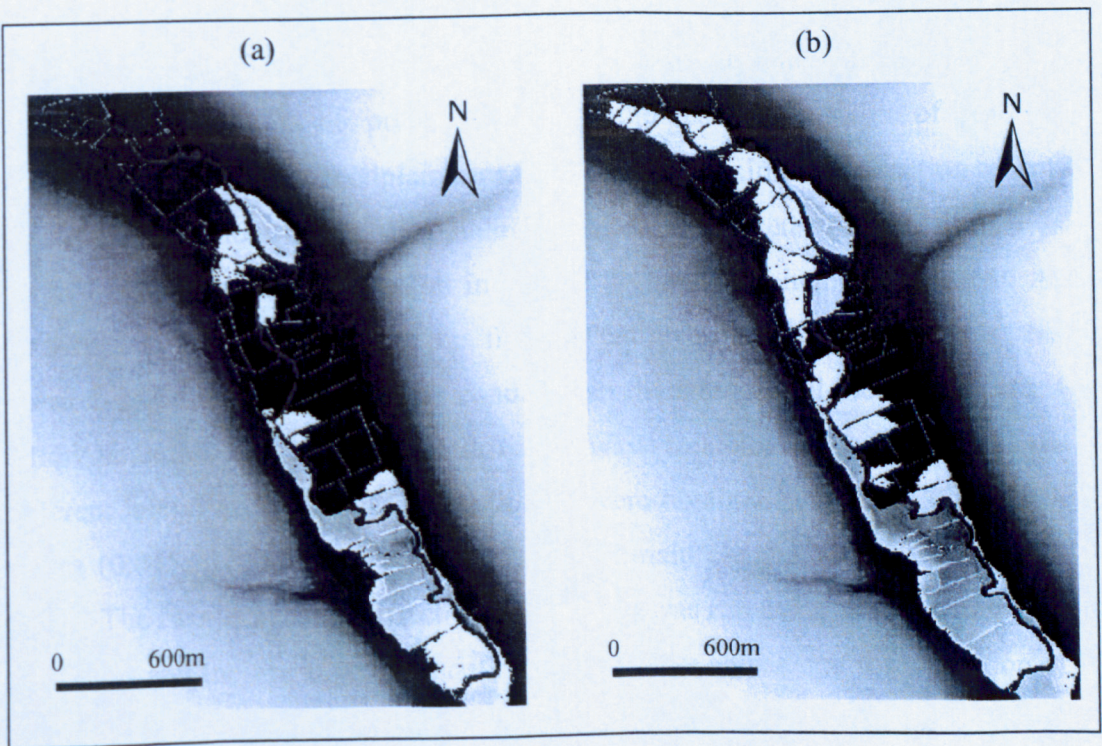
As seen, new areas of the floodplain, mostly in the upstream half of the reach, become inundated as flood magnitude increases. No major change in flooded area is seen in the downstream half of the reach. In the latter part, the effect of more water on the floodplain is reflected in water depth on the floodplain (i.e. darker areas in this part mean deeper water on the floodplain). This resulted in the floodplain areas remaining under water for longer and in this respect it has implications for floodplain management. However, the floodplain in the downstream parts of the study reach is confined and floodplain inundation remains constrained in response to floods bigger than the 0.5-year return period. This is an important finding for these systems as it implies that small floods can result in inundation of certain parts of this floodplain. These floods, unlike more extreme floods, are the ones that are likely to be sensitive to land management change (Evans *et al.*, 2004).

6.4.4 Validation of the model versus inundation extent

In terms of validation data, inundation extents resulting from a flood event that occurred at 4th February 2004, with a peak flow of 47.73 m³/s and a duration of 18.5h was collected using ground survey using RTK GPS and photographs at the time of flooding (see Chapter 3). Given the sensitivity analysis undertaken in section 6.4.2, there is no preference within the reasonable range of possible Manning's *n* values for floodplain area in relation to maximum inundation extent. However, the whole range of Manning's *n* used in the sensitivity analysis was applied in validation of the model in relation to measured inundation extent. As discussed before, by applying the flood event hydrograph considered in this research as an upstream boundary condition in the storage cell model, the lateral inflow boundary conditions of the diffusion wave treatment were provided. Four different lateral inflow boundary conditions were obtained using four different *n* values (0.045, 0.055, 0.060 and 0.065) in the main channel of the storage cell model. The two-dimension diffusion wave model was run using the four boundary conditions and their resultant inundation extents were considered for validation of inundation extent predictions versus the observed data. The diffusion wave treatment was run on an 8 m resolution DEM for all scenarios considered here (see Section 6.4.2.1). The predicted wet and dry cells were projected onto a 2 m

DEM in order to compare these results at the same resolution with the results of the storage cell and normal modes of HEC-RAS. Four accuracy assessment measures: overall accuracy; measure of F; KHAT value; and the Conditional Kappa coefficient (see Section 4.12.1); were estimated for each simulation in order to compare the model's ability in relation to inundation extent predictions. Overall accuracy presents the percentage of inundated and non-inundated areas that are correctly predicted as a fraction of the entire floodplain area. The measure of fit (i.e. F) represents the area correctly predicted as wet by the model as a fraction of area either predicted of observed to be wet. F, therefore, varies between 0 for a model with no overlap between predicted and observed areas and 1 for a model where these coincide perfectly. Using the measure of Fit, it is possible to compare the model performance used here with previous research as their performances have been described by this measure (for example see Horritt and Bates, 2002). If the model accuracy in relation to prediction of both wet and dry cells is of interest, the Kappa test should be considered. In contrast, if the ability of a model in relation to only prediction of wet areas is of interest, then the Conditional Kappa for wet cells is the best statistic to represent this aspect of model ability. Table 6.4 presents the values of the four accuracy assessment measures undertaken at the maximum extent of inundation for the study reach and flood event considered for the research, using different n values.

Table 6.4: Results of four accuracy assessments performed in relation to inundation extent prediction through the diffusion wave treatment, using different n values

Floodplain n	Overall Accuracy	Measure of Fit	Kappa	Conditional Kappa (wet cells)
0.03	0.75	0.61	0.50	0.41
0.04	0.75	0.61	0.50	0.41
0.05	0.75	0.61	0.50	0.41
0.06	0.75	0.61	0.50	0.41
0.07	0.75	0.61	0.50	0.40
0.08	0.75	0.61	0.50	0.40
0.50	0.75	0.61	0.49	0.38

By changing n values, there is no real difference in model performance in relation to inundation extent prediction regardless of the kind of accuracy measure used in this particular reach and flood event. This is not surprising given the poor

representation of inertial process in a diffusion wave model. As discussed in section 6.4.2.4, insensitivity of floodplain flows to friction factors in this particular reach may also be attributed to floodplain confinement. The behaviour of the model in response to floodplain n value changes is consistent with previous studies. For instance, by changing the n values from 0.06 to 0.1 for floodplain area, only a 1% change was seen in the measure of fit between predictions and observations (Horritt and Bates 2001b).

The best fit between the predicted and observed inundation extents are estimated 0.74, 0.61, 0.50 and 0.41 for Overall accuracy, F, KHAT value and Conditional Kappa (predicted wet cells) measures respectively. These simulations were parameterised with the inflow boundary condition obtained using the n value of 0.06 in the main channel. Overestimation of the overall accuracy measure as compared with other accuracy measures is not surprising, as this is biased strongly by the number of cells that are always dry in both predictions and observations.

Model performance using different inflow boundary conditions resulting from the main channel n value variations (0.045, 0.055, 0.06 and 0.065) are summarised in Table 6.5 (see Figures 6.3 and 6.4 for inundation extent maps). Within these simulations, as the effect of floodplain n value is insensitive in relation to inundation prediction, the n value of 0.06 was selected for floodplain areas. Table 6.5 shows that by increasing main channel n values from 0.045 to 0.065, model performance in relation to inundation extent generally improves. However, the change of n value from 0.060 to 0.065 did not result in a marked change in model performance so that two measures (Conditional Kappa and F) increased and two measures decreased (overall accuracy and Kappa) by one percent. As the inundation extent associated with the n value of 0.065 produced a big isolated wet area in the upstream half of the reach (see Figure 6.3), which does not exist in the observed data, the simulation that uses the n value of 0.060 is considered as the optimum model performance with an ability of 61% in predicting inundated and non-inundated area for this particular event and reach.

Table 6.5: Model performance in relation to inundation extent using different n values in the main channel

Accuracy assessment measure	0.045	0.055	0.060	0.065
Overall Accuracy	0.68	0.72	0.75	0.74
Kappa	0.40	0.45	0.50	0.49
Conditional Kappa (wet area)	0.26	0.35	0.41	0.42
Fit	0.47	0.57	0.61	0.62

Given the results obtained in the last two sections, the best performance of the two-dimensional diffusion wave treatment is associated with an n value of 0.060 in the main channel and an n value in the range 0.03-0.08 for floodplain roughness. The inundated area associated with this simulation is presented in Figure 6.10.

Prediction of the maximum extent of inundation does not necessarily mean a realistic assessment of inundation processes throughout the simulation. Inundation process resulting from the raster-based model application in here cannot be truly assessed due to insufficient validation data (i.e. single point in time). This becomes more important when the ultimate goal of the research is to determine the level of complexity necessary for floodplain flow representation. Such insight cannot be achieved without investigating the model behaviour during the whole period of simulation. For instance, the results of the raster-based model in relation to inundation extent prediction for each hour of the simulation time are presented in Figure 6.11, but no judgment can be made in relation to the accuracy of these predictions until the floodplain reaches its maximum inundation extent and can be compared with observed data sets.

Figure: 6.10: The best prediction of inundation extent using the raster-based model

Land lines
Observed shorlines
Main channel
Modelled inundation

0   1 Kilometers

213
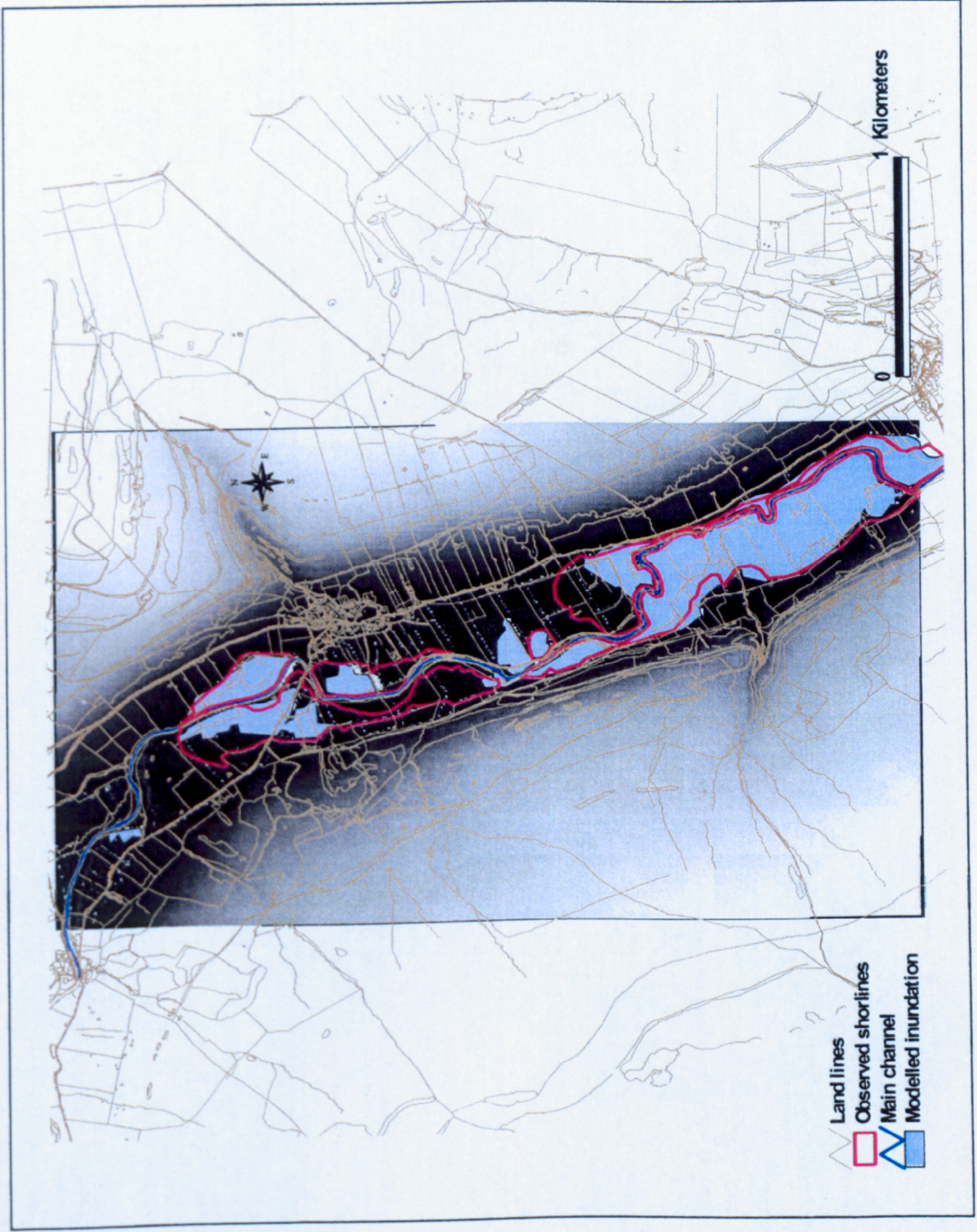
Figure 6.11: Time series of inundation extent prediction using the *n* value of 0.06 on floodplain
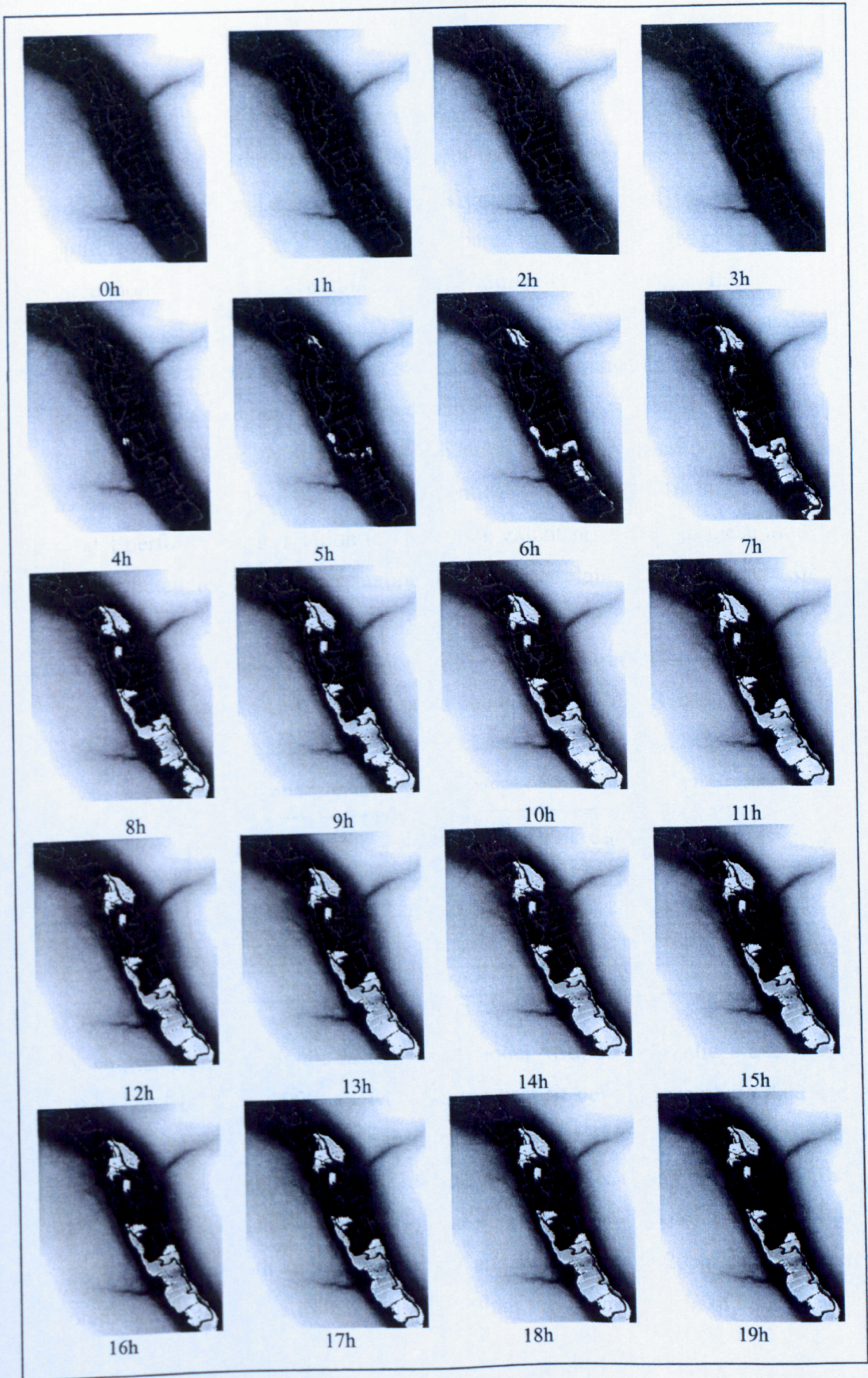
6.6 Comparison of different modelling approaches in terms of inundation extent

If the performance of the two-dimensional diffusion wave model used here is compared with the storage cell and normal modes of HEC-RAS, improvements have been seen in the predictive ability of the diffusion wave model as compared with these models. Table 6.6 compares the performance of the models at their optimised predictions. It should be remembered that the optimised prediction for the three models used here is obtained using a similar 1D model (i.e. HEC-RAS) in the main channel, parameterised with relatively similar n values (0.06 for normal and 2D diffusion models and 0.055 for storage cell model), meaning flows that leave the main channel and enter into the floodplain are relatively similar in terms of volume, location and timing. Moreover, the validation data sources used for the accuracy assessment of the three models were identical (see Figure 4.16-1). Thus, different model performance in relation to inundation extent prediction in these models can be attributed to flow representation on the floodplain. If the measure of fit is considered as an indication of the models' capabilities in relation to inundation extent prediction, the two-dimensional diffusion wave outperforms significantly, by 7% and 11%, the storage cell and normal modes of HEC-RAS respectively.

Table 6.6: Comparison of the performance of models used in the research

	Normal, HEC-RAS	Storage cell, HEC-RAS	Diffusion wave
Overall Accuracy	0.68	0.72	0.75
Kappa	0.39	0.47	0.50
Conditional Kappa	0.27	0.32	0.41
Fit	0.50	0.54	0.61

A similar study using the-raster based model with a kinematic wave treatment (Bates and De Roo, 2000) showed that the best fit between air photo data and the raster model outputs in relation to inundation extent (25 m DEM, steady state and 35 km reach) correctly predicts 81.9% of pixels as wet or dry compared with only 69.5% for the best fit obtained for planar approximation (also on the 25m DEM for 35 km reach). Both the models show an approximately 20% increase in their predictive abilities for inundation extent than the normal mode of HEC-RAS (i.e.

1D model) and the raster-based model used in this research. Their results also revealed that the application of the planar approximation for a 7-km portion of the 35-km reach provide inundation predictions that are almost as good as the raster model outputs (83.7% versus 85.5%). The similar capability of simpler (i.e. HEC-RAS) and more complicated (i.e. the two-dimensional diffusion and TELEMAC-2D) models in relation to inundation extent prediction is a finding that was also acknowledged by Horritt and Bates (2002). They showed three models of HEC-RAS, the two-dimensional diffusion wave treatment and TELEMAC-2D give similar levels of performance, approximately 65% in terms of F at their optimum calibrations.

To be more specific, the performance of the raster-based model used in this research was compared with previous studies that applied raster-based models in relation to inundation extent predictions (Table 6.7). Table 6.7 indicates that the measure of fit in this research has lower values than other studies that applied similar models. For instance, the measure of fit between the model predictions and observations of a diffusion wave model applied over a 4 km reach (similar reach length to this research) with a 70 m^3/s peak flow and 50 m resolution is 84.7% (Horritt and Bates, 2001b) whereas this value is reduced to 61% in this research. In order for validation, they used ERS-1 SAR data representing shorelines with a likely error of ±50m (Horritt and Bates, 2001b). In this research, shorelines are determined precisely using a GPS (RTK) along with ground photographs and observational evidence at the time of flooding. Given that flow processes on the floodplain in both models are treated using diffusion wave and that the two models use an optimal resolution resulting in the best predictions, one possible reason that can explain the difference in the model performances is floodplain configuration. Floodplain configuration can be interpreted as either the topographic complexity of a floodplain surface or floodplain confinement due to surrounding hillslopes. The latter is especially the case in upland floodplains, where strong and direct lateral flows due to the close proximity of the contributing hillslopes, can be involved in expansion of floodplain inundation. Therefore, in hydraulic models where lateral inflow boundaries are not considered in floodplain flow simulations, as it is the case here, the performance of such models may be lower than expected. Horritt and Bates (2002) obtained two different performances using a two-dimensional

diffusion model in steady state for two flood events. They explained that the difference in their maximum performances stemmed from the different sources of validation data used for the two events. The lower performance was associated with ERS-2 image containing large areas of uncertain flood state (see Horritt and Bates, 2002). Hence, the quality of validation data is crucial in evaluating model performance. In this research, the effects of hillslope flows directly or indirectly through tributaries involved in floodplain flooding are not included in inundation predictions, although their contribution to the river channel are included in HEC-RAS. Figure 6.12 clearly show four areas on the floodplain in which discrepancy between predictions of the raster-based model and observations map on to tributaries in areas where the floodplain is not laterally confined.

Table 6.7: The results of previous studies in relation to performance of the raster-based model application for inundation extent prediction

	Study reach characteristics	Peak flow (m3/s) and state	Resolution applied and method	Measure of F%
Bates & De Roo (2000)	35 km reach, River Meuse, 100m channel width, 3 km floodplain width, bankfull discharge 1450 m3/s	2863, steady state	25m kinematic 50m kinematic	77.3% 78.3%
Horritt & Bates (2001a)	60 km reach, River Severn, bankfull discharge 180 m3/s	435, steady state	50m kinematic 250m Kinematic	72.2% 58.6%
Horritt & Bates (2001b)	4 km reach, upper River Thames, meadow and rough pasture on floodplain, bankfull discharge 40 m3/s	73, steady state	50m kinematic 50m diffusion	83.8% 84.7%
Horritt & Bates (2002)	60 km reach, River Severn, bankfull discharge 180 m3/s	435 steady state 391 steady state.	50 m, diffusion	63.8% 41.4%
Yu & Lane (in press)	4 km reach, River Ouse	563, unsteady state	4 m, diffusion 8 m, diffusion 16 m, diffusion 32 m, diffusion	76.4% 78.5% 75.0% 61.3%
Current research	5.5 km reach, upper River Wharfe 10-15 m channel width, 50-500 m floodplain width, bankfull discharge 30.5 m3/s	47.5, unsteady state	8 m, diffusion	61.0%

In Figure 6.12, areas of a, b and c are created as a result of the contribution of tributaries of Birk Gill, Water Gill and Buckden Beck respectively although

hillslope flows affect inundation in these areas as well. In terms of area d, hillslope flows seem to be the only source of inundation. However, it is very difficult to distinguish the relative contribution of each of these sources to floodplain inundation. The existence of such areas was studied in terms of the optimum predictions of inundation extents derived from the storage cell and normal modes of HEC-RAS. Figures 6.13 and 6.14 show that such areas are generally recognisable in all models, but that the normal and storage cell modes have additional differences linked to the flow representation in each model on the floodplain. For instance, as compared with the two-dimensional diffusion model, there is less error in area b in the storage cell model (Figure 6.13). This is because of rapid conveyance of floodplain flows from upstream cells to this area by hydraulic connections between storage cells. Similarly, in this area, a planar approximation of water elevation across the floodplain is responsible for a better correspondence between predictions and observations in the normal mode of HEC-RAS than the two-dimensional model (Figure 6.14). Both of these models perform more effectively than the diffusion wave treatment but this may be for the wrong reasons: field observations suggested that these areas were inundated by tributary/hillslope flows and not the main river. This emphasises the need to consider model design very carefully in studies of inundation extent. Here, parameterisation could optimise model performance, but not necessary for the right reasons.

Another issue that may explain the poorer performance in this particular floodplain is that the floodplain is heavily partitioned by separating walls between fields with gates in between, which strongly affect the direction that the flow takes across the floodplain. If these are not effectively represented in the DEM used as a base in the raster model, their effects on floodplain inundation could be major.

Fig. 6.12: Four areas showing the difference between predictions and observation in the two-dimensional diffusion model
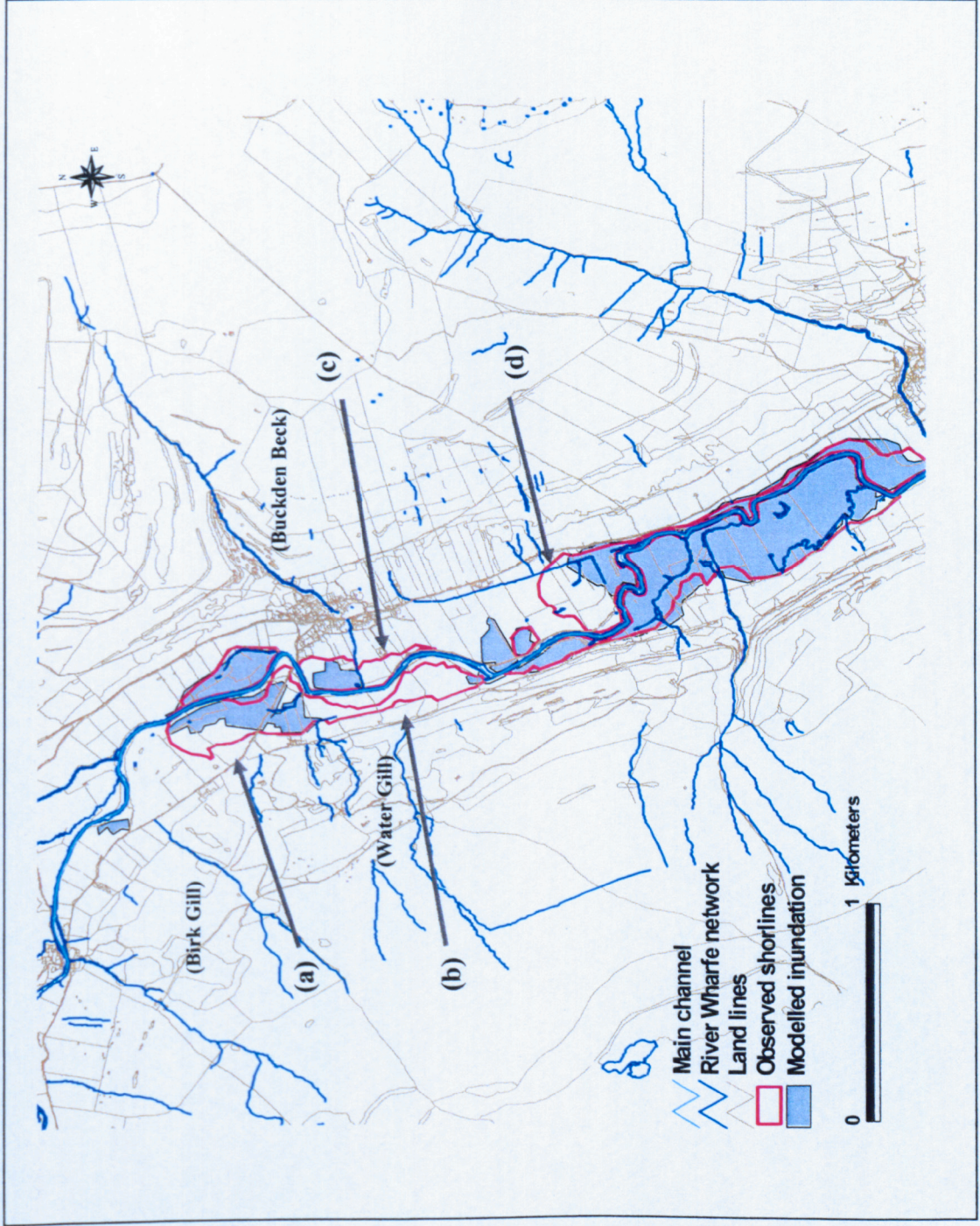
Figure 6.13: Four areas showing the difference between predictions and observation in the storage cell model
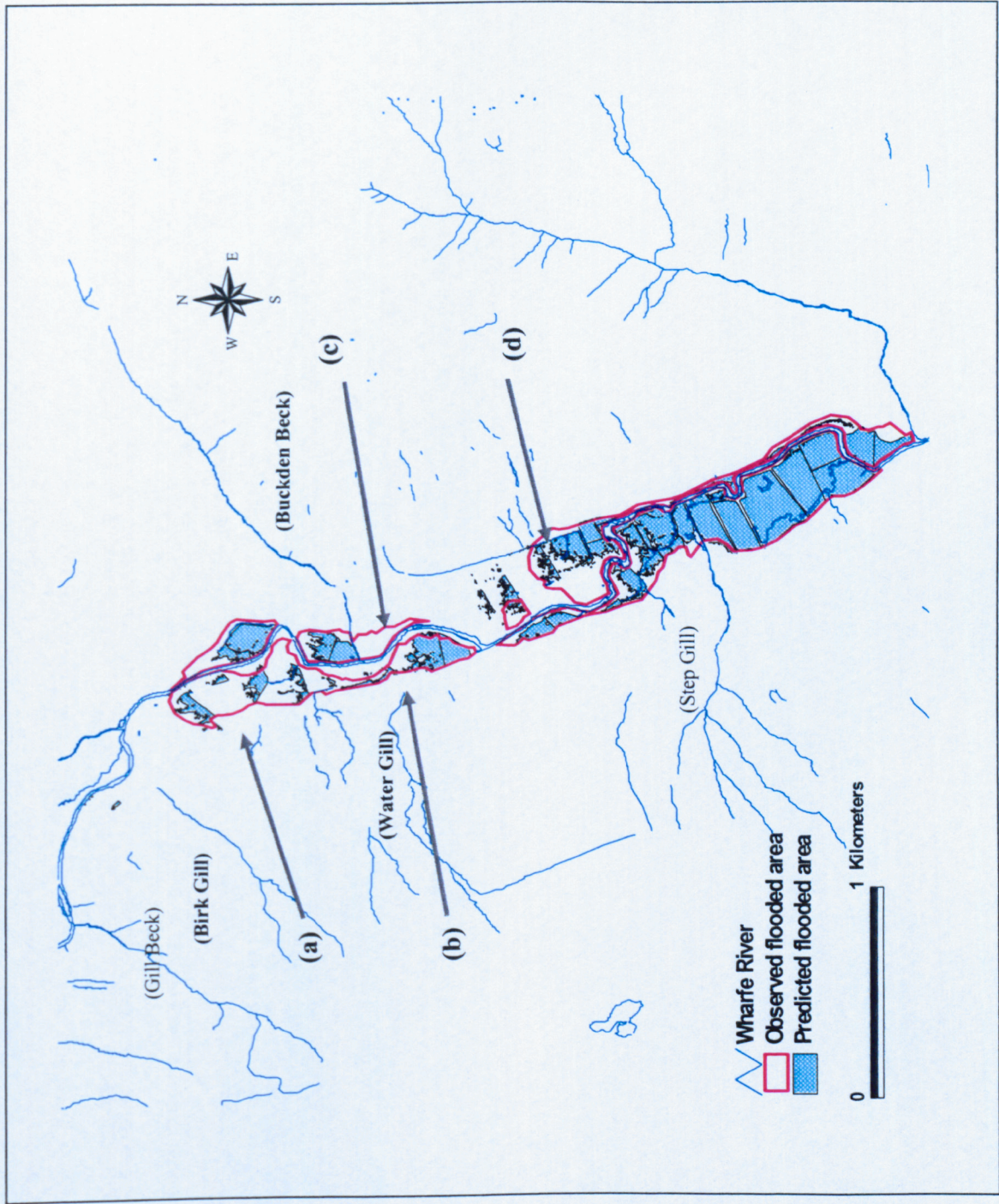
Figure 6.14: Four areas showing the difference between predictions and observation in the normal mode of HEC-RAS
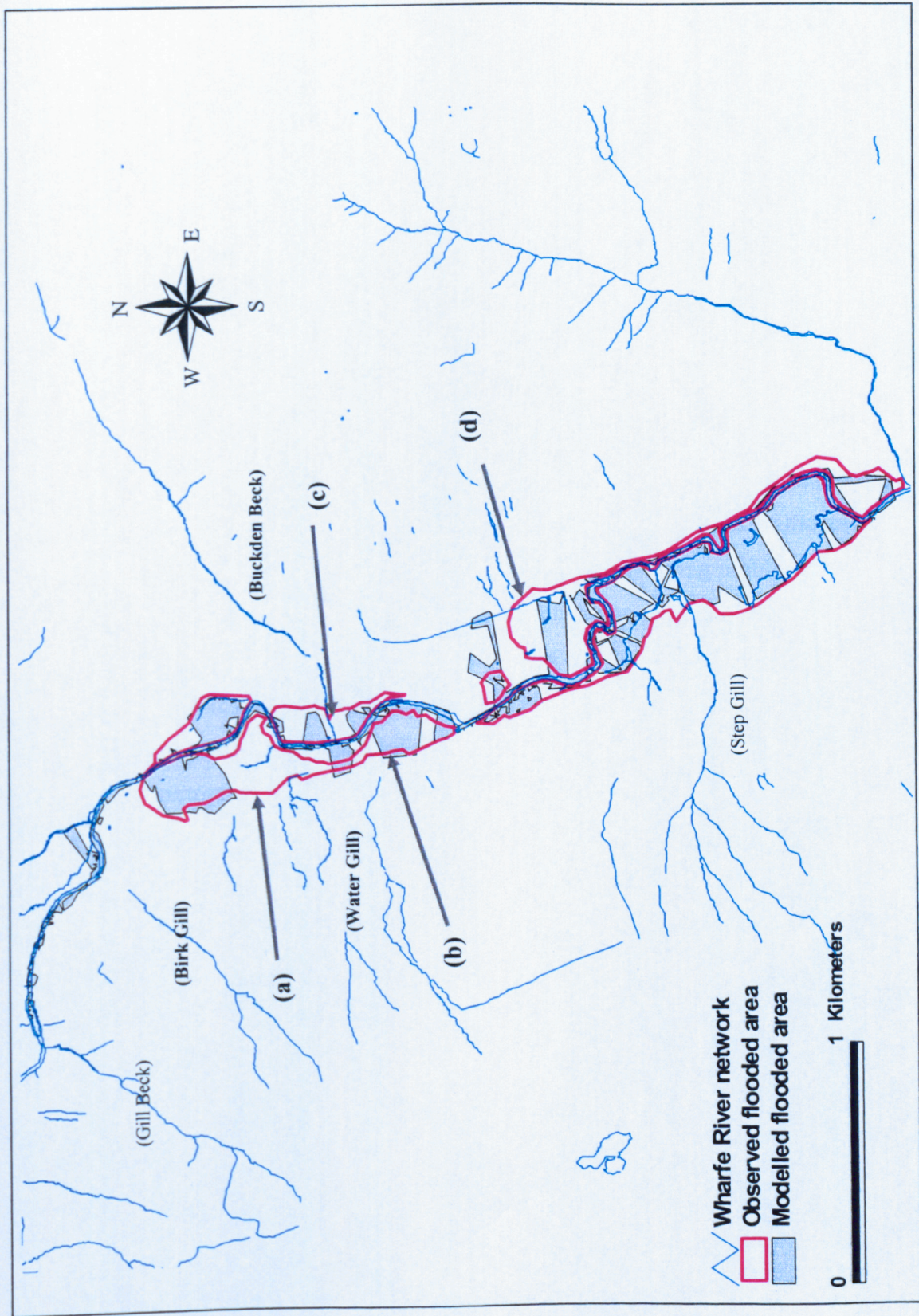
6.7 Discussion of substantive findings in relation to inundation extent prediction

Flood inundation extent resulting from a flood event that occurred on 4th February 2004 with a peak flow of 47.7 m^3/s and flood duration of 19.5 h on a short reach (*c.* 5.5 km) of the upper River Wharfe was simulated using the three kinds of floodplain flow treatment including: (i) one-dimensional treatment (i.e. HEC-RAS in normal mode), (ii) storage cell treatment (i.e. HEC-RAS in storage cell mode) and (iii) two-dimensional diffusion wave treatment. The numerical experiments outlined in Chapters 4, 5 and 6 have revealed some useful properties of these models.

In terms of numerical stability, the storage cell and two-dimensional models have advantages over the normal one-dimensional models as they can simulate a range of floods from 0.5- to 10-year return periods under certain conditions of model set up (see Tables 4.4, 5.1 and 6.1). The main reason for encountering problems with one-dimensional models is basically the floodplain topography complexity, which causes hydraulic properties of two adjacent cross sections to have an abrupt change. In this particular case, levées located along the river reach with large storage areas behind them are the main cause of model instability. In such situations, as soon as a levée is overtopped, it leads to a rapid change in flow hydraulics (ineffective flow area is transferred to effective flow area on floodplain as the model assumes a horizontal water surface on floodplain) between two adjacent cross sections at a certain time step. Solutions presented to resolve the problem (see HEC-RAS, Hydraulic Reference, 2001), are mostly suitable for flood routing studies and their application in models in which inundation extent is a central aim may increase prediction uncertainties. This limitation of 1D models in this respect is of practical importance when it is acknowledged that, until recently, the most popular approaches to flood modelling have been one-dimensional models (e.g. Samuels, 1990; Fread, 1993; Ervine and MacLeod, 1999). Thus, development of models that overcome this limitation is vital particularly where inundation extent prediction is a central aim. In response to such limitations (levées with big storage areas behind them) (HEC-RAS, Hydraulic Reference, 2001) and also floodplains that are well partitioned by embankments, walls, roads etc., floodplain flows can be simulated using storage cells (Chapter 5) (e.g. Estrela, 1994; Zanobetti *et al.*, 1968, 1970;

222

Cunge 1975, 1980) that are hydraulically connected to other storage cells and the main channel as well. Regardless of flow representation in this method, its success is subject to the possibility of defining storage cells on the floodplain.

In terms of sensitivity analysis, the normal mode model had a reasonable sensitivity to the main channel friction factor, with minimal effects of floodplain friction. This finding is consistent with the work of Cunge et al., (1976), Romanwicz et al., (1996), Bates and De Roo (2000) and Horritt and Bates (2001) and contradicts work of Hardy (1997) and Horritt (2000) who noted that floodplain friction controls the bulk flow characteristics. It should be noted that models used by these researchers are based upon different physical process. It is obvious that different process inclusion in each model would mean that the friction values have different physical meanings and cannot be realistically compared with one another (e.g. Horritt and Bates, 2002). As in-channel flows are simulated using the same one-dimensional model for the three numerical experiments conducted in this research, the difference in predictive performance of these models arises from their different response to floodplain flow representation and its response to the calibration process. Hence, the effect of floodplain n can be absolutely compared using the performance indication (i.e. F%). The comparison between the performance of the normal mode of HEC-RAS and the diffusion model in relation to inundation extent prediction shows that the former is more sensitive to floodplain friction so that by varying floodplain n from 0.04 to 0.07, a 7% reduction in the model performance was seen (see Table 4.8). In contrast, the performance of the diffusion model remains unchanged within the range of 0.03-0.5 for the floodplain n. These results are consistent with work of Horritt and Bates (2002) and such behaviour follows the inclusion of inertia and advection terms in the normal mode of HEC-RAS (see Horritt and Bates, 2002; Yu and Lane, in press a). Therefore, different process treatment may require different calibration approaches: the friction parameter is being used to compensate for different problem representations (Horritt and Bates, 2002). In the storage cell model, floodplain flow processes are controlled by the hydraulic connections between cells and the primary capacity of storage cells. Therefore, due to an incomplete treatment of momentum effects on the floodplain surface, the floodplain friction does not impact on model performance.

In addition to the impacts of floodplain flow representation on the calibration of hydraulic models (which in turn affects the performance of the hydraulic model in relation to inundation extent), floodplain configuration is also important. Using different flood magnitudes (1 in 0.5 and 1 in 2 floods) (for example see 6.4.3) in this particular, it was shown that the floodplain is confined laterally, meaning that as flood magnitude increases the extension of inundation, this is also reflected in increased water depth on the floodplain. Figure 6.6 shows that, using the range of n values of 0.03-0.08 on the floodplain, the maximum inundation-time curves gradually separate from each other after some time into simulation, but that as soon as flood inundation is confined laterally, they converge to a maximum value, the ultimate limit of inundation extent. Hence, as floodplain width extends, the effects of Manning's n on inundation process may increase. In this respect, Yu and Lane (in press, a) noted that the effect of n values on the inundation extent might be clearer if the floodplain areas are unconfined. Hence, floodplain confinement may mask the weakness of strengths of different flow treatments in relation to inundation extent prediction and affect model behaviour in response to calibration parameter changes (see Horritt and Bates 2001a; Horritt and Bates 2002). Therefore, the selection of different n values in main channel in optimal calibration (n = 0.055 for the storage cell mode, 0.06 for the normal mode and the 2D diffusion model) (see sections 4.12.2, 5.4.4 and 6.4.4) can be explained by different flow representation on the floodplain and floodplain confinement in this study.

As the precise measurement of friction factors is difficult, a reasonable range of value sets is considered for calibration of hydraulic models. As mentioned before, the friction value is used, to some extent, for compensating flow representation, and hence the actual value may be shifted. This situation becomes worse when the validation data areas are associated with major errors because, in this state, the calibration intends to compensate for the error found in the observation data as well. In such a situation, the existence of other validation data, such as stage and outflow hydrographs and internal observed water level elevations are necessary.

The predictive ability of hydraulic models used here in relation to inundation extent at optimum calibration was estimated using the measure of fit as 50%, 54% and 61% for the normal mode, storage cell mode and two-dimensional diffusion wave models respectively. The comparison of the predictive ability of the raster-based

model relative to similar previous applications showed a reduction in model performances (for example see Table 6.7). For instance, Horritt and Bates (2001b) showed that a two-dimension diffusion wave model used in an upland floodplain with similar reach length, floodplain confinement and boundary conditions to this study classified approximately 84% of the study domain correctly. The performance of a one-dimensional model (i.e. HEC-RAS) and a two-dimensional diffusion wave model in relation to inundation extent, which were used over a 60 km reach, was determined similarly as 64% of inundated and non-inundated areas of the study domain (Horritt and Bates, 2002). The performance of models used in this research compared with examples mentioned above shows a lower ability in terms of inundation prediction (also see Bates and De Roo, 2000; Yu and Lane, in press a). Such a reduction in model performance regardless of flood flow representation on the floodplain, to some extent, may be attributed to a significant degree of uncertainties surrounding inundation extent observations. These uncertainties can generally be divided into two groups: (i) those which stem from the kind of remotely-sensed data and relevant analysis techniques used (e.g. Tholey, 1995; Imhoff, 1997; Horritt, 1999; Horritt and Bates 2001b; Horritt *et al.*, 2002); and (ii) flows which inundated the floodplain flows but are not sourced from the main channel, hillslope and tributary flows. We can add a third source of uncertainty here: associated with inflow uncertainties (see Chapter 3). However, Chapter 5 showed that with n = 0.06, inundation across the weirs at the floodplain-channel interface was well-predicted. The flows used were sufficiently reliable for reasonable water level predictions in the main channel to the observed. The issue of hillslope/tributary flows is particularly the case in upland floodplains where there may be a strong link between floodplains and hillslopes. For instance, a 24% difference was seen in model performances where the predictions of both a one-dimensional model (i.e. HEC-RAS) and a two-dimensional diffusion wave model were validated against different sources of validation data (see Horritt and Bates, 2002). It is worth nothing again that validation data in this research were surveyed using a GPS, and supported by ground photographs and observational evidence, and hence they are reliable in terms of shoreline locations. Lateral inflow onto the floodplain associated with hillslopes and tributaries are the main source of uncertainties in inundation extent observations, which are not considered in predictions. These uncertainties in validation data may be explained by poorer

performance of the models used as compared relatively with similar studies. This is supported given the fact that discrepancies between predictions and observations in the three models used are found in similar parts of the floodplain, most of which are likely to be affected by tributaries (see Figures 6.12, 6.13 and 6.14). In contrast, where inundation extent is less affected by hillslope and tributary flows, a good correspondence between predictions and observations (the downstream half of the reach) is seen, particularly in the models in which the floodplain surface is parameterised with high quality topographic data (i.e. storage cell and diffusion models). This implies that (i) with having more appropriate validation data for this site, better performances of these models could be expected and (ii) the significant role of floodplain topographic characteristics in determining the shorelines in storage cell and diffusion models. However, the validation data used here are insufficiently appropriate to strongly distinguish between floodplain flow representations, and hence the validation of these models becomes confused with the calibration process (i.e. the calibration compensates for the lack of tributary representation and this makes the process realisation in different models difficult to distinguish from one another

The results show that the two-dimensional diffusion wave model, with a maximum ability of 61% in predicting inundation extent in this particular case study and flood event, outperforms the normal mode and storage cell modes of HEC-EAS significantly by 11% and 7% respectively. As mentioned before, given uncertainties surrounding the validation data in this study, and the further influence of calibration in such situations in order to achieve an optimum prediction, the discrimination between floodplain flow representations used here is difficult. However, numerical experiments performed in this research indicate some useful properties of the models used. It is worth commenting on the conceptual difference between normal and storage cell modes, as both have been shown to be problematic in practice. Aside from the fact that both require considerable skills in determining cross section locations (Samuels, 1990) and establishing storage cells and their hydraulic connections, the normal mode is problematic because it allows conveyance of water downstream for all floodplain flows as it does not block downstream flux even when blockages exist. Thus, it only represents momentum effects and does not consider discontinuities in flow due to physical blockage. In contrast, the storage cell mode represents this effect explicitly by conceptualising the floodplain as

discrete cells, with hydraulic connections. However, aside from points of hydraulic connection, there is no representation of momentum effects on floodplain flux rates. Hence, the storage cells allow flux transfer to be very rapid on the floodplain. This is aggravated where floodplains have a steeper general slope so that in such situations the effects of momentum flux is enhanced and the effect of floodplain storage is reduced. Thus, conceptually, both models are inadequate: the normal mode for assuming that a two-dimensional routed flow can be reduced to flux between extended cross sections; and the storage mode for assuming that floodplains are a series of storage ponds that are not affected by dynamic flux transfer processes. Hence, a compromise solution that recognises both storage and flux routing effects may improve model performance. In response to the need, the two-dimensional raster-based model is conceptually superior.

Both the storage cell mode and two-dimensional diffusion models are basically conceptualised as interconnected storage cells on the floodplain. In this state, floodplains comprise a series of discrete areas acting as storage cells, which communicate with their neighbours and/or the main channel. In both models, conceptually, floodplain flows are routed independently of main channel flows. The smaller size of storage cells in the two-dimensional diffusion model enhances flux routing effects, which are conducted using the Manning equation between cells (i.e. pixels) in two directions. This may reduce the effect of the lack of flux routing in floodplain flow processes that results from the storage cell conceptualisation. Moreover, the diffusion wave model involves floodplain topographic characteristics in flow routing on the floodplain, and allows the effects of blockage, where it exists, to be simulated in relation to the resolution of topographic data available. Thus, conceptually, the two-dimensional diffusion model overcomes the limitations of the normal and storage cell modes in terms of the storage and flux routing process and, practically, it improves model performance in relation to inundation extent prediction (see Table 6.6).

6.8 Conclusion

The three models tested here (normal mode of HEC-RAS, storage cell mode of HEC and two-dimensional diffusion wave models) classify correctly 50, 54 and 61% of inundated and non-inundated areas of the study domain at optimum

calibration when compared with validation data taken using a Global Positioning System supported with ground photographs and observational evidence. Conceptually, the two-dimensional diffusion model overcomes the limitations of the normal and storage cell models. Practically, it has improved performance. The improvement is not as great as expected due to floodplain configuration (i.e. confinement) in this study and uncertainties surrounding validation data. Flow on this reach was laterally confined to a relatively narrow valley and we might expect more complex overbank flow patters in wider floodplains. In such cases, the 2D diffusion wave treatment may prove more effective than the other two models. Uncertainties in validation data, in this case, mostly stem from hillslope and tributaries flows and this directly affects model performance. In such situations, model validation is further obscured by the calibration process and the discrimination between different flow process representations in relation to inundation prediction becomes more clouded. Therefore, the results presented here should be treated with caution and the extension of the methodologies used here to other reach and flood events may reveal different behaviour.

Chapter 7

Floodplain inundation in response to changes in river channel configuration and climate

7.1 Introduction

In the last three chapters, three hydraulic models with different physical bases have been used to predict inundation extent for a 5.5 km reach of an upland river and a flood event that occurred on 4th February 2004. The results showed that the two-dimensional diffusion wave treatment has marginally higher capability in relation to prediction of inundation extent in this particular reach and flood event: this was primarily due to a better conceptual representation of flow process on the floodplain and its stability rather than a markedly greater level of agreement with independent validation data. The hydrological response of any given catchment is affected by land management (i.e. landuse change), hydrological elements (e.g. precipitation) (e.g. Stover and Montgomery, 2001) and sediment delivery. The latter, may lead to a reduction in channel capacity that may alter the flooding regime of a river. Thus, the focus of this chapter is the effect of sediment delivery and precipitation changes driven by climate change upon flood inundation. The effects of in-channel geometric changes on flooding were analysed using different cross sectional data sets in conjunction with the same flood event. To investigate the effect of climate change (i.e. precipitation) on flooding, an estimated flood event was reproduced using a rainfall-runoff model driven by downscaled Global Climate Model (GCM) output (Reynard et al., 2001). Therefore, this chapter investigates the changes in inundation extent in response to: (i) change in river configuration (i.e. bed level changes) imposed by erosion and deposition processes along the river; and (ii) climate change. The first part of this chapter addresses the effect of in-channel change on inundation extent using the two geometric surveys undertaken in

December 2002 and April 2004. In the second part, using the monthly percentage precipitation changes simulated by HADRM3 for periods 2050s and 2080s under emission A2 (UKCIP02 scenarios), the flood event considered for this study is modified in order to represent the effect of climate change on the inflow hydrograph. Then, using the modified inflow hydrographs for scenarios in the 2050s and 2080s, the individual effect of climate change and its effects in combination with channel configuration change on inundation extent are studied.

7.2 Sediment delivery, channel change and flooding

The cross sectional form of natural channels is characteristically irregular in outline and locally variable. Cross-sections continually adjust to accommodate the discharge and sediment load supplied from the catchment basin. Hence, channel dimensions are not arbitrary but adjust through the processes of erosion and sedimentation that impact on the river bed and channel banks. These processes are pre-dominantly controlled by the magnitude of flow (Knighton, 1998). However, upstream sediment supply must also be considered as a control of within-channel dynamics especially as it can influence the deposition process (Lane et al., 1996). Lane et al. (1996) showed that the relative timing of discharge and sediment supply processes is critical in determining the nature of morphological change in both the short- and long-term and that the exact effect of these processes is determined by the existing channel morphology. These processes will be more active in the upper part of river reaches as most sediment supply originates in the gills and hillslopes of this part of the catchment, which are hydraulically well-connected to the river channel. The natural response of river channels to sediment deposition is the adjustment of reach-scale channel morphology via deposition of point bars which reduces channel capacity but which is compensated for by erosion of channel banks (Lane, 2001). This ultimately results in the migration of rivers across the floodplain opposite the zone of deposition (Knighton, 1998). The condition becomes worse when river management, concerned with stopping river migration across floodplain and protecting farmlands and properties, is achieved through bank protection measures (Lane, 2001). In this state, the river channel can only deposit sediment, which means that bed level gradually rises and river conveyance is reduced. As river conveyance decreases, this may cause the river banks to be overtopped more frequently and hence results in greater flood risk. This is the case for the River

Wharfe in this study reach, which has a long history of river management through bank protection.

In the literature, the geomorphological impacts of river flows and flooding and the influence of different land management practices (i.e. landuse change, clear cutting, urbanisation and etc.) on downstream flooding have been broadly acknowledged (for example see Rothacher, 1973; Harris, 1973; Hollis, 1975; Ziemer, 1981; Lyons and Beschta, 1983; Jones and Grant, 1996; Thomas and Megaham, 1998; Heritage et al., 2001; Phillips, 2002; Hohensinner et al., 2004). Much less attention has been given in relation to the impact of river channel configuration (i.e. within-channel morphology) on flood risk and inundated extent. For instance, recently, Stover and Montgomery (2001) showed that the stage-discharge relationship of the Skokomish River, USA, exhibited an increased stage for any given discharge, coinciding with an aggradation period of the channel bed. During this period (i.e. reduction in the requisite discharge for a given stage), and given the fact that the peak discharge regime was relatively unchanged, they showed that observed flooding was due to aggradation within the channel. Moreover, they observed a higher frequency of floodplain inundation in the study area at the same time. As increased flooding could arise from either: (i) a change of hydrological response of a river basin resulting from land management, or climate change; or (ii) channel changes that reduce channel conveyance; it is important that the real cause of increased flooding be specified.

7.2.1 Configuration change in the study reach

To investigate the effect of in-channel morphological changes on flooding and inundation extent, cross sectional surveys were undertaken in December 2002 and April 2004, using both traditional surveying methods (levelling) and RTK GPS facilities (the 2004 data were collected by Simon Reid). By comparing these two data sets, it was possible to assess whether or not the study reach had deposited or eroded during this period. Figure 7.1 shows the relative longitudinal profile of bed level values obtained in April 2004 as compared with December 2002. In this Figure, mean bed level values obtained in 2002 were assumed as a datum and the corresponding values in 2004 were compared to them. To calculate the mean bed level in each cross section, each section bed was divided into ten identical spatial

pieces and bed elevations at these points were extracted. Then, using these elevation points, a mean bed level was calculated for each cross section bed. As seen, the profile shows that most parts of the reach possess positive values, meaning that the reach has risen in elevation between 2002 and 2004. As was illustrated in Figure 7.1, the average value of bed level change was estimated to be 10cm along the reach.

Fig 7.1: The realtive rise or fall of bed levels along the study reach between surveys undertaken in 2002 and 2004
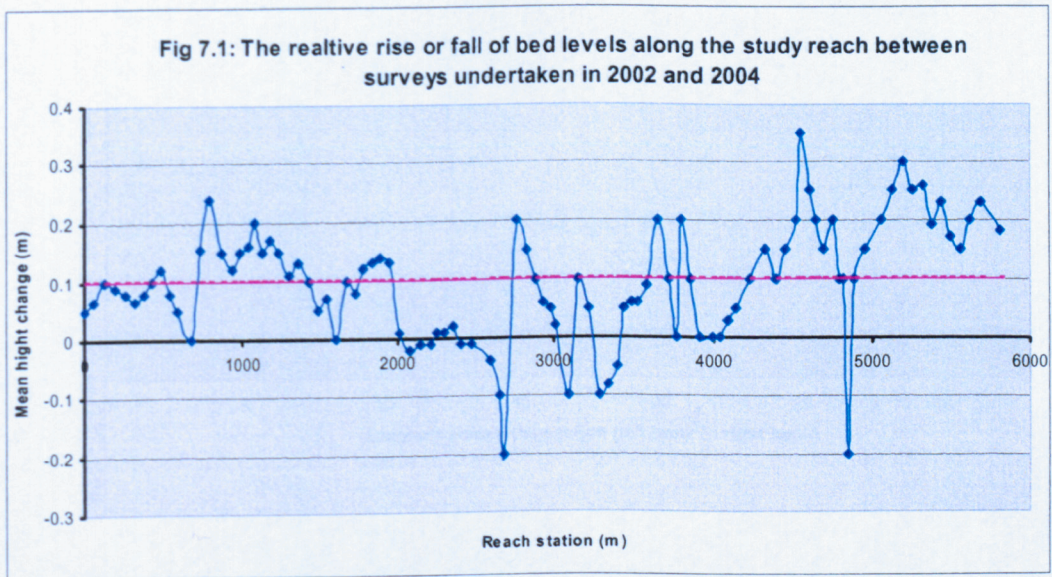
The natural response of the river channel to bed rise is erosion of its banks. Hence, the bed level is not the only parameter that can describe the change of cross sectional form and its effect on river conveyance. Rather, channel width should also be considered. By considering both changes in bed levels and channel width, we can finally specify whether the conveyance of the river channel has been altered or not. Figure 7.2 shows in-channel changes for four cross-sections in the study reach for surveys undertaken in 2002 and 2004.

Figure 7.2: Change of cross sectional forms, observed between 2002 and 2004

Cross section 4715

Cross section 2794

Cross section 1535
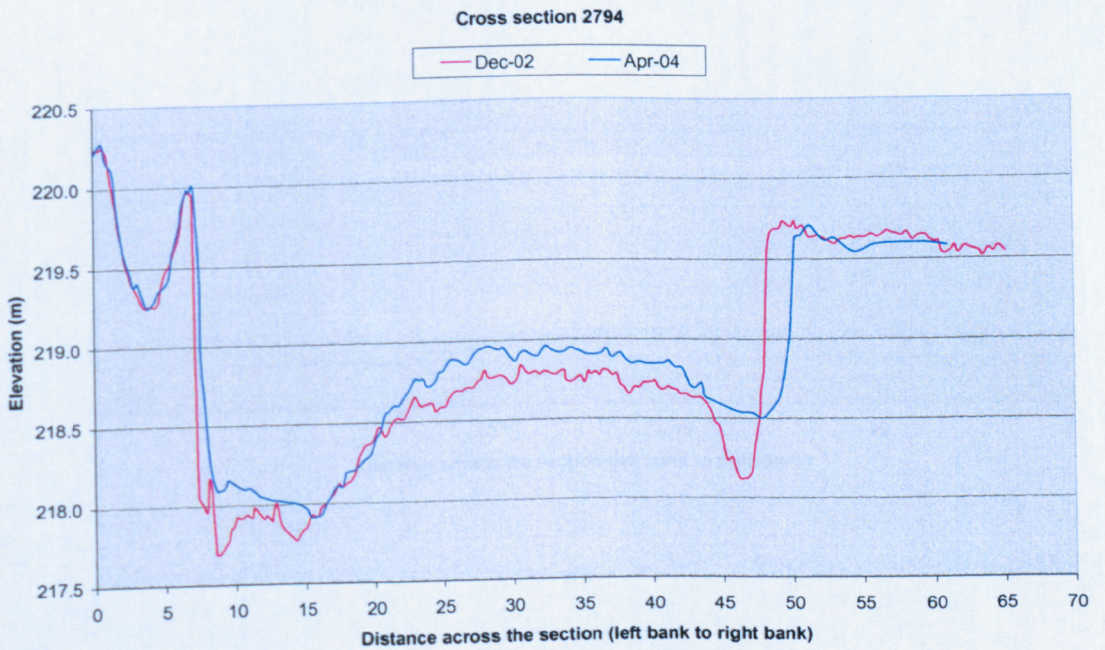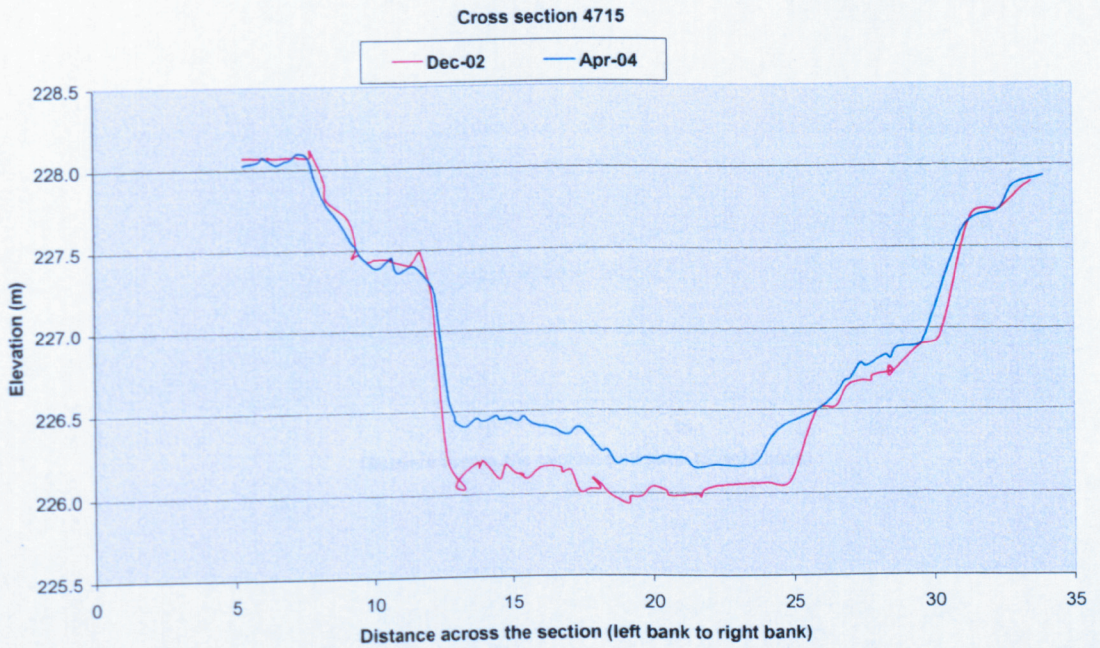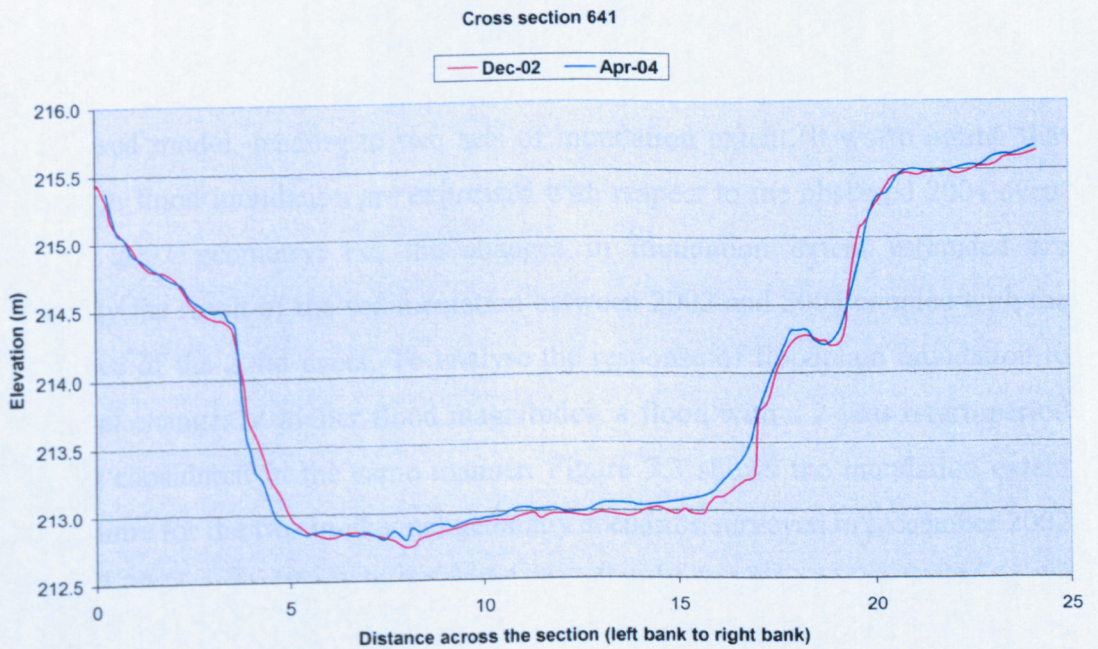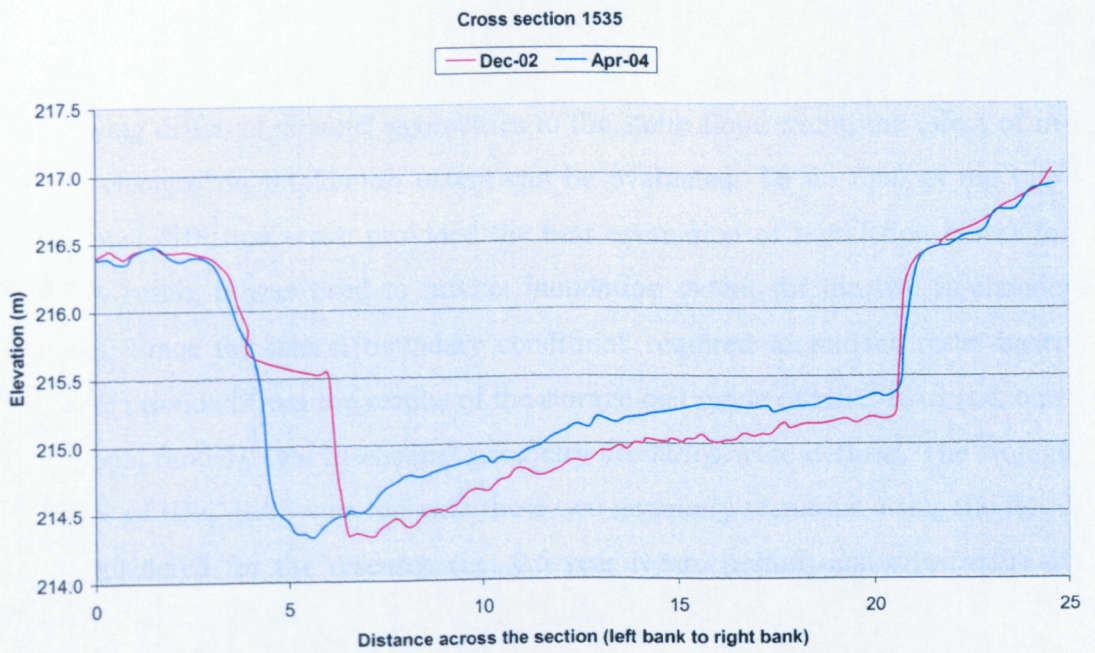
Cross section 641

Figure 7.2 shows that in-channel morphological change varies from one location to another. For instance, the in-channel change in cross section 4715 is constrained to the bed of the cross section. In cross sections 2794 and 1535 it includes channel sides. In cross section 641 no major change is seen.

7.2.3 Comparison of inundation extents using 2002 and 2004 geometric data

By applying different channel geometries to the same flood event, the effect of in-channel changes on inundation extent can be evaluated. To do this, as the two-dimensional diffusion wave provided the best estimation of inundation extent for the study reach, it was used to predict inundation extent for the two in-channel scenarios. Since the lateral boundary conditions required to run the raster-based model are provided from the results of the storage cell mode of HEC-RAS (i.e. one-dimensional model), two in-channel geometry scenarios were defined. The storage cell mode of HEC-RAS was run with these two geometry scenarios, using the flood event considered for the research (i.e. 0.5-year return period) and an n value of 0.055 in the main channel. It should be noted that the choice of main channel n values is less critical here in the sense that the model prediction will not be validated. However, main channel n values will control the magnitude and duration of out-of-bank flow and any changes in flow will be partly conditioned by the value of n used. The two resultant inflow boundary conditions were then used in the raster-based model, leading to two sets of inundation extent. It worth noting that changes in flood inundation are expressed with respect to the observed 2004 event and the 2002 geometry: i.e. the changes in inundation extent estimated are essentially the result of the sedimentation between 2002 and 2004 coupled with the occurrence of the 2004 event. To analyse the response of floodplain inundation to in-channel changes at higher flood magnitudes, a flood with a 2-year return period was also considered in the same manner. Figure 7.3 shows the inundation extent through time for the two in-channel geometry scenarios surveyed in December 2002 and April 2004, using the 1 in 0.5 and 1 in 2 floods. In terms of the timing of the inundation process there is no marked change due to channel configuration changes in both flood events. Figure 7.3 indicates that regardless of the flood event being simulated, the floodplain starts to be inundated after approximately 10000s into the simulation for both channel configuration scenarios. In the same way, channel configuration has no effect on when the maximum inundation extent is approached (approximately 33000s into the simulation). However, the analysis of the maximum inundated areas in response to the observed channel changes showed an increase in inundation area of 5.7% and 7.1% for the 1 in 0.5 and 1 in 2 floods respectively. These values are of great importance because the difference in inundation extent

described here is a product of only 2 years of in-channel fluvial processes. If these changes are considered in the longer term, particularly in relation to their effects on inundation frequency, their implications could be very serious for floodplain management.

Fig. 7.3: Inundation progress on the floodplain, using in-channel forms 2002 and 2004; and two different flood magnitudes
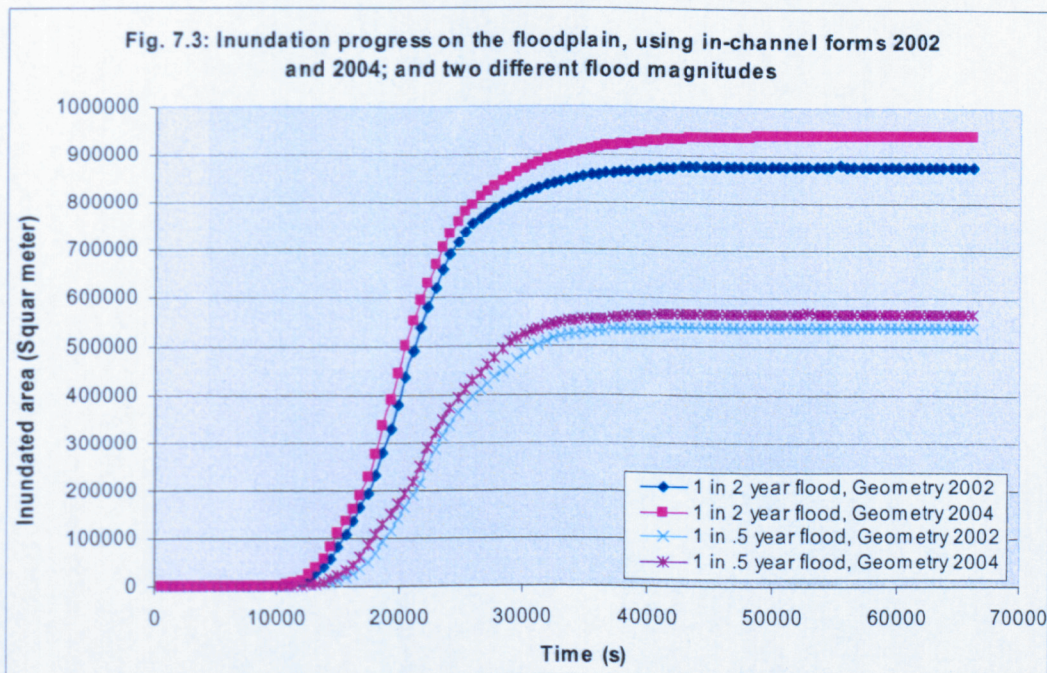
Visual comparison of the inundated areas obtained, using the two geometry scenarios and the floods with 0.5- and 2-year return periods (Figure 7.4a, b, c, d), indicates that development of the inundated area as a result of an average rise of 10cm to the bed levels can result in inundation of new parts of the floodplain that were not affected by 1 in 0.5 and 1 in 2 year floods. For instance, in the case of the 1 in 0.5 year flood, of the 5.7% increase, 2% was due to new cross sections being overtopped and 3.7 % to an increase in inundated areas linked to sections overtopped in both the 2002 and 2004 scenarios, but where the floodplain configuration allowed greater floodplain flow delivery. Under both geometric scenarios and flood events, changes in the down-stream inundation extent were partly limited by high levels of valley confinement. As floodplain confinement has a dominant role in this case study, the percentage of inundated area increases as a result of in-channel geometry rise may be greater where floodplains are not laterally confined.

Figure 7.4: The inundated areas using two in-channel geometry data and two flood events: (a) geometry 2002 and 1 in 0.5 year flood, (b) geometry 2004 and 1 in 0.5 year flood, (c) geometry 2002 and 1 in 2 year flood and (d) geometry 2004 and 1 in 2 year flood.

(c)

0   400m

(d)

0   400m
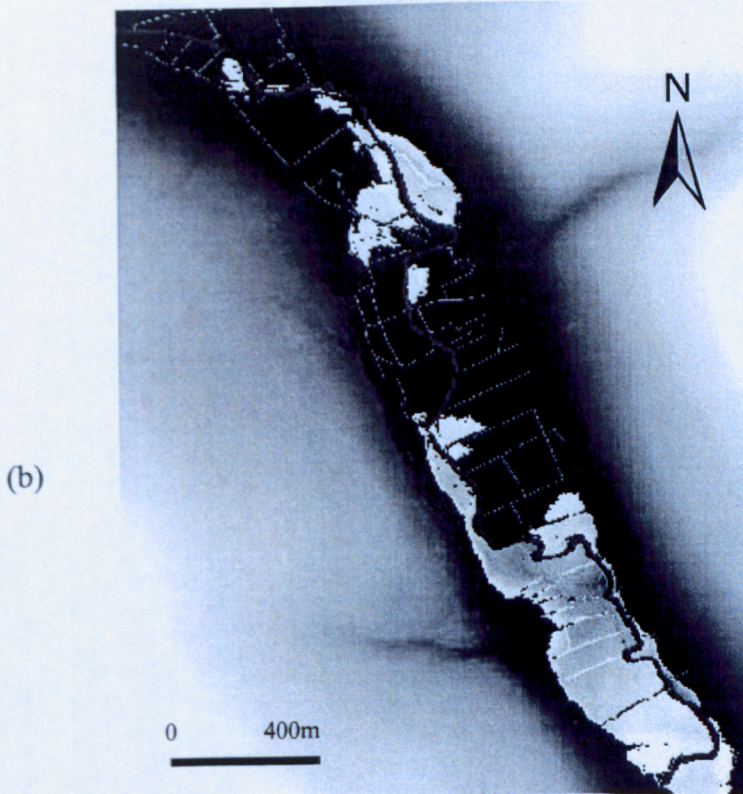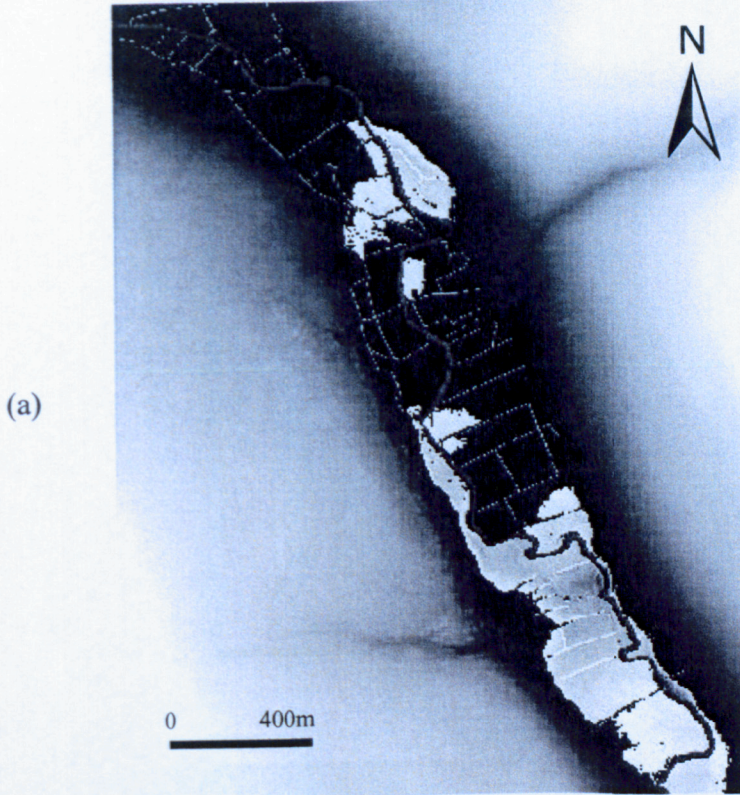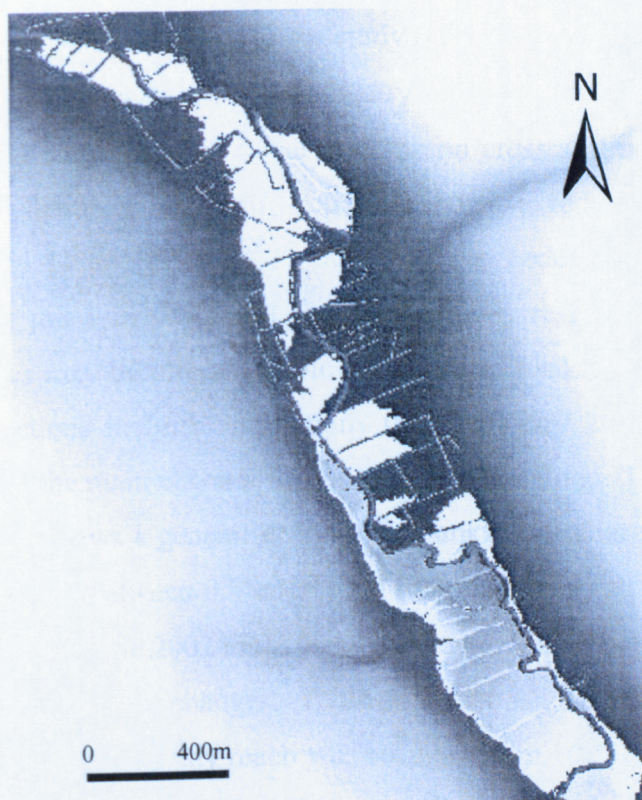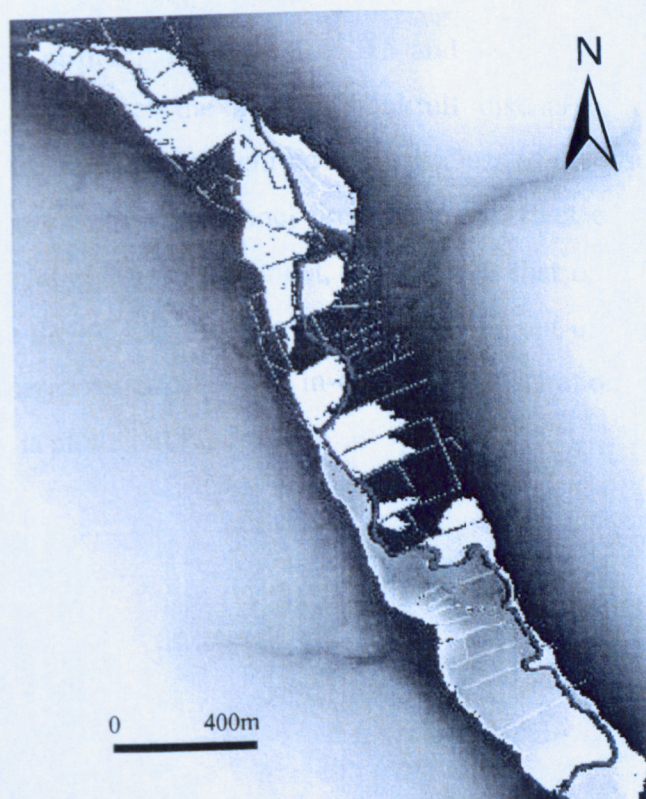
The effects of in-channel geometry change on channel conveyance, bankfull discharge and out-of-bank duration for the study reach using the 1 in 0.5 and 1 in 2 year floods were evaluated. Using the geometry data surveyed in December 2002 and April 2004, the average conveyance of common cross sections that contribute to floodplain inundation in the two scenarios shows a reduction of 3.1% (i.e. reduction from 951.11 to 921.62 m^3/s) and 2.6% (i.e. reduction from 1132.59 to 1103.21 m^3/s) for the 1 in 0.5 and 1 in 2 year floods respectively. As a result, bankfull discharges may be altered. Table 7.1 presents bankfull discharges for all common cross sections in both simulations (i.e. geometry 2002 and 2004) that allow flow to leave the main channel for the 1 in 0.5 year flood. The comparison of bankfull discharges shows a general decrease in bankfull discharge using the 2004 geometry data, varying between 0.5 and 6m^3/s (compare bankfull discharge for the 1 in 0.5 year flood using the 2002 and 2004 geometries, Table 7.1), depending upon local channel configuration changes. Table 7.1 also shows that the discharge required for bankfull in this study reach was reduced from 30.57 to 28.72 m^3/s (i.e. 6.1% decrease) due to an average rise of 10 cm in bed levels along the reach. Using the 2004 geometry data, a similar comparison was made between the estimated bankfull discharges resulting from the 1 in 0.5 and 1 in 2 year floods (see Table 7.1). The results show that the average bankfull discharges remain relatively unchanged using different flood magnitudes. Regardless of the issues as to whether or not the imposed changes in channel form have an effect on the estimation of maximum water level in the main channel, it is obvious that rising bed levels cause more flow to leave the main channel, in turn, prolonging out-of-bank flow duration. The bankfull discharge variation due to in-channel configuration changes using the 1 in 0.5 year flood is plotted in Figure 7.5.

Table 7.1: Bankfull discharge of some cross sections of the study reach, using in-channel geometry 2002 and 2004; and 1 in 0.5 and 1 in 2 year flood

Lateral weir No.	Bankfull discharge m3/s, (Geometry 2002, 1 in 0.5 year flood)	Bankfull discharge m3/s, (Geometry 2004, 1 in 0.5 year flood)	Bankfull discharge m3/s, (Geometry 2004, 1 in 2 year flood)
4345	28.50	25.51	25.31
4255	26.18	23.83	23.86
4160	32.42	31.71	31.68
4120	30.64	30.03	30.04
4115	32.06	31.77	31.90
4070	33.96	32.65	32.64
4020	34.03	32.39	32.43
3520	38.43	38.58	38.45
3480	39.01	39.11	39.11
2710	37.14	37.13	36.95
2680	35.85	35.96	35.83
2620	43.36	40.61	40.58
2615	35.05	34.87	34.90
2235	25.50	24.33	24.65
2175	25.86	23.33	23.80
2105	25.93	23.18	23.47
2035	25.00	21.26	21.40
1965	26.77	23.38	23.52
1870	26.94	26.37	26.50
1820	27.49	24.88	24.97
1765	27.82	25.18	25.21
1760	21.93	20.23	20.44
1710	21.58	20.01	20.11
1705	26.62	23.75	23.86
1635	21.17	22.65	22.76
1525	26.94	23.81	23.45
1350	25.43	23.60	23.45
1335	26.32	22.92	23.05
1280	27.99	26.23	26.22
1275	23.66	20.65	20.61
1205	24.28	21.30	21.19
1170	37.47	34.25	34.16
1165	30.32	28.35	28.31
1125	32.79	30.65	30.55
1120	33.47	31.26	31.45
1080	32.70	31.69	31.94
1030	33.85	32.34	32.30
920	36.60	29.93	29.93
830	28.75	28.30	28.35
825	36.94	35.21	35.11
780	28.80	28.25	28.31
775	31.88	30.37	30.37
715	33.86	32.50	32.62
640	30.34	28.72	28.66
635	35.38	29.01	29.36
575	31.35	28.95	29.31
520	34.98	33.30	33.33
470	33.62	31.38	31.48
410	29.11	27.74	27.91
355	31.48	30.12	30.12
350	30.79	29.50	29.54
300	30.80	29.37	29.33
295	31.29	29.86	29.91
Along the reach	Average 30.57	Average 28.72	Average 28.76

Fig. 7.5: Bankful discharge variation due to in-channel configuration chnage

Geometry 2002, 1 in .5 year flood
Geometry 2004, 1 in .5 year flood
Geometry 2004, 1 in 2 year flood
Average bankful discharge (Geo. 02 & 1 in 0.5 year flood)
Average bankful discharge (Geo. 04 & 1 in 0.5 year flood)
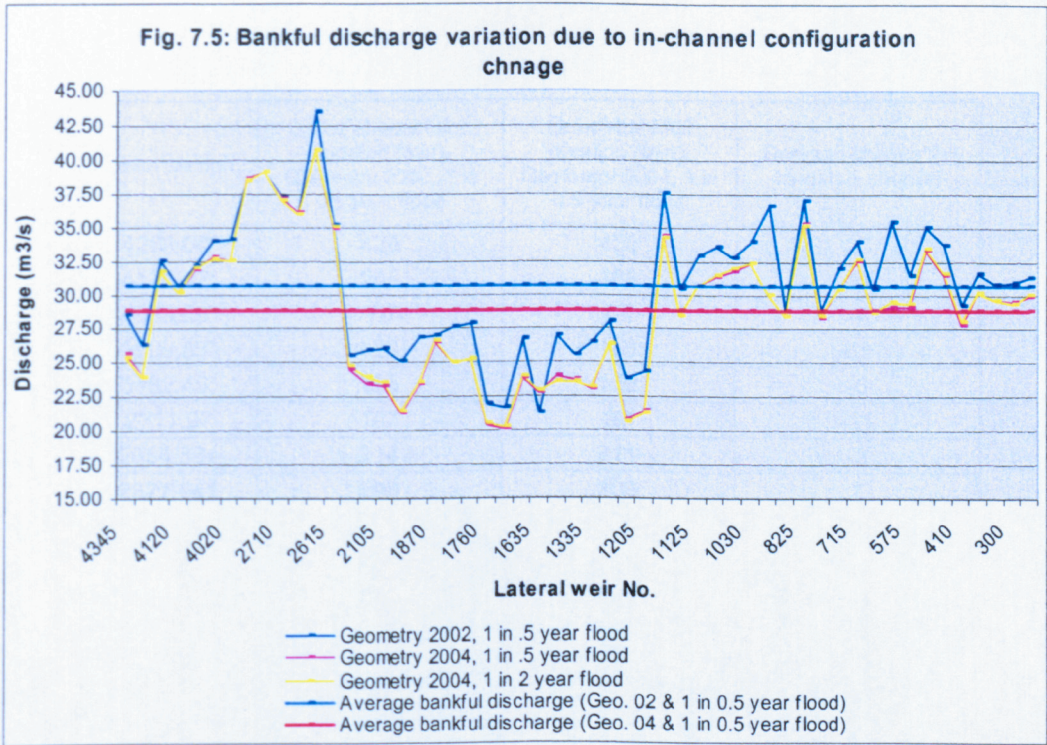
In terms of out-of bank duration, Table 7.2 shows changes in out-of-bank flow duration for cross sections that contribute to inundation extent in both geometry scenarios (2002 and 2004). As seen, the out-of-bank flow duration becomes both longer and shorter according to which cross section is considered. However, the average out-of-bank flow duration increases from 302 minutes to 330 minutes (i.e. 9.5%).

Table 7.2: Out-of-bank duration changes due to in-channel geometry changes

cross section	Out-of-bankfull duration (min), Geometry 2002, 1 in 0.5 year flood	Out-of-bankfull duration (min), Geometry 2004, 1 in 0.5 year flood	Duration change (+ longer, - shorter)
4263.04*	428	456	28
4120.47*	205	186	-19
4073.89*	70	66	-4
3890.83*	123	186	63
3482.49*	165	159	-6
2711.97	107	96	-11
2684.884	214	211	-3
2627.641	296	303	7
2504.182	96	95	-1
2248.16	319	328	9
2179.61*	438	459	21
2111.06*	435	473	38
2042.51*	389	473	84
1973.966	150	302	152
1923.02*	409	470	61
1872.07*	120	129	9
1766.53*	343	331	-12
1712.753	518	541	23
1649.186	430	456	26
1592.46*	324	364	40
1470.59*	316	380	64
1405.447	429	474	45
1343.59*	431	479	48
1281.74*	437	486	49
1219.89	352	404	52
1175.23*	368	407	39
1130.577	269	379	110
1086.27*	243	286	43
1038.347	284	304	20
921.821	27	36	9
836.43	343	327	-16
781.471*	410	417	7
726.024	418	431	13
641.148	375	391	16
585.701*	392	409	17
528.813	295	311	16
472.873*	254	284	30
416.934	194	208	14
359.666*	222	254	32
302.399	377	393	16
234.292*	273	301	28
166.185	102	117	15
Average	302.0	330.0	28.8

7.2.4 Summary of channel configuration change on inundation extent

In the introduction of this chapter it was noted that the geomorphological impacts of river flows and flooding have been broadly acknowledged in the literature (e.g. Jones and Grants 1996; Heritage *et al.*, 2001; Hohensinner *et al.*, 2004) but little studies have been conducted in relation to the impact of river channel configuration on flooding and flood inundation extent. In response to the need, the effect of in-channel configuration change on inundation extent using two cross section surveys undertaken in December 2002 and April 2004 in conjunction with the 1 in 0.5 and 1 in 2 year floods was conducted. The results of this analysis suggested an increase in inundation area of 5.7% and 7.1% for the 1 in 0.5 and 1 in 2 year flood respectively due to an average of 10cm rise in bed levels along the reach. In addition, the analysis of those factors whose values affect inundation extent indicated similar meaningful variations. For instance, a 6.1% reduction in bankfull discharge and a 9.5% increase in out-of-bank duration were demonstrated using geometry data for 2002 and 2004 for the 1 in 0.5 year flood. The result of this analysis highlighted the importance of considering the impacts of channel configuration changes on flooding and inundation extent variation particularly given the time scale over which these changes may occur. However, different scales of river channel and flood events in conjunction with a longer term understanding of channel configuration change may help to provide a better understanding of the impacts of channel configuration changes on inundation extent.

7.3 Climate change and flooding

One of the key elements that can affect the hydrological response of a catchment is climate conditions (e.g. precipitation, evaporation etc.). Climate change directly affects runoff generation through precipitation changes which, in turn, result in changes in flow characteristics. Inundation extent is a function of flow discharge and stage. Hence, climate changes may have a direct impact on flood inundation extent and future flooding and flood risk depends upon future climate conditions. Recent major flooding in the UK has raised the concern that climate change is causing increases in flood frequency and magnitude (e.g. Hunt *et al.*, 2002). To date, there is no clear conclusion as to whether or not climate change is causing

increases in the occurrence and magnitude of flooding given the fact that climate variability is seen to have a very strong impact on flood records, matching any observed trend (Robson, 2002). In contrast, there is clearer evidence that rainfall has become more variable, and that rainfall intensity and the frequency of high intensity rainfall may have increased in some areas, including the UK (Easterling *et al.*, 2000; Osborn and Hulme, 2002). In the UK, to be more specific, long term monthly rainfall series show a tendency to increased winter rainfall and decrease summer rainfall, but with a non-significant trend in the annual rainfall total (Robson, 2002). Thus, in terms of the existing long-term rainfall and flood frequency data sets, it seems that there is a dilemma here. On the one hand, trends have not been noted for the longest flood series and the trends in the recent flood series can reasonably be explained by climate variability. On the other hand, given the known increase in temperature, and indications of increases in winter rainfall, an increase in flooding would seem likely (Robson, 2002; Senior *et al.*, 2002). By accepting the conclusion that flooding in the future is likely to be affected by climate change, through changes in rainfall event characteristics, future climate conditions must be modelled. In this research, to investigate the effect of climate changes on hydrological response, the standard 'impact' approach (Carter *et al.*, 1994) was adopted, translating specified changes in climatic inputs into changes in hydrological responses. This involved (i) the application of a hydrological model using current (i.e. observed) climate data; (ii) the definition of climate scenarios; (iii) perturbation of the original (i.e. observed) input climate data accordingly; and (iv) running the hydrological model under future climatic condition.

7.3.1 Modelling climate change

At present, the only principal sources of information regarding potential climate changes are Global Climate Models (GCMs) whose results can be interpreted at the scale of individual grid boxes (typically 300 km). They attempt to represent the climate and physical process of the atmosphere, ocean, crysphere and land surface using a three-dimensional grid across the globe (Prudhomme *et al.*, 2002). Although they are often run at fine temporal resolutions (e.g. 15-30 minute time steps), the most reliable output variables are at the daily scale (for large-scale circulation indices) and the monthly scale (for 'weather' variables such as temperatures and

precipitation) (Prudhomme *et al.*, 2002). GCMs simulate current and future climate elements, according to different global emissions scenarios. The emission scenarios are based upon varying assumptions about future population and economic growth, technological advancement and social attitudes towards energy use (Reynard *et al.*, 2001). None of these scenarios include targeted global or national strategies but they assume different development paths for the world. The most commonly applied emission scenarios are the 'SRES' scenarios developed by the Intergovernmental Panel for Climate Change (IPCC) and labelled Low Emissions, Medium-Low-Emissions, Medium-High-Emissions and High-Emissions (IPCC, 2001). The GCM outputs in combination with regional topographic and climatic characteristics can be interpreted at the scale of 50 km by using HADCM3 as the most advanced regional model at the UK Meteorological Office, Hadley Centre.

The period 1961-1990 has been chosen internationally as the baseline for predicting future changes (IPCC, 2001, Hulme *et al.*, 2002). Future climate change results are mostly presented for three different time periods; the 2020s; the 2050s; and the 2080s. The 2020s, 2050s and 2080s present the periods 2011-2040, 2041-2070 and 2071-2100 respectively. HADCM3 has been run for all four of the SRES scenarios and for three future time slices. The data sets available from the UK Climate Impacts Programme 2002 (UKCIP02) include 14 climate variables at a spatial resolution of 50 km in the form of monthly averages for the 2020s, 2050s and 2080s time slices. Due to the high degree of variability exhibited in the UK climate, average results for a 30-year period are generally considered more reliable than results for a single year (Reynard *et al.*, 2001).

In terms of climate change, this research has only considered changes in precipitation and focused on changes simulated in 2050 and 2080. UKCIP02 scenarios have been produced for all four of the SRES greenhouse gas emission scenarios. However, only A2, the medium-high emissions scenario is considered here as it is the only one to have been fully simulated by HADRM3. As discussed, the HADRM3 outputs are only reliable at the monthly time scale (given the temporal resolution required for hydrological modelling they must be downscaled). The monthly percentage precipitation changes simulated by HADRM3 for periods 2050s and 2080s under emission A2, for a 50-km grid within which the study site is located are shown in Table 7.3. As Table 7.3 shows, the UKCIP02 scenarios

245

indicate an increase in the seasonality of precipitation for North Yorkshire in the future with a progressive increase in winter rainfall and decrease in summer rainfall (Hulme *et al.*, 2002).

Table 7.3: percentage changes in precipitation relative to the 1961-1990 baseline, as simulate by HADRM3 for the 2050s and 2080s using emission A2 (UKCIP02)

Month	Percentage change in precipitation	
	2050s	2080s
January	11.07	19.47
February	8.51	14.97
March	4.53	7.98
April	-1.29	-2.27
May	-8.62	-15.16
Jun	-15.74	-27.69
July	-20.68	-36.39
August	-20.57	-36.19
September	-13.84	-24.35
October	-3.65	-6.41
November	5.46	9.6
December	10.66	18.75

In this research, to perturb the observed precipitation data (i.e. those data that caused the flood event 4th February 2004), the proportional approach was selected. Accordingly, the percentage increase/decrease in monthly rainfall is applied proportionally to rainfall series in the observed data (i.e. 15-minute intervals). Given the time of the rainfall event considered here (i.e. February), the original rainfall data were proportionally upscaled by 8.51 and 14.97% for scenarios in the 2050s and 2080s respectively. Due to its simplicity, this type of change has been frequently applied in literature (e.g. Arnell, 2003; Prudhomme *et al.*, 2003). The changes applied to the original observed rainfall data for scenarios in the 2050s and 2080s, using the proportional approach, are shown in Figures 7.6a and 7.6b.

Fig. 7.6a: Observed rainfall event versus perturbated rainfall using 2050 scenario for Upper Wharfe River at 4 Feb 2004 (8:15 am to 19:30 pm) at Beckmonds gauge

Fig. 7.6b: Observed rainfall event versus pertubated rainfall usin 2080 scenario for Upper Wharfe River at 4 Feb 2004 (8:15 am to 19:30 pm) at Beckmonds gauge
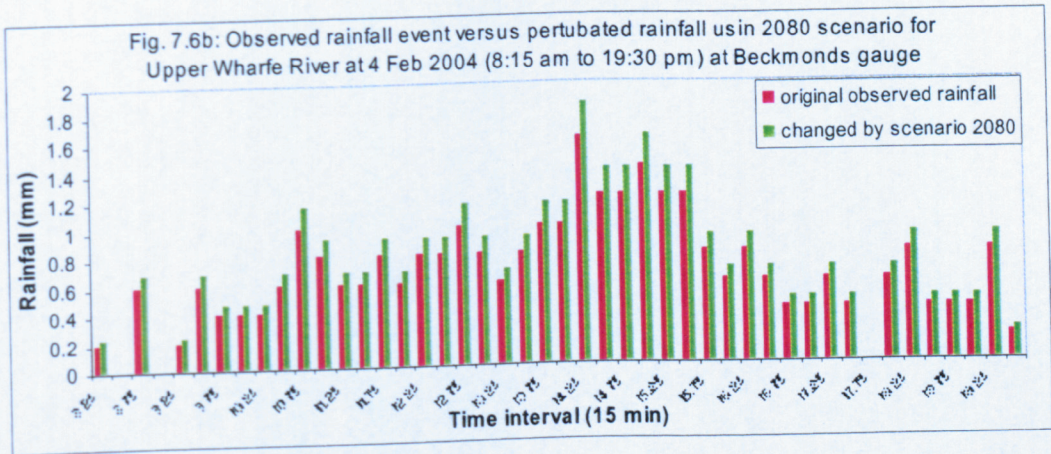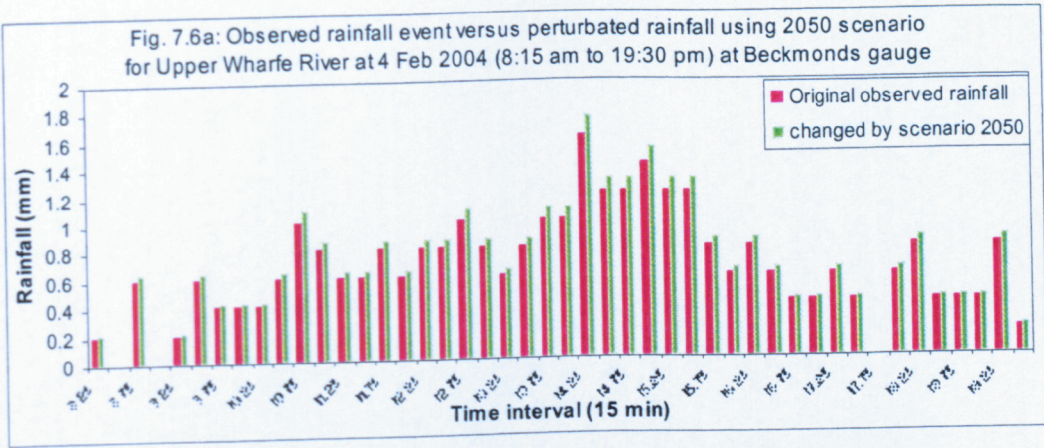
7.3.2 Hydrological modelling

In Chapter 3, the hydrological methods used in this research to estimate flow hydrograph for the rainfall event occurred on 4th Feb 2004 were described. Based on the results achieved, the Flood Estimation Handbook (FEH), using a rainfall-runoff method was specified as the best method for estimating peak flows for this event. In this method, a rainfall input is converted to a flow output using a deterministic model of catchment response (see section 3.5.1). This technique is computationally efficient and the effect of climate change (i.e. rainfall changes) can be considered by altering the input rainfall. It should be noted that we assume no change in parameter values in the deterministic model: only changes in rainfall are simulated. The deterministic model includes parameters such as percentage runoff (PR) and base flow, both strongly depending on land use, soil status and urbanisation index of the catchment that could seriously affect future estimations. By using the original rainfall event and events predicted under 2050s and 2080s scenarios (Figures 7.6a and 7.6b) into the rainfall-runoff model, three flow

247

hydrographs were generated that represent the current flood event (i.e. 4th Feb. flood event) and the corresponding flood events perturbed by climate changes in 2050s and 2080s respectively (see Figure 7.7). Figure 7.7 reveals that the estimated peak flow using climate scenarios for the 2050s and 2080s as compared with the original estimates of peak flow show an increases of 8.2% and 14.7% respectively.

Fig. 7.7: Current flood hydrograph and its changes under climate scenarios 2050s and 2080s
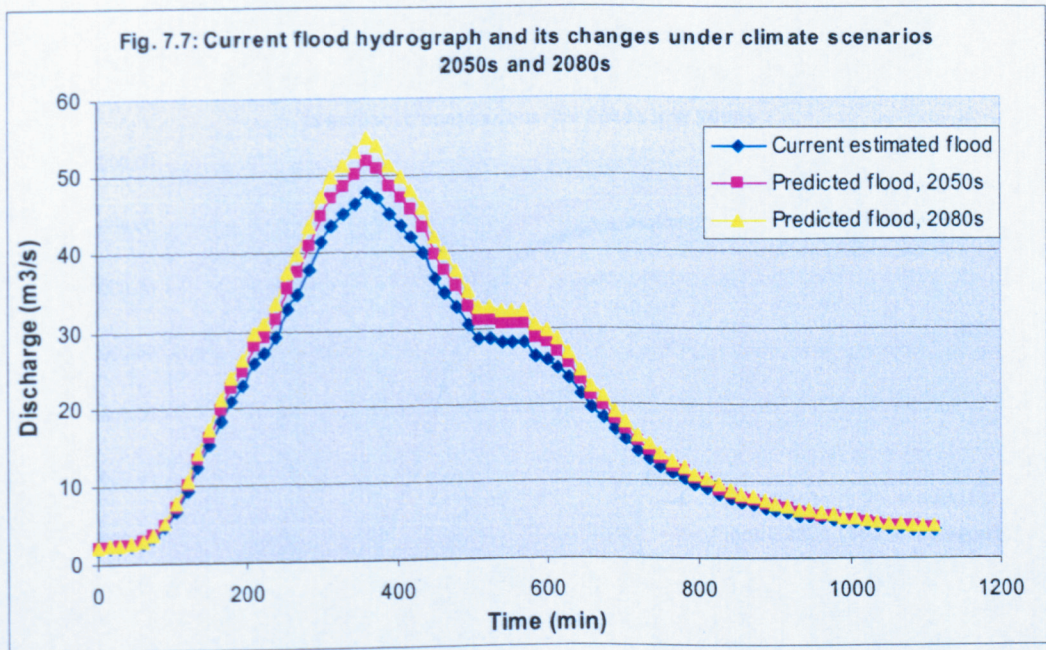
The results obtained here are consistent with Dugdale (2003) in relation to the percentage changes observed in flood magnitudes. In that study, a modified form of TOPMODEL was used in a small sub-catchment upstream of the study reach, Oughtershaw. She found increases of 8.51% and 14.97% in flood magnitude for a 1 in 2 year flood, under the proportional change scenario, for the 2050s and 2080s respectively.

7.3.3 Inundation extent in response to climate change

To evaluate the effect of climate change on inundation extent in the study reach, the raster-based model was chosen as the predictive tool. The boundary conditions for the raster-based model were provided using the above three inflow hydrographs as the upstream boundary condition in the storage cell mode of HEC-RAS. Having generated the boundary conditions for the raster-based model for these three

scenarios, the model was run to generate inundation extent for each scenario. Figure 7.8 shows the progress of inundation and maximum inundation extent using these three scenarios. The timing of inundation for the three scenarios is similar but the maximum flooded area increases as compared with current conditions. Table 7.4 summarises the quantitative changes in inundated area due to climate change impacts on the flood hydrograph considered here under emission scenario A2.

Figure 7.8: Progress and maximum inundated areas using flood events at current condition, climate scenarios 2050s and 2080s
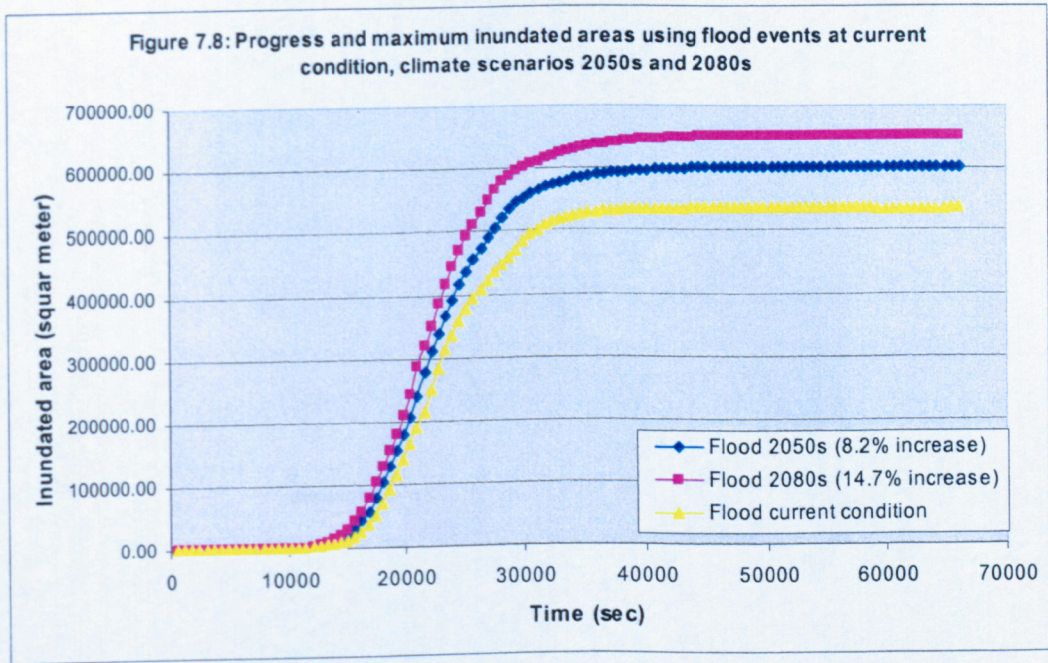
Figure 7.9 shows inundation maps associated with these three scenarios. As seen, the general patterns of inundation remains unchanged despite an increase of 8.2% and 14.7% in peak flow magnitudes resulting from climate change scenarios for the 2050s and 2080s respectively. It means that the flow leaves the main channel from similar places along the river and only its volume and duration vary under climate change scenarios.

Fig. 7.9: Inundation maps associated with: (a) the current 1 in 0.5 year flood, (b) the 1 in 0.5 year flood under scenario 2050, and (c) the 1 in 0.5 year flood under scenario 2080

(a)

(b)

(c)

0   400m
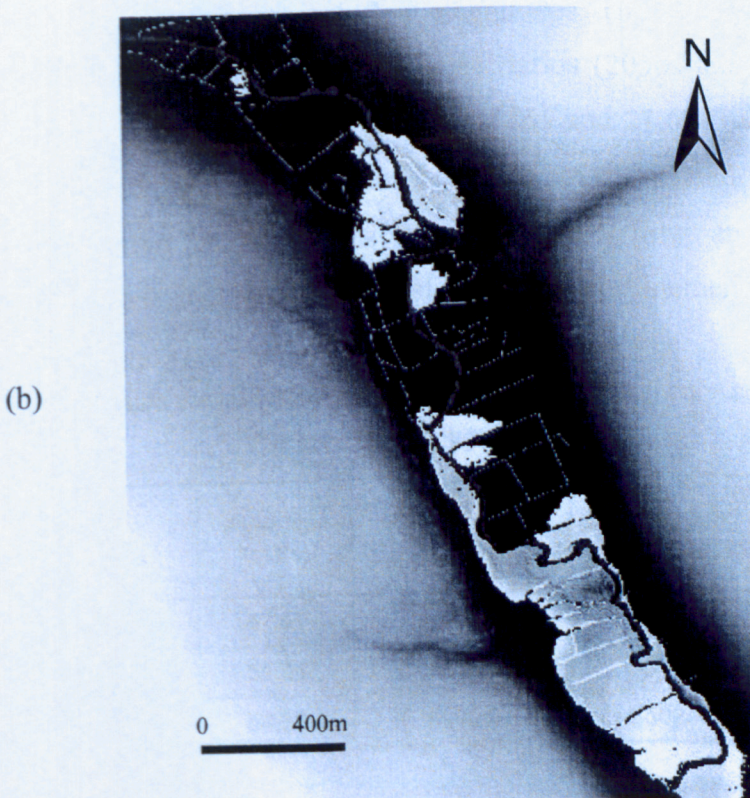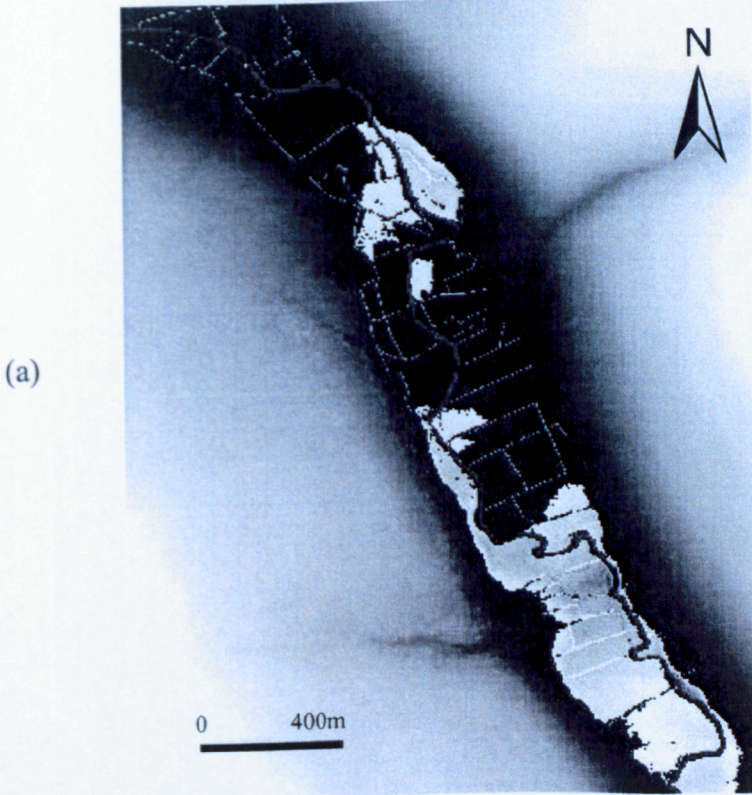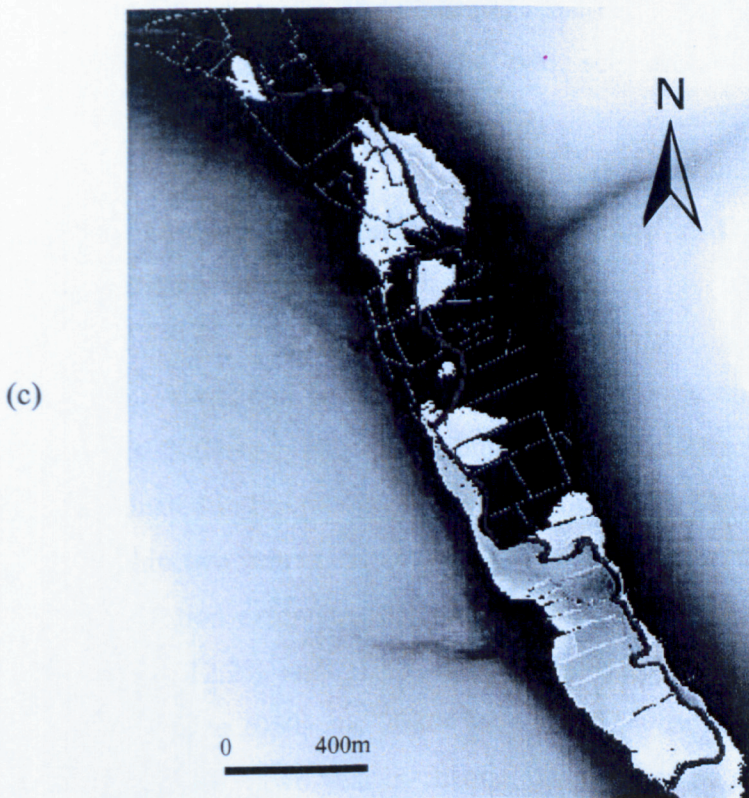
Table 7.4 shows that climate change scenarios for the 2050s and 5080s result in 8.2% and 14.7% increases in peak flow magnitudes. The resultant changes in flow hydrographs due to these climate change scenarios (2050s and 2080s) lead to an increase in maximum inundation extent of 12.2% and 21.6% respectively. In both scenarios, the increase in inundation extent is not associated with areas and is mostly reflected in lateral extension of floodplain flow and water depth on floodplain, which is another indication of floodplain confinement.

Table 7.4: Inundation extent variation using different climate change scenario for 2050 and 2080

Flood	Peak flow (m3/s)	% of peak flow increase to current condition	Inundation extent (m2)	% of Inundation increase to current condition
Current condition	47.41	0%	534784	0%
Under scenario 2050s	51.31	8.20%	599872	12.20%
Under scenario 2080s	54.38	14.70%	650240	21.60%

Moreover, comparison between the percentage increase of flow hydrograph peak and maximum inundation extent in the two scenarios shows a non-linear relationship.

7.4 Interaction between short-term channel change and long-term climate change on inundation extent

Inundation extent variations in response to short-term channel change (i.e. in-channel geometry 2002 and 2004) and long-term climate change (i.e. 2050s and 2080s) were evaluated in the previous sections. The results showed an average bed rise of 10cm within two years (from 2002 to 2004) resulted in an increase of 5.7% and 7.1% in inundation extent for the 1 in 0.5 and 1 in 2 year floods. Inundation extent increased by 12.2% and 21.6% due to changes resulting from the climate change scenarios for the 2050s and 2080s for a 1 in 0.5 year flood. The comparison of the results shows that a two-year in-channel change may be as serious as 50% of the changes that are likely to arise from climate change within the next fifty years, using a flood with a 1-year return period. The relative comparison of inundation variation in response to channel change and climate change reveals that in-channel fluvial process can have more significant impacts on inundation extent than climate change over short term.

Climate change scenarios were established using the period 1961-2000 as a baseline for predicting future climate change. Robson (2002) noted that trends in this period may be explained by climate variability and periods longer than 40 years are needed to distinguish between climate variability and climate change. Climate variability can be thought as the natural variation in climate over time: it is the same as climate change (both climate change and climate variability occur at the same time). Under climate variability, the climate differs from one period to the next but under climate change, a long-term alteration in the climate is occurring. The distinction between climate change and climate variability as a cause attributed to an increase of either rainfall or flooding is not the main focus. Rather, the key issue in addressing climate change and climate variability is that what may appear under climate change within a longer period may occur under climate variability in the shorter term. Thus, there is the possibility that short-term in-channel change occurs

simultaneously with longer term changes imposed on flow hydrographs (climate change or climate variability). Hence, the effect of the combination of in-channel change and climate change/variability on inundation extent prediction was explored. Figure 7.10 shows inundation extents predicted using the in-channel geometry for 2004 (i.e. an average of 10 cm rise in bed levels along the study site) and climate scenarios for the 2050s and 2080s (i.e. 8.2 and 14.7% increase in the peak flow of inflow hydrographs respectively) for the 1 in 0.5 year flood. As seen in Table 7.5, inundation extent increases by 38 and 52%, using the 2004 geometry in conjunction with climate scenarios for the 2050s and 2080s as compared with the inundation extent resulting from the 2002 geometry and the peak flow of the inflow hydrograph observed in the February 2004 event (i.e. 47.41 m^3/s).

Fig. 7.10: inundation extent resulting from geometry 2004 and climate change 2050s (a) and 2080s (b) using the 1 in 0.5 year flood

(a)

0   400m

(b)
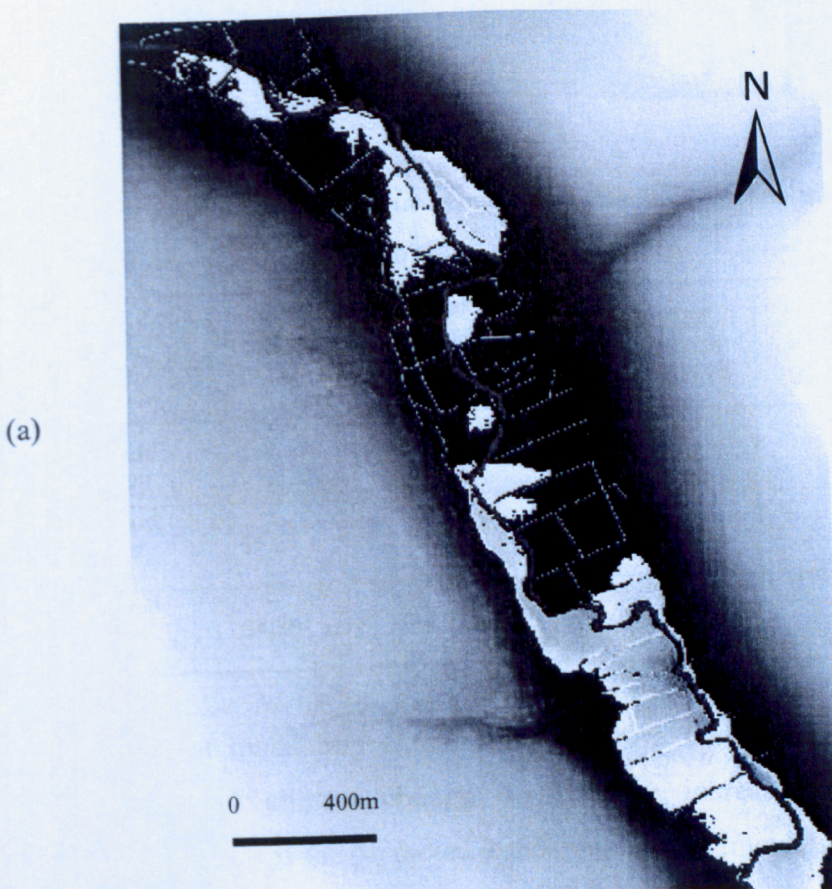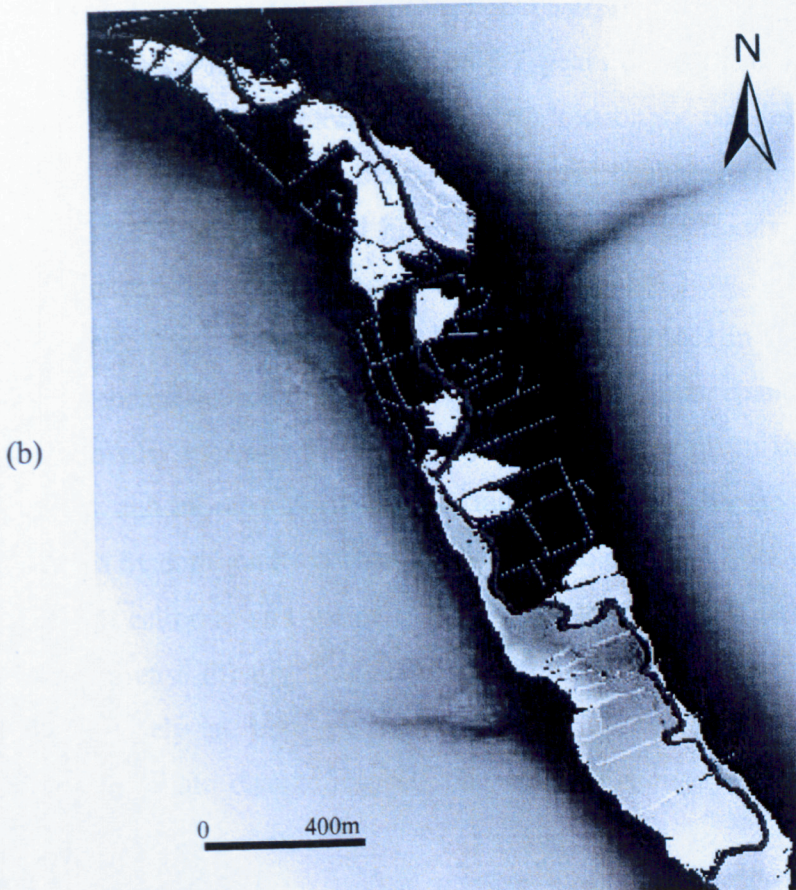
Table 7.5: inundation extent increase due to combined effects of in-channel change and climate change

Flood	Peak flow (m3/s)	% of peak flow increase to current condition	% of inundation increase under geometry 2002	% of inundation increase under geometry 2004
1 in 0.5 year flood current condition	47.41	0%	0%	5.70%
1 in 0.5 year flood under scenario 2050s	51.31	8.20%	12.20%	38.23%
1 in 0.5 year flood under scenario 2080s	54.38	14.70%	21.60%	52.13%

Table 7.5 shows that inundation extent resulting from the combined effects of channel geometry and climate change dramatically increased. The channel configuration change causes the predicted 2050s increase in inundation area to rise from 12.2% to 38.2%. The 2080s increase rises from 21.6% to 52.1%. These are quite dramatic, and they have a number implication. First, they show that the sensitivity of inundated area change to climate changes is strongly conditional by

in-channel sedimentation. Whilst this is not a surprising finding in general, the magnitude of the sensitivity, given that only 2 years of sedimentation and a mean 10cm bed level rise are explored, it implies a strongly non-linear relationship between changes in inundation extent and bed level changes. Second, it should be noted that different results would be obtained for bigger floods: there will be a maximum inundation extent, associated with a potential flow, when the valley is fully inundated. These flows will not be linked to changes in inundation extent, regardless of channel configuration or climate change. Thus, channel configuration changes essentially increase the frequency with which a given inundation extent occurs. Third, and more importantly, the fact that inundation extent is so heavily impacted upon by configuration change causes us to question how we use historical flood events to calibrate and validate flood inundation models based upon surveys of current geometry. Finally, this set of experiments emphasises the need to look much more closely at how geomorphology conditions affect flood risk and, crucially, how climate change impacts on sediment delivery, and hence on flood risk.

7.5 Conclusion

The results obtained in this chapter have highlighted that channel configuration change is of great importance in relation to inundation extent prediction given the short time scale of its change (5.7% over 2 years) as compared with longer term changes of climate (12.2% over 50 years). The combined effects of long-term climate change and short-term channel configuration change resulted in an additional range of 26-47% increase in inundation extent when they are simultaneous. This implies that the rate of increase in inundation extent due to influencing factors (i.e. in-channel geometry and climate change) is non-linear and complex. Given the spatial scale of the study site and the magnitude of flood event considered here, individual or combined effects of channel configuration change and climate change could be more serious if a wider floodplain along with a longer term configuration change were considered. However, it is very difficult to generalise this conclusion in terms of the effects of climate change and channel configuration individually or combined on inundation extent. To a large extent, the conclusion will be floodplain configuration dependent. However, the results

presented here have one main implication: in future flood risk studies, not only focus should be put on climate change effects, but also channel configuration effects especially as management activities (e.g. bank erosion protection) may exacerbate in-channel sedimentation in upland, coarse-grained, river channels.

Chapter 8: Conclusions

8.1 Chapter objectives and structure

The objectives of this chapter are:

(i) to summarise the results of the thesis with respect to the primary thesis aims and the objectives outlines in Chapter 1; and

(ii) to highlight the limitations of the study and to propose future research directions.

This chapter has three main sections. Section 8.2 addresses a synopsis of the main findings of the research with respect to each individual aim and objective of the research, particularly highlighting the strengths and weaknesses of the modelling systems applied in relation to floodplain inundation extent and the effects of short-term channel change and long-term climate change on inundation extent. Section 8.3 provides a summative conclusion. Section 8.4 highlights issues which need to be considered in future research.

8.2 Synopsis of the main research findings

The overriding theme of the research has been the accurate prediction of inundation extent in a topographically-complex upland floodplain. In this respect, the research was based on a context that was both technical (model representation of floodplain

flow inundation) and substantive (the effects of climate change and sediment delivery on flood inundation). Thus, the two main aims of the thesis were:

(i) to evaluate the performance of hydraulic models with one-dimensional (i.e. in normal and storage cell modes) and a simplified two-dimensional process representation (i.e. raster-based diffusion wave treatment) for floodplain flows in conjunction with high resolution topographic data for floodplain inundation extent prediction; and

(ii) *to explore the effects of different in-channel configurations, due to deposition and erosion, and climate change on floodplain inundation extent.*

In Phase 1 of the research, as shown in Chapters 4, 5 and 6, the same one-dimensional flow representation in the main channel was assumed to represent a reasonable level of flow process complexity for the main channel flow representation for large scale flow routing studies (Cunge *et al.*, 1980; Knight and Shiono, 1996). Whit this, the ability of different floodplain flow treatments in relation to inundation extent prediction was then examined. The results showed that the two-dimensional diffusion wave treatment with an optimum performance of 61% outperformed significantly (by 11% and 7%) the normal and storage cell modes of HEC-RAS respectively. A number of issues were involved in obtaining these results. The main issues included the nature of flow processes used in each model, topographic parameterisation in complex floodplains, validation data, calibration and floodplain configuration. Some of these aspects have been acknowledged in previous studies (Gee *et al.*, 1990; Feldhaus *et al.*, 1992; Bates and Anderson, 1992, Bates and Anderson, 1994; Bates *et al.*, 1995, 1996, 1998; Lane, 1998; Hardy *et al.*, 1999; Stewart *et al.*, 1999, Bates and De Roo, 2000; De Roo *et al.*, 2000; Horritt and Bates, 2001a, 2001b, 2002, Nicholas and Mitchell, 2003; Bradbrook *et al.*, 2004; Yu and Lane, in press a, b).

Chapter 7 dealt with the effect of channel configuration change and climate change on inundation extent (Phase 2). In this regard, the results showed the significant effects of main channel geometry changes (as a result of sediment delivery) and boundary conditions (as a result of climate change) in determining inundation extent; issues that have received less attention. The range of performances of

models used in this research, largely resulting from flow process representation and floodplain topographic parameterisation, was about 11% (see Table 6.6). Individual impacts of channel configuration change and climate change on inundation extent for the same flood event were estimated as 5.7% and 12.2% (for the 2050s) (see Table 7.5). However, a dramatic increase in inundation extent was estimated when the impacts of channel configuration change and climate change interacted. The results obtained in this research have implications in relation to the direction of future research, flood inundation studies and flood risk. Hence, more details of the issues involved in Phase 1 and 2 of the research and their consequent implications are addressed in the frame of thesis objectives in the next section. Then, a final conclusion is presented.

8.2.1 Phase 1 objectives

Objective 1: to simulate inundation extent using normal mode of a one-dimensional hydraulic model for floodplain flow representation (i.e. HEC-RAS).

The numerical experiments undertaken using HEC-RAS in normal mode showed that the model is only stable when simulating floods with return periods less than 5 years in this particular reach. Within stable simulations, it responds to input variations in a realistic way. The sensitivity of the model to friction variations showed that the bulk flow characteristics are controlled by main channel friction, with a minimal effect of floodplain friction, a finding that is consistent with previous studies (see Cunge *et al.*, 1976; Romanwicz *et al.*, 1999; Bates and De Roo, 2000). Although the change of floodplain friction did not affect downstream bulk flow characteristics, it did affect the accuracy statistics (Table 4.8) sufficiently to suggest that inundation extent does depend on floodplain friction, which is consistent with the work of Horritt and Bates (2001). The best performance of HEC-RAS in normal mode correctly simulated 50%, (*F%*), of inundated and non-inundated areas of the potential floodplain area (see Table 4.8). This is shown in Figure 4.17, which provides a comparison of model predicted inundation extent with the shorelines derived from GPS data and observational evidence. The model performance obtained here seems not to be promising as compared with previous studies (see Bates and De Roo, 2000; Horritt and Bates, 2002). The negligible

difference between maximum water elevations observed and predicted at a number of cross sections along the study reach at optimum calibration (Table 4.10) suggest that inflow uncertainties (Chapter 3) could not be a major source of poor performance of the model. However, poorer performance may be attributed to a number of issues. First, once the river overtops, the model calculates conveyance of water downstream for all floodplain flows regardless of the local topography of floodplain and does not block downstream flux even when blockages exist. This may be a reasonable conceptualisation for straight channels with steep lateral floodplain slopes (Cunge 1980; Bates and De Roo, 2000) where no major storage and blockage effects exist. Thus, the model only represents momentum effects and cannot represent discontinuities in floodplain flows due to physical blockage. This is more crucial in topographically-complex floodplains where two-dimensional flow behaviour is reduced to flux between extended cross sections. This is the case for the study site in this research, where the floodplain is well partitioned with field walls and public roads, causing flow direction on the floodplain to be independent of the main channel. Second, the fact that the water surface is assumed to be horizontal across the floodplain may affect the model performance in relation to inundation extent. This becomes more important in this case study where the floodplain has a slight lateral slope and the river banks are protected using levées with a higher elevation than the floodplain. Third, there are uncertainties surrounding inundation extent observations, resulting from either the kind of remotely-sensed data and analysis techniques used (e.g. Tholey, 1995; Imhoff, 1997; Horritt, 1999; Horritt and Bates 2001b; Horritt et al., 2002) or lateral inflows onto the floodplain which are not considered in the model. The latter is, to some extent, the case here as the observed inundation extent was associated with contributions from hillslope and tributary flows. Tributary flows were considered as boundary conditions in the modelling system used here but their flow hydrographs were connected only to the main channel. In this state, tributary flows that only contribute to floodplain inundation are simulated as inflow to the main channel and this may reduce the simulated inundation extent.

Objective 2: to simulate inundation extent using storage cell model of a one-dimensional hydraulic model for floodplain flow representation (i.e. HEC-RAS).

HEC-RAS in storage cell mode was numerically more stable and capable of simulating a wider range of flood magnitudes in the particular study site, provided that the model was run with the smallest time step. The downstream response of the model to main channel friction change was complicated (peak discharge increased rather than decreased, as in normal mode) due to two flow processes simultaneously impacting in the main channel and the floodplain. On the one hand, increases of friction in the main channel resulted in a higher water level in the main channel and more transfer of flow onto the floodplain. This, in turn, caused the downstream flow hydrograph to become more attenuated and delayed. On the other hand, given there was no representation of momentum effects in relation to floodplain flux, a rapid downstream transfer of floodplain flow occurred. These two processes act against each other and caused the response of downstream bulk flow characteristics to main channel friction changes to become complex and less sensitive than for the normal mode. As there is a current emphasis on using floodplain storage to attenuate downstream flows, this finding emphasises the need to give very careful attention to how floodplains are represented in one-dimensional models. The best performance of the storage cell mode in relation to inundation extent outperformed the normal mode by 4% (54% versus 50%). This stems only from difference between the floodplain flow treatment used in the two models as the observation data used in validation are similar. Also, a relatively poor performance of the storage cell mode, as with the normal mode, was not due to uncertainties associated with inflow boundary condition as a good agreement between predicted and observed inundation across the weirs at the main channel-floodplain interface was seen (See section 5.4.4). As discussed before, the storage cell mode allows floodplain topographic characteristics to cause some storage and blockage effects to be simulated but there is no representation of momentum effects on floodplain flux. Thus, in storage cell mode, inundation extent is determined by floodplain storage and is not affected by dynamic flux transfer processes. This aggravates the prediction of inundation extent in upland floodplains where the general slope of the floodplain is relatively high, causing the floodplain storage to be reduced and the floodplain flux becomes more significant in relation to flood inundation. Lack of flux flow causes water transfer onto the floodplain to leave the domain rapidly. In such situations, changes in flows that leave the main channel do not necessarily change inundation extent at a similar rate. This is illustrated in Table 5.4 where

different rates of improvement in the measure of F were noted using different n values in the main channel. Therefore, the inundation extent in the storage cell mode was not controlled by the volume of flow that leaves the main channel, but the primary storage capacity of cells (storage capacity below critical elevation of a hydraulic connection) and the effects of backwater and blockage. As the storage cell size becomes bigger, floodplain flux effects become more important and this leads to a poorer agreement between predictions and observations as the storage cell is filled by water from the lowest elevations upwards rather than routing water across the storage cell. Aside from these limitations, the high quality floodplain topographic characteristics used in the storage cell parameterisation aided good agreement between predicted and observed shorelines, where the floodplain is fully inundated (i.e. the downstream part of the floodplain in this research). By using smaller storage cells, the effects of dynamic flux transfer process would be enhanced: this is a central aim in the two-dimensional diffusion model. However, what is defined as critical size depends on channel configuration in relation to flood size. As with the normal mode, the storage cell approach represents only a very poor treatment of actual floodplain processes.

Objective 3: to simulate inundation extent using a two-dimensional diffusion wave treatment for floodplain flow representation.

As mentioned before, both the normal and storage cell mode approaches are inadequate representations of floodplain flow processes for flood inundation. The former only represent the momentum effects of floodplain flows without considering blockage and storage effects that may be caused by physical obstacles on the floodplain. The latter emphasizes storage effects caused by floodplain topographic characteristics. However, the way that flow processes on the floodplain are represented in the storage mode leads to an overly rapid flux rate on the floodplain. The raster-based model conceptually outperforms these models as it represents a compromise solution in terms of storage and flux routing. Reducing the storage cell size, considering a uniform bed level for each cell and using a simplified form of the shallow water equation for routing flows between cells, the effect of flux routing is enhanced in the raster-based models. The optimum size of cells (resolution) is a function of storage and flux routing on the floodplain and

these effects depend on channel configuration (whether acting as storage area or flux routing) (see Horritt and Bates, 2001a). In addition it depends on the local context of channel and floodplain size and flood magnitude (see Yu and Lane, in press, a). Storage effects are affected by topographic characteristics in each cell in the raster-based model. Thus, in the raster-based model, flows are routed given small-scale topographic characteristics of the floodplain whereas in the storage cell, topographic features are only involved in defining the storage capacity of each cell and determining shorelines after the flow simulation.

The raster-based model, unlike the normal mode, is capable of simulating a range of floods with 0.5 to 10 year return periods in this study area (see Table 6.2). Using this model, change of n values in the main channel resulted in changes in inundation extent on the floodplain that could be explained by flow representations in the normal and storage approaches (see section 6.4.2.3). In two-dimensional raster-based models, the effects of n upon flow routing on the floodplain is less-understood. This may be attributed to the poor representation of inertial processes (Bates and De Roo, 2000; Horritt and Bates, 2002). It may be due to floodplain confinement as noted by Yu and Lane (in press, a) and Horritt and Bates (2001a). Similarly, the results in this research showed that maximum inundated area curves were separated from each other but as soon as floodplain confinement is reached, they converged to a maximum value (see Figure 6.6).

Aside from a better representation of flow process conceptually, the model application proved practically a better performance in relation to inundation extent prediction. The model outperformed the normal and storage cell approaches by 11% and 7% percent respectively (61% versus 50% and 54%). Improvements in the raster model predictive ability are partly hidden by good performance of the normal and storage cell models in places but for the wrong reasons. Where field observations suggest inundation is as a result of hillslope/tributary flows, both the normal and storage cell models predict it as channel-sourced inundated areas that, in turn, improve their performance as compared with the diffusion model. This emphasises the need to consider model design very carefully in studies of inundation extent. The predictive ability of the raster-based model used here showed a poorer performance as compared with similar studies (Bates and De Roo, 2000; Horritt and Bates, 2001b; Horritt and Bates, 2002; Yu and Lane, in press a). As noted for the normal mode, this is attributed to uncertainness involved in the

observed inundation extent. This is supported as discrepancies between predictions and observations in all models were found in similar parts of the floodplain, most of which are likely to be affected by tributary/hillslope flows. Where inundation extent is less affected by hillslope and tributaries flows, a good correspondence between predictions and observations was seen (the downstream half of the reach) in the models in which the floodplain surface is parameterised with high quality topographic data, implying the significant role of floodplain topographic characteristics in determining shorelines.

8.2.2 Phase 1 conclusion

Conceptually, the diffusion model outperforms the normal and storage cell models. By testing these models in this research, the two-dimensional raster-based model outperformed the normal and storage cell approaches at optimum calibration. Practically, the improvement in the diffusion wave model was not as great as expected due to floodplain configuration.

The validation data used here are insufficiently accurate for further discrimination between the model behaviours in relation to inundation process. The major difference between simulated and observed inundation extent for the three models used here was seen at certain locations, which correspond to hillslope/tributary flows. Models in which the floodplain surface was parameterised with high quality topographic data, showed a good correspondence between predicted and observed shorelines where floodplain inundation is less affected by tributary/hillslope flows, implying the significant role of floodplain topography in determining shoreline locations.

8.2.3 Phase 2 objective and conclusion

Objective: to evaluate the effect of in-channel configuration change and climate change on inundation extent.

The effect of in-channel configuration change and climate change on inundation extent was explored. The former affects bankfull discharge (see section 7.2.3) and the latter influences the volume of water that enters the study domain. In this

respect, the findings indicated that for the 1 in 0.5 year flood in this case study, the individual effects of two-year in-channel configuration change (6.1% reduction in bankfull discharge following a mean 10cm rise in bed levels) and climate change (scenario 2050s, 8.2% increase in peak flow) are equal to increases of 5.7% and 12.2% of inundation extent prediction. If these values are compared with the difference in the range of model performances obtained in this research (maximum 11%), largely resulting from flow process representation and floodplain topographic parameterisation, it illustrates the significant role of in-channel geometry and inflow boundary condition in predicting inundation extent. This means that the correct estimate of the flow entering into the study domain (affected by climate change) and the flow volume leaving the main channel (affected by in-channel change) are crucial to inundation extent prediction. This is noted by Horritt and Bates (2001b) who showed that, as long as bankfull discharge was approximately correct, the inundation area was also approximately correct using different two 2D models. It means that, for a reasonable level of flow representation, the in-channel geometry and inflow boundary condition have a role even more important than flow representation and calibration in terms of inundation predictions. The channel configuration change caused the predicted 2050s inundated area increase to rise from 12.2% to 38.2% (see Table 7.5). In the case of the 2080s scenario, it rises from 21.6% to 52.1% (see Table 7.5). These are quite dramatic and may have a number of implications. First, they show that the sensitivity of inundated area changes to climate change is strongly conditioned by in-channel sedimentation. Second, different sensitivity would be observed for bigger floods in this case study. However, channel configuration change essentially increases the frequency with which a given inundation extent occurs. Third, the fact that inundation extent is strongly affected by channel configuration changes causes us to question how we use historical flood events to calibrate and validate flood inundation models based upon surveys of current geometry. Finally, given the complex and non-linear impacts of combined climate change and river configuration change on inundation extent, it is vital to explore much more closely the interaction between climate change and sediment delivery and how they impact on flood risk.

8.3 Final conclusion

The numerical experiments undertaken in this research highlighted that conceptually and practically, floodplain flow representation in the two-dimensional raster-based model is a compromise solution in this case study, an upland topographically-complex floodplain, in relation to flood inundation prediction given the known limitations in representing flow processes in the normal and storage cell approaches. Differences in predictive performance were due to different flow representation that causes different responses to friction parameterisations. Aside form the impact of flow representation on calibration, the significance of river channel configuration on model responses was illustrated. A relatively small range of model performance differences (maximum 11%) was attributed to channel configuration role in this particular case that causes the normal mode and storage cell approaches to work more effectively for the wrong reasons. The application of the models in this case study showed that the model is not at the limit of its predictive ability due to uncertainties involved in the validation data. Uncertainties associated with observed inundation were highlighted as controlling elements that affect model performance relative to each other (correspondence between wrong predictions and wrong observations) or the absolute comparison between different studies. This highlights the importance of model design given process representation in reality. Using the storage cell approach and the 2D model, the effective role of floodplain topography in determining shorelines was demonstrated. The research highlighted the importance of model design in relation to model performance given process representation in reality. The impacts of in-channel change and climate change on inundation extent prediction highlighted that they could affect model performance in a similar range of uncertainties stemming from different flow process representation and calibration This emphasised the significance of climate change and in channel-change as a potential flood risk and that model performance should be investigated in the wider context of controlling elements. This has implications for watershed planning and management, those which affect in-channel sedimentation (i.e. bank erosion protection). Thus, a relatively crude model in conjunction with good geometric data may produce results similar to outputs resulting from a more detailed model parameterised with

inaccurate geometric data. Moreover, it noted that investigation of current flood risk should be based on the current geometric data and historical flood event models should not be calibrated or validated with the current geometric data. Given that in-channel change can dramatically increase the effects of climate change on inundation extent, experiments that can explain the relationship between climate change and sediment delivery and in turn their impacts on flood risk are vital.

8.4. Future research directions

There are three important research directions emerging from this thesis.

River channel configuration: The numerical experiments undertaken in this research were conducted in an upland confined floodplain. As discussed, floodplain confinement may affect flow process and model response to calibration. This may, in turn, affect model performance. In this state, the strengths and weaknesses in a model in relation to flow process representation may be masked by the wrong reasons. Use of these models in floodplains in which flows are not confined laterally may help to develop a better understanding of their predictive ability and possibly to define criteria that can anticipate where the models yield acceptable results. The same point is valid for the effects of climate change and in-channel change on inundation extent. More investigations using different river channel configuration, given the fact the inundation is strongly floodplain-topography independent, may aide generalising of their impacts on inundation extent predictions.

Validation data: Further discrimination of flow process representation was not feasible due to uncertainties associated with validation data in this research. This caused the actual predictive ability of the models used in this research to be difficult to specify. Hence, it is suggested that similar numerical experiments be undertaken where validation data are accurate enough to distinguish flow process representation.

Climate change and fluvial process interaction: Given that the effect of climate change on flood risk is dramatically increased by in-channel sedimentation, further

267

research is required to investigate in-channel fluvial process and climate change interaction with respect to flood risk. This requires investigations within a longer framework and a wider number of river channel configurations than was reported here.

References

Ackers, P., 1992a. Gerald Lacey Memorial Lecture- canal and river regime in theory and practice: 1929-92. *Proceedings of the Institution of Civil Engineers, Water, Maritime and Energy* 96,167-178.

Ackers, P., 1992b. Hydraulic design of two stage channels. *Proceedings of the Institution of Civil Engineers, Water, Maritime and Energy* 96, 247-257.

Ackers, P., 1993a. Stage-discharge functions for two-stage channels. *Journal of Hydraulic Research* 31 (4), 509-531.

Anderson, M. G., Bates, P. D., 1994. Initial testing of a two-dimensional finite element model for floodplain inundation. *Proceedings of the Royal Society of London* A 444, 149-159.

Anderson, M. P., Woessner, W. W., 1992. *Applied Groundwater Modelling: Simulation of Flow and Advective Transport. Academic Press*, San Diego, CA.

Aronica G., Bates P. D., Horritt M. S., 2002. Assessing the uncertainty in distributed mode predictions using observed binary patter information within GLUE. *Hydrological Processes* 16, 2001-2016.

Arcement, G. J., Jr, Schneider, V. R., 1989. Guide for selecting Manning's Roughness Coefficients for natural channels and floodplain. *United States Geological Survey Water Supply Paper* 2339.

Baird, L., Gee, D. M., Anderson, M. G., 1992. Ungauged catchment modelling II. Utilization of hydraulic models for validation, *Catena* 19, 33-42.

Barkau, R. L., 1992. UNET, *One-dimensional unsteady flow through a fall network of open channels, Computer Program*, St Louis, MO.

Barnes, H. H., Jr., 1967, Roughness characteristics of natural channels: *U.S. Geological Survey Water-Supply Paper* 1849, 213p.

Bates, P. D., 2000. Development and testing of a subgrid-scale model for moving-boundary hydrodynamic problems in shallow water. *Hydrological Processes* 14, 2073-2088.

Bates, P. D. and Anderson, M. G., 1993. A two-dimensional finite-element model for river flow inundation. *Proceedings of the Royal Society of London* A 440, 481-491.

Bates, P. D., Anderson, M. G., 1996. A preliminary investigation into the impact of initial conditions on flood inundation predictions using a time/space distributed sensitivity analysis. *Catena* **26**, 115-134.

Bates, P. D., Anderson, M. G., 2001. Validation of Hydraulic models. In: *Model Validation: Prospectives in Hydrological Science*, Anderson, M. G., Bates, P. D., (Eds.), Willey, pp.500.

Bates, P. D., Anderson, M. G., Baird, L., Walling, D. E., Simm, D., 1992. Modelling floodplain flow with a two-dimensional finite element scheme. *Earth Surface Processes and Landforms* **17**, 575-588.

Bates, P. D., Anderson, M. G., Hervouet, J. M., 1995. Initial comparison of two two-dimensional finite element codes for river flood simulation. *Proceedings of the Institution of Civil Engineers, Water, Maritime and Energy* **112**, 238-248.

Bates, P. D., Anderson, M. G., Price, R. J. Hardy, R. J., Smith, C. N., 1996. Analysis and Development of Hydraulic Models for Floodplain Flows. In: *Floodplain Processes*. Anderson, M. G., Walling, D. E., Bates, P. D., (Eds.). Wiley, Chichester, pp. 215-254.

Bates, P. D., De Roo, A. P. J., 2000. A simple raster-based model for flood inundation simulation. *Journal of Hydrology* **236**, 54-77.

Bates, P. D., Hervouet, J. M., 1999. A new method for moving boundary hydrodynamic problems in shallow water. *Proceedings of the Royal Society of London*, Series A **455**, 3107-3128.

Bates, P. D., Horritt, M., Hervouet, J. M., 1998a. Investigating two-dimensional, finite element predictions of floodplain inundation using fractal generated topography. *Hydrological Processes* **12**, 1257-1277.

Bates, P. D., Horritt, M., Smith, C., Mason, D., 1997. Integrating remote sensing observations of flood hydrology and hydraulic modelling. *Hydrological Processes* **11**, 1777-1795.

Bates, P. D., Lane, S. N., 1998. Preface: High resolution flow modelling in hydrology and geomorphology. *Hydrological Processes* **12**, 1129-1130.

Bates, P. D., Marks, K. J., Horritt, M. S., 2003. Optimal use of high-resolution topographic data in flood inundation models. *Hydrological Processes* **17**, 537-557.

Bates, P. D., Stewart, M. D., Siggers, G. B., Smith, C. N., Hervouet, J-M., Sellin, R. H. J., 1998b. Internal and External validation of a two-dimensional finite element model for river flood simulation. *Proceeding of the Institution of Civil Engineers, Water, Maritime and Energy* **130**, 127-141.

Beven, K. J., 1979a. A sensitivity analysis of the Penman-Monteith actual evapotranspiration estimates. *Journal of Hydrology* **44**, 169-190.

Beven, K. J., 1989. Changing ideas in Hydrology: the case of physically based distributed models. *Journal of Hydrology* **105**, 79-102.

Beven., K. J., Binley, A. M., 1992. The Future of distributed models – model calibration and uncertainty prediction. *Hydrological Processes* **6** (3), 279-298.

Bhallamudi, S. M., Chaudhury, M. H., 1991. Numerical modelling of aggradation and degradation in alluvial channels. ASCE *Journal of Hydraulic Engineering* **119**, 1145-1164.

Bhomik, N. G., Demissie, M., 1982. Carring capacity of flood plains. *Journal of Hydraulics Research. American Society of Civil Engineers* **108**, 443-452.

Bradbrook, K. F., Lane, S. N., Waller, S. G., Bates, P. D., 2004. Two dimensional diffusion wave modelling of flood inundation using a simplified channel representation. *International Journal of River Basin Management* **3**, 1-13.

Brackett, R. A., Arvidson, R. E., Izenberg, N. R., Saatchi, S. S.,1995. Use of ploametric and interferometric radar for flood routing models: first results for Missouri River. Session 36- Planetary Geology: Radar Remote Sensing of floodplains, mountain belts, and volcanos, Annual Meeting of the Geological Society of America, 5-9 November, New Orleans.

Bray, D. I., 1979. Regime equations for grave-bed rivers. In: *Gravel Bed Rivers*, Hey, R. D., Bathurst, J. C., Thorne, C. R., (Eds.). Wiley, Chichester, pp. 517-42.

Bridge, J. S., Gabel, S. L., 1992. Flow and sediment dynamics in a low sinuosity river: Calamus River, Nebraska Sandhills, *Sedimentlogy* **29**, 499-550.

Chanson, H., 1999. *Hydraulics of Open Channel Flow, An Introduction* Butterworth-Heinemann, 544pp.

Cowan, W. L., 1956, Estimating hydraulic roughness coefficients: *Agriculture Engineering*, v. 37, no. 7, p. 473-475.

Chow, V.T., 1959. *Open Channel Hydraulics*. McGraw-Hill, New York, 680pp.

Cobby D. M., Mason, D. C., Davenport, I. J., 2001. Image processing of airborne scanning laser altimetry data for improved river flood modelling. ISPRS *Journal of Photogrammetry & Remote Sensing* **56**, 121-138.

Congalton, R. G., Green, k., 1999. Assessing the accuracy of remotely sensed data: principles and practices. (Lewis Publisher, CRC Press: Boca Raton) 137 pp.

Cunge, J. A., 1975. Two-dimensional modelling of floodplains. In: Unsteady Flow in Open Channels. Mahmood, K., Yevjevich, V., (Eds.). Vol. II. Fort Collins, CO.

Cunge, J. A., Holly, F. M. and Verwey, A. 1980. *Practical Aspects of Computational River Hydraulics*. Pitman, London, 178 pp.

Davis, C. A., 1995. Hydrologic Engineering Center (HEC), User's Guide and Utility Programs, U.S. Army Corps of Engineering, 120 pp.

De Roo, A. P. J., Wesseling, C. G., Van Deursen, W. P. A., 2000. Physically based river basin modelling within a GIS: the LISFLOOD model. *Hydrological Processes* **14**, 1981-1992.

Dellurs, J. W., Toebes, G. H., Udeozo, B.C., 1967. Uniform flow in idealised channel floodplain geometries. IAHR. Proceedings 12 the congress Fort Collins.

Dietrich, W. E., Whiting, P. J., 1989. Boundary shear stress and sediment transport in river meanders of sand and gravels. In: *River Meandering*, Ikeda, S., Parker, G., (Eds.), American Geophysical Union Monograph, 12. pp. 1-50.

Dugdale, L.J., 2003. A hydrological modelling study to investigate the potential effect of climate change on the flood regime of a small upland catchment: How certain can we be?, Unpublished MSc dissertation, University of Leeds.

Eagleson, P. S., 1970. *Dynamic Hydrology*. McGraw-Hill, New York.

Einstein, H. A., Li, H., 1958. Secondary currents in straight channels. *Transactions, American Geophysical Union*, **39**, 1085-1088.

Emmons, H. W., 1970. *Annual Review of Fluid Mechanics* **2**, 15-36.

Environmental Agency. 1997. *Evaluation of the Lidar Technique to Produce Elevation Data for use Within the Agency*, National Centre for Environmental Data and Surveillance: Bath, UK; 33 pp.

Ervine, D. A., MacCleod, 1999. Modelling a river channel with distant floodbanks. *Proceedings of the Institution of Civil Engineers, Water, Maritime and Energy* **136**, 21-33.

Estrela, T., Quintas, L., 1994. Use of GIS in the modelling of flows on the floodplains. In: White, H. R., Watts, J. (Eds.), *Second International Conference on River Flood Hydraulics*, Wiley, Chichester, pp. 177-189.

Feldhaus, R., Hottges, J., Brockhaus, T., Rouve, G., 1992, Finite element simulation of flow and pollution transport applied to a part of the River Rhine. Falconer, R. A., Shiono, K., Matthews, R. G. S., (Eds.), In: *Hydraulic and Environmental Modelling: Estuarine and River Waters*. Ashgate Publishing: Aldershot; 323-334.

Flood, M., Gutelius, B., 1997. Commercial implications of topographic terrain mapping using scanning airborne laser radar. *Photogrammetric Engineering and Remote Sensing* **63**, 324-366.

Fread, D. L., 1984. Channel Routing, In: *Hydrological Forecasting*. Anderson, M. G., Burt, T. P., (Eds.), Wiley, Chichester, 209 pp.

Fread, D. L., 1993. Flow routing In: *Handbook of Applied* Hydrology. Anderson, M. G., Burt, T. P., (Eds.). McGraw-Hill, New York, 1-36

French, J. R., 2003. Airborne Lidar in support of geomorphological and hydrological modelling. *Earth Surface Processes and Landforms* **28**, 321-335.

French, R. H., 1994. *Open-channel Hydraulics*. McGraw-Hill Education, 705pp.

Galland, J. C., Coutal, N., Hervouet, J. M., 1991. TELEMAC-a new numerical-model for solving shallow-water equations. *Advances in Water Resources* **14**, 138-148.

Gee, D. M., Anderson, M. G., Baird, L., 1990. Large-scale floodplain modelling, *Earth Surface Processes and Landforms* **15**, 513-523.

Gomes Pereira, L. M., Wicherson, R.J., 1999. Suitability of laser data for deriving geographical information a case study in the context of management of fluvial zones. ISPRS *Journal of Photogrammetry & Remote Sensing* **54**, 105-114.

Hardy, R. J., 1997. *Modelling floodplain morpho-dynamics using a two-dimensional finite element approach*. Ph.D. Thesis, University of Bristol, 267pp.

273

Hardy, R. J., Bates, P. D., Anderson, M. G., 1999. The importance of spatial resolution in hydraulic models for floodplain environments. *Journal of Hydrology* 216, 124-136.

Harris, D. D., 1973. Hydrologic change after cleat-cut logging in a small Oregon Coastal watershed. *Journal of Research of the US Geological Survey* 1, 487-491.

Hasse, H., Bock, M., Hergenrother, E., Knopfle, C., Koppert, H. J., Schroder, F., Trembilski, A., Weidenhausen, J., 2000. Meteorology meets computer graphics – a look at a wide range of weather visualisations for divers audiences. *Computers and Graphics* 24, 391-397.

Henderson, F. M., 1996. *Open Channel Flow*. New York: Macmillan. 321 pp.

Heritage, G. L., Broadhurst, L. J., Brikhead, A. L., 2001. The influence of contemporary flow regime on the geomorphology of the Sabie River, South Africa. *Geomorphology* 38, 197-211.

Hervouet, J. M., Van Haren, L., 1996. Recent advances in numerical methods for fluids flows. In: *Floodplain Processes*, Anderson, M. G., Walling, D. E., Bates, P. D. (Eds.), Wiley, Chichester, pp. 183-214.

Hicks, D. M., Mason, P. D., 1991. *Roughness characteristics of New Zealand rivers*. Wellington: Water Resources Survey. 161pp.

Hohensinner, S., NaberSack, H., Jungwirth, M., Zauner, G., 2004. Reconstruction of the characteristics of a natural river-floodplain system and Hydromorphological changes flowing human modifications: the Danube River (1812-1991). *River Research and Applications* 20, 25-41.

Hollis, G. E., 1975. The effect of urbanisation on floods of different recurrence interval. *Water Resources Research* 11, 431-435.

Horritt, M. S., 1999. A statistical active contour model for SAR image segmentation. *Image and Vision Computing* 17, 213-224.

Horritt, M. S., 2000. Calibration and validation of a 2-dimensional finite element flood flow model using satellite radar imagery. *Water Resources Research* 36, 3279-3291.

Horritt, M. S., Bates, P. D., 2001a. Effects of spatial resolution on a raster based model of flood flow. *Journal of Hydrology* 253, 239-249.

Horritt, M. S., Bates, P. D., 2001b. Predicting floodplain inundation: raster-based modelling versus the finite-element approach. *Hydrological Processes* **15**, 825-842.

Horritt, M. S., Mason, D. C., Luckman, A. J., 2001a. Flood boundary delineation from synthetic aperture radar imagery using a statistical active contour model. *International Journal of Remote Sensing* **22**, 2489-2507.

Horritt, M. S., Bates, P. D., 2002. Evaluation of 1D and 2D numerical models for predicting river flood inundation. *Journal of Hydrology* **268**, 87-99.

Howard, A. J., Macklin, M. G., Black, S. and Hudson-Edwards, K. A., 1999. Holocene river development and environmental change in Upper Wharfedale, Yorkshire Dales, England. *Journal of Quaternary Science* **15**, 239-252.

Howes, S., Anderson, M. G., 1988. Computer simulation in geomorphology. In: *Modelling Geomorphological Systems*, Anderson, M. G., (Edt.). John Wiley, Chichester, 421-440.

Hydrologic Engineering Center, 1995. RD-41, A Comparison of the One-Dimensional Bridge Hydraulic Routines from: HEC-RAS, HEC-2, and WSPRO, U.S. Army Corps of Engineers, Davis C.A.

Hunt, J. C. R., 2002. Floods in a changing climate: a review. *Philosophical Transactions of The Royal Society of London* A **360**, 1531-1543.

Jones, J. A., Grant, G. E., 1996. Peak flow response to clear-cutting and roads in small and large basins, western Cascade, Oregon, *Water Resources Research* **32**, 959-974.

Imamoto, h., Ishigaki, T., Shiono, K., 1993. Secondary flow in a straight open channel. Annals of the Disaster Prevention Research Institute, Kyoto University, No. 36 B-2, April,ppl-9 (in Japenese).

IPCC, 2001. *3rd Assessment Report: Climate Change*. Cambridge University Press, Cambridge, pp 398.

Knight, D. W., 1989. Hydraulics of flood channels. In: Beven, K., Carling, P. (Eds.), *Floods: Hydrological, Sedimentological and Geomorphological Implication*, Wiley, Chichester, pp. 83-105.

Knight, D. W., Cao, S. 1994. Boundary shear in the vicinity of river banks. *Proceedings of ASCE National Conference On Hydraulic Engineering*, Buffalo. New York, August, Vol. 2, pp. 954-958.

275

Knight, D. W., Patel, H. S. 1985. Boundary shear stress distributions in rectangular duct flow. *Proc. 2nd Int. Symp. on Refined Flow Modelling and Turbulence Measurements,* Iowa. USA Sept., Paper 122, pp.1-10, Hemisphere Publishing Co., Iowa, USA.

Knight, D. W., Shiono, K. 1996. River Channel and Floodplain Hydraulics. In: *Floodplain Processes.* Anderson, M. G., Walling, D. E., Bates, P. D., (Eds.). Wiley, Chichester, pp. 139-181.

Knight, D. W., Samuels, P.G., Shiono, K., 1990. "River flow simulation: research and developments". *Journal of the Institution of Water and Environmental Management,* 4(2), 163-175.

Knight, D. W., Shiono, K., Pirt, J., 1989. Prediction of depth mean velocity and discharge in natural rivers with overbank flow. *Proc. Int. Conf. on Hydraulic and Environmental modelling of Coastal. Estuarine and Rivers Waters,* (Ed. R.A. Falconer *et al.*), University of Bradford. Gower Technical Press, Paper 38, pp.419-428.

Knight, D. W., Demetrious, J. D., Hamed, M. E., 1983. "Hydraulic analysis of rivers with floodplains" *Proc. Int. Conf. on Hydraulic Aspects of Floods,* British Hydromechanics Association, BHRA, Cranfield, Spte., Paper E1, pp.129-144.

Knight, D. W., Demetrious, J. D., Hamed, M. E., 1984."Stage-discharge relationships for compound channels". *Proc. Int. Conf. on Hydraulic Design of channel Control Structures in Water Resources Engineering: Channels and Channel Control Structures* (Ed. K. V. H. Smith), Southampton, April, pp. 4.21-4.25, Springer-Verlag, Heidelberg.

Knight, D. W., Yuen, K. W. H., Alhamid, A. A. I. 1994. Boundary shear stress distributions in open channel flow. In: *Physical Mechanisms of Mixing and Transport in the Environment.* Beven, K. Chatwin, P. and Millbank, J. (Eds.). Wiley, Chichester, pp. 51-87.

Lane, S. N., 1998. Hydraulic modelling in hydrology and geomorphology: A review of high-resolution approaches. *Hydrological Processes.* 12, 1113-1150.

Lane, S. N., 2000. The measurement of river channel morphology using digital photogrammetry. *Photogrammetric Record* 15, 937-961.

Lane, S. N., 2001. Upper Wharfedale Best Practice Project. Information Series No. 4.

Lane, S. N., 2003. Numerical modelling in physical geography: understanding, explanation and prediction. In: *Key Methods in Geography,* Clifford N. J. and Valentine G. (Eds.), 263-290.

Lane, S. N., Bradbrook, K. F., Richards, K. S., Biron, P. A. and Roy, A. G. 1999. The application of computational fluid dynamics to natural river channels: three-dimensional versus two-dimensional approaches. *Geomorphology* **29**, 1-20.

Lane, S. N., Richards, K. S. 1998. High resolution, two-dimensional spatial modelling of flow processes in a multi-thread channel. *Hydrological Processes* **12**, 1279-1298.

Lane, S. N., Richards, K. S. 2001. The 'Validation' of Hydrodynamic Models: Some Critical Perspectives. In: *Model Validation: Perspectives in Hydrological Sciences*, Anderson, M. G., Bates, P. D., (Eds.),Wiley.

Lane, S. N., Richards, K. S., Chandler, J. H., 1994. Application of distributed sensitivity analysis to a model of turbulent open channel flow in a natural river channel. *Proceedings of The Royal Society of London* A **446**, 49-63.

Lane, S. N., Richards, K. S., Chandler, J. H., 1996. Discharge and sediment supply controls on erosion and deposition in a dynamic alluvial channel. *Geomorphology* **15**, 1-15.

Langben, W. B., 1966. A random walk model of hydraulic friction. *Bulletin of The International Association of Scientific Hydrologist* **11**, 5-9.

Li, C. S., 1997. Waveform sampling LiDAR applications in complex terrain. *International Journal of Remote Sensing* **18**, 2087-2104.

Liggett, J. A., Chiu, C. L., Miao, L. S., 1965. Secondary current in a corner. *Journal of Hydraulics Division*, ASCE **91**, 99-117.

Limerions, J. T., 1970. Determination of Manning coefficient from measured bed roughness in natural channels. *United States Geological Survey Water Supply Paper* **1898B**.

Lyons, J. K., Beschta, R. L., 1983. Landuse, floods, and channel change: Upper Middle Fork Willamette River, Oregon (1936-1980). *Water Resources Research* **19**, 463-471.

Marks, K. and Bates, P. D., 2000. Integration of high-resolution topographic data with floodplain flow models. *Hydrological Processes* **14**, 2109-2122.

Mason, D. C., Cobby, D. M., Daveport, I. J., 1999. Image processing of airborne scanning laser altimetry for some environmental applications. *Image and Signal Processing for Remote Sensing V, SPIE*, Vol. 3871. International Society for Optical Engineering, Bellingham, WA, pp. 55-62.

Mason, D. C., Cobby, D. M., Horritt, M. S., Bates, P. D., 2003. Floodplain friction parameterisation in two-dimensional river flood models using vegetation heights derived from airborne scanning laser altimetry. *Hydrological Processes* 17, 1711-1732.

McCuen, R. H., 1973. The role of sensitivity analysis in hydrologic modelling. *Journal of Hydrology* 18, 37-53.

Melling, A., Whitelaw, J. H., 1976. Turbulent flow in rectangular duct. *Journal of Fluid Mechanics* 78, 289-315.

Miller, A. J., 1994. Debris-fan constructions and flood hydraulics in River Canyons: Some implications for two-dimensional flow modelling. *Earth Surface Processes and Landforms* 19, 681-698.

Nelson, J. M., Smith, J. D., 1989a. Flow in meandering channels with natural topography, In: *River Meandering*, Parker, G., American Geophysical Union Monograph, 12. pp. 69-102.

Nelson, J. M., Smith, J. D., 1989b. Evolution and stability of erodible channel beds, In: *River Meandering*, Parker, G., American Geophysical Union Monograph, 12. pp. 321-377.

Nicholas, A. P., Mitchell, C. A., 2003. Numerical simulation of overbank processes in topographically complex floodplain environments. *Hydrological Processes* 17, 727-746.

Nicholas, A. P., and Walling, D. E., 1997. Modelling floodplain hydraulics and overbank deposition on river floodplains. *Earth Surface Processes and Landforms* 22, 59-77.

Nicholas, A. P. and Walling, D. E. 1998. Numerical modelling of floodplain hydraulics and suspended sediment transport and deposition. *Hydrological processes* 12, 1339-1355.

Niekerk, A. Van, Vogel, K. R., Slingerland, R. L., Bridge, J. S., 1992. Routing of heterogeneous sediment over mobile bed: model development, *ASCE Journal of Hydraulic Engineering* 118, 246-263.

Olson, R. M., Wright, S. J. 1990. *Essentials of Engineering Fluid Mechanics*. Harper Row, New York. 638pp.

Osborne, T. J., Hulme, M., 2002. Evidence fro trends in heavy rainfall events over the UK. *Philosophical Transactions of The Royal Society of London* A **360**, 1313-11325.

Penning-Rowsell, E. C. and Tunstall, S. M. 1996. Risks and Resources: defining and managing the floodplain. In *Floodplain Processes*, Anderson, M. G., Walling, D. E., Bates, P. D. (Eds). Wiley, Chichester,493-533.

Perkins, H. J., 1979. The formation of streamwise vorticity in turbulent flow. *Journal of Fluid Mechanics* **44**, 721-740.

Phillips, J. D. 2002. Geomorphic impacts of flash flooding in a forested headwater basin. *Journal of Hydrology* **269**, 236-250.

Pinder, G. F., Gray, W. G., 1977. *Finite Element Simulation in Surface and Subsurface Hydrology*. Academic Press, New York, 259 pp.

Poof, N. L., 2002. Ecological response to and management of increased flooding caused by climate change. *Philosophical Transactions of The Royal Society of London* A **360**, 1497-1510.

Priestnall, G., Jaafar, J., Duncan, A., 2000. Extracting urban features from LiDAR-derived digital surface models. *Computers, Environment and Urban Systems* **24**, 65-78.

Rhodes, D. G., Knight, D. W. 1994a. Distribution of shear force on boundary of smooth rectangular duct. *Journal of Hydraulic Engineering*, ASCE **120**, 787-807.

Rhodes, D. G. and Knight, D. W., 1994b. Velocity and boundary shear in a wide compound duct. *Journal of Hydraulic Research*, IAHR **32**, 743-764.

Richardson, E. V., Simons, D. B., Julien, P., 1990. Highways in the River Environment, FHWA-HI-90-016, Federal Highway Administration, U.S. Department of Transportation, Washington, D. C.

Robson, A. J., 2002. Evidence for trends in UK flooding. *Philosophical Transactions of The Royal Society of London* A **360**, 1327-1343.

Rodi, W., 1980. *Turbulence models and their Application in Hydraulics. IAHR*, Delft.104 pp.

Rodi, W., Pavlovic, R. N., Srivatsa, S. K. 1981. "Prediction flow and pollutant spreading in rivers". In Fischer, H. B. (Ed.), *Transport Models for Inland and Coastal Waters*. Academic Press, New York. 542 pp.

Rogers, C. C. M., Beven, K. J., Morris, E. M., Anderson, M. G., 1985. Sensitivity analysis, calibration and predictive uncertainty of the institute of hydrology distributed model. *Journal of Hydrology* **81**, 179-191.

Romanowicz, R., Beven, K. J., Tawn, J., 1996. Bayesian calibration of flood inundation models. In: Anderson, M. G., Walling, D. E., Bates, P. D. (Eds.), *Floodplain Processes*, Wiley, Chichester, pp. 333-1439.

Rothacher, J., 1973. Does harvesting in west slope Douglas-fir increase peak flow in small harvest date stream? Res. Pap. PNW-163, US For. Serv. For., Northwest For. and Range Exp. Stn., Corvallis, OR.

Salmuels, P. G., 1985. Modelling of river and floodplain flow using the finite element method, *Hydraulics Research Technical Reports*, **SR61**, Wallingford, UK.

Salmuels, P. G., 1990. Cross section location in one-dimensional models. In: White, W. R. (Ed.). *International Conference on River Flood Hydraulics*, Wiley, Chichester, pp. 339-350.

Schmitz, G., Seus, G. J., Czwitzty, H. J., 1983. Simulating two dimensional flood flows. *British Hydrometric Research Association*. International Conference on the Hydraulic Aspects of Flood and Flood Controls. pp. 195-206.

Sellin, R. H. J., Willets, B. B. 1996. Three-dimensional structures memory and energy dissipation in meandering compound channel flow. In: *Floodplain Processes*. Anderson, M. G., Walling, D. E. and Bates, P. D. (Eds.), Wiley, Chichester, pp. 255-298.

Senior, C., Jones, R. G., Lowe, J. A., 2002. Predictions of extreme predictions and sea-level rise under climate change. *Philosophical Transactions of The Royal Society of London* A **360**, 1301-1311.

Shiono, K. and Knight, D. W. 1991. Turbulent open channel flows with variable depth across the channel. *Journal of Fluid Mechanics*, **222**, 617-646 (and 231, 693).

Shimizu, H., Itakura, T., 1989. Calculation of bed variation in alluvial channels, *ASCE Journal of Hydraulic Engineering* **115**, 367-348.

Shimizu, H., Yamaguchi, H., Itakura, T., 1990. Three-dimensional computation of flow and bed deformation. *ASCE Journal of Hydraulic Engineering* **116**, 1090-1106.

Siggers, G. B., Bates, B. P., Anderson, M. G., Walling, D. E., He, Q., 1999.A preliminary investigation of the integration of modelling floodplain hydraulics with estimation of overbank floodplain sedimentation derived from Pb-210 and Cs-137 measurements. *Earth Surface Processes and Landforms* **24**, 211-231.

Singh, V. P., 1996. *Kinematic Wave Modeling in Water Resources, Surface-Water Hydrology*. Wiley-Interscience, 1424pp.

Stewart, M. D., Bates, P. D., Anderson, M. G., Price, D. A., Burt, T. P. 1999. Modelling floods in hydrologically complex lowland river reaches. *Journal of Hydrology*, **223**, 85-106.

Stover, S. C., Montgomery, D. R., 2001.Channel change and flooding, Skokomish River, Washington. *Journal of Hydrology* **243**, 272-286.

Struiksma, N., Crosato, A., 1989. 'Analysis of a two-dimensional bed topography model for rivers', in Parker, G. (Edt.), *River Meandering*, American Geophysical Union Monograph, 12. pp.153-180.

Thomas, R. B., Megahan, W. F., 1998. Peak flow response to clear-cutting and roads in small and large basins, western Cascade, Oregon: a second opinion. *Water Resources Research* **34**, 3393-3403.

Thomas, T.G., Williams, J. J. R., 1995. Large eddy simulation of turbulent flow in an asymmetric compound open channel. *Journal of Hydraulic Research* **33**, 27-41.

Tracy, H. J., 1965. Turbulent flow in a three-dimensional channel. *Journal of the Hydraulics Division*, ASCE, **91** (HY6), 9-35.

US Army Crops of Engineers, Hydraulic Engineering Center, 1995. *HEC-RAS, Hydraulic Reference Manual*, Version 1.0. 121 pp.

Upper Wharfedale 'Best Practise' Project, 1998. *Feasibility Study, Final Report*. ARK AURP. 63 pp.

U.S. Army Corps of Engineers, 1965. *Hydraulic Design of Spillways*, EM 1120-2-1603, Plate 33.

Walling, D. E., Quinne, J. A., He, Q., 1992. Investigating contemporary rates of floodplain sedimentation. In: *Lowland Floodplain Rivers: Geomorphological Prespective*. Carling, P. A., Petts, G. E., (Eds.). Wiley, Chichester, 166-184.

Westway, R. M., Lane, S. N., Hicks, D. M., 2001. Airborne remote sensing of clear water, shallow, gravel-bed rivers using digital photogrammetry and image analysis. *Photogrammetric Engineering and Remote Sensing* 67, 1271-1281.

Westway, R. M., Lane, S. N., Hicks, D. M., 2003. Remote survey of large-scale braided rivers using digital photogrammetry and image analysis. *International Journal of Remote Sensing* 24, 795-816.

Wheater, H., 2002. Progress in and prospects for fluvial flood modelling. *Philosophical Transactions of The Royal Society of London* A 360, 1451-1460.

Wormleaton, P. R., Allen, J., Hadjipanos, P., 1982. Discharge assessment in compound channel flow. *Journal of Hydraulics Division, ASCE* 108, 975-994.

Younis, B. A., 1992. *Is Turbulence modelling of any use?* AIRH Conference. Institution of Civil Engineers, London, April 1992.

Younis, B. A., 1996. Progress in turbulent modelling for open channel flows. In: Anderson, M. G., Walling, D. E., Bates, P. D. (Eds.). *Floodplain processes*, Wiley, Chichester, pp. 299-332.

Young, P. C. 2002. Advanced in real time forecasting. *Philosophical Transactions of The Royal Society of London* A 360, 1433-11450.

Yu, D., Lane, S. N., in press a. Urban fluvial flood modelling using a two-dimensional diffusion wave treatment: 1. Mesh resolution effects. Paper forthcoming in Hydrological Processes

Yu, D., Lane, S. N., in press b. Urban fluvial flood modelling using a two-dimensional diffusion wave treatment: 2. Development of a sub grid-scale treatment. Paper forthcoming in Hydrological processes.

Yuen, K. W. H., 1989. A study of boundary shear stress, flow resistance and momentum transfer in open channels with simple and compound trapezoidal cross section. PD. thesis, University of Birmingham, UK. 196 pp.

Zanobetti, D., Lorgere, H., Preissmanm, A., Cunge, J. A., 1968. Le modele mathematique du delta du Mekong. *La Houille Blanche*, No. 1, 4 and 5.

Zanobetti, D., Lorgere, H., Preissmanm, A., Cunge, J. A., 1970. Mekong Delat mathematical model program construction, *Journal of The Waterways and Harbors Division*, ASCE, 96, No. WW2, May, 143-159.

Zeike, W., Urban, W., 1981. Two-dimensional modelling of rivers with floodplains. International Association of Hydraulics Research, Numerical Modelling of River Channel and Overland Flow for Water Resources and Environmental Applications, Delft, Netherlands.

Ziemer, R. R., 1981. Storm flow response to road building and partial cutting in small stream in Northern California. *Water Resources Research* 17, 907-917.

Zhelenznyakov, G. V., 1971. Interaction of channel and floodplain streams. *Proceedings. 14th International Conference of the International Association of Hydraulics Research*. Paris, France, pp. 17.